Advanced GPS signal processing techniques for LBS services

Hanaa Al Bitar-El Natour

N° d'ordre : 2497

THESE

présentée

pour obtenir

LE TITRE DE DOCTEUR DE L'INSTITUT NATIONAL POLYTECHNIQUE DE TOULOUSE

École doctorale : Informatique et Télécommunications

Spécialité : Réseaux, Télécommunications, Système et Architecture

Par MM Hanaa AL BITAR

Titre de la thèse Techniques avancées de traitement du signal GPS pour les services LBS

Advanced GPS signal processing techniques for LBS services

Soutenue le 6 Juillet 2007 devant le jury composé de :

M.	Francis CASTANIE	Président
M	Christophe MACABIAU	Directeur de thèse
MM	Marie-Laure BOUCHERET	Directrice de thèse
M	Bernd EISSFELLER	Rapporteur
M	Thierry CHONAVEL	Rapporteur
M	Michel MONNERAT	Membre
M	Jean-Luc ISSLER	Membre
MM	Anne-Christine ESCHER	Membre

"*What difference does it make to the dead, the orphans, and the homeless, whether the mad destruction is wrought under the name of totalitarianism or the holy name of liberty and democracy*"

Mahatma Gandhi

Résumé

Par le passé, il était indispensable, pour le bon fonctionnement du GPS (*Global Positioning System*), que le signal soit en vision directe entre le satellite et le récepteur, et les signaux faibles n'étaient pas exploitables. Mais l'extension du GPS aux services LBS (*Location Based Services*) et à d'autres applications de navigation a changé ce paradigme. Par conséquent, on prévoit une augmentation considérable de techniques de localisation de plus en plus performantes, surtout dans des environnements du type indoor ou urbain. Les exigences de la localisation dans ce type d'environnements posent un véritable défi pour la conception des récepteurs GPS.

Le but de la thèse est d'optimiser les techniques existantes de traitement du signal GPS pour la localisation dans des milieux contraints, dans le cadre de l'AGPS (*Assisted GPS*). Ce système suppose que le récepteur GPS est connecté ou introduit dans un téléphone portable. Ce genre de couplage permet de transférer au récepteur GPS des données d'assistance via le réseau GSM (*Global System for Mobile communications*). Ces données fournissent au récepteur GPS la liste des satellites visibles, mais aussi des valeurs estimées de leur Doppler et leur retard de code, réduisant ainsi la fenêtre de recherche de ces paramètres. Les travaux de la thèse consistent à explorer différentes techniques d'acquisition du signal GPS pour réduire le temps d'acquisition nécessaire ou TTFF (*Time To First Fix*), sans affecter la sensibilité du récepteur GPS. Ceci est réalisé après une étude du canal GPS radio.

L'étude débute par une revue du GPS et de la structure du signal utilisé dans ce système. Le processus d'acquisition est ensuite décrit en détails: l'acquisition classique est décrite en premier pour mettre en évidence par la suite l'effet du milieu de propagation sur cette étape du traitement du signal. A cet effet, les milieux contraignants (Indoors et Urbains) seront modélisés et analysés. Cette analyse permettra de mettre en évidence les problèmes subits par les ondes radio se propageant dans ce type d'environnements. On notera que le canal urbain a été analysé en utilisant un modèle déjà existant élaboré par Alexander Steingass et Andreas Lehner du DLR (*Centre Aérospatial Allemand*) [*Steingass et al., 2005*]. D'autre part, un modèle statistique du canal indoor a été développé par l'ESA (*European Space Agency*) dans le cadre du projet intitulé "Navigation signal measurement campaign for critical environments" et présenté dans [*Pérez-Fontán et al, 2004*]. Mais ce modèle considère un canal statistique invariable dans le temps. Pour cela nous avons développé un modèle Indoor qui envisage plutôt un canal variant avec le temps, en prenant en compte les variations temporelles de certains paramètres du canal, comme le retard et la phase de la fonction de transfert. Les valeurs initiales de ces paramètres utilisés dans notre modèle sont toutefois basées sur les distributions statistiques fournies par le modèle de l'ESA. L'étude des canaux de propagation porte surtout sur les multitrajets, les inter-corrélations, et le masquage du signal. Les multitrajets sont particulièrement gênants dans le cas de milieux urbains, les inter-corrélations et le masquage sont par contre plus gênants dans les milieux indoors. Ces phénomènes peuvent impliquer des erreurs dans la position calculée par le récepteur. Pour y remédier, une des solutions est d'augmenter la durée d'observation du signal pour améliorer le rapport signal sur bruit. Mais ceci conduit à des temps d'acquisition beaucoup plus longs. Par conséquent, la qualité commerciale du récepteur est mise en cause vues les contraintes sur le TTFF nécessaires pour fournir une première solution. Ces contraintes en termes de temps

de traitements sont aussi importantes que les contraintes en termes de précision pour les utilisateurs du GPS. Mais ces deux contraintes vont en général l'une à l'encontre de l'autre. Par conséquent, une solution idéale consistera à réduire le temps d'acquisition sans pour autant affecter la sensibilité du récepteur.

Ainsi, dans la suite de l'exposé des méthodes avancées de traitement du signal dans la phase d'acquisition seront présentées. La plupart de ces méthodes vise à réduire le temps total d'acquisition plutôt qu'à améliorer la sensibilité du récepteur: ceci permet de tolérer) le traitement de signaux plus longs - afin d'améliorer la sensibilité - sans augmenter la durée globale de traitement. Ces méthodes seront tout d'abord caractérisées en évaluant les avantages et les inconvénients de chacune d'elles. Une évaluation de performances de ces algorithmes, utilisant des signaux générés avec un Spirent STR4500 sera conduite dans une étape finale de cette étude.

Abstract

In the past, in order for GPS (*Global Positioning System*) to work accurately, the presence of an unobstructed LOS (*Line-Of-Sight*) signal was necessary. Weak signals were not suitable for use because they may have large associated noise and other errors. The expansion of GPS to LBS (*Location-Based Services*) and other navigation applications all over the world, such as the E-911 and the E-112 mandates in the United States and Europe respectively, changed the paradigm. Consequently a dramatic increase in the need for more and more performant positioning techniques is expected, especially in urban and indoor environments. These rising localization requirements pose a particularly difficult challenge for GPS receivers design.

The thesis objective is to evaluate and enhance existing GPS signal acquisition techniques for positioning goals in harsh environments, in the context of AGPS (*Assisted GPS*). The AGPS system assumes that the GPS receiver is connected to or introduced in a mobile phone. This allows for the transfer of AD (*Assistance Data*) to the GPS receiver via the GSM (*Global System for Mobile communications*) cellular network. Amongst others, the AD provides the GPS receiver with the list of visible satellites and estimates of their Dopplers and code delays, thus reducing the search window of these parameters. This work consists in exploring different GPS signal acquisition to reduce the acquisition time or TTFF (*Time To First Fix*), without affecting the receiver sensitivity. This is done after a prior study of the GPS radio channel.

The study starts out with a revue of the GPS system and the GPS transmitted and received signal structure. The acquisition process is then described in details: the classical acquisition is first described in order to proceed afterwards with the impact of the propagation environment on this stage of the signal processing. For this purpose, harsh environments (urban and indoor) are modelled and analysed. This analysis enables to study the problems which encounter the radio frequency signal propagation through such environments. Note that the urban channel is studied using an existing statistical model developed by Alexander Steingass and Andreas Lehner at the DLR (*German Aerospace Center*) [*Steingass et al., 2005*]. On the other hand, an indoor channel model was developed by the ESA (*European Space Agency*) in the frame of a project entitled “Navigation signal measurement campaign for critical environments” and presented in [*Pérez-Fontán et al, 2004*]. But this model considers a time invariant statistical channel. Consequently, we developed an Indoor model which rather considers a time variant channel, by taking into account temporal variations of some channel parameters, like the transfer function delay and phase. The initial values are however based on the statistical distributions provided by the ESA model. The channels are analysed is terms of multipaths, cross-correlations and signal masking. The multipaths replicas are particularly disturbing in urban environments while the cross-correlations and masking effects are more disturbing in indoor environments. These phenomena may induce errors in the final solution calculated by the receiver. In order to avoid this error, one solution consists in increasing the signal observation duration in order to enhance the signal to noise ratio. But this generally implies longer acquisition time, thus affecting the receiver

performance, commercially speaking. Indeed, the time requirements are as important as sensitivity requirements for GPS users. However, these two requirements are not generally compatible with each other. Consequently, an ideal solution consists in reducing the acquisition time without greatly affecting the receiver sensitivity.

Accordingly, such advanced methods for acquisition signal processing are described next. Most of these methods aim at reducing the total acquisition time, rather than enhancing the receiver sensitivity. This means however that longer signal blocks can be processed (thus enhancing sensitivity) without affecting the global processing duration. At first, each of these methods is evaluated through the description of its advantages and drawbacks. A performance evaluation of these algorithms, using signals generated with a Spirent STR4500, ensues as a final step of this study.

Acknowledgements

I would like to express my heartfelt thanks and gratitude to my supervisor, Dr. Christophe Macabiau, for his patience, encouragement, and guidance throughout my research. His expertise and the numerous technical discussions we had during these three years added considerably to my graduate experience. His pleasant character, great sense of humor and frequent hearty laughs made our time here much more enjoyable. I would also like to thank him for the succulent "fois gras de Montauban" that he often offered to us on happy occasions.

I would like to thank Eng. Michel Monnerat and Stéphane Corazza from Thales Alenia Space for their technical support, and especially Stéphane Corazza for his kindness and friendship.

In addition, I would like to acknowledge Anne-Christine Escher for her help with this dissertation, and Olivier Julien for his insightful critiques and valuable technical discussions prior to my Ph.D defense.

I would also like to express my gratitude to Professor Francis Castanié, director of the TéSA laboratory, for his support and encouragement, and for being the chairman of the jury, as well as all the TéSA team for their friendly welcome.

I would like to thank my reviewers, Prof. Bernd Eissfeller and Dr. Thierry Chonavel for taking the time to read my thesis and for their valuable remarks which were essential to improve the quality of my report.

I appreciate the camaraderie of my coworkers at ENAC, Emilie, Damien, Anaïs, Mathieu, Benjamin, Christophe, Na, Antoine, Philippe, Audrey, Gael, ….

I particularly wish to thank my great officemates, Emilie and Damien.

Emilie, thank you for always managing to put some order in the office despite our messy presence and bad memory. Also, thank you for being a precious guide in all the travels we made to the United States.

Damien, I hope your new colleagues are not always freezing "either in winter or in summer", as was the case for us, and hope you are enjoying your new personal cooling system.

I owe a unique word of gratitude to my family, especially my parents and my husband for their immense support. Ahmad, thank you for all what you did, and especially for the colorful power point presentations you created out of my rather poor slides.

Maman, te remercier du fond du cœur pour tous les sacrifices que tu as faits et continues à faire pour nous n'est que très insuffisant. J'espère que je pourrais un jour te rendre une partie même infime de tout ce que tu m'as donné sans répit. الجنة تحت أقدام الأمهات

Finally, this research would not have been possible without financial assistance of the French Ministry for Education and Research via a research fellowship, and Thales Alenia Space who complemented this fellowship.

Table of Contents

List of Figures

List of tables

List of abbreviations

A/D	Analog to Digital
AD	Assistance Data
AGPS	Assisted GPS
AOA	Angle Of Arrival
ARNS	Aeronautical Radio Navigation Services
BPSK	Binary Phase Shift Keyed
BSC	Base Station Controller
BTS	Base Transmission Station
C/A	Coarse/Acquisition
CDF	Cumulative Distribution Function
CDMA	Coded Division Multiple Access
CGI	Cell Global Identifier
COO	Cell Of Origin
CTP	Conventional Terrestrial Poles
DFT	Discrete Fourier Transform
DGPS	Differential GPS
DLR	German Aerospace Center
DoD	Department of Defense
DSSS	Direct Sequence Spread Spectrum
E-FLT	Enhanced Forward Link Triangulation
EIRP	Effective Isotropic Radiated Power
ENAC	Ecole Nationale de l'Aviation Civile

E-OTD	Enhanced OTD
ESA	European Space Agency
FCC	Federal Communications Commission
FFT	Fast Fourier Transform
GNSS	Global Navigation Satellite Systems
GPS	Global Positioning System
HOW	Hand Over Word
HSGPS	High Sensitivity GPS
IF	Intermediate Frequency
IFFT	Inverse FFT
INS	Inertial Navigation System
IR	Infra Red
LBS	Location Based Services
LMMCM	Land Mobile Multipath Channel Model
LMU	Location Measurement Unit
LNA	Low Noise Amplifier
LOS	Line Of Site
MCS	Master Control Station
MEO	Medium Earth Orbit
MLC	Mobile Location Centre
MS	Mobile Station
MSC	Mobile Switching Centre
NAVSTAR	NAVigation Satellite Timing and Ranging
NLOS	Non LOS
OTD	Observed Time Difference

OCS	Operational Control Segment
P	Precision
PDA	Personal Data Assistant
PDE	Position Determination Equipment
PDF	Probability Density Function
PFA	Probability of False Alarm
ppm	part per million
PPS	Precise Positioning Service
PR	Pseudo Range
PRN	Pseudo Random Noise
PSAP	Public Safety Answering Point
PSD	Power Spectral Density
PVT	Position, Velocity and Time
RF	Radio Frequency
RRLP	Radio Resource LCS Protocol
RRC	Radio Resource Control Protocol
RTD	Real Time Difference
SA	*Selective Availability*
SMLC	Serving Mobile Location Centre
SNR	Signal to Noise Ratio
SPS	Standard Positioning Service
SOR	Sum Of Replicas
TA	Time Advance
TDOA	Time Difference Of Arrival
TOA	Time Of Arrival

TTFF	Time To First Fix
WGS84	World Geodetic Reference 84
WGN	White Gaussian Noise
XOR	eXclusive OR

List of symbols

L_1	L_1 carrier frequency 1575.42 *MHz*
L_2	L_2 carrier frequency 1227.6 *MHz*
L_5	L_5 carrier frequency 1176.45 *MHz*
λ_{L1}	L_1 carrier wavelength 19.03 *cm*
A	Signal amplitude
d	Binary NRZ materialisation of the navigation data bits
c	Binary NRZ materialisation of the spreading code
P	Precision code
h	Channel impulse response
h_{FE}	Front End filter impulse response
H_{FE}	Front End filter frequency response
h_{CI}	Coherent integration low pass filter impulse response
H_{CI}	Coherent integration low pass filter frequency response
γ	Satellite elevation angle
r_e	Earth radius
r_s	Distance between the earth's center and a satellite
m_b	Mean noise level in the correlation matrix
δ	Dirac distribution function
$\overline{T}$	Mean acquisition time

T_D	Data bit duration
T_c	C/A code chip duration
T_P	P code chip duration
T_s	Sampling period
T_p	Coherent integration duration
f_s	Sampling frequency
f_I	Intermediate frequency
f_c	C/A code rate 1.023 *MHz*
f_p	Coherent integration bandwidth
f_d	Carrier Doppler frequency
f_{dc}	Code Doppler frequency
v_d	Doppler velocity
Δf_{DOP}	Width of Doppler frequency bin
Δf_{FFT}	FFT frequency resolution
f_{inst}	Carrier instantaneous frequency
M	Number of non-coherent accumulations
N_c	Number of C/A code periods coherently accumulated
N_{rec}	Number of satellite signals in the received composite GPS signal
N_{loc}	Number of local replicas added together in the SOR algorithm
R	Autocorrelation function
τ	Propagation delay
θ	Carrier phase delay

φ	Carrier instantaneous phase
B	Font-end selective filter double-sided Bandwidth
C	Carrier power
$\frac{C}{N_0}$	Carrier to noise power density ratio
SNR_{pre}	Signal To Noise ratio at the output of the front end filter
SNR_{post}	Signal To Noise ratio after coherent integration
I	In-phase correlation value
Q	Quadra-phase correlation value
λ	χ^2 distribution non-centrality parameter
Pf_a	Probability of false alarm
P_d	Probability of detection
G_c	Coherent gain
G_n	Non-coherent gain
G_c	Coherent gain
G_{tot}	Total coherent and non-coherent gain
P_R	PRN peak range due to time and location uncertainties

Résumé du chapitre 1

L'objectif de cette thèse est double : tout d'abord, il s'agit de caractériser le canal GPS d'un point de vue de l'acquisition, et ensuite de proposer une solution de traitement de signal optimale pour améliorer le processus d'acquisition.

Dans un contexte de localisation par satellite, les environnements urbains et indoors présentent pratiquement les mêmes problèmes, mais le problème de l'atténuation du signal est plus prononcé dans un environnement indoor. Ainsi, une étude des caractéristiques du canal GNSS est particulièrement importante pour mieux comprendre les problèmes de ce type de canaux, et trouver une technique de traitement adaptée.
La caractérisation du canal a été réalisée en utilisant un modèle de canal qui soit le plus en conformité avec le canal réel : un modèle basé sur des tests statistiques réels, tout en permettant de contrôler l'environnement de test. Pour cela, un modèle pour l'environnement indoor a été développé dans le cadre de cette thèse. Pour l'environnement urbain, c'est le modèle du DLR (centre spatial Allemand) qui a été utilisé.
Les résultats obtenus ont permis de tirer quelques conclusions concernant les problèmes rencontrées lors de l'acquisition d'un signal GPS. Ces conclusions ont conduit à la deuxième partie de cette thèse qui consiste à trouver une solution optimale pour le processus d'acquisition.

Le but de cette deuxième partie est donc de trouver des techniques avancées de pour le traitement di signal en acquisition, de les décrire, et de comparer leurs performances, en termes de sensibilité et de temps d'acquisition.

Ainsi, cette thèse est répartie en sept chapitres organisés comme suit :
Le premier chapitre donne le background nécessaire et résume les objectifs de la thèse.

Le deuxième chapitre décrit les bases du système GPS et de la phase d'acquisition du signal dans ce système. Il illustre en outre les performances d'un récepteur GPS de base en acquisition avec les résultats obtenus par un test réalisé au cours de cette thèse.

Le troisième chapitre présente une caractérisation de canal GPS, en le modélisant dans un premier temps, puis en réalisant plusieurs tests en pouvoir en tirer des conclusions.

Le chapitre IV présente deux techniques d'améliorations des récepteurs GPS standalone : le HSGPS et AGPS. Chacune des ces techniques sera décrite et ces performances évaluées.

Le chapitre V consiste en une exploration approfondie de différentes techniques avancées de traitement du signal GPS en acquisition. Plusieurs techniques ont été étudiées. Seules les plus significatives d'entre elles ont été reportées dans cette thèse.

Le chapitre six présente une comparaison des performances des techniques décrites dans le chapitre V, en termes de sensibilité (évaluée via le paramètre C/N_0) et le temps d'acquisition. Les méthodes ont été implémentées sous Matlab® 7.1.

Finalement le chapitre VII présente une synthèse des résultats obtenus et des recommandations pour des travaux futurs.

Il est à noter que les chapitres IV, V, et VI ont été réalisés avec la collaboration de Thalès Alenia Space, dans le cadre des activités de recherche du projet européen LIAISON. LIAISON est un projet de recherche dirigé par Thalès Alenia Space et engage 34 partenaires Européens, qui vise à développer les services LBS pour des marchés professionnels.

Chapter 1

Introduction

Contents

GNSS (*Global Navigation Satellite Systems*) navigation solutions are being more and more integrated in our daily life. With the emerging LBS (*Location Based Services*) and other positioning applications, the need for positioning is absolutely justified. In the United States, the primary LBS driver is the E-911 mandate issued by the FCC (*Federal Communications Commission*), phase II of which was due for implementation by October 2001 [*FCC, 2000*]. The E-911 mandate requires that the position of a cellular phone be available to the appropriate emergency PSAP (*Public Safety Answering Point*). Operators who deploy network-based solutions (which are independent of handset type, software, etc) must locate callers within 100m at least 67% of the time, and within 300m accuracy 95% of the time. Operators selecting handset solutions (requiring specialized handsets with location capability like GPS enabled handsets) have more rigorous requirements of 50 m at 67% of the time and 150m at 95% of the time. The E-112 mandate is the European counterpart of the E-911.

The most promising technologies to achieve this on a continental level was cellular phone network-based TDOA (*Time Difference Of Arrival*) methods (refer to appendix D for more details on cellular network based positioning methods) and GPS, if the latter could be made to operate under attenuated signal conditions. Early developments and testing of cellular phone network-based TDOA methods resulted in promising results with the use of GPS to precisely time synchronise signal transmissions [*Klukas et al, 1997 & 1998*]. However, the additional cell equipment required proved to be a challenge. In addition, with TDOA being a hyperbolic location method, observability was found to be low in an urban environment given the rapidly changing geometry of the available cells. Outside urban areas, the cell geometry was not present to meet availability requirements. Furthermore, the exclusive use of network

based technologies yielded a position accuracy that is generally much lower than GPS-based solutions [*LaMance et al., 2002*].

The main goal of modern satellite positioning is primarily to provide a worldwide solution in all kinds of environments. This solution is subject to precision and computation speed requirements, especially when dealing with real time commercial applications.

The American GPS (*Global Positioning System*) is currently the only operational satellite based positioning system as the European Galileo system is planned to roll out by 2012 [*Mathieu, 2006*], [*PriceWaterHouseCoopers, 2001*]. One of the advantages of a satellite positioning system is that the users are not required to transmit anything to the satellites, so there is no limit to the number of users that can use the system simultaneously. This thesis only deals with GPS receivers.

Although the GPS was originally designed as a military system, with the primary goal of providing land, air and marine positioning capabilities to the U.S. armed forces and its allies, GPS is currently freely available to all civilian users. Given the existing space-based infrastructure and coverage advantages of GPS, Research and Development efforts on improving GPS performance intensified rapidly, and the number of civilian users is already far greater than the military users and tremendous innovation is occurring within the civilian sector, with the development of technology and procedures that are permanently increasing. So far, the recent advances in integrated circuit technology have made it possible to produce highly sophisticated GPS receivers in volumes that are cheap enough for mass usage, and also small enough to be integrated into small autonomous devices such as PDAs (*Personal Data Assistants*) and cellular mobile phones. These technologies have particularly contributed to a faster integration of the GPS by the general public. The small size also indicates low power consumption, and results in more possibilities for the integration of a GPS receiver into ever-smaller cellular phones.

I.1 Background and motivations

The main goal of satellite positioning is to provide an all time/all weather solution. For this, it has to deal with many types of operational environments which may be generally classified as:

- **Rural environments**: they refer to unobstructed environments with very good satellite visibility. In such environments many direct LOS (*Line Of Site*) satellite signals are generally available at the receiver level. This means that the received signal is strong enough to be easily acquired and tracked.

- **Urban environments**: in these environments a LOS satellite signal is not always available. The signal generally reaches the receiver after multiple reflections or diffractions or after going through various possible materials like walls or foliage for example, giving rise to multipaths and shadowing phenomena. This causes the signal to be attenuated compared to the theoretical LOS signal. Furthermore, the presence of NLOS (*Non LOS*) signals leads to inaccurate solutions, since they have different

delays, or are very attenuated, compared to the original signal. Cross-correlations may also appear if two signals have different strengths.

- **Indoor environments**: these environments refer to in-building sites, where a LOS is not very likely to be available at the receiver. In most cases the signal must cross one or several concrete walls and ceilings to reach the receiver. This implies an important attenuation of the signal power, depending on the building materials. Note that cross-correlation problems may also arise in the case where two signals with very different signal strengths reach the receiver (with one reaching it through a window, and the other one going through a wall for example).

Generally speaking, the urban and indoor environments have practically the same problems, but the attenuation problem is much more significant in indoor environments. Hence, a subtle study of the channel characteristics is particularly valuable in order to gain a greater understanding of the GPS channel problems, and thus to find an optimal signal processing technique to be adopted.

Many studies aimed at characterizing the different GPS channels, especially the indoor and the urban channels. The studies were conducted using either simulated channel models [*Steingass et al., 2005*], [*Gligorevic, 2002*], [*Mangold et al., 1998a,b*] and [*Chandra, 2002*], or field tests [*Pérez-Fontán et al., 2004*], [*Steingass et al., 2004*], [*van Diggelen, 2001a*], [*Deshpande et al., 2004a*], [*Kavak et al., 1999*] and [*Saleh et al., 1987*].

The indoor model developed by the ESA (*European Space Agency*) and presented in [*Pérez-Fontán et al., 2004*] is a statistical model based on field tests realized using a GPS signal simulator placed on board a helicopter, and a GPS receiver in a 6 stores building. The tests were conducted for the GPS receiver being placed on different stores of the building and more or less close to that building external walls. The problem with this model is that it is static and assumes that the channel parameters do not vary with time. For this reason, a new indoor model was developed in the frame of this thesis based on the statistical results of the ESA model, but with time-varying parameters.

The DLR (*German Aerospace Center*) developed an urban channel model that is available for public use [*Steingass et al., 2005*]. This model was used to assess the main characteristics of this channel. This model is rather an optical model, based on ray tracing and statistical results obtained through different field tests. It is a time varying model. In this thesis, the urban channel was studied using both the DLR model, and a modified version of our indoor model to match with the urban channel.

The results obtained allowed for deriving some conclusions about the GPS signal acquisition main problems. These conclusions drove the subsequent search of an optimal solution for the acquisition process.

Conventional GPS receivers were initially designed to operate in open sky, i.e. in the presence of unobstructed LOS, and the received satellite signals usually conform to the minimum strength requirement specified by the ICD-GPS-200C [*ICD200C, 2000*]. The expansion of GPS to LBS, changed the paradigm, and GPS is utilized in increasingly difficult operational environments such as urban and indoor channels where path loss is very severe most of the time. As conventional GPS is unlikely to operate properly in such environments, HSGPS (*High Sensitivity GPS*) and AGPS (*Assisted GPS*) techniques have been developed.

While the HSGPS uses long signal integration time [*Shewfelt et al., 2001*] and [*Akos et al., 2000*], the AGPS rather relies on external navigation data aiding to acquire and track weak signals much lower than conventional GPS, which makes GPS useable in signal degraded environments. These new techniques have made it possible to use the GPS receivers in various signal degraded environments. The AGPS technique is particularly interesting and is recognized as a very promising technique [*Karunanayake et al., 2004*], [*Goran et al., 2001*], [*LaMance et al., 2002*] and [*Changlin, 2003*]. The HSGPS mainly enhances GPS signal tracking, but does not enhance acquisition. The GPS receiver conducts operations of acquisition, tracking, and navigation message demodulation. Acquisition is a coarse synchronization process giving estimates of the code offset and the carrier Doppler. The estimated PRN code offset and carrier Doppler are used to initialise the tracking loops which along with bit synchronization and sub-frame synchronization perform a finer search over the two parameters, and keep track of the carrier and code as well as computing pseudorange and carrier phase measurements, and demodulating the navigation message. Finally the navigation solution is calculated. Prior to determining the code delay and the carrier phase, a search for the PRN code to be used may be necessary, especially if the receiver has been shut down for long time. The acquisition is the most difficult stage to be carried on. This is particularly true in degraded environments.

The present thesis only deals with acquisition aspects. Different software acquisition approaches were tested and compared in terms of sensitivity and computation time. The performance evaluation is traditionally carried out using field tests, which is costly, time-consuming and introduces possible uncertainties due to the uncontrolled testing environments. An alternative method is to implement a simulator in a laboratory environment. Through such tests, GPS signals are replicated under strictly controlled conditions and verification of the receiver performance can be conducted. GPS hardware simulators are designed to accomplish this task. They are effective and cost-efficient tools for verifying new GPS product designs because of their capabilities to reproduce the RF (*Radio Frequency*) signals of GPS satellites. A series of Spirent Communications Inc. hardware GPS signal simulation systems is now available to generate L_1, L_2 and L_5 carriers with C/A (*Coarse/Acquisition*) code, P (*Precision*) code and navigation data. In this thesis only the L_1 C/A code GPS signal acquisition is addressed. The Spirent STR4500 simulator that was used through out this thesis has 12 independent channels with GPS L_1 carrier frequency, and C/A code. It has the capability of generating different scenarios and provides full user control over the power of different satellite signals. The models developed can also be used in such performance tests.

I.2 Thesis objective

The thesis objectives are twofold: first, to characterize the GPS channel from the acquisition point of view, and second, to propose optimal software solutions to improve the acquisition process.

The channel characterization is conducted using a channel model which has to match with field signals in a satisfactory manner. Therefore, it is based on field test statistics, while allowing for a full control of the simulated signal parameters, the main goal being to provide representative results while controlling the testing environment. The channel is studied in an acquisition context, i.e., with requirements corresponding to those of the acquisition phase of

the GPS signal processing. Different types of channels are used in order to derive general conclusions on the GPS channels.

Once the different channels are described and characterized, and the acquisition problems mitigated, the next step is to try to find advanced software techniques for acquisition, describe them and compare their performance using either simulated and/or real signals. The TTFF and the sensitivity are the key drivers for GPS receivers acquisition performance evaluation. The TTFF is the time needed for a GPS receiver to provide a first position. It accounts for both the signal observation time and the signal processing time. The sensitivity refers to its ability to acquire and possibly track weak signals. For commercial solutions, an efficient receiver is a receiver with reduced TTFF and high sensitivity. But generally, enhancing the sensitivity results in an increased TTFF and vice versa. In fact, one way to enhance the receiver sensitivity is to use longer coherent integration times leading to higher SNR (*Signal to Noise Ratio*) at correlator output [*van Diggelen, 2001b*]. But this increases the TTFF. As a result, a compromise must always be found between the receiver sensitivity and the TTFF. Note however, that modifying the acquisition algorithm in order to reduce its complexity, enables the use of longer coherent/non-coherent integrations to increase sensitivity, without eventually increasing the overall TTFF. This will be the key driver of the advanced techniques studied in this research.

I.3 Thesis outline

Characterizing the GPS channel and testing different advanced acquisition techniques are the core parts of this Ph. D. The dissertation comprises seven chapters organized as follows:

This first chapter gives the necessary background information and establishes the intent of this thesis.

Chapter II provides an overview of GPS and the acquisition signal processing phase. It starts with a brief description of the GPS architecture and the transmitted and received signals structure. Next, it describes the acquisition process and reports on its main limitations before recalling the classical sequential acquisition algorithm and the FFT (*Fast Fourier Transform*) algorithm principles. In the last part, it reports on some results illustrating, the standalone GPS performance.

Chapter III addresses the issue of the GPS channel characterization. This is carried out by first modelling the channel and then carrying different test cases, which leads to some concluding remarks about this channel and its main problems. One of these conclusions is that the standalone GPS cannot be used in constrained environments and augmentation systems are a must.

Two main improvement techniques are dealt with in chapter IV: the HSGPS and the AGPS. These two systems are first described each alone with some results assessing their respective performance. Subsequently they are compared with each other and conclusions are drawn finally. Experiments realized in the Toulouse downtown and the ENAC (*Ecole Nationale de l'Aviation Civile*) campus provide a useful insight on these two systems functioning properties.

Chapter V consists in an in-depth investigation of different advanced software acquisition techniques. Much more techniques were examined, but only the six most significant methods are reported here for further analysis and performance comparison. This chapter introduces these advanced techniques. Their advantages and drawbacks are evidenced using either theoretical considerations and/or some illustrating examples. The first five techniques dwell with improving the acquisition algorithm for one satellite, thus assuming a "mono-satellite" search at each execution of the algorithm. The sixth is rather a "multiple-satellite" algorithm where many satellites are searched for in parallel. The latter acquisition method can be optimised by combining it with one of the five aforementioned techniques. But due to the algorithm structure, not all of these techniques can be combined with it, as it will be discussed.

A performance comparison of all these methods is assessed in chapter VI through the computation of the C/N_0 (signal power to noise power density ratio) and the acquisition time for different values of the integration duration (coherent and non-coherent) and signal strengths. The algorithms were implemented using Matlab® 7.1. The chapter reports on the set of experiments conducted in this context. A first set of experiments provides a comparison of the different algorithms at similar parameter values, in terms of complexity and sensitivity. A second one yields a performance comparison with rather threshold values, to compare the limits in sensitivity for each method.

Last, Chapter VII synthesises all the results obtained through out this thesis with some concluding remarks, and recommendations for future works.

It is noteworthy that part of this thesis (Chapters IV, V and VI) was realised in collaboration with Thales Alenia Space in the frame of the research activities of the European project LIAISON. LIAISON is a research project led by Thales Alenia Space and involving 34 other European partners, which aims at developing LBS for professional markets. LIAISON has received research funding from the Community's Sixth Framework Program.

Résumé du chapitre II

Le signal GPS civil de la porteuse L_1 utilise une modulation BPSK, les codes utilisés étant des codes dits C/A qui sont des codes de la famille de Gold. Chaque satellite est caractérisé par son code C/A qui lui unique. Ces codes ont des propriétés de corrélation caractéristiques : Leur autocorrélation présente un lobe principal ayant une forme triangulaire quand les deux codes sont en phase, et des valeurs très faibles de l'ordre de 1/1023 si les codes ne sont pas en phase. Cela permet d'identifiant le retard du code en corrélant le signal reçu avec une réplique identique du code C/A utilisé dans ce signal.

La localisation par satellite est basée sur le principe de la triangulation, qui exige la réception d'au moins quatre signaux satellites. Chacun de ces signaux est corrélé à la réception avec le code C/A correspondant afin de se mettre en phase avec le signal reçu. Ceci permet par la suite la démodulation des données contenue dans le signal.

L'acquisition est la première étape du traitement de signal GPS. Pour cette phase on dispose en général de peu d'information sur le signal reçu. Cette étape d'acquisition est suivie par une étape de poursuite qui se base sur l'information grossière fournie à la sortie de l'acquisition pour l'affiner et la mettre à jour de façon continue. Il est connu que l'acquisition est l'opération la plus difficile et longue pour un récepteur GPS. Ceci est particulièrement vrai dans des environnements sévères où le récepteur GPS utilisé pour le positionnement doit être amélioré en software et/ou en hardware. Cette thèse considère plutôt une amélioration en software car ces techniques présentent plusieurs avantages par rapport aux techniques hardware :

- La facilité d'évolutions futures
- La capacité de travailler avec des signaux discrets
- La flexibilité dans la conception et l'implémentation, fournissant ainsi aux chercheurs et développeurs une flexibilité accrue pour tester et évaluer les performances d'une technique ou d'un système donnés.
- Une indépendance de la partie hardware qui permet d'éviter des composants qui aient des réponses non linéaires en fonction de la température et du temps.
- La possibilité d'utiliser des algorithmes de traitement de signal assez sophistiqués pour pouvoir capter des signaux qui soient très en dessous des niveaux nominaux.

Il est à noter que l'acquisition ne consiste pas uniquement à faire une recherche sur les différents retards du code du signal reçu pour se mettre en phase avec celui, mais aussi une recherche sur les différents Dopplers possibles subits par la porteuse du signal reçu. En effet, le signal en se propageant dans l'atmosphère subit un décalage temporel et fréquentiel en même, causant ainsi la porteuse de se déplacer légèrement de sa valeur d'origine. Le doppler fréquentiel est en général estimé à quelques *KHz*, et les pas de recherche fréquentielle sont de l'ordre de quelques centaines de *Hz* à quelques dizaines de *Hz*, suivant la durée d'intégration

du signal. Le pas de recherche temporelle lui est de l'ordre d'un demi chip en général. Mais quand il s'agit de signaux discrets, le pas de recherche temporelle se réduit au pas d'échantillonnage, dépendant ainsi de la fréquence d'échantillonnage utilisée.

La décision sur la détection ou non du signal se fait en comparant le résultat de l'acquisition à un seuil défini en fonction de la probabilité de fausse alarme et de la durée d'intégration (cohérente et non-cohérente). Si ce seuil est dépassé, la case correspondante définie par une valeur de la fréquence Doppler et du retard de code, est supposée contenir du signal utile, sinon elle uniquement formée de bruit. Notons que l'intégration cohérente est un paramètre très important dans l'acquisition. Ce paramètre a des effets opposés sur la probabilité de détection du signal et le temps d'acquisition. Si on augmente le temps d'intégration cohérente, la sensibilité du récepteur aux signaux faibles se trouve améliorée, mais cela implique un temps d'acquisition beaucoup plus élevé, le rapport entre l'augmentation du temps d'intégration et le temps d'acquisition n'étant pas linéaire. Cela signifie que suivant l'environnement dans lequel on se trouve, les temps d'intégration cohérents et non cohérents doivent être adaptés pour qu'un compromis soit atteint entre la sensibilité aux signaux faibles et le temps d'acquisition.

Deux schémas principaux de recherche en Doppler et en retard du code sont présentés dans ce chapitre : la recherche séquentielle, où les cases de recherche sont explorées l'une à la suite de l'autre. Bien entendu, cet algorithme de recherche, appelé algorithme Tong est très coûteux en temps de calcul, mais n'a aucune exigence mémoire. La deuxième technique de recherche se base sur la FFT pour réaliser une recherche en parallèle sur tous les retards possibles du code pour une fréquence Doppler donnée. Donc la recherche en fréquence Doppler se fait toujours en séquentiel.

Finalement, un test d'acquisition a été réalisé en utilisant le récepteur GPS OEM4, et le générateur de signaux GPS Spirent STR4500. Ce test montre que la limite de sensibilité de ce récepteur GPS classique est à peu près égale à 38.6 *dBHz*, une valeur très élevée par rapport au niveau des signaux reçus dans les milieux urbains et en indoors.

Chapter 2

Classical GPS acquisition

Contents

Acquisition is the first stage of the GPS signal processing and assumes little a priori information on the signal received depending on the application, as already mentioned in the introductory chapter. It is followed by a tracking stage which is based on coarse information provided by the acquisition process in order to refine it and constantly update it. It is commonly recognized that acquisition is the most difficult and time-consuming operation in a GPS receiver. This is particularly true in degraded environments where GPS positioning must be enhanced through software and/or hardware upgrading of the receiver. This thesis rather

deals with software enhancement techniques because software approaches offer many advantages over conventional hardware approaches:

- ease of upgrade
- capability of working with discontinuous signals
- flexibility in design and implementation, thus providing researchers and developers with more evaluation and testing flexibility
- hardware independence which allows for avoiding non-linear temperature-dependent and age-dependent components
- the potential for using sophisticated signal processing programs to work with signals far below normal levels

Before describing the optimisation techniques proposed, it is necessary to describe the GPS signal structure and the acquisition process in details, then to describe the radio frequency propagation channel in order to be able to better determine the problems and consider the possible solutions. This chapter focuses on describing the GPS signal classical acquisition principles and chapter III deals with the GPS channel and its constraints.

II.1 GPS overview

II.1.1 GPS basics

The NAVSTAR (*NAVigation Satellite Timing and Ranging*) GPS satellite radio-navigation system was first developed by the United States DoD (*Department of Defense*) to allow the military members [*Parkinson, 1996*] to accurately determine their 3D PVT (*Position, Velocity and Time* information) anytime, anywhere in the world. 10 years later, in 1983, it was decided to allow the civilian use of the GPS system. The Full Operational Capability of the GPS system for civilian use was announced in 1995 [*Kowoma, 2005*].

The GPS architecture is composed of three segments:

- **The space segment** contains the MEO (*Medium Earth Orbit*) satellite constellation which currently consists of 30 Block II/IIA/IIR/IIR-M satellites (at least 24 satellites are active at a time [*Kennedy, 2002*]). They are all arranged in six earth centred orbit planes. The nominal orbital period of a GPS satellite is equal to the duration of half a sidereal day (about 11 hours and 58 minutes). With no obstruction, up to 12 satellites may be visible at once [*Germroth et al., 2005*]. The satellite payload contains four atomic clocks, two based on Rubidium and two on Caesium, for a precise signal generation.
  The GPS satellites use today two carrier frequencies to broadcast users radionavigation signals: L_1 (1575.42 *MHz*) and L_2 (1227.6 *MHz*) carriers [*ICD200C, 2000*]. A third carrier frequency, L_5 (1176.45 *MHz*), will be mainly used for safety-of-life purposes such as ARNS (*Aeronautical Radio Navigation Services*) [*DoD, 95*]. But it is not expected to be fully operational before 2011. The satellite signals require a direct line to GPS receivers and can hardly, if not impossibly, penetrate water, soil, walls or other obstacles. Two kinds of codes are broadcast on the L_1 frequency: C/A (*Coarse Acquisition*) code and P (*Precision*) code. The C/A code is available to civilian GPS users and provides the SPS (*Standard Positioning Service*). It provides

the users with navigation accuracy less than $13\,m$ 95% of the time in the horizontal plane and less than $22\,m$ 95% of the time on the vertical axis [*Assistant Secretary of Defense, 2001*], after may 2000, when SA (*Selective Availability*) was removed following a decision made by President Clinton [*Clinton, 2000*]. The SA process was intended to prevent potential adversaries of the United States from using low-cost GPS receivers for certain military functions. The signal transmitted for civilian purposes is the result of a BPSK (*Binary Phase Shift Keyed*) modulation of the L_1 carrier frequency by data bits and C/A code chips. Each satellite is assigned a unique C/A code which is a PRN (*Pseudo Random Noise*) sequence. The P code is broadcast on both the L_1 and L_2 frequencies. The P code, used for the PPS (*Precise Positioning Service*) is only available to the United States government and its allied countries military users (France for example). It is further encrypted into a classified Y code and the two codes are referred to collectively as P(Y) code [*ICD200C, 2000*]. Using the P code on both frequencies, a military receiver can achieve better accuracy than civilian receivers. This thesis only deals with the L_1 carrier modulated by the C/A code, which is of primary commercial interest.
The data bits sent at $50\,Hz$ are summed with the code sequence using a DSSS (*Direct Sequence Spread Spectrum*) technique, providing CDMA (*Coded Division Multiple Access*) modulation schemes, to ensure the channel multiple-access [*Peterson et al., 1995], [Spilker, 1997*]. The message sent contains two important elements: the almanacs and the ephemeris data. The almanacs contain orbital data about the location of all the satellites in the constellation and time information. They are regularly updated from ground stations monitoring the constellation. The ephemeris data consist in short-lived data about the orbit of the particular satellite sending it and time information also. They are valid for four hours, and are transmitted every two hours. More details on the data navigation message can be found in appendix A.

- **The OCS (***Operational Control Segment***)** tracks the satellites in space, monitors the satellite health and signal integrity, and updates the clock corrections, ephemeris and almanac, and other parameters essential to determine user PVT. The U.S. DoD maintains an MCS (*Master Control Station*) at Falcon Air Force Base in Colorado Springs. There are four other monitor stations located in Hawaii, Ascension Island, Diego Garcia and Kwajalein.

- **The user segment** is composed of the user receiver equipment which performs the navigation, timing, surveying by processing the L-band signals transmitted from the satellites. One of the GPS system advantages is that the GPS receiver is passive, i.e. it does not need to send signals back to satellites: it depends exclusively on the received signal. Consequently, the number of GPS receivers can be unlimited, with the possibility for these receivers to be static or mobile. There are civilian applications for GPS in almost every field, from surveying to transportation, natural resource management, and agriculture.

The next section briefly describes the principle of triangulation used for GPS positioning.

II.1.2 Principle of GPS positioning

The ephemeris information transmitted by each satellite is necessary to determine the user position which is usually determined by measuring the propagation delay of at least four received GPS satellite signals. The calculated delays are proportional to the distance the signal travelled from the satellite (its range). These distances are called pseudo-ranges (not ranges) due to some residual clock errors between the receiver and the transmitting satellite. The travel time of GPS satellite signals can be altered by atmospheric effects: when a GPS signal passes through the ionosphere and troposphere it is refracted, causing the speed of the signal to be different from the speed of a GPS signal in space. Sunspot activity also causes interference with GPS signals. Other sources of error are distortion of the signal caused by electrical interference or errors inherent in the GPS receiver itself. Errors in the ephemeris data (the information about satellite orbits) also causes errors in computed positions. Small variations in the atomic clocks (clock drift) on board the satellites can translate to large position errors: a clock error of 1 nanosecond translates to 3 meters user error on the ground, for example. The receiver clock bias is also an important error source. This bias is however common to all received signals. In order to avoid time inaccuracies leading to such errors, this bias is considered as an additional unknown to the three dimensional position unknowns. This is why at least 4 satellite signals are needed to compute an accurate 3D position.

The position determination using calculated pseudo-ranges is called triangulation (figure II-1). The receiver generates a replica of the received signal code using its own clock. A classical receiver estimates the correlation function between the received signal and the computed C/A code replica by multiplying the incoming signal with this replica at different time lags over a $1\,ms$ interval (corresponding to one C/A code period) and summing (or integrating) the result. If the code samples do not line up with the signal from the satellite, the sum of multiplied signal will be close to zero. The lags that are close to the correct time offset will sum to larger values (because more of the bits in the code line up). Once the received satellite code and the replica code have both the same state, the receiver is able to determine the phase shift of the local signal with respect to the received signal, and then deduce the exact propagation delay: this state corresponds to the maximum of the correlation function. The signal processing will be detailed in the next section.

For each measurement, the receiver can be positioned on a sphere centred on the signal emitting satellite and having as radius the measured satellite-to-user pseudo-range plus or minus the satellite to user clock bias. The position can then be determined as the intersection of at least three spheres, as illustrated in figure II-1 below. A fourth measurement enables to solve for the time information, as already explained.

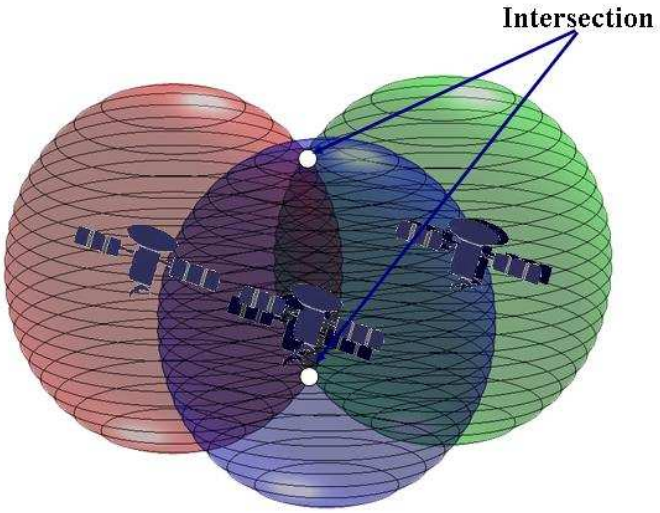

Fig II-1: The triangulation method for determining the user position

The earth shape is not a perfect sphere and the surface model must represent an appropriate model which is an approximation for the earth's surface. The satellites positions are computed by the user from the broadcast ephemeris data in the reference frame called WGS84 (*World Geodetic Reference* 84) [*Kaplan, 1996*]. Thus the user position is nominally expressed in the WGS84.

II.2 The GPS signal structure

In this section, the GPS transmitted and received signal structures and spectral characteristics are described.

II.2.1 The GPS transmitted signal

The GPS L_1 signal generation is described in the following block diagram (figure II-2):

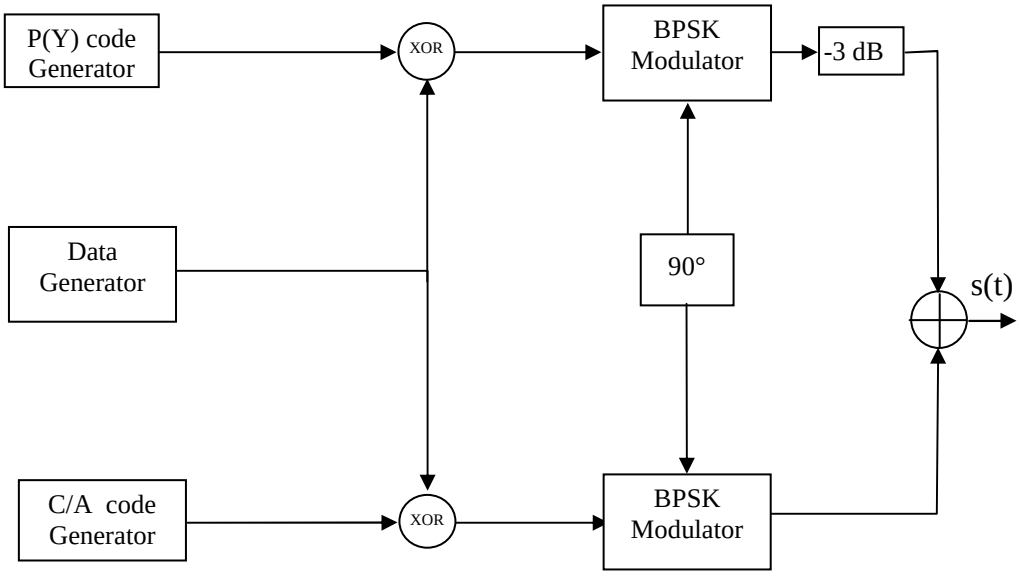

Fig II-2: GPS L_1 carrier modulation

The P(Y) code has a chipping rate of 10.23 *M*chips/*s* whereas the C/A code is at 1.023 *M*chips/*s*. The data has a bit rate of 50 bps. In order to generate the L_1 signal, the data bits are first combined with the P(Y) code and the C/A code, respectively using a XOR (*eXclusive OR*) process. The resulting signal is used to modulate the L_1 carrier at 1575.42 *MHz* using a QPSK (*Quadrature Phase Shift Keying*) scheme: a BPSK (*Binary Phase Shift Keying*) scheme is used for each code. The C/A code modulates the inphase component of the L_1 signal, while the quadrature phase component is modulated by the P(Y) code. The long and secure P(Y) code has a period of seven days, while the Gold code C/A code has a 1ms period.

The satellite payload is designed such that all clock signals are derived from only one reference clock.

The signal of satellite *i* transmitted on the L_1 carrier can be expressed as:

$$s^i(t) = A \cdot d^i(t) \cdot c^i(t) \cdot \cos(2\pi L_1 t) + A/\sqrt{2} \cdot d^i(t) \cdot p^i(t) \cdot \sin(2\pi L_1 t) \quad \textbf{(II-1)}$$

where s^i, is the signal transmitted by satellite *i,*

A, is the signal amplitude,

d^i, is the data message to be sent by satellite *i,* $d^i(t) = \left[\sum_{k=-\infty}^{+\infty} d^i(k) \cdot \delta(t - kT_D) \right] * rect\left[\frac{t - T_D/2}{T_D} \right]$, $d^i(k) \in \{1,-1\}$, with T_D the data bit duration (20*ms*),

c^i, is the C/A code of satellite *i,* $c^i(t) = \left[\sum_{k=-\infty}^{+\infty} c^i(k) \cdot rect\left(\frac{t - T_c/2 - kT_c}{T_c} \right) \right]$, $c(k) \in \{1,-1\}$, with T_c the PRN code chip duration ($T_c = \frac{1}{f_c}$ with $f_c = 1.023\,MHz$ the C/A code rate),

p^i, is the P(Y) code of satellite *i,* $p^i(t) = \left[\sum_{k=-\infty}^{+\infty} p^i(k) \cdot rect\left(\frac{t - T_p/2 - kT_p}{T_p} \right) \right]$, $p(k) \in \{1,-1\}$, with T_p the PRN code chip duration, and,

L_1, is the carrier frequency of 1575.42 *MHz* .

The $1/\sqrt{2}$ coefficient in front of the P(Y) signal refers to the –3 *dB* gain applied by the transmitter to the P(Y) code signal. The spreading factor is given by the ratio T_c/T_D. In practice, T_D is chosen to be a multiple of the temporal repetition period of the PRN sequence; $T_D = nLT_c$, where L is a one spreading code period length in chips. In the case of the C/A code of length L=1023 chips per period, n is set to 20.

The data and the codes are synchronised with each other, such that the data bit transitions occur at code chip transitions.

Since this thesis only deals with civil applications, thus only the C/A component of the GPS L_1 signal will be considered in what follows, that is:

$s(t) = A \cdot d(t) \cdot c(t) \cdot \cos(2\pi L_1 t)$ (for a given satellite)

The PSD (*Power Spectral Density*) of the resulting transmitted signal can be computed by first calculating its autocorrelation function, assuming that the three signal components are independent (data, C/A code and carrier):

$$R_s(\tau) = R_d(\tau) \cdot R_c(\tau) \cdot R_{s_a}(\tau) \quad \textbf{(II-2)}$$

where $R_d(\tau)$ is the autocorrelation function of the data signal, $d(t)$

$R_c(\tau)$ is the autocorrelation function of the materialised PRN code signal, $c(t)$

$R_{sa}(\tau)$ is the autocorrelation function of the signal $s_a(t) = A\cos(2\pi L_1 t)$

Then, assuming the three signals to be independent, and according to the Wiener-Kintchine theorem, the PSD of $s(t)$ is given as:

$$S_s(f) = S_d(f) * S_c(f) * S_{s_a}(f) \quad \textbf{(II-3)}$$

Where $S_{s_a}(f) = \frac{A^2}{4}\left[\delta(f - L_1) + \delta(-f - L_1)\right]$, the PSD of the carrier s_a

$S_d(f) = T_D \cdot \sin_c^2(\pi f T_D)$, the PSD of the data $d(t)$

$S_c(f) = \frac{1}{LT_c} \sum_{j=-\infty}^{\infty} |C(j)|^2 \left| M\left(\frac{j}{LT_c}\right) \right|^2 \delta\left(f - \frac{j}{LT_c}\right)$, the PSD of the code $c(t)$ as derived in [*Macabiau, 2001*], with $C(f)$ the C/A Discrete Fourier Transform over its period, and $M(f)$ the Fourier Transform of the C/A code materialization function $m(t)$.

The shape of the signal spectrum $S_s(f)$ is illustrated below.

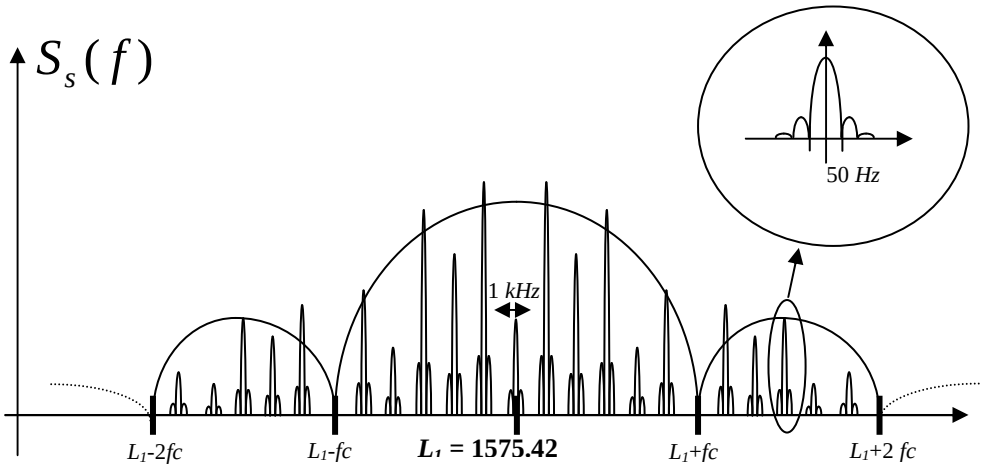

Fig II-3 : PSD of the GPS L_1 transmitted signal

The energy of the signal is centered on the L_1 carrier, and the spectrum is spread mainly in the main lobe over a bandwidth of about 2 *MHz* (corresponding to the C/A spreading code main lobe bandwidth) [*Watson, 2005*].

$s(t)$ travels through the atmosphere, over a distance of approximately 20,000 *km*. This distance is long enough to cause a non negligible loss of the signal power. At reception, the nominal signal power is of –160 *dBW* approximately [*MacGougan, 2003*], but most GPS satellites emit signals at 3 to 7 *dB* higher than the specified minimum with an average power level typically 5.4 *dB* above the minimum [*Spilker, 1996*], and a typical C/N_0 ratio of about 45 *dBHz* (for more details on the GPS link budget see appendix B).

After having described the structure of the transmitted GPS signal, the next section describes the received signal structure and characteristics.

II.2.2 The GPS received signal structure

Many signals are present at the receiver antenna:

- the main signal, which has experienced delays, phase shifts and possibly power losses;
- different delayed versions of this signal due to multipath;
- signals from other satellites and their respective reflected versions;
- noise;
- interference…..

The received signal may be expressed as:

$$r(t) = \left\{ \sum_{i=1}^{N} \sum_{k=0}^{M^i-1} A_k^i \cdot d^i\left(t-\tau_k^i\right) \cdot c^i\left(t-t_k\right) \cos\left(2\pi L_1 t - \theta_k^i\right) \right\} + j(t) + n(t) \qquad \textbf{(II-4)}$$

where N is the number of satellite signals reaching the receiver. N is lower or equal to the number of visible satellites.

M^i is the number of the multipath replicas of the i^{th} satellite,

τ_k^i is the delay experienced by the k^{th} multipath replica of the i^{th} satellite,

θ_k^i is the carrier phase shift experienced by the k^{th} multipath replica of the i^{th} satellite,

$j(t)$ represents possible interference (from other radio signals), and,

$n(t)$ is the channel additive noise.

In what follows, $j(t)$ is not taken into consideration (for more details about the impact of other radio frequencies interference on the GPS signal, refer to [*Deshpande et al., 2004b*]).

The other sources of interference are discussed in details in Chapter III. The next section focuses on the acquisition process.

II.3 GPS Signal Acquisition

Acquisition is a coarse synchronization process giving estimates of the C/A code offset and the carrier Doppler frequency. It must ensure that the signal is acquired at the correct code phase and carrier frequency. Among other minor effects, the code offset is mainly due to the satellite-receiver clock offset with respect to the system time and the position of the receiver with respect to that of the satellites; the carrier Doppler is mainly due to the satellites and the receiver dynamics, and the frequency drift of the receiver local oscillator.

As mentioned previously, prior to determining the code delay and the carrier phase, a search for the PRN code to be used may be necessary: in fact in the case of a cold start, that is when the receiver has been shut down for a few hours, it must start by searching for the visible satellites; thus it determines the C/A codes to be used for despreading, and then tries to estimate each code delay and carrier phase offset.

The GPS signal two-dimensional search acquisition process is conducted in an uncertainty region defined by the windows width of the code delay and the carrier Doppler uncertainty to be explored. The correct alignment is identified by the measurement of the output power of the correlators. The result of this two dimensional search is an estimate of the code Offset to within half a chip and of the carrier Doppler to within half the Doppler search bin size (several Hz to several hundreds of Hz).

II.3.1 Fundamental acquisition scheme

At the receiver level, the radio frequency signal is acquired according to the block diagram illustrated in figure II-4 below, where T_s is the sampling period, and $\hat{\theta}$ and $\hat{\tau}$ are respectively the estimated values of the carrier phase and the code delay shift:

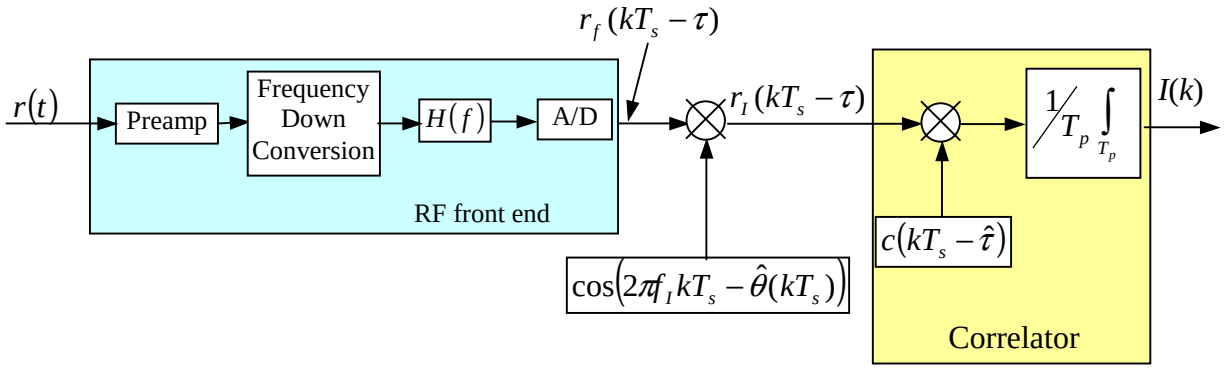

Fig II-4 : GPS received signal demodulation block diagram

The GPS signal processing is discussed in details in [*Ward, 1996*] and [*van Dierendonck, 1996*]. In the block diagram of figure II-4, the channel was supposed to act as a pure delay filter with impulse response $\delta(t-\tau)$ for illustration purposes.

Hence, the received signal may be modelled as:
$r(t) = s(t-\tau) + n(t) = Ad(t-\tau)c(t-\tau)\cos(2\pi L_1 t - \theta) + n(t)$,
where $n(t)$ is an AWGN (*Additive White Gaussian Noise*) noise, $\theta(t) = 2\pi L_1 \tau - \varphi_0$ is the carrier phase, with φ_0 and θ_0 random initial phases. Thus the carrier instantaneous phase is given as:
$\varphi(t) = 2\pi L_1 t - 2\pi L_1 \tau + \varphi_0$

The corresponding instantaneous frequency is defined as the derivative of the instantaneous phase:
$$f_{inst} = \frac{1}{2\pi}\frac{d\varphi(t)}{dt} = L_1 - L_1\frac{d\tau}{dt}$$

The group delay is a function of the distance *d* traveled by the signal between the satellite and the receiver: $\tau = \frac{d}{c}$. This distance *d* is variable with time due to the satellite-to-receiver relative motion and the earth's rotation. Assuming that *d* has linear variations with time (this is true for a relatively short time interval of a few seconds), that is $d = v_d t + d_0$, with d_0 the initial distance between the satellite and the receiver, this gives for the instantaneous frequency:
$$f_{inst} = L_1 - L_1\frac{v_d}{c}$$

The carrier Doppler shift defined as $f_d = L_1 - f_{inst}$ becomes: $f_d = -L_1\frac{v_d}{c}$, which finally leads to: $\theta(t) = 2\pi L_1 \tau - \varphi_0 = -2\pi f_d t + \theta_0$.

The signal is first preamplified in order to set the overall gain and the noise figure of the receiver. Next, it is filtered and down-converted to an IF (*Intermediate Frequency*) which is specific to each receiver. An anti-aliasing front-end filter is then used. It is assumed to have a double-sided bandwidth *B*. Its bandwidth determines the amount of C/A code information, but also of thermal noise introduced into the GPS correlator. A larger bandwidth allows more C/A code signal information along with more noise in the acquisition process. In general a compromise is made on the font-end filter bandwidth. The GPS signal is then digitised using an A/D (*Analog to Digital*) converter, with a sampling rate adapted to the filtering characteristics and the sampling scheme (at least $2.046 MHz$). At the output of the RF front end, the signal is modelled as:

$$\begin{aligned} r_f(kT_s - \tau) &= A \cdot d(kT_s - \tau) \cdot c_f(kT_s - \tau) \cdot \cos(2\pi f_I kT_s - \theta(kT_s)) + n_f(kT_s) \\ &= s_f(kT_s - \tau) + n_f(kT_s) \end{aligned} \quad \textbf{(II-5)}$$

where $c_f(kT_s - \tau)$ is the filtered C/A code

$n_f(kT_s)$ is the filtered WGN with a PSD of $S_{n_f}(f) = |H_{FE}(f)|^2 S_n(f) = \frac{N_0}{2}|H_{FE}(f)|^2\ dBW \cdot Hz^{-1}$. N_0 is of the order of $-200\ dBHz$ to $-204\ dBHz$ (see appendix B for more details on GPS link budget).

The useful signal PSD is given as :

$S_{s_f}(f) = |H_{FE}(f)|^2 S_s(f)$

with $S_s(f)$ derived previously in equation II-3: $S_s(f) = S_d(f) * S_c(f) * S_{s_a}(f)$

And the global PSD module of $s_f(kT_e - \tau)$ looks like:

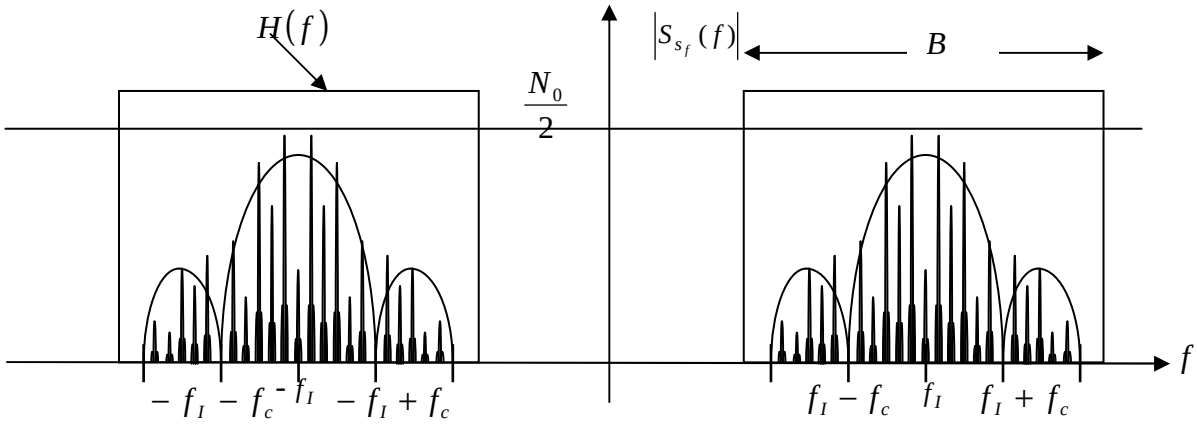

Fig II-5 : The PSD of the signal at the output of the selective filter

The SNR (*Signal to Noise Ratio*) at the output of the receiver selective filter is:

$$SNR_{pre} = \frac{P_{s_f}}{P_{n_f}} = \frac{2\int_{-\infty}^{+\infty} |H_{FE}(f)|^2 \cdot S_s(f) \cdot df}{N_0 B}$$

with P_s the incoming filtered signal power and P_{n_f} the filtered noise power.

According to the Wiener-Kintchine theorem, $SNR_{pre} = \frac{2\int_{-\infty}^{+\infty} |H_{FE}(f)|^2 \cdot S_s(f) \cdot df}{N_0 B} = \frac{2R_{s_f}(0)}{N_0 B}$,

with $R_{s_f}(0) = \frac{A^2}{2} R_{c_f c}(0)$. This gives for the final expression of the SNR at the output of the front end filter:

$$SNR_{pre} = \frac{A^2 R_{c_f c}(0)}{N_0 B} = \frac{A^2 R_{c_f c}(0)}{N_0 B} \qquad \textbf{(II-6)}$$

The impact of the front-end filter Bandwidth on the signal is not studied in this thesis. Indeed, it was shown by van Dierendonck [*1996*], and confirmed by Olivier Julien [*Julien, 2005*] that the front end filter does not have a large impact on the overall receiver resistance to noise. For a Front End filter that would just filter the main lobe of the C/A code ($\cong 2$ *MHz*), the signal power loss would be equal to approximately 0.45 *dB*. And with larger filter bandwidth the power loss approaches 0 *dB*.

The signal code despreading is carried out at this stage. First, the signal is translated back to base band by multiplying it with a replica of the last IF carrier using an estimation of

the Doppler frequency. Next, the signal is multiplied by a replica of the spreading code with code delay estimation.

The signal at the input of the correlator (after base band translation) is:

$$\begin{aligned} r_I(kT_s-\tau) &= r_f(kT_s-\tau)\cdot\cos\left[2\pi\left(f_I+\hat{f}_d\right)kT_s-\hat{\theta}_0\right] \\ &= A\cdot d(kT_s-\tau)c_f(kT_s-\tau)\cos\left[2\pi(f_I+f_d)kT_s-\theta_0\right]\cos\left[2\pi\left(f_I+\hat{f}_d\right)kT_s-\hat{\theta}_0\right] \\ &\quad + n_f(kT_s)\cos\left[2\pi\left(f_I+\hat{f}_d\right)kT_s-\hat{\theta}_0\right] \end{aligned}$$

The double frequency is eliminated by the integrator which acts a low pass filter. The above expression becomes

$$\begin{aligned} r_I(kT_s-\tau) &= \frac{A}{2}d(kT_s-\tau)c_f(kT_s-\tau)\cos\left[2\pi\left(f_d-\hat{f}_d\right)kT_s-\left(\theta_0-\hat{\theta}_0\right)\right] \\ &\quad + n_f(kT_s)\cos\left[2\pi\left(f_I+\hat{f}_d\right)kT_s-\hat{\theta}_0\right] \end{aligned} \quad \textbf{(II-7)}$$

That gives:

$$\begin{aligned} r_I(kT_s-\tau)\cdot c(kT_s-\hat{\tau}) &= \frac{A}{2}d(kT_s-\tau)\cdot c_f(kT_s-\tau)\cdot c(kT_s-\hat{\tau})\cdot\cos\left[2\pi\left(f_d-\hat{f}_d\right)kT_s-\left(\theta_0-\hat{\theta}_0\right)\right] \\ &\quad + n_f(kT_s)\cos\left[2\pi\left(f_I+\hat{f}_d\right)kT_s-\hat{\theta}_0\right]\cdot c(kT_s-\hat{\tau}) \end{aligned} \quad \textbf{(II-8)}$$

In what follows, the symbol *k* will be used instead of kT_s to refer to the k^{th} sample of the signal.

The next step is the averaging process, which is equivalent to low pass filtering the signal, with a bandwidth that is inversely proportional to the averaging duration, T_p. This low pass filtering may be modeled as:

$$h_{CI}(t)=\frac{1}{T_p}rect\left(\frac{t-T_p/2}{T_p}\right)$$

Setting $n_I(k)=n_f(k)\cos\left[2\pi\left(f_I+\hat{f}_d\right)kT_s-\hat{\theta}_0\right]\cdot c(kT_s-\hat{\tau})*h_{CI}(t)$, the signal at the output of the correlator becomes [*Holmes, 2000*]:

$$I(k)=\frac{A}{2}\cdot d(k)\cdot\frac{\sin(\pi\Delta f_{DOP}T_p)}{\pi\Delta f_{DOP}T_p}\cdot R_{c_fc}[\tau(k)-\hat{\tau}(k)]\cdot\cos\left[\theta(k)-\hat{\theta}(k)\right]+n_I(k) \quad \textbf{(II-9)}$$

with $I(k)$ is the inphase component of the signal,
n_I is a centred Gaussian noise,
R_{c_fc} is the cross-correlation between the received filtered spreading code (which has been filtered by the RF front-end filter) and the local replica code,
$\hat{\tau}$ is an estimation of the group propagation delay,
$\hat{\theta}$ is an estimation of the carrier phase shift,

Δf_{DOP} is the Doppler frequency estimated error between the received and the local carriers, $\Delta f_{DOP} = f_d - \hat{f}_d$,

T_p is the coherent integration time and $f_p = \frac{1}{T_p}$.

If $\hat{\tau}$, $\hat{f}_d$ and $\hat{\theta}$ are accurately estimated, $I(k)$ becomes:

$$I(k) = \frac{A}{2} \cdot d(k) + n_I(k) \quad \textbf{(II-10)}$$

The decision on the symbol value can be made by sampling at the end of the integration period, and it greatly depends on the noise power at this instant. The noise power at the output of correlator is derived hereafter:

Recall that $n_I(k) = n_f(k)\cos\left[2\pi\left(f_I + \hat{f}_d\right)kT_s - \hat{\theta}_0\right] \cdot c(kT_s - \hat{\tau}) * h_{CI}(t)$.

Let us denote $n_{\text{int}} = n_f(k)\cos\left[2\pi\left(f_I + \hat{f}_d\right)kT_s - \hat{\theta}_0\right] \cdot c(kT_s - \hat{\tau})$. Then according to the Wiener-Lee theorem, the noise PSD is given as:

$$S_{n_I}(f) = S_{n_{\text{int}}}(f) \cdot |H_{CI}(f)|^2$$

In order to compute $S_{n_{\text{int}}}(f)$, we first calculate its autocorrelation function, assuming that all of its components (the filtered noise, the C/A code and the cosine term) are independent:

$$R_{n_{\text{int}}}(\Delta k) = E\left[\begin{array}{l} n_f(k)\cos\left[2\pi\left(f_I + \hat{f}_d\right)kT_s - \hat{\theta}_0\right] \cdot c(kT_s - \hat{\tau}) \\ \cdot\, n_f(k + \Delta k)\cos\left[2\pi\left(f_I + \hat{f}_d\right)(k + \Delta k)T_s - \hat{\theta}_0\right] \cdot c((k + \Delta k)T_s - \hat{\tau}) \end{array}\right]$$

$$R_{n_{\text{int}}}(\Delta k) = \frac{1}{2} R_{n_f}(\Delta k) \cdot R_c(\Delta k) \cdot \cos\left(2\pi\left(f_I + \hat{f}_d\right)\Delta k T_s\right)$$

This gives the PSD of n_{int} as:

$$S_{n_{\text{int}}}(f) = \frac{1}{4} S_{n_f}(f) * S_c(f) * \left[\delta\left(f + f_I + \hat{f}_d\right) + \delta\left(f - f_I - \hat{f}_d\right)\right]$$

Assuming a bandpass front end filter, centred around f_I, we have:

$$S_{n_f}(f) = \frac{N_0}{2}|H_{FE}(f)|^2 * \left[\delta(f + f_I) + \delta(f - f_I)\right] \quad \textbf{(II-11)}$$

Consequently, $S_{n_{\text{int}}}(f) = \frac{N_0}{4}|H_{FE}(f)|^2 * S_c(f) * \left[\delta\left(f + \hat{f}_d\right) + \delta\left(f - \hat{f}_d\right)\right]$

Note however, that the bandwidth *B* (>2 *MHz*) of the signal n_{int} is very large compared to $\hat{f}_d$ (of the order of a few *kHz*). This leads to:

$$S_{n_{\text{int}}}(f) \cong \frac{N_0}{4}|H_{FE}(f)|^2 * S_c(f)$$

Thus, the noise PSD after integration is:

$$S_{n_I}(f) = S_{n_{\text{int}}}(f) \cdot |H_{CI}(f)|^2 = \frac{N_0}{4}|H_{FE}(f)|^2 * S_c(f) \cdot |H_{CI}(f)|^2$$

The coherent integration low pass filtering, $H_{CI}(f) = e^{-i\pi f T_p} \cdot \frac{\sin(\pi f T_p)}{\pi f T_p}$, has a narrow bandwidth ($1/T_p$) compared to that of the selective filter, *B*. In other words, $S_{n_{\text{int}}}(f)$ may be considered as constant over the integrator bandwidth, which gives: $S_{n_I}(f) = S_{n_{\text{int}}}(0) \cdot |H_{CI}(f)|^2 = \frac{N_0}{4} \int_{-\infty}^{+\infty} |H_{FE}(f_1)|^2 \cdot S_c(f_1) df_1 \cdot |H_{CI}(f)|^2$.

And finally, the noise power is given as:

$$P_{n_I} = \frac{N_0}{4} \int_{-\infty}^{+\infty} \int_{-\infty}^{+\infty} |H_{FE}(f_1)|^2 \cdot S_c(f_1) df_1 \cdot |H_{CI}(f)|^2 \cdot df = \frac{N_0}{4} \int_{-\infty}^{+\infty} |H_{FE}(f_1)|^2 \cdot S_c(f_1) df_1 \int_{-\infty}^{+\infty} |H_{CI}(f)|^2 \cdot df$$

$$P_{n_I} = \frac{N_0}{4T_p} \int_{-\infty}^{+\infty} |H_{FE}(f)|^2 \cdot S_c(f) df$$

In the case of a rectangular front end filter, the noise power becomes:

$$P_{n_I} \cong \frac{N_0}{4T_p} \quad \textbf{(II-12)}$$

Obviously, the expression of the noise power shows that the greater the integration duration T_p, the lower the noise power and the higher the resulting SNR.

The useful signal power is (assuming no Doppler, code delay or phase errors): $P_I = \frac{A^2}{4} R_{c_f c}^2(0)$,

The resulting signal noise ratio at the output of the correlator taken on the *I* component is:

$$SNR_{post} = \frac{A^2 T_p R_{c_f c}^2(0)}{N_0} \quad \textbf{(II-13)}$$

This is the expression of the SNR after correlation assuming no Doppler, phase or code delay errors.

Reconsidering equation II-9, it can be noticed that the correlation output is weighted by three factors:

- $\frac{\sin(\pi \Delta f_{DOP} T_p)}{\pi \Delta f_{DOP} T_p}$ due to the Doppler estimation error,
- $R_{c_f c}(\tau(k) - \hat{\tau}(k))$ due to the code delay estimation error,
- $\cos(\theta(k) - \hat{\theta}(k))$ due to the phase estimation error.

The reduction in the correlation maximum resulting from the cosine term, $\cos(\theta(k) - \hat{\theta}(k))$, can be avoided by taking into consideration the quadrature component of the signal obtained by multiplying the signal by $\sin(2\pi f_I k T_s - \hat{\theta}(k))$. Squaring the signals on the two correlation channels, the inphase and the quadrature channels, and then adding the result, thus allows to remove this reducing factor. This is why in general the two signal components are used in the acquisition schemes. The complete acquisition scheme becomes:

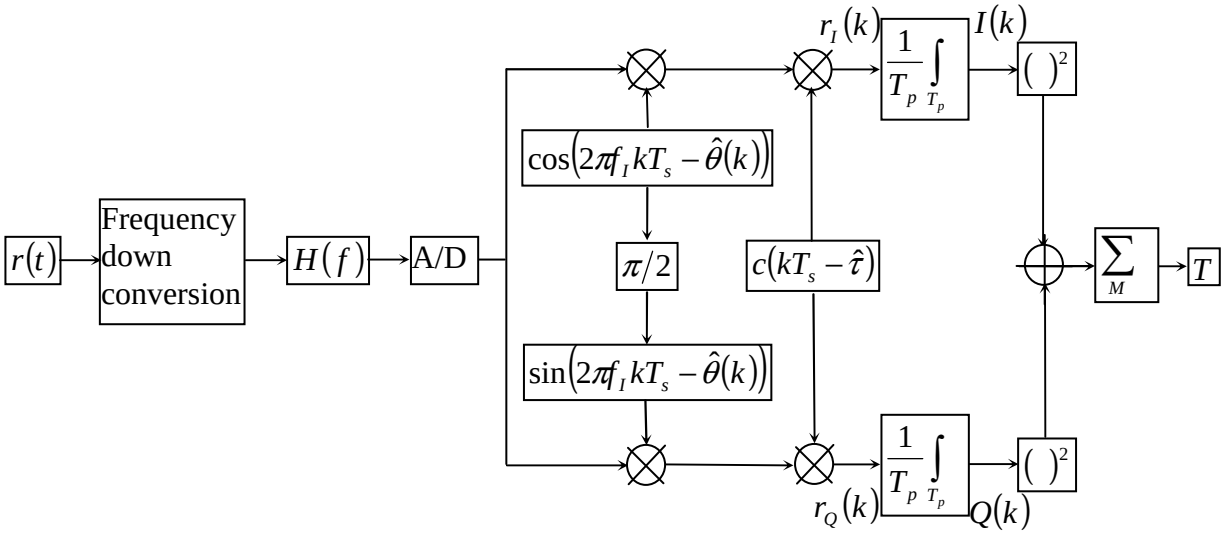

Fig II-6 : The complete block diagram of the acquisition process

Averaging the inphase and the quadrature components respectively, before squaring them, is called coherent integration. This reduces the impact of noise on the signal as explained above.

The whole process can be repeated *M* times and the squared coherently integrated components are respectively summed in order to further reduce the impact of noise. This is called non-coherent integration.

The final detection criterion can be expressed as:

$$T = \sum_{k=1}^{M} \left(I^2(k) + Q^2(k) \right) \qquad \textbf{(II-14)}$$

with M the number of non-coherent integrations

$$I(k) = \frac{A}{2} \cdot d(k) \cdot \frac{\sin(\pi \Delta f_{DOP} T_p)}{\pi \Delta f_{DOP} T_p} \cdot R_{c_f c}\left(\tau(k) - \hat{\tau}(k)\right) \cdot \cos\left(\theta(k) - \hat{\theta}(k)\right) + n_I(k)$$

$$Q(k) = \frac{A}{2} \cdot d(k). \frac{\sin(\pi \Delta f_{DOP} T_p)}{\pi \Delta f_{DOP} T_p} \cdot R_{c_f c}\left(\tau(k) - \hat{\tau}(k)\right) \cdot \sin\left(\theta(k) - \hat{\theta}(k)\right) + n_Q(k)$$

$A^2/2$ is the total (I+Q) components signal power at the output of the receiver antenna

n_I and n_Q are respectively the inphase and quadrature components of the correlator output noise. They are centered WGN components,

After describing the fundamentals of GPS acquisition, some key parameters of the acquisition stage - namely the definition of the search space, the detection criterion and the coherent and non-coherent integration times are detailed in the subsequent sections.

II.3.2 The search space

The first step to be done prior to beginning the acquisition process is to set the boundaries for the search space, or uncertainty region. This region must cover the full range of uncertainty in the code and the Doppler offset, assuming that the PRN code to be used is known. Figure II-7 below illustrates the acquisition uncertainty region:

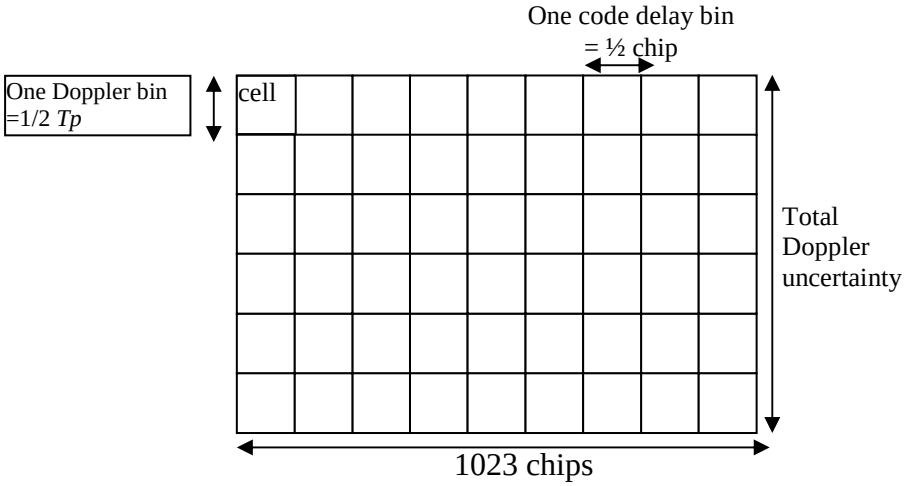

Fig II-7 : The acquisition uncertainty region

II.3.2.1 The code delay range and uncertainty

The period of the C/A code being fairly short, 1 *ms* (1023 chips), typically, the search range includes all possible code offset values. The tracking process requires a minimum precision of half a chip on the code delay; this is why usually ½ chip increments are considered. Assuming an ideal normalized code autocorrelation function, if the code search cell width is half a chip, the maximum code uncertainty ε_τ is a quarter of a chip, which corresponds to $\varepsilon_\tau = \pm 0.25\,\text{chip}$ (figure II-8). This implies a worst case degradation of $20 \cdot \log_{10}(1-0.25) = -2.498 \cong -2.5\ dB$ in the useful signal power at the correlator output.

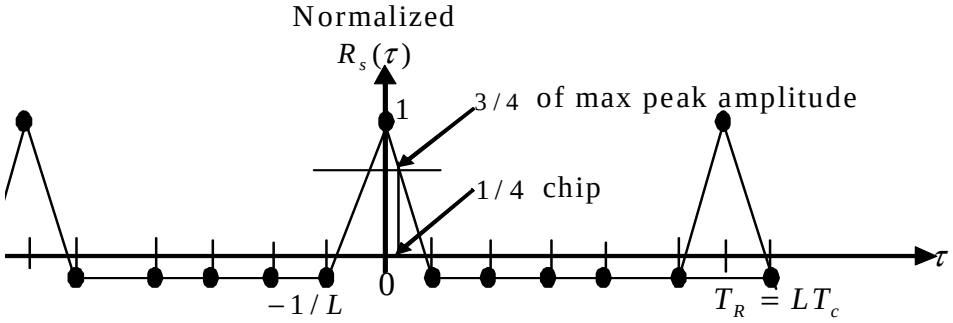

Fig II-8: Degradation of the C/A code autocorrelation function (normalized) for a code phase uncertainty of ¼ chip

II.3.2.2 The Doppler offset range and uncertainty

The range of the Doppler uncertainty is governed by the vehicle and GPS satellite dynamics and the stability of the receiver oscillator. Consequently, the maximum user velocity plus the maximum satellite radial velocity for a stationary user must be considered.

Recall that $f_d = -L_1 \frac{v_d}{c}$. The maximum satellite radial velocity is $v_{d\max} \cong 929\,m/s \cong 2078\,miles/h$ [*Kaplan, 1996*] (see appendix C).

The corresponding maximum Doppler frequency shift (absolute value) for the L_1 frequency is then:

$$f_d = \frac{L_1 v_{d\max}}{c} = \frac{1575.42 \times 929}{3 \times 10^8} \cong 4.9\ kHz$$

When considering the local oscillator drift, approximately $\pm 1\ kHz$ uncertainty must be added to this value to get f_d (depending on the receiver clock oscillator performance measured in *ppm* where 1ppm induces an error of $10^{-6} \times 1.57542 \times 10^9 = 1.57542 \times 10^3\ Hz$). The user motion also affects the Doppler shift. If the user is moving towards the satellite, the overall received frequency is increased. Otherwise, it is reduced. The user motion must thus be considered for users travelling at high speeds (cars, planes, …).

In short, for a terrestrial user with a 1 *ppm* clock, a minimum Doppler range of $\pm 6\ kHz$ must be searched.

The frequency resolution depends on the coherent integration time T_p, and the acceptable frequency degradation at the output of the correlator. As it was stated previously, the Doppler frequency uncertainty affects the correlator output through the scaling factor $\frac{\sin(\pi \Delta f_{DOP} T_p)}{\pi \Delta f_{DOP} T_p}$ (refer to equation II-9). This factor has a direct impact on the correlator output amplitude, and then on the detected power. The shape of the function $\left[\frac{\sin(\pi \Delta f_{DOP} T_p)}{\pi \Delta f_{DOP} T_p}\right]^2$ is illustrated in figure II-9 below:

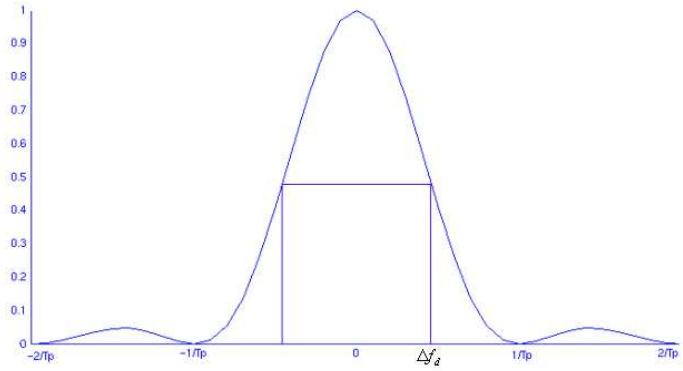

Fig II-9 : The signal attenuation due to a Doppler frequency error

For a worst case signal power degradation of 1 *dB* due to Doppler frequency, a frequency bin of approximately $\Delta f_{DOP} = 1/2T_p$ must be considered. Indeed, in this case, where the cell width is half the predetection bandwidth, the worst uncertainty is a quarter of this bandwidth ($\Delta f_{DOP} = T_p/4$), and the corresponding frequency degradation is of $20 \cdot \log_{10} \sin_c(\pi \times 0.25) = -0.91 \cong 1\ dB$. The coherent integration time T_p varies from $1\ ms$ ($500\ Hz$ Doppler bins), for strong signals, up to 20 *ms* (25 *Hz* Doppler bins), for weak signals. This means that T_p is based on the expected C/N_0 ratio. The poorer this expected C/N_0, the longer the coherent time must be in order to successfully acquire the signal. Longer integration times may be considered; the coherent integration time limits will be discussed in details in the next section.

In conclusion, the total worst case degradation resulting from code phase and frequency uncertainty is $\cong -3.5\ dB$.

II.3.3 Maximum length of coherent or non-coherent integration times

Increasing the coherent integration time T_p during the acquisition process, improves the SNR ratio at correlator output, because the correlator output noise power, $\sigma_n^2 = \frac{N_0}{4T_p}\int_{-\infty}^{+\infty}\left|H_{FE}(f)\right|^2 \cdot S_c(f)\cdot df$ (appendix C), is inversely proportional to this time, and will be lowered. However, this involves more calculations and hence, is time consuming. The time consumption does not increase linearly with T_p since a higher T_p implies simultaneously an increased number of data points to be processed, and an increased number of frequency cells to be searched as the frequency bin size is of $\Delta f_{DOP} = \frac{1}{2\cdot T_p}$, as was shown earlier. These are not however the only limits to increasing coherent integration length. Amongst other parameters, the local oscillator drift, a possible data bit transition and the Doppler effect on the C/A code also set limits to T_p.

The local oscillator drift results in an additional Doppler which depends on the oscillator clock precision, and varies from one receiver to another. This parameter generally limits the data length processed coherently to a few hundreds of milliseconds [*Kaplan, 1996*]. This limitation is not very dramatic for the acquisition process where the coherent integration time rarely reaches or exceeds this limit.

Obviously, the probability that a data bit transition occurs during coherent integration increases with the coherent integration time T_p. A transition causes a reduction of the detected energy. This will degrade the acquisition result. Since the navigation data is $20\ ms$ or 20 C/A code periods long, the maximum data record free of data bit transitions that can be used for coherent integration is $20\ ms$. On the other hand, since the C/A code has a period of $1\ ms$, generally, the acquisition is performed on at least $1\ ms$ of data in order to avoid correlation losses.

The other limit of the data length for coherent integration rises from the Doppler effect on the C/A code, when no Doppler compensation is used. If the maximum C/A code shift allowed is ½ chip, in the worst code Doppler shift case, i.e. $3.2\ Hz$ (refer to appendix C equation C-1), it takes about $156\ ms$ (½ x1/3.2) before a ½ chip shift occurs. Therefore, this is not a very constraining limit compared to that imposed by the data bit transitions every $20\ ms$.

Note however, that in weak signal conditions, higher integration times may be needed. In this case, either aiding information about data bits transitions is needed or non-coherent accumulations can be used. For a non-coherent integration, there are no limits on the data record length other than the acquisition time. This parameter is important to be shortened for real time applications.

Non-coherent detection is particularly interesting when the phase of the received signal is random, i.e., very difficult to be predicted. The non-coherent detection is insensitive

to phase errors since these errors are the same for the inphase and quadrature components of the incoming signal. In the case of a non-coherent detection, these latters are first squared and then added together thus eliminating the effect of phase error. This is generally the case in the acquisition stage of the GPS signal processing. Nonetheless, the non-coherent gain is lower than the coherent gain since the latter implies squaring losses not induced by the coherent gain, as it will be derived in the next paragraph (equations II-17 to II-20).

II.3.4 The detection criterion

In the presence of noise, a threshold is set, and the search process is applied until this threshold is reached. Any cell envelope that is at or above the threshold is detected as the possible presence of the signal. Any cell envelope that is below the threshold is detected as noise. In weak signal conditions, in order to provide a solution in any case, a simple correlation maximum search may be applied if the PRN code is already known (in the case of the AGPS for example) and a solution is provided. The reliability of this solution is then verified using algorithms, like RAIM, for instance. The cell envelope detection is done through a measurement of the correlator output (equation II-14):

$$T = \sum_{k=1}^{M} \left(I^2(k) + Q^2(k) \right)$$

If the input and local signals are aligned, the amplitude of the recovered signal at the correlator output is maximum. This amplitude is compared to the predefined threshold. The detection of the signal is thus a statistical process based on a two hypothesis test:

- hypothesis H_0: the useful signal is not present, and the considered cell contains only noise.
- hypothesis H_1: the considered cell contains noise with signal present.

The threshold is usually based on an acceptable probability that a noisy measurement which does not contain the signal will appear to match the replica. This is called the PFA (*Probability of False Alarm*).

When hypothesis H_0 is verified, i.e. if no signal is present, the criterion, or in other words the expression of the test statistics, is:

$$T_0 = \sum_{n=1}^{M} \left[n_I^2(k) + n_Q^2(k) \right]$$

n_I and n_Q are assumed to have a normal distribution $N(0, \sigma_n^2)$ [*Macabiau, 2001*] and [*O'Driscoll, 2006*]. They can be written as: $\sigma_n n_I^{'}$ and $\sigma_n n_Q^{'}$ with $n_I^{'}$ and $n_Q^{'}$ two unitary variance centred Gaussian random variables.

As a result, $\frac{T_0}{\sigma_n^2} = \sum_{k=1}^{M} \left[n_I^{'2}(k) + n_Q^{'2}(k) \right]$ is a centred chi square distribution with $2M$ degrees of freedom. This implies that, for a given false alarm probability $P_{fa} = \Pr\left[T_0 > Th / H_0 \right]$, the threshold Th can easily be deduced. For instance, if the false alarm probability has the value $P_{fa} = 10^{-3}$ then $Th = 59.7\sigma_n^2$.

In presence of the useful signal (H_1), and setting $\varepsilon_\tau = \tau(k) - \hat{\tau}(k)$ and $\varepsilon_\theta = \theta(k) - \hat{\theta}(k)$, the criterion becomes:

$$T_1 = \sum_{k=1}^{M} \left[\left(\frac{A}{2} d(k) R(\varepsilon_\tau) \frac{\sin(\pi \Delta f_{DOP} T_P)}{\pi \Delta f_{DOP} T_P} \cos(\varepsilon_\theta) + n_I(k) \right)^2 + \left(\frac{A}{2} d(k) R(\varepsilon_\tau) \frac{\sin(\pi \Delta f_{DOP} T_P)}{\pi \Delta f_{DOP} T_P} \sin(\varepsilon_\theta) + n_Q(k) \right)^2 \right] \quad \textbf{(II-15)}$$

$$T = \sum_{k=1}^{M} \left[\frac{A^2}{4} R^2(\varepsilon_\tau) \left[\frac{\sin(\pi \Delta f_{DOP} T_P)}{\pi \Delta f_{DOP} T_P} \right]^2 + \left[n_I(k)^2 + n_Q(k)^2 \right] + N \right]$$

with $N = Ad(k) R(\varepsilon_\tau) \frac{\sin(\pi \Delta f_{DOP} T_P)}{\pi \Delta f_{DOP} T_P} \cos(\varepsilon_\theta) n_I(k) + Ad(k) R(\varepsilon_\tau) \frac{\sin(\pi \Delta f_{DOP} T_P)}{\pi \Delta f_{DOP} T_P} \sin(\varepsilon_\theta) n_Q(k)$

Equation II-15 shows that the final signal contains a significant term $\frac{A^2}{4} R^2(\varepsilon_\tau) \left[\frac{\sin(\pi \Delta f_{DOP} T_P)}{\pi \Delta f_{DOP} T_P} \right]^2$ and two other noise terms that could eventually cause signal masking. In order to reduce these noise terms the code delay and the carrier Doppler must be estimated as accurately as possible.

On the other hand, as in the case of hypothesis H_0, it can be proven that the test statistic $\frac{T_1}{\sigma_n^2}$ is a noncentral chi square distribution with $2M$ degrees of freedom, the noncentrality parameter being:

$$\lambda = \frac{2M}{f_p} \frac{C}{N_0} R^2(\varepsilon_\tau) \left(\frac{\sin(\pi \Delta f_{DOP} T_P)}{\pi \Delta f_{DOP} T_P} \right)^2 \quad \textbf{[Bastide et al., 2002]} \quad \textbf{(II-16)}$$

where C is the RF (*Radio Frequency*) signal power.

The PDFs (*Probability Density Function*) of these two hypotheses are plotted in figure II-10 next.

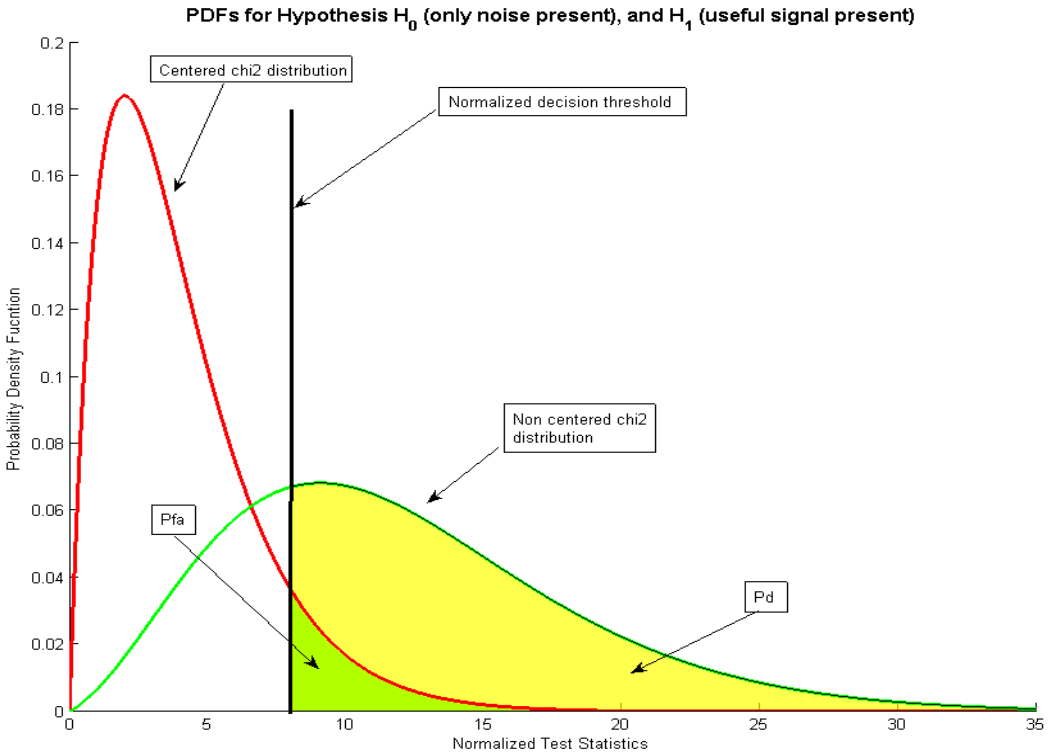

Fig II-10: Unbiased and biased test statistic distribution for hypothesis H_1 and H_0

The detection probability $P_d = \Pr[T_1 > Th / H_1]$, where Th is the decision threshold, was computed for different values of M and T_p in order to illustrate the influence of the choice of these two parameters on the detection probability. First, we set $T_p = 5\,ms$, and consider different values of $M = 20$, $M = 10$ and $M = 5$ respectively to assess the impact of the non-coherent integrations on the detection probability. The results are shown in figure II-11 below.

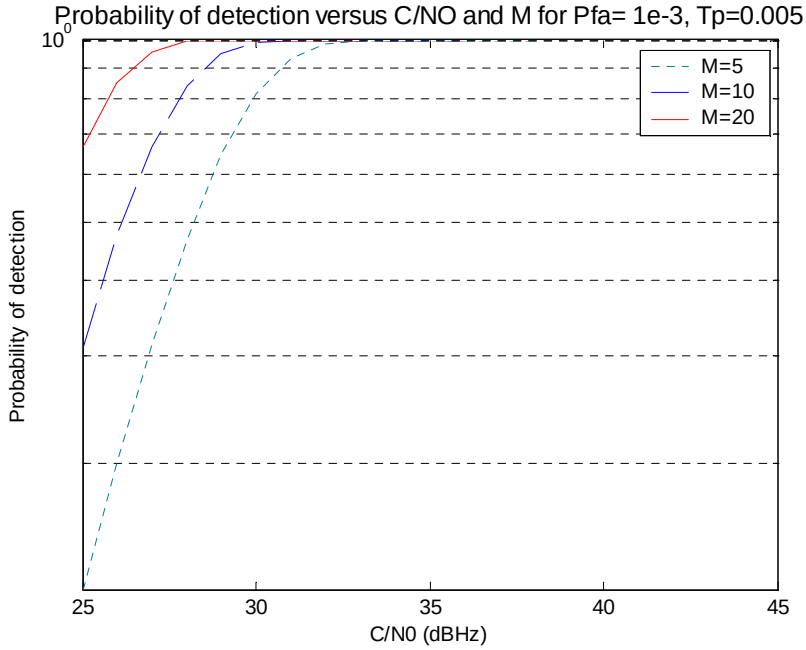

Fig II-11: Probability of detection for a Probability of false alarm equal to 10^{-3}, $T_p = 5ms$ and $M = 20$, $M = 10$ and $M = 5$ respectively

Figure II-12 illustrates the same result for $M = 5$ and $T_p = 5ms$, $T_p = 10\,ms$ and $T_p = 20\,ms$, respectively.

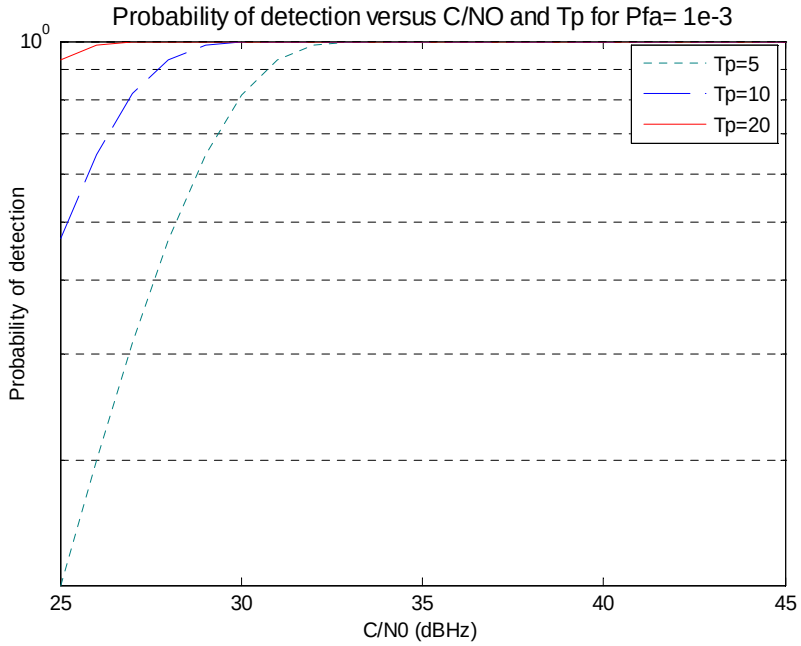

Fig II-12: Probability of detection for a Probability of false alarm equal to 10^{-3}, $M = 5$ and $T_p = 5\,ms$, $T_p = 10\,ms$ and $T_p = 20\,ms$ respectively

The results show a clear influence of the non coherent and the coherent integration times over P_d; the higher these values, the higher the detection probability, or in other words the lower the $\frac{C}{N_0}$ ratios that can be detected. The price to pay is a longer search time.

Furthermore, a comparison of the two figures shows that for the same dwell time (the total coherent and non-coherent integration time: MT_p), a higher coherent integration time provides better probability of detection. This is illustrated in figure II-13.

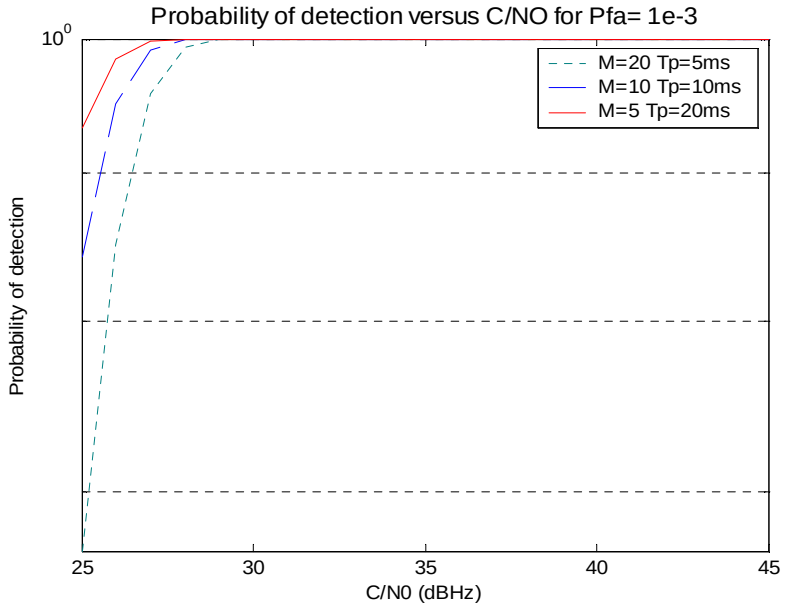

Fig II-13: Probability of detection for a constant dwell time and a Probability of false alarm equal to 10^{-3}

Indeed, for higher coherent integrations the increase in the detection probability is more significant than for higher non-coherent integrations. At this stage, it is useful to introduce the notions of coherent, non-coherent and total gains: the coherent gain is the ratio of the SNR after coherent integration to the SNR before coherent integration. The non-coherent gain is the ratio of the SNR after non-coherent integration to the SNR before non-coherent integration. Note that squaring the inphase and quadrature phase in non-coherent accumulation results in squaring the noise, which results in what is called squaring loss defined in equation II-19 below. The total gain is the sum between the coherent and non-coherent gains.

Figure II-13 shows that the coherent gain is higher than the non-coherent gain. The coherent gain can be calculated based on equations II-6 and II-12:

$$G_c = 10\log\left(\frac{SNR_{post}}{SNR_{pre}}\right) = 10\log\left(B \cdot T_p \cdot R_{c_f c}(0)\right) \quad \textbf{(II-17)}$$

Assuming that the Front End filtering introduces no errors on the C/A code correlation function, the coherent gain becomes:

$$G_c = 10\log\left(B \cdot T_p\right) \quad \textbf{(II-18)}$$

The non-coherent gain is given by [*Lin, 2002*] and [*Karunanayake, 2005*]:

$$G_n = 10\log_{10}(M) - L(M)$$

$$L(M) = 10\log_{10}\left[\frac{1+\sqrt{1+M\,9.2/D_C(1)}}{1+\sqrt{1+9.2/D_C(1)}}\right] \quad \textbf{(II-19)}$$

$$G_{tot} = G_c + G_n \quad \textbf{(II-20)}$$

where B is the pre-detection bandwidth in Hz, i.e., the front end selective filter bandwidth,
T_p is the coherent integration time in sec,
M the number of non-coherent integrations,

$L(M)$ the non-coherent squaring loss,
$D_C(1)$ the ideal detectability factor defined as: $D_C(1) = [erfc^{-1}(2P_{fa}) - erfc^{-1}(2P_d)]^2$,
G_{tot} is the total processing gain in dB.

The total gain resulting from coherent and non-coherent integrations and the minimum $\frac{C}{N_0}$ for acquisition are depicted in figures II-14 and II-15, respectively, as a function of the dwell time. The results are computed assuming $P_{fa} = 10^{-3}$ and $P_d = 0.9$.

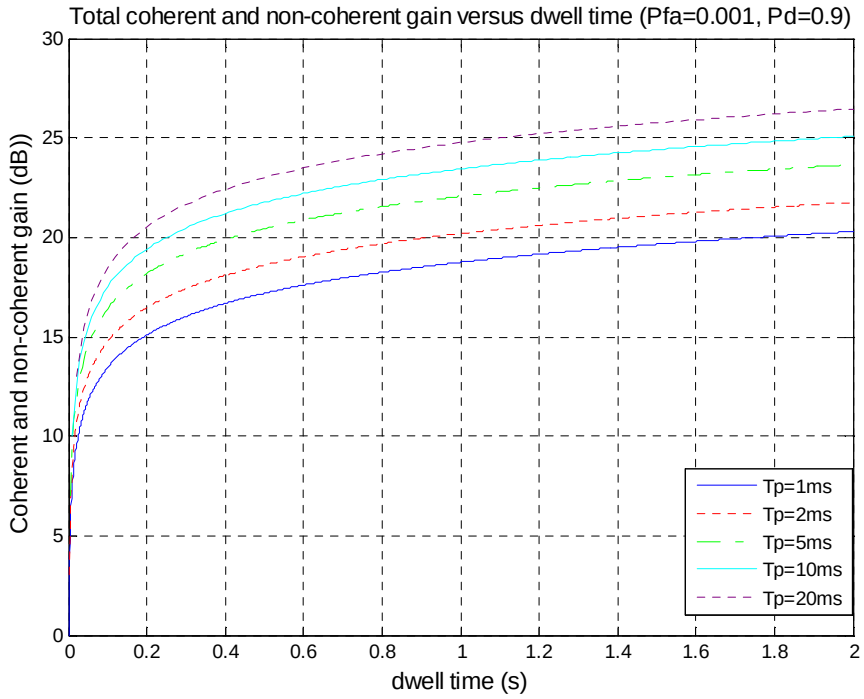

Fig II-14 : Total coherent and non-coherent gain versus dwell time, with a $p_{fa} = 10^{-3}$ and $p_d = 0.9$

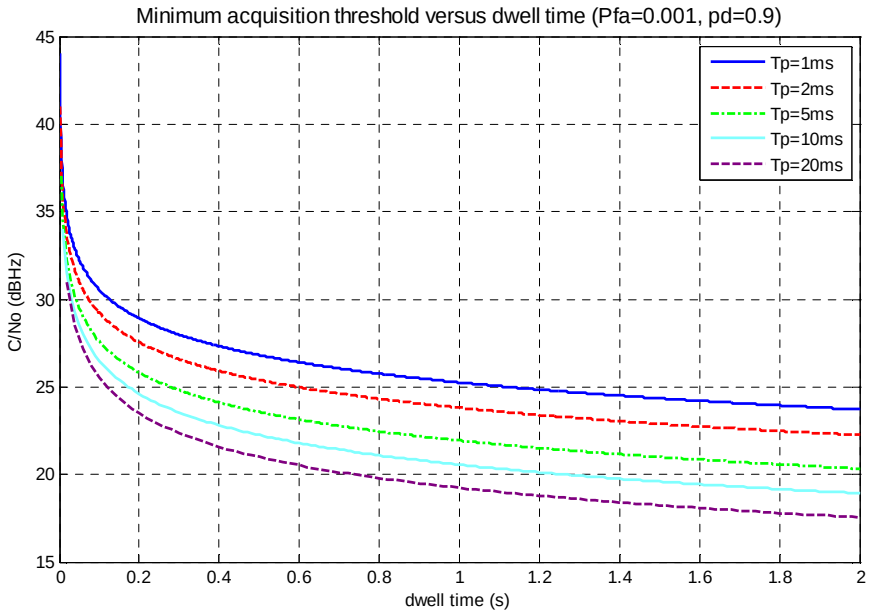

Fig II-15 : Minimum acquisition threshold versus dwell time, with a Pfa a $p_{fa} = 10^{-3}$ and $p_d = 0.9$

Note that by minimum acquisition threshold, illustrated in figure II-15, we refer to the minimum $\frac{C}{N_0}$ ratio that can be detected in acquisition, which is different from the decision threshold. It is obvious in these figures that for longer coherent integrations, lower dwell times are needed to achieve successful acquisition, with $P_d = 0.9$.

The acquisition parameters depend on the acquisition scheme used by the receiver. The classical and FFT (*Fast Fourier Transform*) acquisition schemes are described in the next paragraphs. More advanced schemes will be the object of Chapters V and VI after different GPS radio channel problems are highlighted in Chapters III and IV.

The next paragraph introduces the classical GPS acquisition scheme.

II.4 GPS classical acquisition scheme (linear search)

This algorithm is simple to be implemented. As the name suggests, linear search simply linearly increments the phase and the Doppler frequency. Figure II-16 illustrates a classical acquisition search scheme.

The serial search algorithm usually uses a constant Doppler bin size. Typically, the search pattern starts from the known mean value of the Doppler uncertainty (zero Doppler when there is not any expected value). All code possible delays are then searched over. If this fails, the search is carried on to the next Doppler bin. The search is usually done in the range direction from early to late in order to best avoid false acquisition of a multipath signal. Indeed, the direct arrival of a signal subject to multipath is always ahead in time with respect to the reflected arrivals.

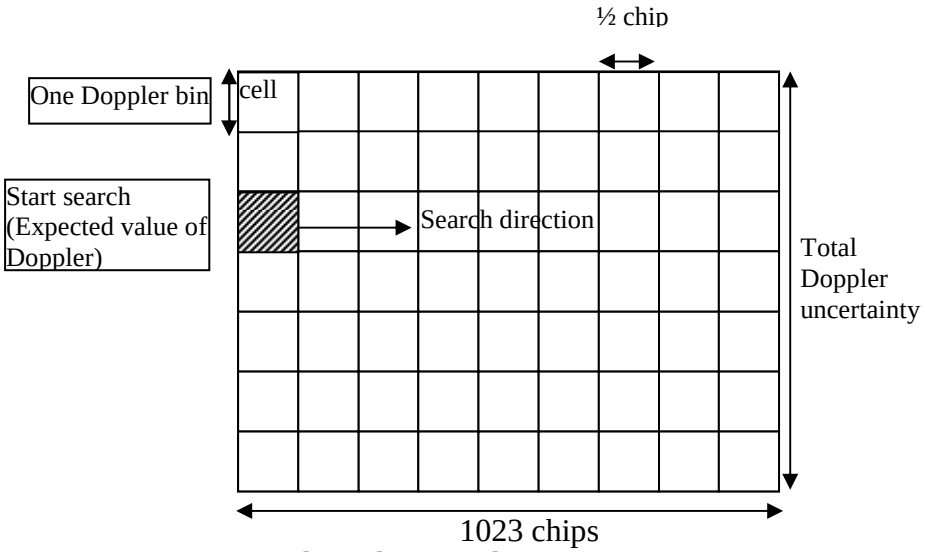

Fig II-16: A typical search map in the acquisition uncertainty region

The final estimated code phase and carrier frequency Doppler are fixed in the centre of the cell wherein detection occurs.

The classical algorithm can be otherwise illustrated, as in figure II-17 below:

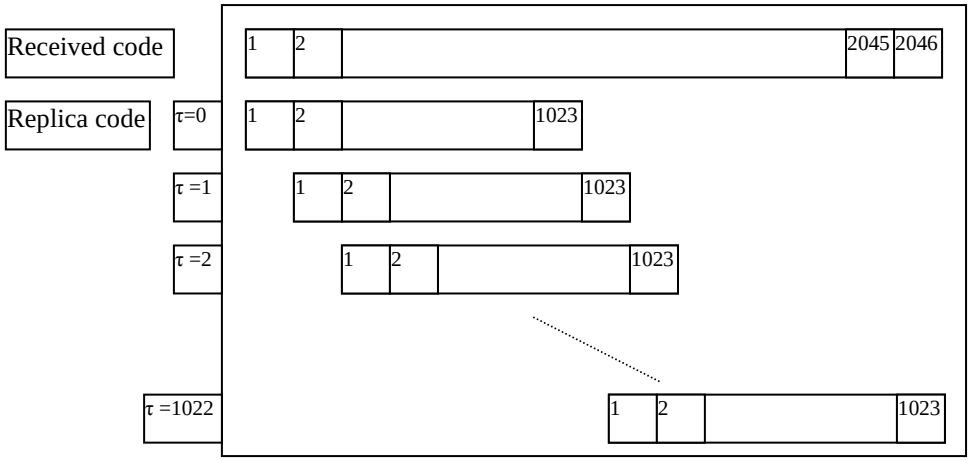

Fig II-17: Linear search algorithm with the C/A code GPS signal

In this figure, τ is the delay in chips between the input and the local C/A codes having a period of 1023 chips. The correlation between the received and local replicas is given as:

$$R(m) = \frac{1}{N}\sum_{k=0}^{N-1} c_r(k)c_l(k-m) \qquad \textbf{(II-21)}$$

where $c_r(k)$ and $c_l(k)$ are respectively the received and the local C/A codes. This correlation has a complexity of $O(N^2)$ for *N* correlation samples.

The acquisition performance is directly related to the receiver sensitivity to weak signals and to the TTFF. As already mentioned, increasing the coherent and/or non-coherent integration times enhances the final SNR, and thus the sensitivity. But it increases the TTFF, as shown in equation II-22 below [*Holmes, 1990*].

$$\overline{T} = \frac{2 + (2 - P_d)(q-1)(1 + KP_{fa})}{2P_d} MT_p \qquad \textbf{(II-22)}$$

where $\overline{T}$ is the mean acquisition time,

P_d is the probability of detection,

P_{fa} is the false alarm probability,

q is the uncertainty region,

M is the number of non-coherent accumulations,

T_p is the coherent integration duration,

K is the penalty factor chosen, here, so that $K\tau_d = 1$ *s*, is the time lost if a false alarm occurs

The uncertainty region is defined as the number of cells to explore to achieve code acquisition. Total uncertainty region is the product of the code and frequency respective uncertainty regions. In the case of a GPS signal with a maximum Doppler range of ± 6 *kHz* (i.e. a 12 *kHz* Doppler window with frequency bins of $1/2T_p$), the Doppler uncertainty region contains: $12\,kHz * 2T_p = 24000T_p$ cells. Assuming a code delay bin of half a chip, the code

delay uncertainty region contains 2046 cells. The total uncertainty region is then composed of: $49104000 \cdot T_p$ cells.

An example depicting the mean acquisition time as a function of the C/N_0 ratio, and the coherent and non-coherent durations is shown in figure II-18 below.

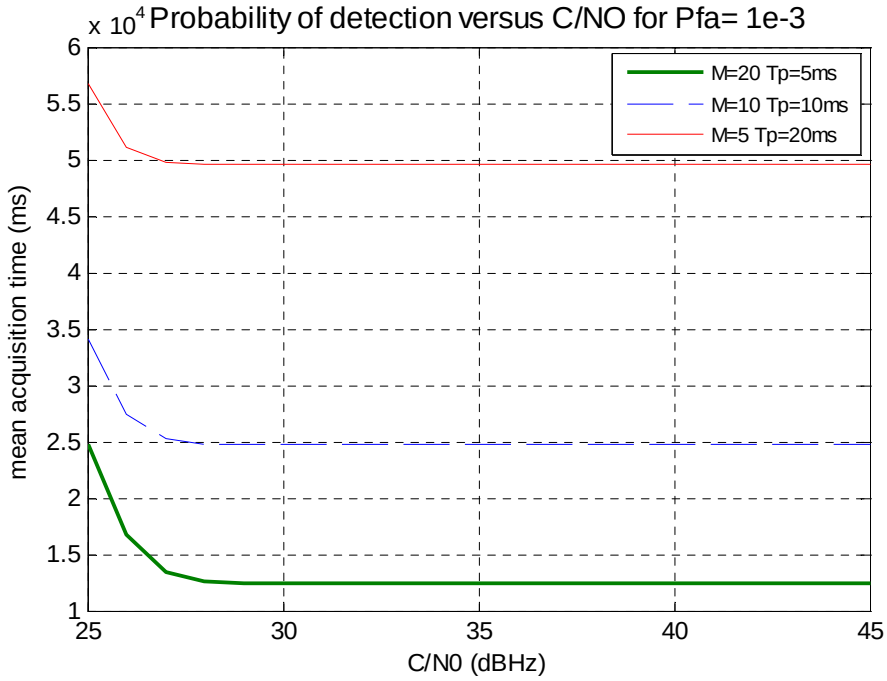

Fig II-18: Mean acquisition time (in ms) versus $C/N_0\,(dBHz)$ for a constant dwell time and $p_{fa} = 10^{-3}$

This figure shows that the acquisition time performance is much better with smaller coherent integration durations. Indeed, with *Tp*=5 *ms* and *M*=5, 12 *s* are needed to acquire a C/N_0 of 30 *dBHz*, while 50 sec are needed to acquire the same C/N_0 ratio with *Tp*=20 *ms* and *M*=5. However, in terms of acquisition sensitivity performance (i.e. probability of detection), for a given dwell time, lower C/N_0 could be acquired with the same probability of detection for higher coherent integration durations.

As a result, a compromise must always be found between the receiver sensitivity and the time performances. The best compromise is found when the acquisition algorithm is modified such that its complexity is reduced without or with negligible impact on its sensitivity performance. This allows for longer coherent/non-coherent integrations, implying enhanced sensitivity performance, while keeping a relatively constant TTFF, knowing that the TTFF depends on the signal observation and processing durations.

The FFT (*Fast Fourier Transform*) algorithm is one modified acquisition algorithm that reduces the complexity of the classical one. It will be the object of the next paragraph.

II.5 FFT search algorithm

Instead of linearly shifting the code phase, as in the serial search process, the replica code can rather be circularly shifted as shown in figure II-19. The application of this algorithm to the GPS signal is possible since the replica is periodic, thus cyclic correlation is possible.

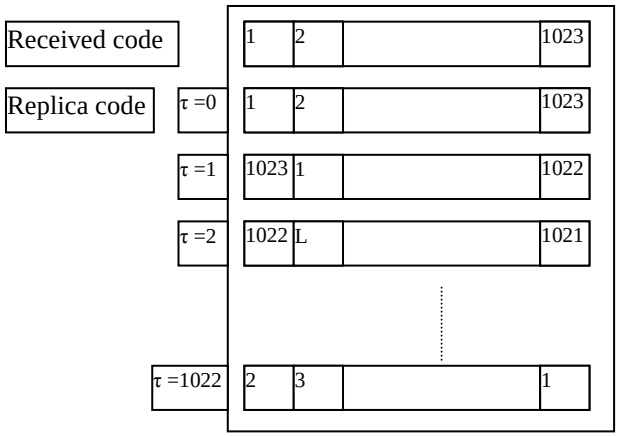

Fig II-19: Circular search algorithm

The cyclic correlation is performed using a DFT (*Discrete Fourier Transform*). The DFT allows for calculating the correlation for an entire range dimension of duration T_p, for a selected Doppler, in a single step. The DFT acquisition process, which can be used to replace the classical temporal correlation algorithm, is detailed in what follows.

The DFT of an N points sampled signal $s(k)$ is given as

$$S(n) = \sum_{k=0}^{N-1} s(k) \exp(-j2\pi k \frac{n}{N})$$

Multiplying the DFTs of two signals $s(k)$ and $y(k)$ and taking the inverse DFT of the product corresponds to convolution in the time domain. However since the incoming GPS signal is correlated with the reference signal in the time domain, this corresponds to multiplying the DFT of $s(k)$ with the conjugate DFT of $y(k)$, and then taking the inverse DFT of the product. This is proved in the following.

First recall that the C/A code autocorrelation function over N samples, is defined as (equation II-21):

$$R(m) = \frac{1}{N} \sum_{k=0}^{N-1} c(k)c(k-m)$$

with N corresponding to a multiple of the C/A code period of 1*ms*. The received code being periodic with period L, its autocorrelation function is also periodic with the same period L. The expressions of $c(k)$ and $c(k\text{-}m)$ respectively as a function of the DFT $C(n)$ of the code $c(k)$ are:

$$c(k) = \frac{1}{N} \sum_{n=0}^{N-1} C(n) e^{i2\pi \frac{kn}{N}} \text{ and } c(k-m) = \frac{1}{N} \sum_{n=0}^{N-1} C(n) e^{i2\pi \frac{n(k-m)}{N}}$$

Replacing these expressions in the expression of the C/A autocorrelation function gives:

$$R(m) = \frac{1}{N}\sum_{k=0}^{N-1}\left(\frac{1}{N}\sum_{n=0}^{N-1}C(n)e^{i2\pi\frac{kn}{N}}\right)\left(\frac{1}{N}\sum_{l=0}^{N-1}C(l)e^{i2\pi\frac{l(k-m)}{N}}\right)$$

$$R(m) = \frac{1}{N}\sum_{n=0}^{N-1}\sum_{l=0}^{N-1}\frac{1}{N^2}C(n)C(l)e^{-i2\pi\frac{lm}{N}}\sum_{k=0}^{N-1}e^{i2\pi\frac{(n+l)k}{N}} \qquad \textbf{(II-23)}$$

Yet we know that, $\sum_{k=0}^{N-1}e^{i2\pi\frac{(n+l)k}{N}} = 0$ for $n+l \neq 0$, and $\sum_{k=0}^{N-1}e^{i2\pi\frac{(n+l)k}{N}} = N$ for $n+l = 0$.

Consequently, equation II-23 becomes

$$R(m) = \frac{1}{N^2}\sum_{n=0}^{N-1}C(n)C(-n)e^{i2\pi\frac{nm}{N}},$$

which may also be written as:

$$R(m) = \frac{1}{N}DFT^{-1}\left[C(n)C(-n)\right] = \frac{1}{N}DFT^{-1}\left\{DFT\left[c(k)\right]\cdot conj\left(DFT\left[c(k)\right]\right)\right\}$$

This last result shows that a DFT algorithm is equivalent to the classical one and thus it can be used in the acquisition process. Hence, once T_p *ms* of signal are received, the algorithm is applied.

Figure II-20 below illustrates the receiver structure with a DFT algorithm:

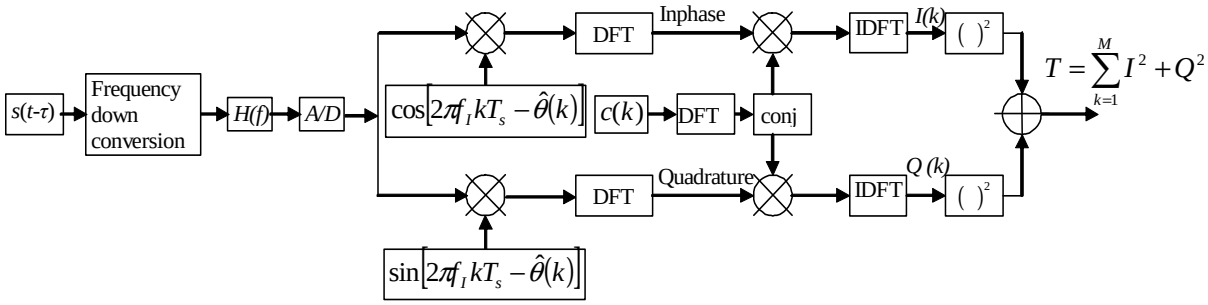

Fig II-20: DFT acquisition scheme

A DFT is applied to the inphase and the quadrature components of the incoming signal. The inphase and quadrature components of the signal may also be derived by multiplying the signal with a complex exponential: $\exp\left[2\pi f_I kT_s - \hat{\theta}(k)\right]$. The result is multiplied by the conjugate DFT of the replicated signal. The inverse DFT of the product gives the correlation result in the time domain for all of the code phase offsets. Note that this method is in terms of complexity, similar to the conventional time domain technique: for the *N* point DFT, O(N^2) arithmetical operations are required which is the same as in the case of the time domain serial search.

Note however, that the periodicity of the C/A code autocorrelation allows for using the FFT algorithm which realizes a circular correlation. It is this algorithm which is used in practice to compute the DFT. This algorithm was developed by Van Nee and Conen [*1991*] and is much faster than the implementation of the DFT expression. One implementation of the FFT algorithm called radix-2 Cooley Tukey algorithm requires only O($N\log_2 N$) arithmetical operations for example, to compute the FFT of an *N* point sequence, if *N* is a power of 2. For other values of *N*, the speed is slightly degraded. Other FFT algorithms may

have better performances. Further details on the different FFT algorithms complexities may be found in [*Mitra et al., 1993*].

II.6 Standalone GPS acquisition performance illustration

In this section, the acquisition performance of the Novatel OEM4 receiver was studied for illustration purposes, using a Spirent STR4500 GPS signal simulator. The performance test focuses on two essential parameters of the GPS localization, namely the receiver sensitivity to weak signals and the TTFF. Recall that the TTFF is the time elapsed before a first position is delivered by the receiver. It is thought that the classical sequential acquisition method is used in this receiver.

II.6.1 Test Setup

The test setup used during simulations has the following configuration:

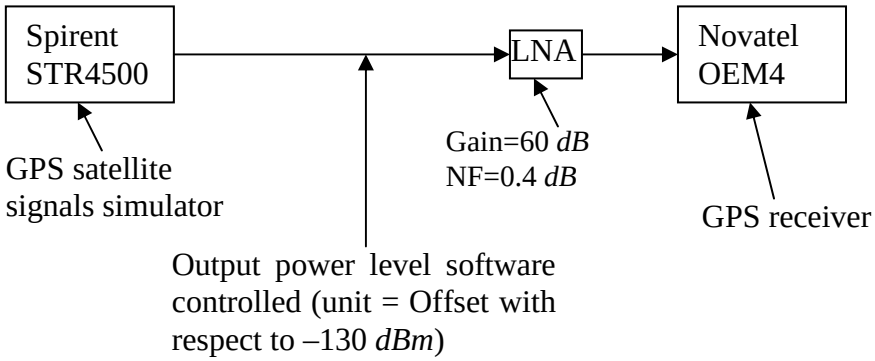

Fig II-21: Test setup for a Novatel OEM4 receiver acquisition performance

The Spirent front panel is illustrated in figure II-22, next.

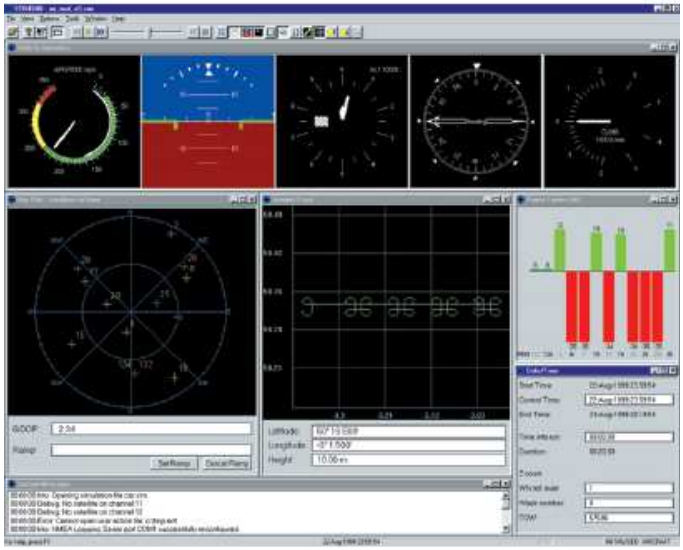

Fig II-22: Spirent STR4500 front panel

The LNA (*Low Noise Amplifier*) acts to set the signal conditions (i.e. noise floor) to values similar to real GPS receivers [*Van Dierendonck, 1996*].

The Spirent runs a scenario on the 17th of May 2000, with a static user. It lasts 8 hours with 11 satellites in view at the beginning of the scenario.

II.6.2 Test results

The acquisition performance test considers a scenario where all of the satellites are at the same power level: we start from -130 *dBm*, and reduce the power level by 1 *dBm* for each subsequent measure until no position fix can be obtained.

For each signal power level, we noted the average C/N_0 given by the receiver, and the TTFF. The results obtained are summarized in the following table:

Satellites powers	TTFF	C/N_0
-130 *dBm*	1 *min* 50 *s*	41.6 *dBHz*
-131 *dBm*	2 *min* 30 *s*	40.6 *dBHz*
-132 *dBm*	3 *min* 39 *s*	39.6 *dBHz*
-133 *dBm*	4 *min* 32 *s*	38.6 *dBHz*
-134 *dBm*	23 *min* 08 *s*	37.6 *dBHz*
-135*dBm*	31*min* 45 *s*	36.6 *dBHz*
-136 *dBm*	1 *h* 30 *min*	35.6 *dBHz*

Tab II-1 : Acquisition performance when all the satellites have the same power

No tests were conducted for lower power levels because the TTFF is already very high at –136 *dBm* to be affordable in practice.

This test shows that the acquisition threshold for the Novatel OEM4 is approximately $-133\,dBm$ or $38.6\,dBHz$. For this value the TTFF is of about several minutes which ultimately can be afforded by a GPS user. These results are confirmed by Karunanayake et al. [*2004*].

II.7 Conclusion

This chapter illustrates some of the GPS fundamentals: the system architecture, the positioning triangulation principle, the transmitted and the received signal structure. It also presents the general acquisition theory, the classical serial algorithm and the FFT based algorithm. It shows the impact of the coherent integration on the probability of detection and the acquisition time. The coherent integration turns out to have opposite impacts on these two key acquisition performance parameters. A higher coherent integration results in better sensitivity to weak signals, but higher acquisition time. This means that depending on the environment and the context the GPS receiver is being used in, the coherent and non-coherent integration durations are of major importance and must be adjusted such that the best compromise is found between the receiver sensitivity to weak signals which induces more complex algorithms, and the need for short TTFF which implies lighter algorithms.

In the aim of illustrating the standalone GPS performance, a test has been conducted using Spirent STR4500 generated signals and an OEM4 receiver. The results show that the acquisition sensitivity limit of the OEM4 receiver is approximately equal to 38.6 *dBHz*! This value is very high compared to signal levels in urban or indoor environments.

Chapter III gives a more detailed insight of the GPS channel and its constraints. It presents GPS indoor and urban channel models that were used to meet this goal, and the results obtained.

Résumé du chapitre III

Les pertes dans les liens de communication radio sont souvent influences par le masquage du signal et les effets des multitrajets: les signaux transmis par les satellites à un utilisateur terrestre sont souvent masqués ou très atténués à cause de la propagation à travers les arbres dans les rues et les immeubles. Les pertes qui en résultent sont appelées 'shadowing'. Les immeubles, et les autres surfaces peuvent aussi agir comme des réflecteurs du signal causant la réflexion ou la diffraction du signal direct dit LOS. L'effet résultant est connu sous le nom de multitrajets. L'atténuation du signal causées par et/ou l'autre des ces effets peut être de l'ordre de 20 dB ou plus en dessous du niveau nominal du signal direct. Dans le passé, les récepteurs n'utilisaient pas les signaux faibles et se limitaient aux quelques signaux forts reçus, réduisant ainsi la disponibilité du service GPS et sa précision. Mais avec l'arrivée des services LBS, les contraintes sont devenues plus importantes et les récepteurs doivent fonctionner dans des environnements assez sévères tout en fournissant des résultats viables. C'est pour ces raisons que ce chapitre présente une caractérisation détaillée de ces environnements, en se focalisant sur les aspects concernant les multitrajets, les intercorrélations (corrélation du signal reçu avec d'autres codes C/A ne correspondant pas au code particulier utilisé dans ce signal) et le masquage du signal.

Pour étudier le canal indoor, un modèle a été développé qui permette de tenir des variations temporelles de ce canal. A l'aide de ce modèle, trois types de signaux ont été générés : un signal direct LOS, un signal composite formé du signal direct LOS et de plusieurs répliques multitrajets, et un signal formé uniquement de multitrajets NLOS.
L'étude s'est focalisée sur le pouvoir de détection d'un pic de corrélation, ou en d'autres termes la sensibilité, et la fiabilité des estimés du retard de code et de la fréquence Doppler. Le temps total nécessaire pour réaliser l'acquisition n'a pas été analysé. Un temps d'intégration total de 200 *ms* a été fixé de façon que les signaux qui puissent être acquis ne aient un niveau moyen de l'ordre de 20 *dBHz*.
Les résultats montrent que pour le cas indoor, les répliques de multitrajets ont un effet mineur et ne perturbent pas l'acquisition du signal en présence d'un signal LOS direct. Dans certains cas, ils ont induit une légère hausse du niveau de bruit. Dans le cas du signal NLOS, les multitrajets ont pu être utilisés pour fournir une solution (même si cette solution n'est pas très précise). Cependant ils sont dans ce cas très atténués par rapport au signal direct, et des temps d'intégration beaucoup plus longs sont nécessaires pour les acquérir. L'atténuation relative des multitrajets par rapport au LOS observée durant les simulations avec notre modèle indoor est de l'ordre de 14 à 17 *dB*. Le retard de code et la fréquence Doppler estimés sont corrects cependant.
Les intercorrélations sont particulièrement gênantes, surtout quand un signal très fort arrive en même avec un signal faible. Mais cette situation n'est pas très commune, à moins de recevoir un signal à travers une fenêtre et un autre a travers le toit d'une maison par exemple. Dans ce cas des problèmes d'intercorrélations se posent pouvant induire des erreurs de l'ordre du *Km* !

Pour les environnements urbains, le modèle du DLR a été utilisé : LMMCM.
Les résultats montrent une corrélation directe entre les délais maximaux et l'angle d'élévation du satellite : Ceux-ci diminuent quand l'angle d'élévation des satellites augmente. Des délais très courts de l'ordre de $50\,\eta s$ $(15\,m)$ ont été relevés pour des angles d'élévation de 90°. De

tels délais ne sont pas gênants dans un contexte d'acquisition du signal GPS L_1 C/A, mais sont très difficiles à être identifiés à ce stade ; Par conséquent, les boucles de poursuites seront initialisées avec des valeurs erronées. Il est par contre à noter que la solution finale résultante peut s'avérer acceptable pour quelques types d'applications.
L'atténuation maximale des signaux dans les environnements urbains variait entre $-5\,dB$ et $-18\,dB$, et n'a pas présenté une corrélation assez claire avec la position du satellite.
Dans les environnements du type downtown et canyon urbain, le signal direct LOS a pu atteindre le récepteur la plupart du temps. Mais dans certains cas, il était totalement absent causant ainsi l'acquisition d'un écho plutôt, et des problèmes d'inter-corrélation. Cependant, dans de mauvaises conditions, et selon l'application visée, il serait éventuellement préférable de fournir une solution mêmes si celle-ci n'est pas très précise pour pouvoir initialiser les boucles de poursuite ; donc en d'autres termes de réaliser le positionnement à l'aide d'un signal réfléchi plutôt que de ne pas être capable de fournir une solution, mais ceci bien entendu dépend des contraintes de l'application visée.

On notera, que comparés aux pics de multitrajets, les pics d'intercorrélation résultent en général de très grandes erreurs, car les pics correspondants peuvent survenir à des retards de code totalement aléatoires à l'intérieur d'une période de code donnée, alors que les délais correspondants aux multitrajets eux dépendent du signal direct, et sont progressivement atténués au fur et à mesure que leurs retards augmentent. Ceci est vrai pour les environnements indoor et urbains.

Une conclusion commune et évidente à tous les résultats présentés dans ce chapitre est qu'en présence d'un signal direct, ou si celui-ci n'est pas très atténué, il n'y a pas de problèmes d'acquisition. Et l'étape suivante serait soit de trouver des techniques de résistance aux intercorélations ou bien d'améliorer la sensibilité du récepteur aux signaux faibles pour assurer une probabilité de détection assez élevée. La suite de cette thèse se focalisera sur l'amélioration des capacités de détection de signaux faibles des récepteurs GPS.

Chapter 3

Challenging radio frequency channels

Contents

The GPS radio communication link losses are often influenced by signal shadowing, and multipath effects: the signals transmitted by the satellites to a land user are obstructed or greatly attenuated due to propagation through roadside trees and buildings. The resultant signal losses are referred to as shadowing. Buildings, and other surfaces, may also act as signal scatterers causing the LOS to be reflected or diffracted. The resultant effect is referred to as multipath propagation. The signal received by the receiver is thus subject to signal fading (i.e. variations in the amplitude and phase of the received signal). These fades may be of the order of 20 *dB* or more below the mean signal level [*MacGougan et al., 2003*]. In the past, an unobstructed LOS signal was necessary for the GPS to work properly. Weak signals whether they are attenuated LOS signals or multipath signals were not desirable for use because they were too weak compared to the noise and other disturbing signals. But this is no more the case with the expansion of GPS to LBS. The resulting stringent localization requirements imply GPS localization in degraded environments, such as indoor and urban channels, where path loss is very severe most of the time, which poses a particularly difficult challenge for system designers.

This chapter focuses on characterising, modelling and analysing the GPS radio frequency channels. It mainly addresses the issues of multipaths, cross-correlations and shadowing.

III.1 Channels characteristics

The positioning applications involve many types of operational environments which were classified and detailed in Chapter I. Each environment basic characteristics are recalled in table III-1 below:

	Main characteristics
Rural environments	- Very good satellites visibility - Availability of LOS - Strong received signal (>30 *dBHz*) - Ease of acquisition - Low probability of false detection
Urban environments	- Partial availability of LOS - Multipaths (due to signal multiple reflections) - Shadowing (due to buildings, and dense foliage for example) - Weak received signal (<30 *dBHz*) - Signal acquisition subject to eventual errors - High probability of false detection
Indoor environments	- Partial or quasi null LOS availability - Very weak signal available at the receiver (<25 *dBHz*) - Multipaths problems - Difficulties in signal acquisition

Tab III-1 : Different GPS operational environments and their main characteristics

Indoor and urban environments are the most constraining. This is why the subsequent work mainly focuses on these channels.

In urban environments, two kinds of obstacles can be defined: large fixed objects, like buildings and trees, on one hand, and people and vehicles moving around on the other hand. However, the impact of buildings and other large objects dominate the characteristics of these channels.

In indoor environments, also two types of obstacles can be defined: those being part of the physical structural components of the building, and those formed by the office or the home furniture and fixed or movable/portable structures. These parameters will be explained below.

The fading phenomenon in a radio GPS channel is primarily affected by the multipath propagation, the mobile relative velocity, the surrounding objects velocity and the cross-correlations between different satellite signals. These parameters will be explained below:

- Multipath is essentially caused by reflection, diffraction and scattering which are the three basic mechanisms of radio propagation [*S. Rappaport, 1996*]. All three phenomenon cause radio signal distortions and give rise to signal fades, as well as additional signal propagation losses. This is because they create additional radio propagation paths beyond the direct optical LOS path between the transmitter and the receiver, resulting in multipath fading (it was the same effect that caused ghost images on television when antennae on the roof were still more common instead of today's satellite dishes). The multipath induced signal attenuation is mainly driven by the number, strength and delay of the multipath signals. The signal components arriving from indirect paths (which are delayed and attenuated versions of the original signal) and the direct LOS path (if it exists), combine and produce a distorted version of the transmitted signal. This combination may cause constructive and/or destructive interference effects [*Lachapelle et al., 2003*]. Large path length differences between different multipath signals cause large differences in the corresponding arrival times resulting in a time delay of the signal arrival. The range of time within which most of the delayed signals arrive can be estimated by measuring the channel delay spread. For GPS indoor environments, at a carrier frequency of approximately 1.5 *GHz*, the delay spread is of the order of 10 to 50 ηs [*Hashemi, 1993*], [*Titus Lo et al., 1994*], hence it is very small compared to half a C/A code chip duration of 500 ηs. This means that indoor multipath must not disturb GPS acquisition where the code delay error must be bounded to within half a C/A code chip duration. This result will be validated by simulations described in the next sections. For urban channels, the delay spread is of about $1\,\mu s$ [*Hashemi, 1993*], [*Pérez-Fontán et al., 2004*]. In this case also, the multipaths delays must not disturb the acquisition.

- As for the relative motion between the mobile receiver and the moving satellite, it causes random frequency modulation due to Doppler shift. The randomness of this Doppler shift makes it very difficult to be estimated at the receiver, which results in Doppler frequency errors, and thus further attenuation of the resulting C/N_0 ratio at the output of the receiver correlator.

- On the other side, if some of the surrounding objects are moving, their velocity may influence the Doppler shifts on multipath signals, causing it to be more important. The surrounding objects may be ignored if their speed is lower than that of the receiver. This is generally the case for the GPS channels. In the model developed herein, the surrounding objects are supposed to be fixed, and the corresponding Doppler shifts are ignored.

- Finally, cross-correlations are caused by interference between GPS signals received from different satellites. The GPS receiver is subject to cross-correlations when it receives many satellite signals with power levels very different from each other. In an indoor channel, this may be the case when one of the signals reached the receiver through a window, whereas another one reached it through a wall or a ceiling for example. Attenuation due to dense foliage may also lead to cross-correlations in urban environments. J. Miller et al. [*1995*] estimated typical signal attenuations due to foliage shadowing. At a 1.55 *GHz* carrier frequency (as for the GPS L_1), the signal experienced attenuations are between 4 and 5.6 *dB* for a 35% tree density, and between 6.9 and 10.8 *dB* for an 85% tree density, where the tree density is defined as the percentage of optical shadowing it causes at an elevation angle of 45°. The result of such situations is

processing one (or more) very strong received signals while the others are very weak. The weak signals are masked by the stronger one(s), thus leading to positioning errors. The cross-correlations cannot be theoretically characterized by a channel parameter, since they are completely random, and depend on the visible satellites geometry, the environment geometry, and the position and velocity of the receiver at a given time. Consequently they will be quite evaluated experimentally.

Once the channels characteristics are described, the next sections focus on modelling and analysing the indoor and urban channels based on theses characteristics. The next section describes the different models that were used to build up our custom indoor model used for analysing the indoor environments.

III.2 Modeling the indoor channel

As discussed before, radio signals reach the receiver through very hardly predictable paths. These are completely characterized by parameters namely each path amplitude, time of arrival, and phase. If the signal $s(t)$ is transmitted in an indoor environment, then the signal $r(t)$ received via many paths at the receiver location is:

$$r(t) = s(t) * h(t,\tau) \qquad \textbf{(III-1)}$$

with $h(t,\tau)$ a complex impulse response of a linear time varying filter used to model the random and time-varying channel. $h(t,\tau)$ is given by [*Hashemi, 1993*]:

$$h(t,\tau) = \sum_{k=0}^{R(\tau)-1} a_k(t)\,\delta\left[\tau - \tau_k(t)\right] e^{j\varphi_k(t)} \qquad \textbf{(III-2)}$$

where t and τ are the observation time and application time of the impulse, respectively
$R(t)-1$ is the number of multipath components
$a_k(t), \tau_k(t), \varphi_k(t)$ are random time-varying amplitude, time of arrival, and phase of the LOS ($k = 0$) and the multipath replicas

This model allows for obtaining the response of the channel to the transmission of any signal $s(t)$ by convolving it with $h(t,\tau)$ and adding noise, $n(t)$, as illustrated in figure III-1 below.

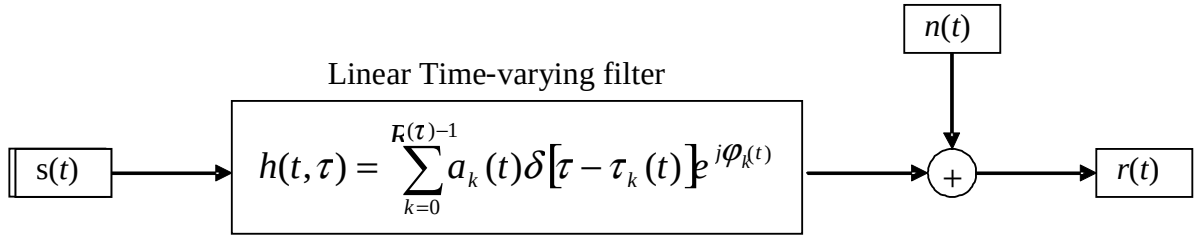

Fig III-1: An indoor channel model

where $r(t) = \int_{-\infty}^{+\infty} s(\tau)h(t,\tau)d\tau + n(t)$ **(III-3)**

The channel modelling is described by the parameters a_k, τ_k, φ_k and R which can be statistically characterized through real tests [*Pérez Fontan et al., 2004*] or using ray tracing methods [*Mudhafar, 2002*], for example. For the indoor channel we rely on a statistical model developed in the course of an ESA project (2002-2003) entitled "Navigation signal measurement campaign for critical environments", carried out by JOANNEUM RESEARCH (Austria) with subcontracts to the DLR and the University of Vigo (Spain) [*Pérez Fontan et al., 2004*]. In this project, the ESA investigated a statistical non-time-varying model which provides the PDF (*Probability Density Function*) for each of the four parameters used to characterize the channel: the number of paths, each path's amplitude, delay, and phase. These parameters were set to be constant over time. In our model we generate a first signal which stands for a direct LOS signal, and many reflected and diffracted replicas of this signal. This model has been developed using Matlab. The difference between our custom model and that of the ESA is that each path delay and phase have rather been assumed to be time-varying. For the sake of simplicity, the relative amplitudes and the number of paths were assumed to be constant during the acquisition duration: these two parameters are chosen at the beginning of the simulation according to their respective distributions presented in the ESA paper. This ESA model will be described in the next paragraph. A detailed description of our model follows.

III.2.1 ESA model

The ESA statistical model is based on a measurement campaign carried out using a channel sounder on board a helicopter. The helicopter was flown around a six floors building where a receiver was located. Different flights were carried out to cover several elevation angles. The receiver was also placed in different locations at different floors within the building so that different penetration conditions could be studied.

The main parameters of the channel impulse response (delays, amplitudes, phases, number of rays) are considered as random variables with a PDF estimated from the measured data. This random time-invariant channel's impulse response has a transfer function defined by equation III-4.

$$h(t) = \sum_{k=0}^{R-1} a_k \delta(t - \tau_k) e^{j\varphi_k} \quad \textbf{(III-4)}$$

with $R-1$ is the number of multipath components. It has random values with a PDF that is estimated from the field test measured data

a_1 is the amplitude of the direct ray (input parameter)

τ_1 is the corresponding delay, set to zero

$a_k, \tau_k, (k \geq 1)$ are the delays and amplitudes of the reflected rays, with PDF obtained from the measurements

φ_k are the direct and reflected paths phases supposed to be uniformly distributed in $[0;2\pi]$

This channel impulse response has the same shape and parameters characteristics as that described in [*Saleh et al., 1987*].

The ESA paper provides the CDFs (*Cumulative Distribution Functions*) of the reflected rays relative amplitudes, and the reflected rays delays. The curves are provided for the ground floor, the fourth and the sixth floors, and for different flights, i.e., different

elevation angles. The paper also provides the distribution of the number of rays, the CDF and the PDF, only for the fourth floor and for an elevation angle of 30°. In what follows the corresponding results are illustrated.

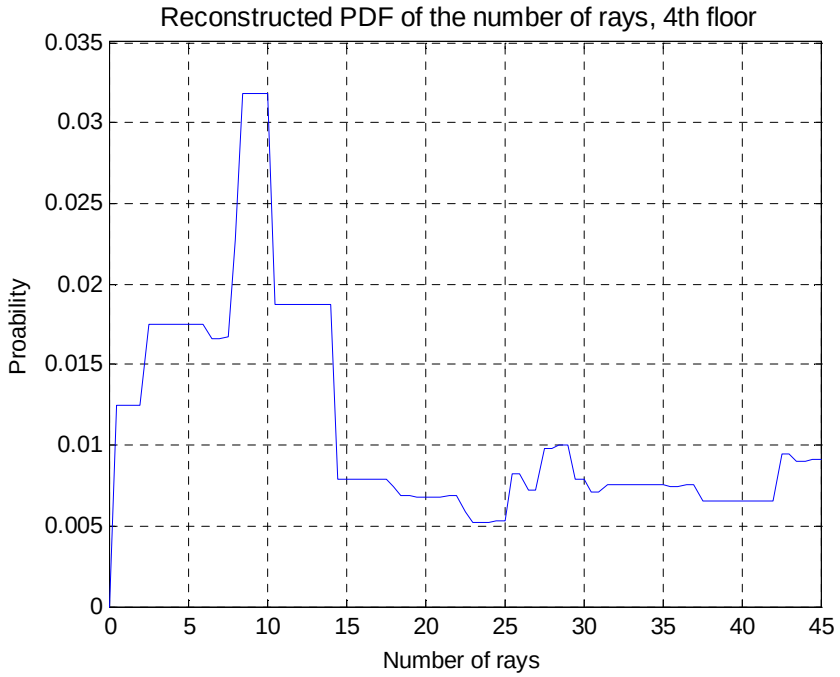

Fig III-2: Number of snapshots with a given number of rays inside the dynamic range. The values for a number of rays greater than 29 have been extrapolated. Measurements realized on the fourth floor [*Pérez Fontan et al., 2004*]

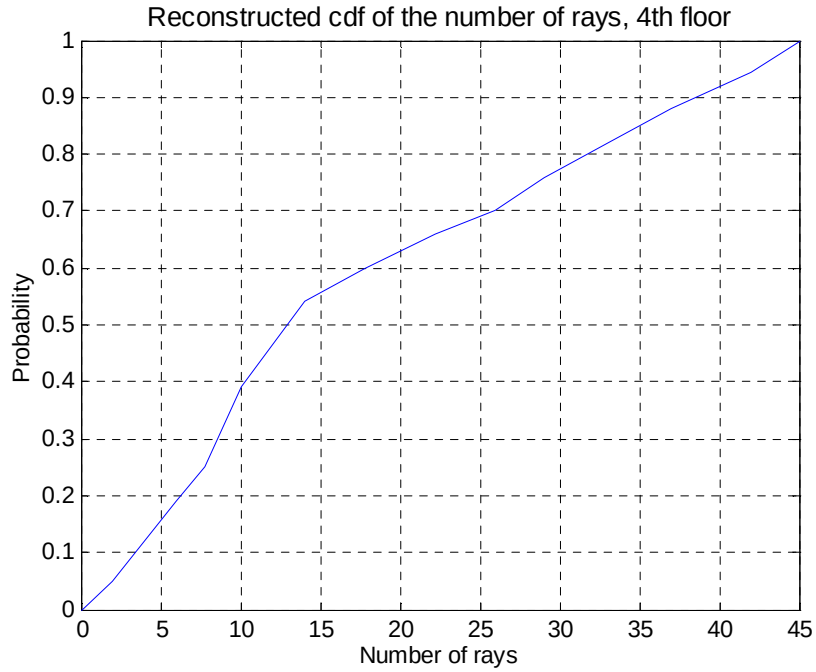

Fig III-3: Estimated and corrected CDF of the number of rays for the circular flight on the 4th floor [*Pérez Fontan et al., 2004*].

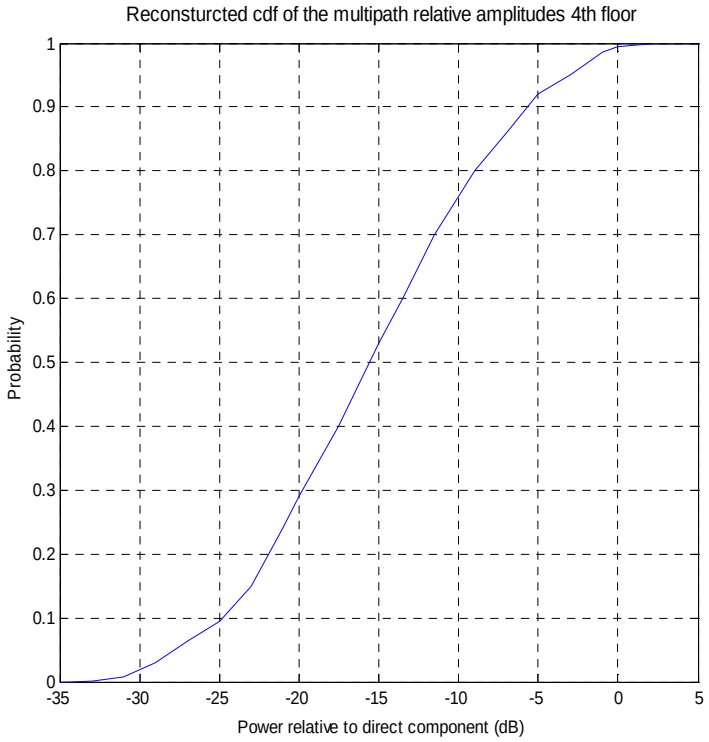

Fig III-4: Estimated CDFs of the relative powers of the reflected rays on the fourth floor [*Pérez Fontan et al., 2004*]

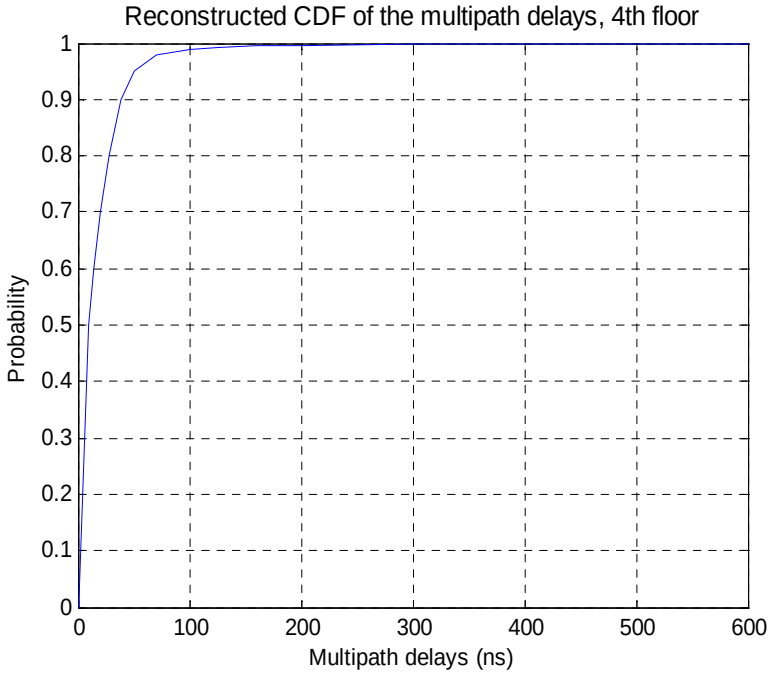

Fig III-5 : CDF of the multipath delays on the fourth floor [*Pérez Fontan et al., 2004*]

In our model, the ESA model is essentially used to provide the needed statistical distributions for the different multipath rays. They are used to initialise our channel parameters.

III.2.2 Custom model

In our model [*El Natour et al., 2005*], variations of the channel parameters as a function of time have been considered. The ESA model is used to derive values for the multipath relative amplitudes a_i which were supposed to be constant over the simulation duration (~1 second), and the initial delays, τ_{0i}, of the different multipath rays. These values are derived such that they have the same distribution as in figures III-4 and III-5 respectively. The receiver which yielded the results shown in these figures was placed in an office with external building walls. For the sake of simplicity, the number of rays *R* is set once and for all to its most probable value, namely 10 rays. All of the results presented here deal with a static user since we found that the results obtained with a dynamic user (with a velocity of $1\,m/s$) were similar. Besides, this assumption means that the LOS replicas are assumed to have the same relative attenuation (compared to the LOS) throughout each simulation. The phase is uniformly distributed over $[0;2\pi]$ as it was the case for the ESA model.

The time-varying indoor GPS channel transfer function is then given by:

$$h(t) = \sum_{k=1}^{R} a_k \cdot \delta[t - \tau_k(t)] \cdot e^{j\varphi_k(t)} \qquad \textbf{(III-5)}$$

where R is the number of rays that reach the receiver. This set of rays may either contain a direct LOS or not. R is constant over the duration of the simulation, and is chosen according to the most probable value given by the distribution of the number of rays reaching the receiver given in [*Pérez-Fontán et al., 2004*] (*R*=10),

a_k is the multipath replicas relative amplitude with respect to that of the direct ray. This parameter is considered to be constant over the duration of the simulation, and is also chosen according to the distribution of the rays powers given in [*F. Pérez-Fontán et al., 2004*],

$\tau_k(t)$ is the delay experienced by the direct LOS ray and the reflected rays respectively. This delay is essentially due to the signal propagation from the satellite to the receiver. This parameter is supposed to be variable with time, with initial values derived according to the corresponding distributions given by the ESA model,

$\varphi_k(t)$ is the phase distortion introduced by the channel. $\varphi_k(t) = 2\pi L_1 \tau_k(t) + \varphi_0$, with φ_0 a random initial phase.

Let us now focus on the received signal. Assuming that the GPS signal transmitted (normalized amplitude) over the channel is modelled as:
$s(t) = c(t) \cdot d(t) \cdot \cos(2\pi L_1 t)$,

The signal that is supposed to reach the receiver is modelled as:

$$r(t) = s(t) * h(t) = \sum_{k=1}^{R} a_k \cdot c[t - \tau_k(t)] \cdot d[t - \tau_k(t)] \cdot \cos[2\pi L_1 t - \varphi_k(t)]$$
$$r(t) = \sum_{k=1}^{R} a_k \cdot c[t - \tau_k(t)] \cdot d[t - \tau_k(t)] \cdot \cos\{2\pi L_1 [t - \tau_k(t)] + \varphi_0\} \qquad \textbf{(III-6)}$$

with L_1 the GPS carrier frequency (1575.42 *MHz*), c the NRZ C/A code, d the NRZ data bits.

When processing the GPS signal, it is assumed that the carrier frequency has already been shifted to an IF (*Intermediate Frequency*) denoted by f_I; the studied signal is then:

$$r(t) = \sum_{k=1}^{R} a_k \cdot c[t - \tau_k(t)] \cdot d[t - \tau_k(t)] \cdot \cos(2\pi f_I t - 2\pi L_1 \tau_k(t) + \varphi_0) \qquad \textbf{(III-7)}$$

Without loss of generality, the phase φ_0 is not considered here ($\varphi_0 = 0$).

The delay $\tau_k(t)$ is assumed to have linear variations with time over short durations. Its value depends on two types of multipath replicas: reflected replicas and diffracted ones (Scattered replicas are supposed to have the same representation as diffracted ones, the scattering coefficient being essentially represented by the path amplitude, and the angle of arrival being random). These two cases are illustrated in figure III-6:

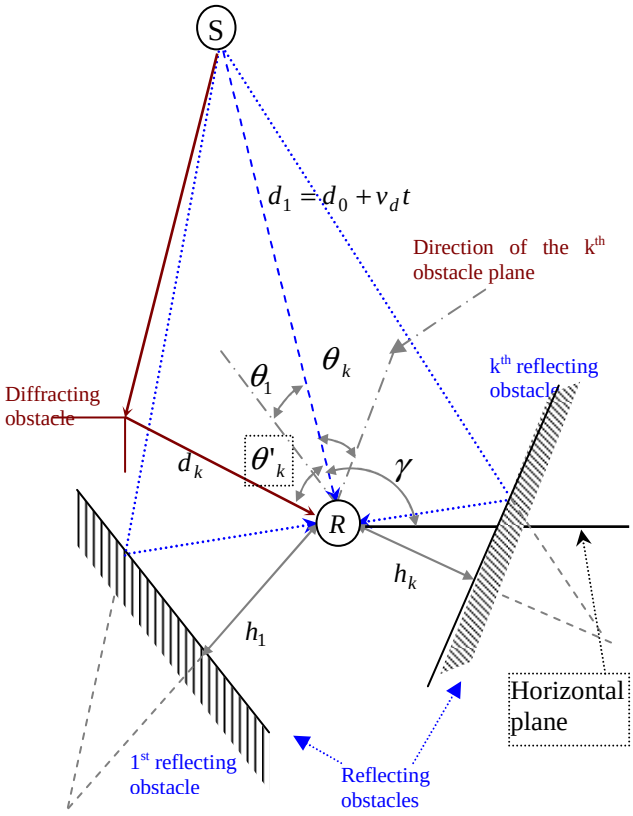

Fig III-6 : Reflected and diffracted rays of a GPS signal. Reflected rays are in dotted lines and diffracted rays are in solid lines. The direct LOS is represented with a dashed line

In the figure above, both diffracting and reflecting obstacles have been illustrated (in red and blue respectively). We denote by d_1 the direct LOS and d_k for $k > 1$ the delayed path.

The receiver is supposed to be at $1\,m$ above the ground level, i.e. in the hand of a user. It is also supposed to be moving horizontally, and the distance between the receiver and the different obstacles around it varies between 0 and $5\,m$ approximately (the user is assumed to be in an office or in a hall).

The delay experienced by the direct LOS ray is:

$$\tau_1 = \frac{d_1}{c} \quad \textbf{(III-8)}$$

where c is the speed of light in vacuum.

$d_1 = d_0 + v_d t$ with d_0 the initial distance between the satellite and the receiver,

v_d the Doppler velocity corresponding to the considered satellite elevation angle. It is given by: $v_d = \frac{v_s r_e \cos\gamma}{\sqrt{r_e^2 + r_s^2 - 2 \cdot r_e \cdot r_s \cdot \sin\gamma}}$ (refer to appendix C), where v_s is the satellite linear velocity, r_e is the earth's radius, r_s is the orthogonal distance between the earth's centre and the satellite, γ is the satellite elevation angle. v_d is also considered constant over the duration of the simulation.

The delays experienced by the multipath replicas are defined with respect to that of the direct LOS. In the case of reflected rays, this is done using a classical model of reflection. The path followed by the reflected ray d_k differs from that of the direct ray d_1 by $2h_k \sin\theta_k$, where θ_k is the angle between the direct ray and the obstacle plane. It has a random value uniformly distributed in $[0;2\pi]$. And, h_k is the distance between the receiver and the obstacle plane. h_k is also supposed to have linear variations with respect to time: $h_k = h_{0k} + v_r t \cdot \sin(\theta_k - \gamma)$, with h_{0k} the initial distance between the receiver and the obstacle; it takes a random value between $[0\ m; 5\ m]$. v_r is the receiver velocity.

Hence, the delay experienced by a reflected ray is expressed as:

$$\tau_k = \frac{d_0}{c} + \frac{v_d t}{c} + 2\frac{h_k}{c}\sin\theta_k \quad \textbf{(III-9)}$$

For diffracted and scattered rays, the delay is given by the ratio of the length of the total path followed by the ray divided by the speed of light. Using figure III-6, Al-Kashi law gives:

$$\tau_k = \frac{\sqrt{(d_0 + v_d t)^2 + (d_k)^2 - 2 \cdot (d_0 + v_d t) \cdot d_k \cdot \cos(\theta_k')}}{c} + \frac{d_k}{c} \quad \textbf{(III-10)}$$

where $d_k = \sqrt{(d_{0k})^2 + (v_r t)^2 - 2 \cdot (d_{0k}) \cdot (v_r t) \cdot \cos(\gamma - \theta_k')}$, and d_{0k} is a random initial distance that lays within $[0\ m; 5\ m]$ also.

The following steps have been followed to generate and acquire a simulated indoor GPS signal according to the model described above:

Generate the signal that is supposed to reach the user based on the signals characteristics model described above,

Add noise to it. The additive noise is such that the carrier to noise density ratio C/N_0 is an input parameter. A 2-bit quantification process is then used. An attenuation of approximately 1.5 *dB* is further induced due to this quantification [*Spilker et al., 1996*],

Acquire the signal using different coherent and non coherent integration times. Throughout the acquisition process the carrier Doppler frequency, the code delay and the C/N_0 ratio are estimated. The result is illustrated by a correlation matrix as was explained in Chapter II. Recall that the detection of the signal is a statistical process based on a hypothesis test:

Hypothesis H_0 : The signal is not present, and the considered cell contains only noise.

Hypothesis H_1 : The considered cell contains noise with signal present.

The threshold was calculated for a PFA of 10^{-3}. In the case of H_1, when it is thought that the Doppler frequency and code delay are found in the best cell, the attenuation due to Doppler and code shift errors is supposed to be negligible, and the value of the peak detected is supposed to be: $\max \approx \frac{A^2}{4} + m_b$ (refer to equation II.13), where m_b is the estimated mean noise level of the correlation matrix and A is the signal amplitude. This allows for computing the power of the useful signal as: $C = \frac{A^2}{2} = 2 \cdot (\max - m_b)$. In other words, once a peak is found at the end of the acquisition process, the signal power can be estimated.

During our simulations, we check the accuracy of the Doppler and the code delay found at the end of the acquisition process, as these two parameters are known a priori for each signal. Indeed, the user-to-satellite distance and the satellite Doppler velocities are input parameters. The delays are calculated according to equations (III.8, III.9, III.10), and the Doppler frequency is calculated to $f_d = -L_1 v_d / c$, with v_d the satellite Doppler velocity (input parameter).

Once the accuracy of the code and Doppler parameters is checked, the signal is said to be successfully acquired only if the correlation peak has the right code and Doppler shifts. A peak which is higher than the threshold, but which is not the right one does not imply a successful acquisition in our tests.

The results reported next are classified in two categories:
1. Impact of multipath on the acquisition performance
2. Impact of cross-correlation on the acquisition performance

III.2.3 Impact of indoor multipath on acquisition performance

In order to study the impact of multipath on the acquisition performance, three types of signals were studied:
- first a LOS only signal (without multipath),
- second a composite signal containing a LOS ray along with different multipath replicas,
- and third a signal with only multipaths rays (NLOS).

These signals are compared with each other. Different GPS signals were tested with different PRNs, code delays, Doppler frequencies, and different multipath parameters with PDF of initial values derived from the ESA model. The multipath replicas have different relative powers, delays and angles of arrival. However, in a given simulation and for the sake of comparison, all of these parameters will be the same in the three cases described above: the LOS only, the composite LOS with multipath replicas and the NLOS case for a specific GPS signal PRN.

For each of these composite signals we try to acquire the original signal using the FFT acquisition algorithm described in Chapter II. First, the coherent integration time, T_p , is set to $1\,ms$ in order to avoid any possible data bit transitions problems. *M* is set to 200, thus yielding a total dwell time of 200 *ms*. The value of *M* was chosen because the signals to be acquired are not too strong, nor too weak. As explained earlier, the acquisition is said to be successful if the detected peak corresponds to the right values of Doppler frequency and code delay of the considered satellite in the input scenario.

For illustration purposes, the results obtained with one of these signals, PRN 1, will be presented here. Its Doppler frequency and code delay were set to $f_d = -4666\ Hz$ and $\tau = 608.276$ chips respectively. These values of the Doppler frequency and code delay, and those used for the upcoming tests, were chosen randomly. The results below show the minimum C/N_0 value that could be acquired in each case.

As illustrated in figure III-7, for a LOS signal without multipath replicas the minimum C/N_0 that could be successfully acquired with a total signal integration time of $0.2\ s$, is $26\ dBHz$.

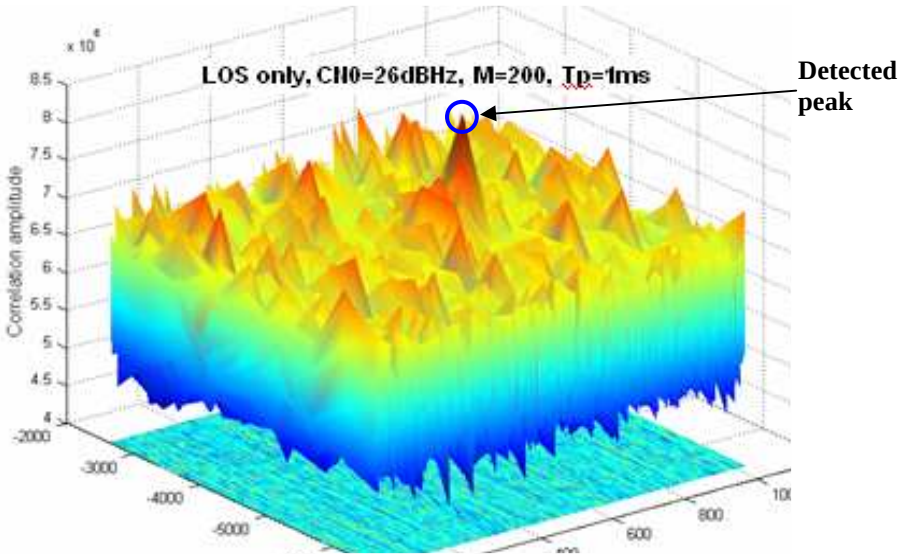

Fig III-7: LOS without multipath replicas; $C/N_0 = 26\ dBHz$ **; true values: Doppler frequency** $-4666\,Hz$ **, code delay** 608.27 **chips; estimated values: Doppler frequency** $-4666\,Hz$ **, code delay** 608.27 **chips**

Theoretically, the minimum C/N_0 that can be detected with such a dwell time and a coherent integration of $1ms$ is: $\cong 28\,dBHz$ for a P_d of 0.9 and $P_{fa} = 10^{-3}$ used here (refer to Chapter II, paragraph II.3.4). The C/N_0 found here is a little lower than the theoretical value. The difference may be due to the test procedure where a limited number of tests were run and

successful acquisition was observed a reasonable number of times. Indeed, these tests were repeated for approximately twenty different signals with different Doppler frequencies, code delays and PRNs.

In the case of a LOS signal with multipath replicas, the minimal C/N_0 that could be detected was rather 27 *dBHz* compared to 26 *dBHz* in the LOS without multipath signal case. This increase in the detectable C/N_0 may be explained by the presence of multipath replicas which raise the global noise level. But even with this small increase in the global noise level, the minimum detectable C/N_0 ratio is still more optimistic (lower) than the theoretical limit. This can be achieved for the same reasons given previously. The output correlation function is represented in figure III-8:

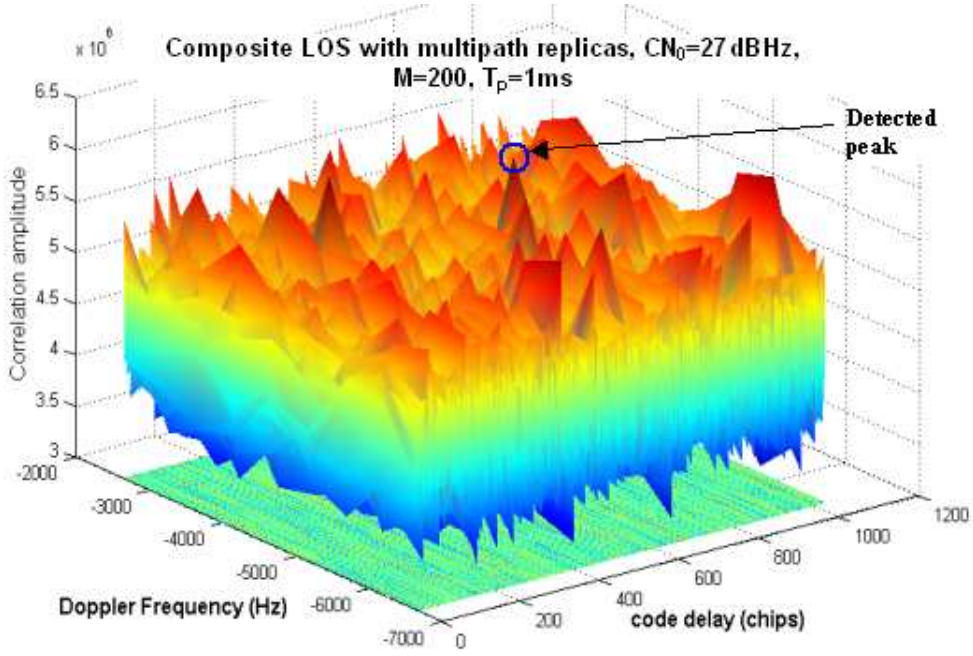

Fig III-8: Composite LOS with multipath replicas; $C/N_0 = 27\,dBHz$ **true values: Doppler frequency** $-4666\,Hz$ **, code delay** 608.27 **chips; estimated values: Doppler frequency** $-4666\,Hz$ **, code delay** 608.27 **chips,**

Notice that the estimated values of the Doppler and the code delay are accurate. Hence multipath replicas did not disturb the final output of the acquisition process. They introduced however a small increase in the global noise level, resulting in a higher threshold C/N_0 (1 *dB* difference in this case) compared to the previous case where the signal studied only comprises a LOS ray.

Figure III-9 shows the output correlation function resulting from the acquisition of a NLOS signal, or in other words of an echo only signal. These multipath replicas are supposed to be those originating from a $44\,dBHz$ LOS signal (the nominal case for a received GPS signal), which was completely masked by walls or ceilings for example. That is, these rays have C/N_0 much lower than $44\,dBHz$ since reflection and diffraction may cause severe attenuations. The lower the signal power, the lower the resulting relative multipaths powers. In this case where the LOS ray is completely masked and only its multipaths replicas are available at the receiver level, an original LOS of at least $44\,dBHz$ was necessary so that its corresponding multipaths replicas could be detectable (with the dwell time of 0.2 *ms* used

here). In other words, for this signal, if a direct LOS signal had a C/N_0 ratio lower than $44\,dBHz$ and could not reach the receiver, the multipath replicas generated cannot be acquired with a dwell time of 0.2 *ms*.

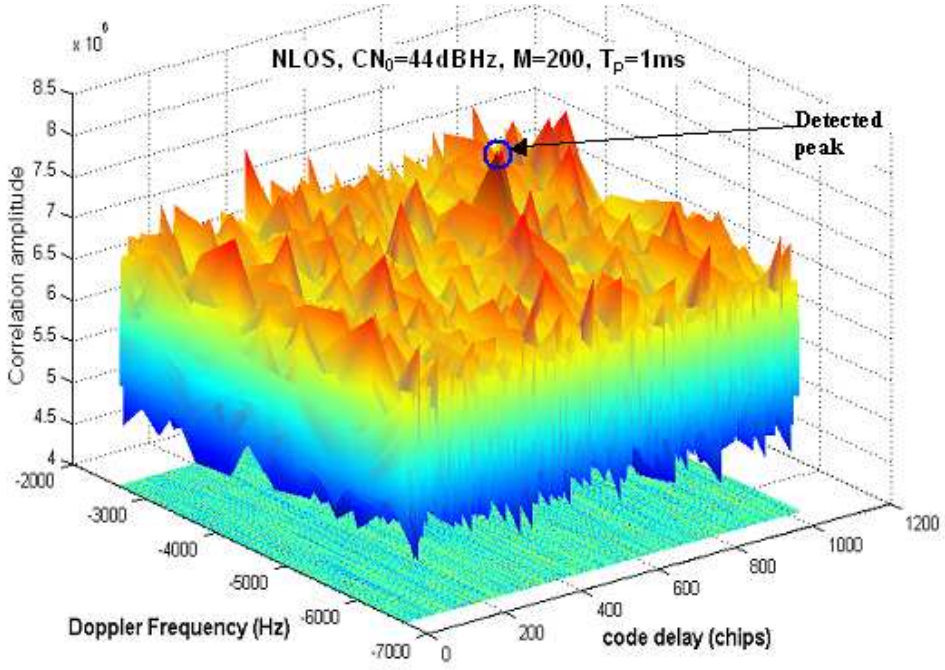

Fig III-9: NLOS signal, multipath replicas only; $C/N_0 = 50\,dBHz$ **(**C/N_0 **of the LOS that could not reach the receiver); true values (of the LOS): Doppler frequency** $-4666\,Hz$ **, code delay** 608.27 **chips; estimated values: Doppler frequency** $-4666\,Hz$ **, code delay** 608.27 **chips**

Comparing this result with that of the composite LOS, there is a difference of 17*dB* between the respective minimum C/N_0 ratios: 27 *dBHz* in the case of the composite LOS versus $44\,dBHz$ in the NLOS case. This 17dB difference between the minimum C/N_0 ratios corresponds to an attenuation with respect to the LOS of 17 *dB*. Thus, supposing that the minimum detectable C/N_0 is 27 *dBHz*, the multipath replicas must be at least at this C/N_0 level to be detected. Notice that the code delay and the Doppler frequency found in the case of the NLOS signal are the same as in the case of the composite signal, yielding that the difference between the detected multipath replica code-Doppler values and those of the LOS (not present) lies within the tolerated acquisition errors for this dwell time where the Doppler accuracy needed is of 250 *Hz* and the code delay accuracy needed is $0.2\,\mu s$ corresponding to a sampling frequency of $5\,MHz$ used here.

The results obtained with other signals were similar to those presented here: for a LOS only signal, the minimum detectable C/N_0 using $0.2\,s$ of dwell time with $1\,ms$ of coherent integration is approximately 26 *dBHz*. In the case of a composite LOS signal, the minimum detectable C/N_0 varied between 26 *dBHz* and 27 *dBHz*. In the case of NLOS signals, the limit C/N_0 was between 40 and $44\,dBHz$ for the masked LOS.

The Doppler frequency and code delay found at the end of the acquisition process in the case of a NLOS signal are a good first approximation of these two parameters to be able to launch the tracking process. However, the final position is sure biased. The bias depends on the multipath characteristics, but at least it provides a solution. The bias is expected to be of

the order of several tens of meters (the indoor delay is most likely of the order of several tens of *ns* as shown in figure III-5) compared to the accuracy reached if the LOS was rather acquired.

In all cases multipath replicas did not induce failures of the signal acquisition, but induce errors on the estimated code delay and Doppler frequency when tracking. This is why it turns out to be the main source of error in indoor environments for tracking issues [*Lachapelle et al., 2004*].

III.2.4 Impact of indoor cross-correlation on the acquisition performance

After having studied the effect of multipath on signal fading in indoor environments, the next step is to study the impact of interference between different GPS satellite signals. In fact there are situations where a strong signal may interfere with another weak signal path. In this case, acquiring the weak signal is very difficult, as it may be affected by cross-correlation peaks. In the case of zero Doppler offset, this cross-correlation peak is generally expected at approximately -23.9 *dBHz* below the autocorrelation peak [*Proakis, 1995*]. Thus theoretically, if two signals have C/N_0 ratios about 24 *dB* apart from each other, the autocorrelation peak of the weaker signal is approximately at the same level as that of the strong signal cross-correlation peaks and thus is masked by the this strong signal. To illustrate this situation, we used the same model that was developed for the multipath simulation, and extended it to support different satellite signals by adding these signals together. Different tests were conducted using one simulated satellite signals with different powers, interfering with each other. The number of interfering GPS signals was set to only two signals for the sake of simplicity. Although it may seem optimistic, this assumption can be a good first step. Note that in indoor environments the number of strong signals is not likely to be high (one or two strong signals at most).

The results obtained for signals emitted by PRNs 1 and 11 are presented hereafter. The PRN numbers were randomly chosen. The C/N_0 ratio for PRN 1 was set to 50 *dBHz*, while that of PRN 11 was set to 25 *dBHz* with a difference of 25 *dBHz* between the two signals so that cross-correlation peaks could appear in the cross-correlation function. Satellite 1 has a null Doppler, while satellite 11 has a Doppler frequency of $-4075\,Hz$. The 2 satellites have also different code delays: 608.276 and 604.035 chips respectively. We tried to acquire PRN 11. The dwell time was increased up to 1 second but no right peak could be detected. The result of acquisition is depicted in figure III-10.

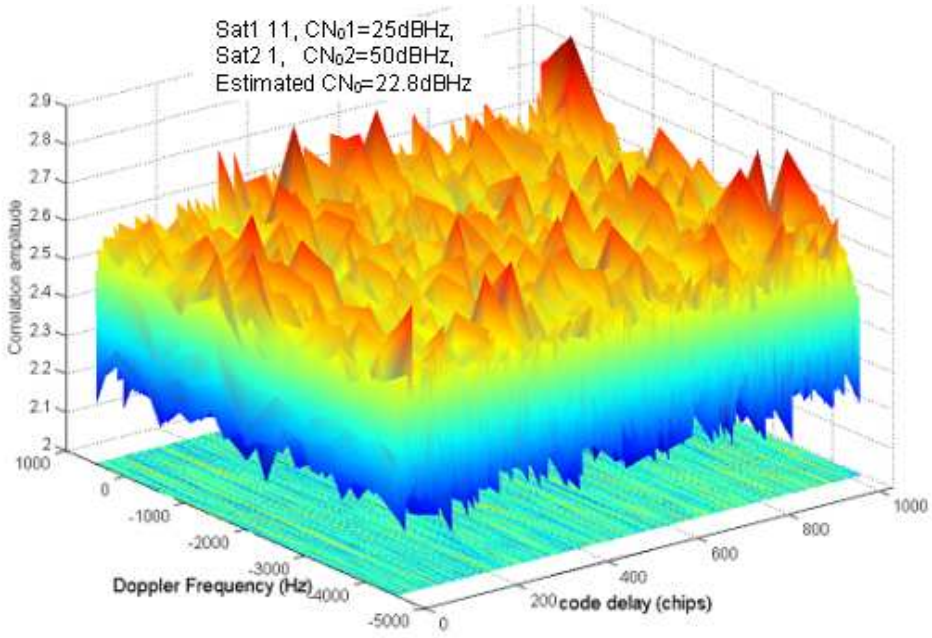

Fig III-10: Cross-correlation between 2 GPS signals: 1- LOS signal of satellite number 11 with multipath replicas, true Doppler $-4075\ Hz$ **, true delay** 608.27 **chips, initial** $C/N_0 = 25\ dBHz$ **2- LOS signal of satellite number 1 without multipath replicas, true Doppler** $0\ Hz$ **, true delay** 604.03 **chips,** $C/N_0 = 50\ dBHz$ **. The signal acquired is that of PRN 11. Estimated values: Doppler frequency 0Hz, code delay** 280.24 **chips,** $C/N_0 = 22.8\ dBHz$

The peak detected after acquisition does not match with the code delay and Doppler frequency of PRN 11 (0 *Hz*; 980.239 chips), nonetheless, it is higher than the acquisition threshold. This means that the acquisition algorithm would have as outputs the code delay and Doppler frequency corresponding to this peak, rather than rendering a failed attempt. In addition, this peak is found at approximately $-27\,dBHz$ below the initial C/N_0 applied to the signal of this satellite, namely 50 *dBHz*. By accounting for the attenuation due to the quantification process (1.5 *dB* approximately), the estimated C/N_0 corresponding to this peak will be very close to the theoretical value for cross-correlation peaks, $-25dBHz$ approximately. This leads us to assume that this peak is most probably a cross-correlation one, not a noise peak. Note that the error resulting from the difference between the detected peak delay (980.239 chips) and the true delay (608.276 chips), is in this case greater than 300 chips, that is 300 μs . This error results in a 90 *km* range error!

In order to be sure that the detected peak is a cross-correlation one, we correlated the signal of PRN 1 alone without noise, with the C/A code of satellite 11, in order to compute the cross-correlation matrix of the signal of sat1 with PRN 11. The detected peak has the same (Doppler frequency, code delay) couple as that of figure III-10.

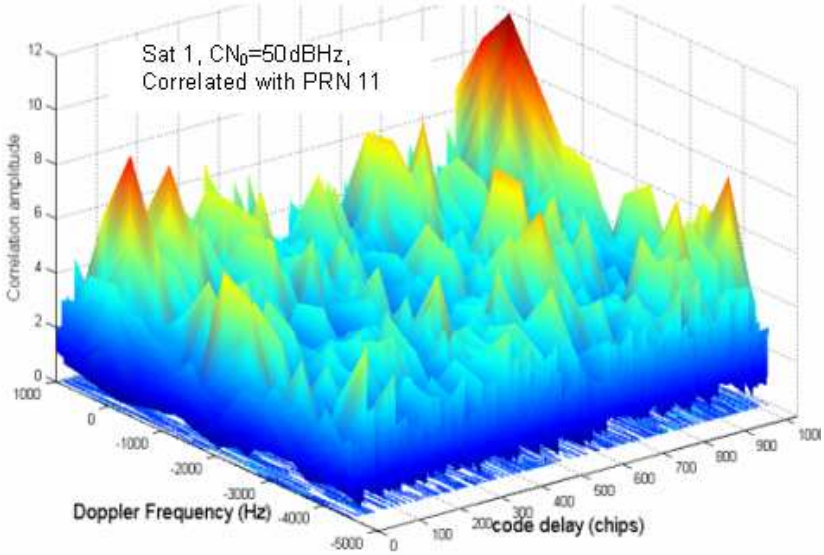

Fig III-11: LOS signal of satellite number 1 without multipath replicas or noise, true Doppler $0\ Hz$ **, true code delay** 608.27 **chips, signal correlated with C/A code of satellite number 11. Estimated values: Doppler frequency** $0\ Hz$ **, code delay** 980.03 **chips**

Figure III-11 shows the result of the cross-correlation between the signal of satellite 1 and PRN code 11.

Generally, the cross-correlation matrix is not supposed to have peaks which are stronger than others. Theoretically, all peaks must have the same amplitude. But this is not the case in figure III-11 where many peaks are stronger than others. This may be due to the additive noise, and the effect of the code Doppler drift, which may cancel or increase some cross-correlation peaks.

Figure III-12 illustrates another case where a cross-correlation peak is detected. It was also verified that the detected peak is a cross-correlation one by the same way as before.

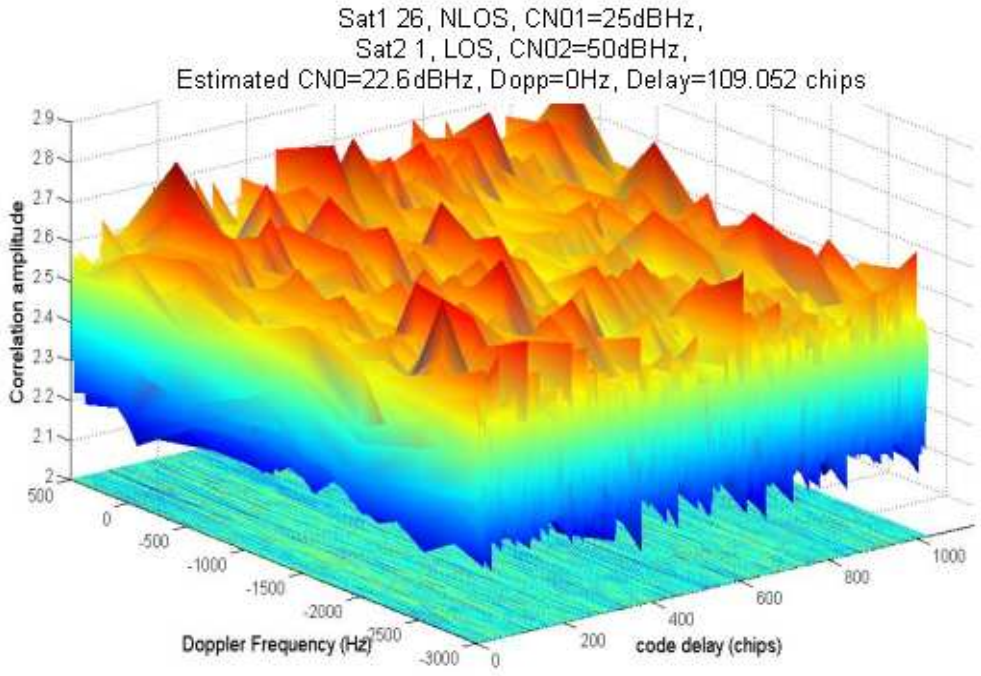

Fig III-12: Cross-correlation between 2 GPS signals: 1- Non LOS signal of satellite number 26 (just multipath replicas), true Doppler $4000\ Hz$ **, true delay** 604.03 **chips, initial** $C/N_0 = 25\ dBHz$ **2- LOS signal of satellite number 1 with multipath replicas, true Doppler** $0\ Hz$ **, true delay** 608.27 **chips, initial** $C/N_0 = 50\ dBHz$ **. Estimated values: Doppler frequency** $0\ Hz$ **, code delay** 109.05 **chips,** $C/N_0 = 22.6\ dBHz$

In this second case the delay error is of 500 chips approximately, inducing a 150 *Km* range error!!

Figures III-10 and III-12 show that the cross-correlation induced errors may be far from the acquisition error bounds. In fact, the cross-correlation resulting error is only limited by the C/A code period of 1ms, i.e. 1023 chips. This error is completely random within this period. Consequently, cross-correlation peaks disturb the acquisition, unlike multipath replicas, especially in the case of a weak signal in the presence of a strong one. It must be mentioned that the weakest signal, that of satellite 11 at 25 *dBHz* in the first case for example (figure III-10), could be easily acquired using the same dwell time, if there were no interfering signal apart from noise.

In conclusion, the main impact of GPS cross-correlation on the acquisition performance is a probable cross-correlation peak, which leads to inaccurate values of the Doppler frequency and the code delay, and hence to inaccuracies in the user position estimation.

On the other hand, the peak detected by the acquisition algorithm is likely to be a false alarm one. Thus it is generally difficult to be sure that a peak is a cross-correlation one or not, making it more difficult to deal with such peaks. A partial solution allowing for avoiding some cross-correlation peaks is inherent to the AGPS (*Assisted GPS*) technique. This will be explained in details in Chapter V. Many other methods for cross-correlation peak detection and/or cancellation were studied [*Norman et al., 2004 & 2001*], [*Turetzky, 2004a & b*], [*Mattos, 2003*], [*Krasner, 2001*]. Norman et al. [*2004, 2001*] describes for example a method which consists in finding the strongest PRN in the received signal, to correlate it with each of the other PRNs of this signal, and subtract the resulting cross-correlations from each PRN auto-correlation function. This method is called strong signal cancellation.

As a conclusion on the indoor channel acquisition, it was found that the cross-correlations are much more problematic than multipaths replicas. This is only true from an acquisition point of view. But in the context of a complete positioning scheme (acquisition, tracking, demodulation of navigation data bits, navigation solution computation), detecting false alarms in the acquisition stage is much better than detecting them after that, since this will be a waste of time. Consequently, in this case multipaths are an important source of error, and more disturbing than cross-correlation peaks since they are very hard to be detected earlier.

In what follows, we focus on the urban channel.

III.3 Modelling the urban channel

The urban channel has not been modelled by our work. Instead, we have used an existing time varying model developed by the DLR for this purpose. It is briefly described in the next paragraph.

III.3.1 Land Mobile Multipath Channel Model

This model, called LMMCM (*Land Mobile Multipath Channel Model*), is based on both deterministic and stochastic processes within an artificial scenery that can be parameterized. The model is available for download. Figure III-13 below presents an example of an urban environment simulated using LMMCM [*Steingass et al., 2004, 2005*].

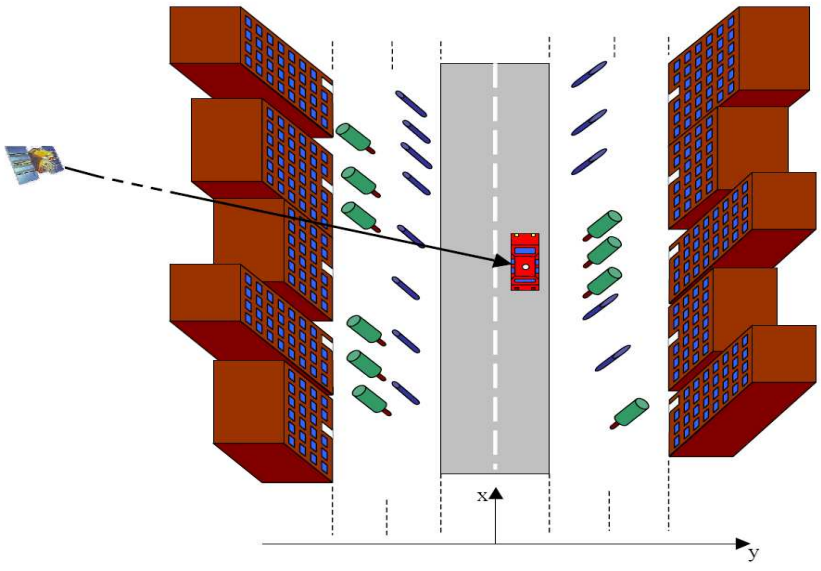

Fig III-13: Artificial scenery [*Steingass et al., 2005*]

The model parameters were derived based on real measurements carried out using a channel sounder.

For this model, the GPS receiver is assumed to be onboard a car that is moving in the north direction. All the components of this scenery can be parameterised, like the car velocity, the road width, the building and house heights, shapes and separations, the trees and pole positions, the satellite position, etc. The satellite position is determined by its azimuth and elevation angles. During this study, for comparison purposes, the buildings shape is considered to be the same, only the impact of the satellite position and the road width will be studied. It must be mentioned that in this model the LOS path is handled in a special way. Due to diffraction effects that can occur at building obstacles the LOS is split into two or three separate paths for certain geometries. These diffracted replicas are considered as LOS; thus the LOS delay may differ from zero if it is diffracted at a house front.

III.3.2 Impact of urban multipath on acquisition performance

The impact of multipath on acquisition performance is assessed by analysing the two parameters which characterise multipath echoes: their relative delays and powers, as for the indoor environment [*El Natour et al., 2006b*]. Two tests are reported here for each environment, using correspondingly two different road widths. In each test the satellite elevation angle and azimuth vary and their effect is analysed. For narrow streets, the environment corresponds to downtowns: the buildings considered have mean heights and are supposed to have small separation distances between them. Larger streets point out to canyons where the buildings are very high with large separations between them. Low elevation angles (<30°) are not considered because they are supposed to be masked. The car velocity is kept at 50*km*/*h*. Table III-1 summarizes the parameters used in each test. The road width and building average height and separation parameters were chosen according to typical values recommended by a civil engineer, and an architect.

	Road width (*m*)	Satellite Elevation(°)			Satellite Azimuth(°)			Buildings average Height (*m*)	Buildings average separation (*m*)
Test A	4 *m*	30	60	90	-30	0	60	12	2
Test B	12 *m*	30	60	90	-30	0	60	60	30

Tab III-2 : Parameters used in tests conducted to study the impact of urban multipath on acquisition performance

Note that a null azimuth corresponds to the north direction. The positive values refer to azimuth in the east whereas negative values correspond to the west direction. 5000 iterations (position and received rays calculations) are considered for each test case, with a sampling frequency of 150 *Hz*. Furthermore, each test case is repeated 5 times. 18 different simulations are necessary to cover all the possible combinations of the satellite elevation angles and its azimuth angles for both the downtown and urban environments. In the following subsections, only the most representative figures for the simulation results obtained in downtown and urban canyon environments are reported and a summary of all the results obtained is given in tables III-3 and III-4 with some concluding remarks on all of these tests following. The output is the PDF that an echo exists at a defined power level and a defined delay relative to the direct path.

Test A: Downtown environment (most representative figures): road width 4 *m*, one way road, car driving in the middle of the road, 1 *m* large sidewalks, no trees nor poles, mean buildings height 12 *m*, mean separation 2 *m*.

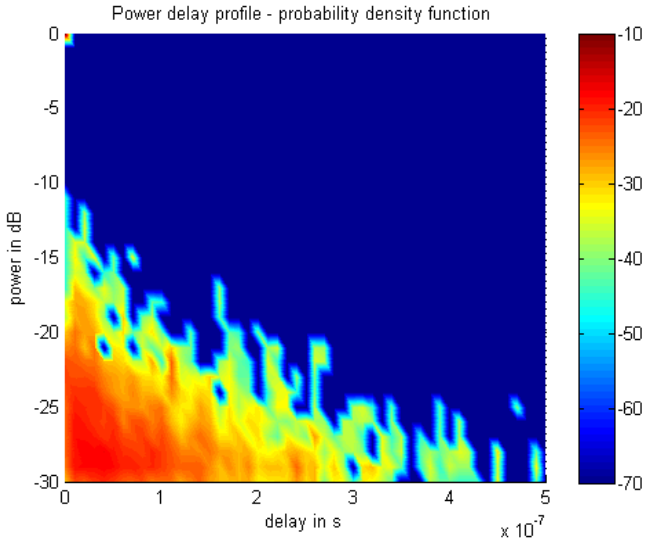

Fig III-14 : PDP and PDF for a satellite elevation angle of 30° and an azimuth of 0°, for test A (downtown environment)

The colour bar on the right represents the PDF in a base 10 logarithmic scale (log). The LOS (with its diffracted replicas) can be seen at null delays, where the original LOS signal is seen at a null power (recall that the y axis corresponds to the echoes relative power with respect to that of the LOS). Other attenuated signals with null delays are most probably LOS diffracted replicas, however there may be some reflected signals with nearly null delays also. In this figure, the maximum excess delay of the channel is higher than $0.5\,\mu s$. The echoes with quasi null delays appear at an attenuation of –10 *dB*, followed by peaks at ($0.02\,\mu s$, -11 *dB*) representative of multipaths having travelled a few meters more than the LOS (6 *m* in this case). Note that according to these figures, the maximum probability density is obtained for echoes occurring at $(0.04\,\mu s, -28.5\,dB)$.

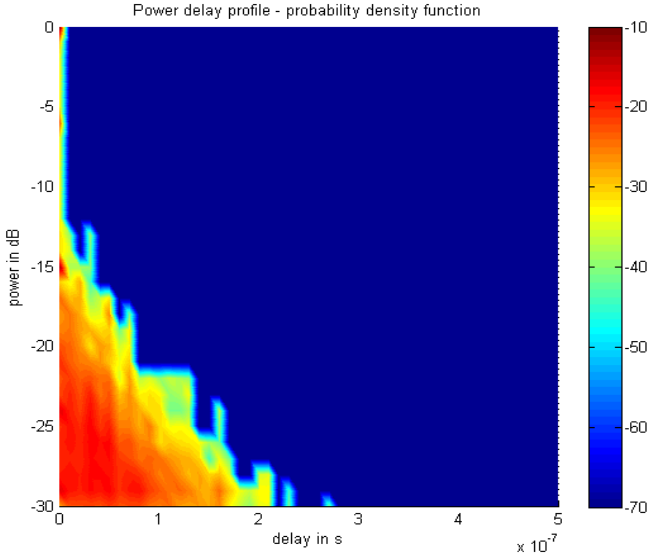

Fig III-15 : PDP and PDF for a satellite elevation angle of 60° and an azimuth of 60°, for test A (downtown environment)

For the elevation angle of 60° and an azimuth of 60°, the maximum excess delay is of $0.28\,\mu s$. The echoes are a little bit more attenuated than before, where the elevation angle was of 30° and the azimuth was of 0°. Notice the presence of high power-null delays replicas in this case which imply more diffracted signals than before.

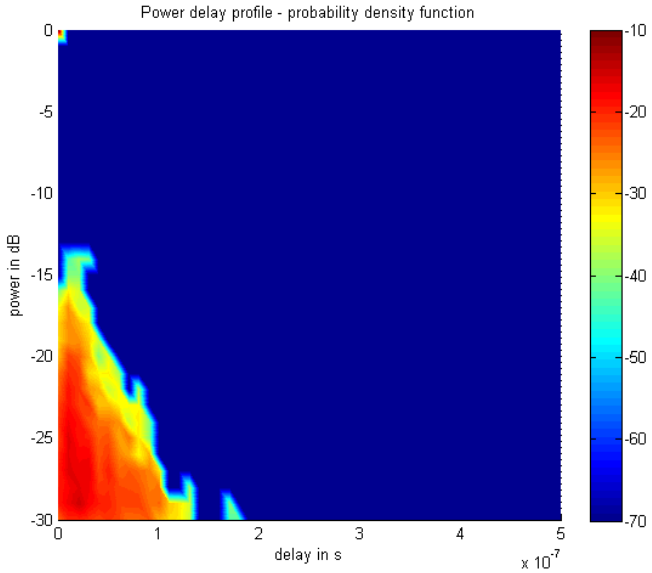

Fig III-16 : PDP and PDF for a satellite elevation angle of 90° and an azimuth of -30°, for test A (downtown environment)

The maximum excess delay in the case of an elevation angle of 90° and an azimuth angle of –30°, is still lower than in the case of a 60° elevation angle and 30° azimuth. The replicas at null delays are more attenuated (-15 *dB*), while a peak appears at $(0.01\,\mu s, -12\,dB)$. This delay corresponds to a distance of 3 *m* which is representative of the distance separating buildings from the car antenna (2 *m* approximately). The most probable echoes occur at $(0.02\,\mu s, -29\,dB)$.

Test B: Urban canyon (most representative figures): road width 12 *m*, two ways road, car driving on the right side, 3 *m* large sidewalks, road boarded with trees and poles on the

two sides, mean buildings height 60 *m*, mean separation 30 *m*. The trees attenuation is in average equal to 6 *dB*. This attenuation corresponds to the limit between light (35%) and dense (80%) foliage [*J. Miller et al,. 1995*].

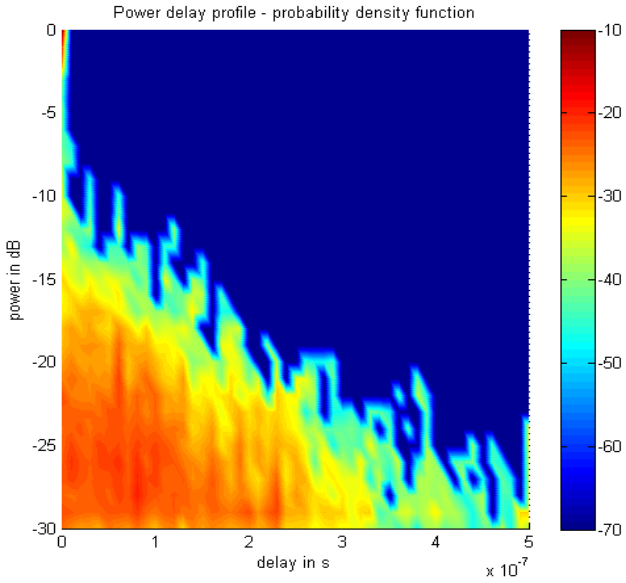

Fig III-17 : PDP and PDF for a satellite elevation angle of 30° and an azimuth of 60°, for test B (urban canyon)

In this case where the elevation angle is of 30° and the azimuth angle is of 60°, the maximum excess delay is once again higher than $0.5\,\mu s$, which is very penalizing in the case where the LOS would be completely masked. On the other hand, the first echoes occur with only –6 *dB* attenuations compared to the LOS. Strong multipaths ($-8dB$) appear also at $0.03\,\mu s$ corresponding to $9\,m$. This distance is higher than that found in test A, reflecting a correlation between the strongest multipath delays and the road width, or the distance between buildings and the receiving antenna.

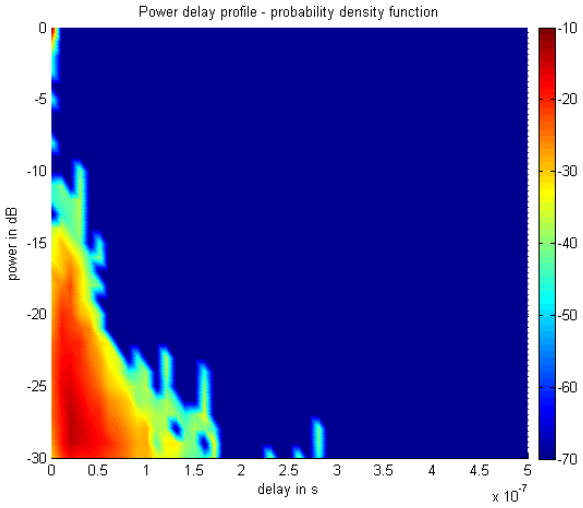

Fig III-18 : PDP and PDF for a satellite elevation angle of 60° and an azimuth of 0°, for test B (urban canyon)

In this case where the elevation angle is of 60° and the azimuth is of 0°, strong multipaths can be found at ($0.03\,\mu s, -10\,dB$) as before, which is not surprising since the buildings and road

parameters are still the same. The most probable echoes occur at $(0.021\,\mu s, -28\,dB)$, compared to $(0.08\,\mu s, -28\,dB)$ in the previous case, yielding that most probably the echoes occur at -28 *dB* attenuation approximately, with delays depending on the satellite elevation: shorter delays for higher satellites.

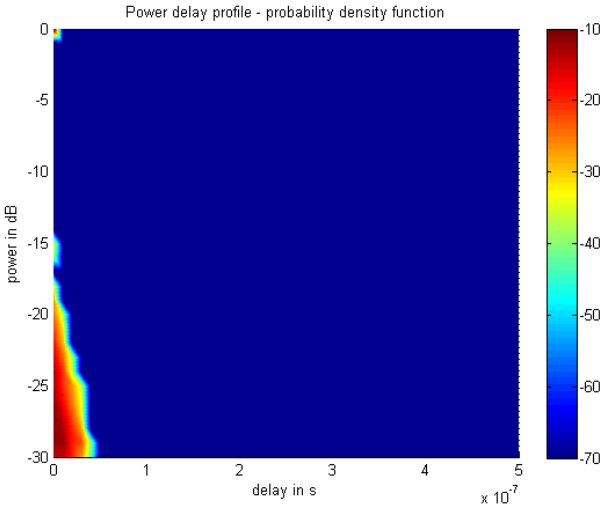

Fig III-19 : PDP and PDF for a satellite elevation angle of 90° and an azimuth of -30°, for test B (urban canyon)

A clear drop in the maximum excess delay ($0.05\,\mu s$) of the channel can be seen in this figure. Furthermore, no strong echoes can be found at null delays, the first one being at -15 *dB* away from the LOS.

Tables III-3 and III-4 summarize the results obtained in all the 18 cases tested, where the minimum attenuation parameter corresponds to the minimum attenuation of a multipath replica compared to the LOS.

Elevation angle	30°			60°			90°		
Azimuth	-30°	0°	60°	-30°	0°	60°	-30°	0°	60°
Maximum excess delay (μs)	≥0.5	>0.5	>0.5	0.33	0.29	0.28	0.2	0.48	0.25
Minimum attenuation (*dB*)	-15 to -12	-10	-12 to -9	-10 to -5	-5 to -10	-12	-15 to -12	-15	-10 to -8
Most probable echoes	0.03 μs (9 *m*); -28.5*dB*	0.04 μs (12 *m*); -28.5 *dB*	0.05 μs (15 *m*); -28 *dB*	0.01 μs (3 *m*); -27 *dB*	0.042 μs (12.6 *m*); -28 *dB*	0.02 μs (6 *m*); -29 *dB*	002 μs (6 *m*); -29 *dB*	0.02 μs (6 *m*); -28.5 *dB*	0.04 μs (12 *m*); -28 *dB*

Tab III-3 : Results obtained in test A (downtown environment)

Elevation angle	30°			60°			90°		
Azimuth	-30°	0°	60°	-30°	0°	60°	-30°	0°	60°
Maximum excess delay (μs)	0.5	0.45	≥0.5	0.32	0.29	0.28	0.05	0.18	0.15
Minimum attenuation (*dB*)	-10	-18	-5	-10	-11	-10	-15	-7	-9
Most probable echoes	0.02 μs (6 *m*) -28 *dB*	0.03 μs (9 *m*) -28.8 *dB*	0.08 μs (24 *m*) -28 *dB*	0.04 μs (12 *m*) -28.5 *dB*	0.02 μs (6 *m*) -28 *dB*	0.01 μs (3 *m*) -28 *dB*	0.06 μs (18 *m*) -28.5 *dB*	0.01 μs (3 *m*) -29 *dB*	0.008 μs (2.1 *m*) -28 *dB*

Tab III-4 : Results obtained in test B (urban canyon)

The first remark that comes out from the comparison of these two tables is that for downtown environments multipaths attenuations have larger variation ranges than for urban canyons, as it can be observed through the comparison of the respective "Minimum attenuation" entries of tables III-3 and III-4. Indeed, for urban canyons, the minimum attenuations obtained throughout the different tests were very close to each other, with maximum differences of 1 *dB* from one simulation to another. This may be explained by the increasing complexity of such environments.

According to the results of these tests, the maximum excess delays depend on the satellite elevation angle. They decrease with increasing elevation angles: $(\cong 0.5\,\mu s, 30°)$, $(\cong 0.3\,\mu s, 60°)$ and $(\cong 0.2\,\mu s, 90°)$ in average. We could not derive a conclusion on the relation between the maximum excess delays and the azimuth angle, although the street is oriented North-South. The attenuation of the strongest echoes was not neither clearly related to the elevation and azimuth angles. It varied between –5 *dB* and –18 *dB*. We noticed however a small increase in the average multipaths relative powers at elevation angles of 60° and 90°.

On the other hand, in all cases the LOS was likely to reach the receiver, but at some epochs of the simulations no LOS was available resulting in the acquisition of an echo only signal, which is problematic for the overall performance. Note that the availability or not of the LOS and multipath echoes could be seen while the simulation was running thanks to another output of the algorithm which visualises the LOS and echoes amplitudes and phases in "real time". But the quasi exponential shape of the impulse response implies that echoes with very large delays occur at very low relative powers. The PDF distribution also suggests that these echoes are not very probable. This means that according to these results, in urban environments, echoes with large delays are not very likely to occur and will be weak. Thus from an acquisition point of view, the delays fall within the tolerated error on the code delay, and do not disturb acquisition. Conversely, in the absence of a LOS, the tracking loops are launched with such delays leading to positioning errors; this is why it is always desirable to eliminate such errors in the acquisition stage, as already explained. However as already explained in the case of indoor multipaths, when absolutely no LOS is present these multipaths lead to errors but at least provide a solution with errors most probably of the order of 3 to 24 *m*, according to the results obtained here. The precision constraints depend on the final application requirements. Integrity algorithms may be used to accept or reject such solutions.

III.3.3 Impact of cross-correlations on acquisition performance

Cross-correlations could not be thoroughly studied using the LMMCM, since it only handles one satellite transmitting at a time. However, the results conducted to study the impact of multipath showed that globally the LOS is likely to be present, especially in urban canyons. But the availability of this LOS depends on the studied environment and more specifically on the satellite position. This means that in the case of more than one satellite, with each one having its own elevation and azimuth angles, their LOS have different probabilities to reach the receiver. If one of these signals is masked, or greatly attenuated, cross-correlation problems arise; the most probable echoes or diffracted LOS attenuations (signals at null delays), is 28 *dB* according to the previous results, thus large power discrepancy may exist between 2 satellite signals reaching the receiver together. This is a typical situation leading to cross-correlation problems, knowing that a cross-correlation appears when the relative powers are approximately 24 *dB* apart. Consequently, cross-correlations are highly possible sources for large pseudorange errors in urban environments. This result is confirmed by [*MacGougan, 2003*].

III.4 Synthesis of the GPS indoor and urban channels problems

In this chapter the impact of multipath and cross-correlation on the GPS signal acquisition has been investigated for indoor environments using our time varying model developed for this purpose, based on statistical analysis given by [*Pérez-Fontán et al., 2004*], and for the urban environment using the LMMCM model developed by the DLR (*German Aerospace Centre*).

First for indoor environments, three types of GPS signals have been generated and tested: a direct LOS only signal, a composite LOS signal with multipath replicas, and a NLOS signal which contains only multipath replicas. The cross-correlation effect has been studied by adding two of these signals together.

The study has focused on the capacity of detection of a correlation peak or, in other words, on sensitivity issues, and the accuracy of the code and Doppler predictions; the total time needed for acquisition was not analysed. Instead, a fixed dwell time of 200 *ms* has been chosen such that the signals that can be acquired are not very low nor very strong (C/N_0 around 27 *dBHz*).

The results show that for indoor cases the multipath replicas have minor impact and do not disturb the acquisition performance, when a direct LOS is present. In some cases they induced a small increase in the noise floor (1 *dB* at a maximum). But they do not influence the output Doppler frequency and code delay. In a NLOS case, multipaths could be used for acquisition (that is acquired in order to provide a solution even if it is not very accurate), but they are much attenuated compared to the LOS signal, and longer dwell times are needed to acquire them. The relative attenuation of multipath replicas (compared to the LOS amplitude) observed during simulations with our indoor channel model, varied between 14 and 17 *dB*. The output code delay and Doppler frequency were within the proper code and Doppler tolerated error bins, for the acquisition process. The minimum detectable C/N_0 ratios found in indoor with the 0.2 *s* dwell time used, are: approximately 26 *dBHz* for LOS only signals,

about 27 *dBHz* for composite LOS signals, and between 40 and 44 *dBHz* for NLOS signals, where 40 and 44 *dBHz* are the C/N_0 ratios of the LOS before complete shadowing.

Cross-correlations are particularly disturbing when a strong and a weak signal reach the receiver together. But this is not very common [*MacGougan, 2003*] unless a signal reaches the receiver through a window for example. In such situations, a cross-correlation peak is likely to cause a false alarm, and consequently a very high range error (in the *Km* level).

The results presented in this chapter concerning indoor environments, correspond to rooms with external building walls, i.e. walls that form the building outer shape; for more confined rooms the performances are expected to be much more degraded.

Second, two types of urban environments were studied using the LMMCM model: a downtown and a canyon environment. Again, the multipath and cross-correlation impacts on acquisition were studied.

The tests conducted with the LMMCM showed a clear correlation between the maximum excess delays and the satellite elevation angle: the maximum excess delays decrease with increasing satellite elevation angles. Very short delays of the order of $50\,\eta s$ ($15\,m$) were found at an elevation angle of $90°$. Such delays though not perturbing for acquisition purposes for GPS L_1 C/A, are very difficult to be identified in the acquisition; thus the tracking loops are launched with erroneous delays. Note however that the resulting solution may be acceptable for some applications. No clear correlation was found between this value and the azimuth angle.

On the other hand, the attenuation of the strongest echoes in urban environments varied between $-5\,dB$ and $-18\,dB$, and did not present a clear correlation with the satellite position.

In the downtown and the canyon environments, the LOS could reach the receiver most of the time. But could be non available in some cases inducing the acquisition of echo only signals and cross-correlation problems as well. Yet when the conditions are bad, depending on the application, it may be better to provide the tracking loops with these initialisation values, which may be a good first approximation, and even to do the position determination with a reflected signal than not being able to determine a position at all.

Notice that compared to multipath peaks, cross-correlation peaks generally result in very large error since the corresponding peaks may occur at random code delays, whereas the multipaths delays depend on the LOS delay, and they are progressively attenuated with increasing delays. This is true for indoors and urban environments.

An obvious common conclusion to all of these results is that when the LOS signal is not hardly attenuated or masked, there would not be any problem. At this stage, the next step would be either to analyse the cross-correlations and find means to detect them and eliminate them or enhance the receiver sensitivity to weak signals so as to ensure a higher detection probability. Different solutions already exist to eliminate cross-correlations and most of them are patented. Another technique to reduce cross-correlation effects is to use the AGPS as it is explained in Chapter IV.

As for weak signals, they consist in signals with C/N_0 lower than $30\ dBHz$ (the approximate performance limit of a normal receiver as it was found in Chapter II). In fact, below this limit, cross-correlation problems become possible (since a gap of 24 *dB* is then possible between two zero Doppler signals knowing that the maximum possible C/N_0 for a GPS signal is of 50 *dBHz* approximately). Consequently, availability and accuracy appear to be problematic for a standalone GPS receiver and enhancements must be provided to this localization technique. HSGPS (*High Sensitivity GPS*) and AGPS (*Assisted GPS*) are yet more interesting methods also used to enhance the GPS receiver performance. These two methods will be the object of the next chapter.

Beyond these system enhancement techniques, rigorous signal processing methods must also be used to perform acquisition. Processing such signals implies a need for longer processing times, and thus longer TTFF. Obviously, an efficient acquisition algorithm is a mandatory in this case, in order to lessen complexity and reduce processing time. This is particularly true for the acquisition where little a priori information is available and the search space is maximal. Such advanced signal processing techniques will be the object of Chapters V and VI.

Résumé du chapitre IV

Les récepteur GPS conventionnel n'étant pas capable de fonctionner tout seul dans des environnements sévères, ce chapitre présente deux techniques d'amélioration de ce type de récepteurs, notamment l'AGPS ou le GPS assisté et le HSGPS ou GPS à haute sensibilité.

Par définition, la technique dite HSGPS est toute technique permettant d'augmenter le gain réaliser lors du traitement du signal GPS à des niveaux supérieurs au niveau standards pour être capable de détecter des signaux faibles. De façon générale, l'implémentation de cette technique est basée sur l'intégration cohérente et non-cohérente sur des périodes supérieures à $20\,ms$, pouvant atteindre quelques centaines de ms voire même quelques secondes dans certains cas. Cependant, à des niveaux de signaux aussi faibles, les problèmes d'intercorrélations, de multitrajets et d'autres types d'interférences sont beaucoup plus significatifs. Les récepteurs conventionnels ne descendent pas à ces niveaux assez faibles car ils n'intègrent pas des techniques de détection et de réjection de telles perturbations. Les récepteurs HSGPS eux sont capables de traiter des signaux très faibles à l'aide de longues intégrations et doivent ainsi combiner de telles techniques de réjection.
Cette technique présente plusieurs problèmes, dont le traitement des transitions des bits de données qui ont lieu toutes les $20\,ms$ et qui résultent en une inversion du signe de la corrélation dans un contexte de longues corrélations, pouvant ainsi résulter en un résultat nul ou très faible. En outre, même si les bits de données étaient connus au préalable, des intégrations aussi longues nécessitent une résolution Doppler beaucoup plus fine. Dans ce cas, toute erreur fréquentielle résiduelle après la compensation en Doppler pourrait causer l'atténuation de la puissance du signal à la sortie du corrélateur. Et finalement, les intégrations assez longues induisent une complexité accrue du récepteur.
En résumé, la réduction du niveau de bruit à la sortie du corrélateur pour l'acquisition et la poursuite de signaux faibles relèvent de la maximisation de l'intervalle d'intégration tout en minimisant les erreurs fréquentielles résiduelles. Ainsi, prédire les transitions des bits de données et limiter les erreurs résiduelles en fréquence pendant la corrélation cohérente sont nécessaires pour obtenir un gain optimal avant d'intégrer en non-cohérent. La technique du AGPS permet de prédire les bits de données avant d'entamer le traitement du signal.

En effet l'AGPS est reconnue pour être la technique la plus promettant en termes de positionnement, de couverture et de précision pour pouvoir remplir les conditions assez contraignantes des services LBS. Cette technique peut être utilisée indépendamment de la technique HSGPS, comme elle peut lui être complémentaire.
La solution de l'AGPS pour compenser le manque d'information lors de l'acquisition et pour améliorer la sensibilité et diminuer la complexité de cette étape du traitement du signal GPS, est de fournir au récepteur GPS une information de temps et/ou des données de positionnement à l'aide d'un récepteur GPS de référence qui aurait une vision directe avec les satellites de la constellation. Ces données dites d'assistance sont envoyées au récepteur mobile via le lien cellulaire (GSM par exemple). La réduction de la complexité de l'acquisition d'une part diminue le temps nécessaire à cette étape, le temps étant un paramètre très important dans la commercialisation de tels produits. Elle permet d'autre part, de réduire la consommation en puissance, ce qui est également très important pour des appareils mobiles.

Avec ces données d'assistance, le récepteur mobile n'a donc plus besoin de télécharger les données d'éphémérides ou toutes autres données de navigation du message de données du satellite GPS. Ces données lui sont plutôt fournis via le lien cellulaire du téléphone mobile en parallèle avec une information de temps et de position approximatifs fournis par le réseau cellulaire. La présence des données d'éphémérides permet au récepteur d'effectuer les mesures de pseudorange en utilisant des temps d'intégration plus longs, même dans le cas de signaux très faibles. En d'autres termes, le récepteur n'est plus obligé d'attendre pendant 30 secondes avant de pouvoir démoduler le message de données pour en extraire les éphémérides et autres données nécessaires au positionnement, et sans non plus exiger la présence d'un signal fort. En outre, le récepteur mobile connaissant la liste des satellites en visibilité, il pourra acquérir plus de satellites que dans le cas normal où il ne pourra détecter la présence de satellites dont les signaux sont faibles.

Les résultats des tests réalisés avec des récepteurs HSGPS et des récepteurs AGPS permettent enfin de conclure que l'AGPS est une technique de positionnement très performante, surtout dans un contexte d'acquisition. De plus elle peut facilement être intégrée avec des techniques de haute sensibilité. Il est à noter que du point de vue de la poursuite, les deux techniques s'avèrent être à peu près équivalentes.

Chapter 4

HSGPS and AGPS

Contents

A conventional GPS receiver is unlikely to operate properly in environments such as indoor or urban canyons to meet the LBS requirements. Indeed, The GPS signals are inherently very weak signals. The received power of a LOS GPS signal is about –160 to $-155\,dBW$ at the output of a right hand circular polarized antenna, on the surface of the earth. This is a very low power signal, and it is much weaker than the surrounding noise. Moreover, in serious attenuation/fading environments, such as urban canyons or inside buildings, the C/N_0 of an incoming GPS signal may be at or even lower than the level of $20\,dBHz$, which is below the tracking threshold of a conventional GPS receiver and thus sure below the acquisition threshold. In these situations, an enhanced GPS receiver is needed.

HSGPS and AGPS techniques have been developed to enhance conventional GPS receiver acquisition and tracking. This chapter gives a brief description of these two methods which may be complementary, and provides a comparison of their performances.

IV.1 HSGPS

High Sensitivity GPS is any technique that increases GPS signal processing gain beyond standard levels to receive and measure weak signals [*Watson, 2005*]. Such techniques enable GPS signal measurements in some environments where previously not possible, like indoors, under dense foliage or in urban canyons.

With this ability, HSGPS offers higher availability and wider applicability compared to conventional GPS. HSGPS receiver manufacturers are aiming for tracking sensitivity levels where the received power is in the range of -182 *dBW* to -188 *dBW*, i.e. ≈ 14 to $20\ dBHz$ assuming a noise density ratio of $N_0 = 202\ dBHz^{-1}$ [*Ray, 2002*]. This allows the receiver to work at attenuations of 27 to 33 *dB* with respect to the average typical received power of $-155\ dBW$.

Nevertheless, HSGPS is associated with received GPS signal levels which come close to disturbing signal level, incurring multiple measurement fault sources ranging in magnitude up to kilometres in some cases [*Lachapelle et al., 2003*]. These are due to multipath errors, measurement noise associated with the low-power of the remaining signals, echo-only and cross-correlation signal tracking. These large ranging errors are then weighted by the poor geometry. Consequently, special measurement processing is required to obtain a reliable solution with HSGPS positioning. The receiver output must include an accurate estimate of the errors [*Collin et al., 2003*].

The next section is dedicated to the description of the HSPGS theory, with a performance test using the BT338 HSGPS receiver following, for illustration purposes.

IV.1.1 Theory of HSGPS

The theory of HSGPS lies in the improved ability to process weak GPS signals. In general, HSGPS implementations rely on coherent and non-coherent integration over periods longer than 20 *ms*. More precisely, the prime characteristics for indoor signal processing are coherent signal integration and non-coherent signal accumulation over periods of several hundred milliseconds up to several seconds. Note however that at such low signal power levels the problems of cross-correlations, multipaths and other interferences are much more relevant. In conventional receivers, low power signals were not processed because they do not integrate techniques for detecting and rejecting such perturbations. HSGPS receivers are able to process weak signals through long integrations, so they must combine such rejection techniques.

The total gain using coherent and non-coherent accumulations is (equation II-20):

$$G_{tot} = 10\log(B \cdot T_p) + 10\log M - L(M)$$

This equation shows that longer dwell times allow for weaker signal acquisition. Longer coherent integration is of particular interest for sensitivity issues, since the higher it is, the

lower is the noise floor at the output of the correlator. Furthermore, it does not introduce additional losses, as the squaring losses introduced by the non-coherent integration (due to squaring the noise component). Yet, increasing the coherent time is limited by the data bits transitions which occur every $20\,ms$, residual frequency errors (caused by satellite motion, receiver clock instability, and user motion), and receiver complexity. Each of these issues is discussed hereafter:

- The navigation bit transition can change the sign of the corresponding correlation result, which may reduce the overall correlation peak obtained after coherent correlation. This 20 *ms* duration of the data bits limits coherent integration of the GPS signal unless the navigation bits are known a-priori. Accordingly, the HSGPS receiver first acquires and tracks the signal with low coherent integration durations, then demodulates the message received to extract the ephemeris, HOW (*Hand Over Word*), and other needed data to compute a position, but also to estimate the data bits transitions such that long coherent integrations become possible. But using low coherent integration times does not allow for the acquisition of very weak signals, as it can be seen in figure II-15. As a result, the HSGPS cannot perform long coherent integration during acquisition, since the data bits are not yet estimated, unless four or more strong signals were already acquired and tracked [*Karunanayake, 2005*]. Hence, in some environments where the signal levels are very weak, the receivers may never be able to download this data reliably. Instead, the receiver must be initialized at first, by acquiring and tracking at least four signals in a strong signal environment so as to enable tracking in urban and indoor environments.
  Furthermore, waiting for the ephemeris and time information in the data message to be demodulated induces a minimum TTFF of at least $30\,s$, since the latters are broadcasted once every $30\,s$ (see appendix A for more details on the data message structure). In real world conditions of urban canyons and dense foliage, where the receiver is usually moving, it can often take up to several minutes to obtain all the ephemeris data the receiver needs to perform its calculations and obtain a fix. This results in a long period with a great deal of location uncertainty before navigation can begin.

- Yet, even if the data bits were known, it is difficult to increase the coherent integration beyond a few tens of milliseconds. It is mainly because longer coherent integration requires finer resolution in Doppler frequency search process. This results in a high frequency selectivity due to a narrower main lobe of the $\sin_c$ component of the signal correlation function as expressed in equation II-9. Recall that the frequency bins used for Doppler removal have a width of $\frac{1}{2T_p}$ with T_p the coherent duration. This level of Doppler frequency search resolution is used to minimize the loss from the insufficient frequency search resolution. Any residual frequency error after Doppler removal can cause the useful signal component power at the correlator output to decrease such that there is no point in further integration. The local oscillator is a major source of frequency drift errors for extended integration durations. An oscillator drift of 0.5 *ppm* (*part per million*) for example, results in a frequency drift of 787.71 *Hz* per second.

- Finally, long coherent integrations require high receiver complexity. The increase in computation complexity with the coherent duration is twofold: long coherent integration implies a larger number of data blocks to be processed at once (thus more complexity and possibly more memory requirements also), and smaller frequency bins as well

($\Delta f_{DOP} = 1/2T_p$), rendering more frequency bins to be tested in a predefined frequency range.

Massive correlators and signal frequency prediction are techniques used amongst others to decrease the acquisition time:

- Massive correlator technique: Several thousands or as many as several hundreds of thousands correlators are used in parallel (200 000 in the Sirf STAR III chipset). Thus, the GPS receiver can search multiple bins at the same time to decrease acquisition time.
- Signal frequency prediction technique: the frequency search region can be dramatically narrowed down if the frequency drift can be roughly estimated. Indeed, the Doppler frequency caused by the GPS satellite velocity can be easily predicted; the receiver clock induced Doppler can be estimated via aiding information; and the user motion component can be predicted in low dynamic situations.

Other software techniques may also be used to speed up the acquisition process. These will be the object of Chapters V and VI.

The non-coherent integration period, can be much longer compared to the coherent integration. Recall that the non-coherent integration is the sum of the squared coherent correlation outputs. With this method, navigation bits become irrelevant, since non-coherent integration is not sensitive to data bit edges. In addition, some residual frequency errors during non-coherent accumulation that are within the carrier tracking bandwidth of the receiver can be tolerated. However, squaring of the signal in non-coherent accumulation results in squaring loss, introduced in equation II-19. Van Diggelen [*2001a*] shows that the squaring loss is significant if the post coherent correlation SNR is low. Thus, maximal coherent integration prior to non-coherent integration results in less squaring loss, which is capital for beneficial non-coherent accumulation.

In summary, reducing the noise level at the correlator output for the acquisition and tracking of weak signals is a matter of maximizing the coherent integration interval while minimizing residual frequency errors (through the use of more stable local oscillators for example). Predicting the data bit transitions and limiting residual frequency errors during coherent correlation is necessary to obtain optimal gain prior to non-coherent accumulation. As it will be discussed later, the AGPS provides the ability to predict the data bits prior to signal processing. The performance of different HSGPS receivers will be the object of the next section, to bring additional illustrations on HSGPS performance.

IV.1.2 HSGPS test results

An HS receiver performance test was conducted at the ENAC. The receiver used is a bluetooth enabled BT338 with a Sirf Star III chipset shown in figure IV-1. The receiver was used in unaided mode (HSGPS mode). It outputs raw measurements which are recorded for subsequent analysis.

Fig IV-1 : The BT338 receiver

Since no aiding data information is available at first, the receiver failed to acquire signals in weak signal environments. Hence, it was first initialised for about 10 to 15 minutes through LOS acquisition and tracking before starting the test bed. The user was moving through the ENAC campus at low speed (pedestrian). The test trajectory is illustrated in figure IV-2.

Fig IV-2 : Test trajectory through the ENAC campus

This trajectory includes many paths in indoors and going under trees.

The instantaneous estimated trajectory is plotted in figure IV-3 below, with the colors corresponding to the number of satellites used to compute the position (light colours imply no or few satellites tracked):

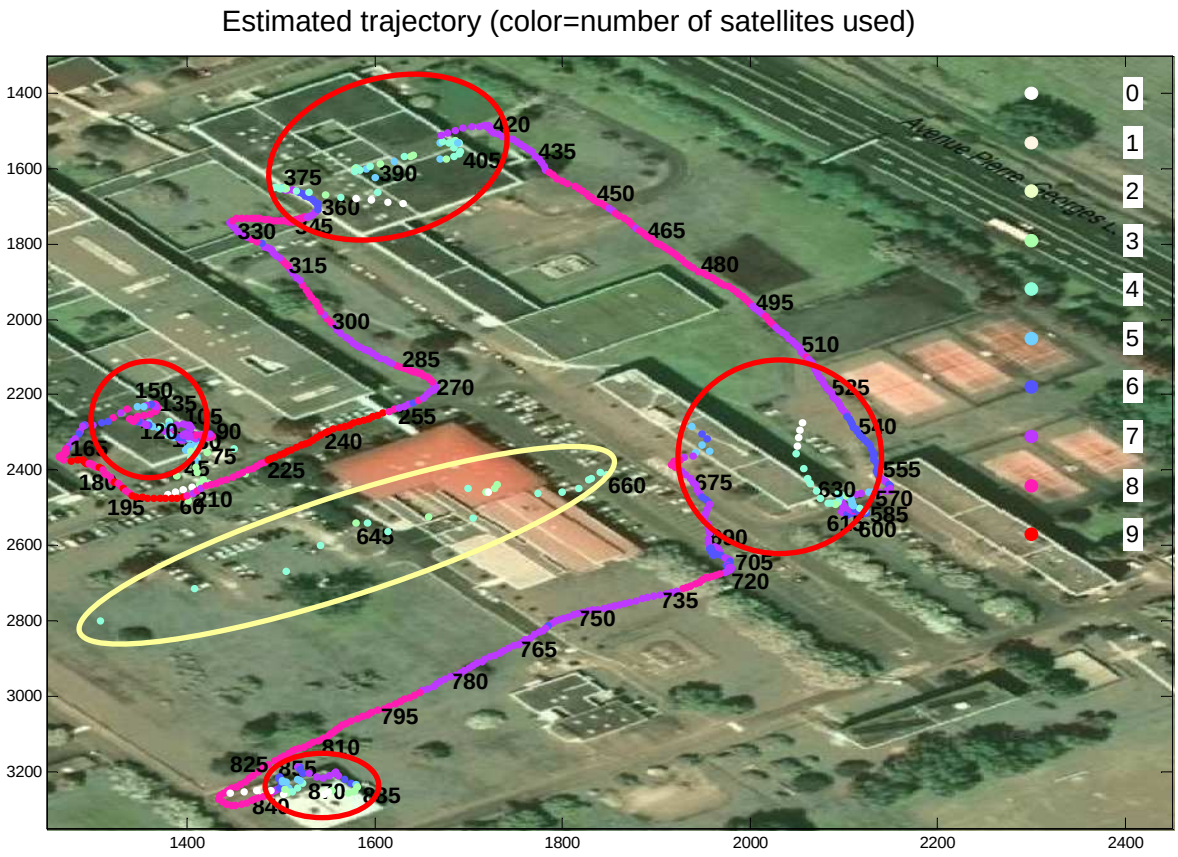

Fig IV-3 : Number of satellites tracked through out the test

It is obvious in this figure that in covered areas (red circles) the satellites availability is much reduced, resulting in very large positioning errors in some cases: a position error of about a few hundreds of meters for example can be observed (yellow circle on the figure) at around 650 seconds from the beginning of the test. But the receiver could in some cases still provide a solution.

The number of satellites tracked as long as the solution type (no solution, 1D fix, 2D fix, or 3D fix) and the estimated satellites signal C/N_0 are depicted in figure IV-4.

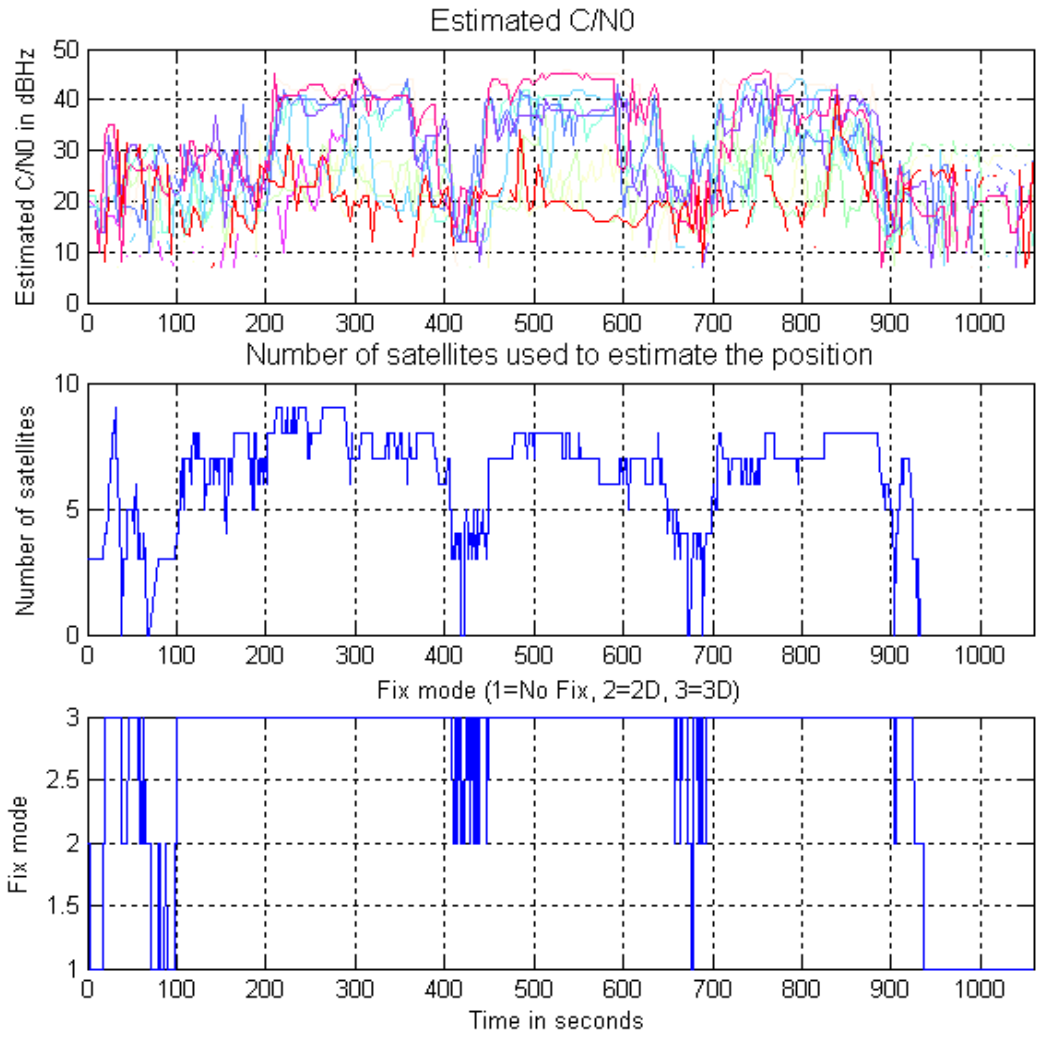

Fig IV-4 : Satellites power in *dBHz*

The minimum estimated C/N_0 that could be tracked is lower than 10 *dBHz*! But it seems that there was an error on this estimated C/N_0 value. A high correlation can be observed between the fix mode and the number of satellites tracked, as could be expected. This figure also highlights the direct correlation between the satellites signal C/N_0 ratio and the type of environment (indoors or outdoors). According to the results on the C/N_0 at around 100, 400, 650 and 900 seconds, an attenuation of more than 20 *dB* compared to the C/N_0 in open environment can be noticed.

Amongst others, Collins et al [*2003*], and MacGougan et al. [*2002*, *2003*] also conducted many tests to evaluate the performance of HSGPS in constrained environments. They also used Sirf HS receivers and studied their performances compared to those of a Novatel OEM4 receiver, in different environments: forests, urban canyons, and residential garage areas. These test results are reminded in the next three sections.

IV.1.2.3 Forests areas

The results showed an enhanced availability (almost 100%) of the HS receiver in forest areas compared to the OEM4, with an average of 9 satellites tracked. Collins et al.

[*2003*] found a position average error of $20\,m$ approximately, whereas MacGougan et al. [*2002*] evidenced errors of the km level!

A kinematic test conducted by MacGougan clearly showed one of the distinct advantages of the HS approach compared to the conventional one: the HS receiver had nearly continuous tracking while the conventional one experienced fast intermittent signal blockages because the latter had to reacquire the signals often and thus the measurement availability is low (for the OEM4) (30%). By measurement availability, we refer to the percentage of successful trials, i.e. trials which could provide a position. It is over 90% for the HS receiver. Last, note that MacGougan used a Spirent STR-6560 GPS simulator to evaluate the HSGPS tracking threshold compared to that of the OEM4, and he found that the HSGPS could still track down to $18\,dBHz$ and possibly lower (since this is the limit of the Spirent), while the conventional receivers would stay at $32\,dBHz$ as a tracking threshold. We could not conduct tests in forested areas due to lack of time.

IV.1.2.4 Urban areas

For the urban environments, HSGPS was still tracking signals almost continuously, even though the average received signal power level was lower than in a forested environment. The HSGPS receiver provided more measurements than the conventional receivers. However, in the tests conducted by Collins et al. [*2003*] the average number of satellites tracked by the HSGPS was 7.5 versus 4.5 for the OEM4; whereas, MacGougan et al. [*2003*] rendered 4 to 5 satellites tracked by the HSGPS versus 2 to 3 for the OEM4. Once again, this could be explained by the constellation geometry at that time. This difference in the number of satellites tracked was echoed by the accuracy results, where the errors were of the order of $100\,m$ and $389km$ (as a maximum error) respectively! In the urban environment case, our results were closer to those obtained by Collins, where the average number of satellites tracked is approximately 7 satellites. In a kinematic test, MacGougan evidenced once again an enhanced availability of the HS receiver and less variation in the number of satellites tracked indicating less frequent loss of signal lock. But in this case also, the conventional receiver solution indicated more accurate positioning.

IV.1.2.5 Light indoors

The biggest difference in availability of HSGPS solution versus conventional GPS was found in the light indoors tests, where only HSGPS was providing position solutions without frequent loss of signal tracking. Collins et al. [*2003*] and MacGougan et al. [*2003*] placed the receiver in a residential garage for these tests. Collins found that the mean number of satellites tracked by the HSGPS receivers was 7.4 versus 5 to 9 satellites for MacGougan. The OEM4 could not provide solutions in the tests conducted by Collins, but could track an average of 2 satellites in the tests conducted by MacGougan. The position error was of a $20\,m$ level in the two cases. This is a relatively low error indicating that short delay multipath is the primary error sources in this environment. In addition, as the ratio of strong to weak signals was never very high, no cross-correlation errors was reflected in the position domain which results in that no very large position errors occurred. In our case however, very large errors (in the order of a few hundreds of meters) were experienced in covered areas (figure IV-3, red circles). This is because these areas had large windowed interfaces which may have led to cross-correlation large errors.

For all these tests, the signal fading with respect to open sky conditions was between 25 and 30 *dB*.

In terms of acquisition, Karunanayake [*2005*] conducted tests on HSGPS acquisition performance using a Sirf XTrac receiver and a Spirent STR6560 signal generator. A first test where all the satellites are at the same power level, disclosed an acquisition threshold of $-140\,dBm$, that is approximately $32\,dBHz$ (a noise power density of $-202\,dBHz^{-1}$ approximately is assumed). With one of the satellites at $-130\,dBm$ ($\approx 42\,dBHz$), the HSGPS receiver acquisition threshold did not change. For the OEM4 conventional receiver, the acquisition threshold was found at about $38\,dBHz$, in a similar test realised using the Spirent STR4500 signal generator (see chapter II, paragraph II-6-2). In this acquisition test, the SirfXTrac HSGPS receiver used had better acquisition performances than the OEM4 conventional receiver. As explained before, the HSGPS mainly enhances tracking, not acquisition, unless a prior initialization is carried out for that receiver. But the SirfXTrace is an HSGPS receiver that is improved in terms of acquisition and tracking sensitivity.

IV.1.3 Conclusion on HSGPS

The use of HSGPS receivers results in higher availability of observations in constrained environments. Position fixes were obtained more frequently with the HS receivers than the conventional receivers tested under foliage and in urban canyons. In the indoor environment tested, the conventional receivers could not operate while the HS unit could still provide positions. However, a degraded level of positioning accuracy performance was observed when comparison was possible between the HS receiver and OEM4 receivers. In fact, the conventional receiver was not able to provide as many measurements as the HS receiver, but when it does, the associated errors are lower. This is due to increased influence of multipath signals as more signals at lower elevations were tracked, errors due to echo-only signal tracking, and in some cases very large errors due to tracking of false correlation peaks caused by signal cross-correlation. In short, applications that will use HSGPS must balance solution availability with positioning accuracy unless fault detection and exclusion is integrated to ensure reliable navigation. It is noteworthy that by enhancing the solution availability, the HSGPS allows for avoiding repeated signal loss and reacquisition.

The tracking threshold of the High Sensitivity receivers was tested by Karunanayake [*2005*] using a GPS hardware simulator and found to be at 14 to 15 *dB* lower than the conventional mode GPS receivers tested in the course of this thesis (32 *dBHz*): that is approximately 18 *dBHz*. The acquisition threshold of the HSGPS SirfXTrac receiver, which is improved in terms of acquisition and tracking sensitivity, was also found by Karunanayake [*2005*] at 32 *dBHz* approximately rendering that the HSGPS by itself is not robust enough to be used in degraded signal environments.

IV.2 Assisted GPS

AGPS is recognized as the most promising positioning technology, in terms of accuracy and coverage, for fulfilling the stringent requirements of the positioning accuracy needs for various LBS [*Biacs et al., 2002*].

Besides emergency services, numerous geolocation based applications are envisioned. Among them are network optimisation, where spatio-temporal wireless traffic distribution is

to be used in planning, design, and operation of wireless networks; information services, which are to provide mobile users with directions to gas stations, restaurants, hotels and the like, tracking of personnel, vehicles, and assets in managing company operations, and location sensitive billing of mobile users, to enable more precise rate structure for wireless service providers. People who work in dangerous jobs (such as security guards), those who work alone (such as field engineers) and those who are commonly in need of assistance (such as nurses and health care workers) are also a target market for AGPS techniques [*Djuknic, 2001*].

Nonetheless, it is not only the performance that promotes AGPS as the backbone of cellular positioning, but also the recent advances in integrated circuit technology, which have made it possible to produce highly sophisticated GPS receivers in volumes cheap enough for mass usage, and also small enough to be integrated into cellular phones. The small size also comes with low power consumption, and results in more possibilities for the integration of a GPS receiver into ever-smaller cellular phones.

As already stated, standalone GPS cannot work properly when no direct LOS is available. It is worth noting that cellular networks based positioning techniques are not efficient neither when they are used alone; cellular based solutions like the Cell ID, the AOA (*Angle Of Arrival*) techniques and others (refer to appendix D for more details), have their own advantages and drawbacks. Their main advantage is the ability to provide a position in all conditions; this is a characteristic of cellular signals. Meanwhile, their accuracy is far below that of the GPS. It depends on the size of the transmitting BTS (*Base Transmission Station*). In the case of rural areas for example, where BTSs are very scarce, the position estimation error is of the order of 30 *km*. In addition, some techniques need hardware and software upgrades of the BTS and the MS (*Mobile Station*). On the other hand, even in urban areas, cellular networks have a lack in synchronization which degrades the positioning performance. The AGPS is a hybrid positioning technique, where the cellular network provides AD (*Assistance Data*) that is used to aid the GPS system for positioning purposes. This is the general principle of the AGPS technique. In this thesis, the AGPS reference position is supposed to be provided using the Cell ID cellular positioning.

The AGPS solution to compensate for the missing information and to improve acquisition sensitivity and complexity, is to provide the GPS receiver with accurate time and/or location data from a reference GPS receiver that has a clear path to satellites via a cellular link. Reducing the acquisition complexity positively affects the receiver's power consumption. Hence, power savings are the immediate consequences of assisted acquisition, because the receiver knows exactly which signals to look for, and where to look for them in time and frequency domains. No extra time, i.e. no extra power, has to be spent on searching for non-visible satellites. This is a decisive factor for the AGPS operation, since the introduction of the GPS receiver within a mobile phone, makes it subject to the same constraints of bulk and overall consumption.

The next two sections are dedicated first, to the description of the APGS theory and then, to the illustration of AGPS performance with some test results.

IV.2.1 Theory of AGPS

Unlike the normal GPS receiver, the AGPS receiver does not have to extract the ephemeris or any other navigation data from the GPS satellite data message. This is instead provided over the phone's communication channel from a network-based resource, along with an approximate time and position. This has two major benefits: first, the phone's receiver can make a faster signal acquisition as it already knows the satellites in-view. Thus it only searches for the visible satellites. Second, the receiver can make pseudorange measurements, using longer integration interval, even when the available C/N_0 ratio is very low, thus preventing from being constrained to accurately demodulate the ephemeris data from the navigation message, since the receiver already has this data. In other words the receiver is able to provide a solution without having to wait 30 seconds before demodulating the ephemeris data since it already has it, and without requiring the presence of a strong signal to be able to accurately demodulate this data. Since it is not necessary to demodulate the ephemeris data, the AGPS- capable mobile handset can focus on acquisition and position computation earlier (without having to wait for at least 30 seconds), which leads to a much lower TTFF. Another benefit of the AGPS is that the receiver can acquire much more satellites when it has the list of satellites in view. Indeed, some of the satellites being weaker than others (<30 *dBHz* for example) would not be visible to the receiver in conventional or in HSGPS modes (without Assistance Data).

Delivering aiding data from the network requires a server with a reference GPS receiver that has clear LOS views of available satellites. It is assumed that the rover/user receiver is within 100 *km* of the reference station and therefore, both receivers have roughly the same visible satellites [*Garin et al, 1999*]. From this information, an AGPS receiver (i.e. a mobile cellular phone user) can know the satellites in view, and get the corresponding ephemeris and clock data.

The general functioning process of the AGPS is illustrated in figure IV-5.

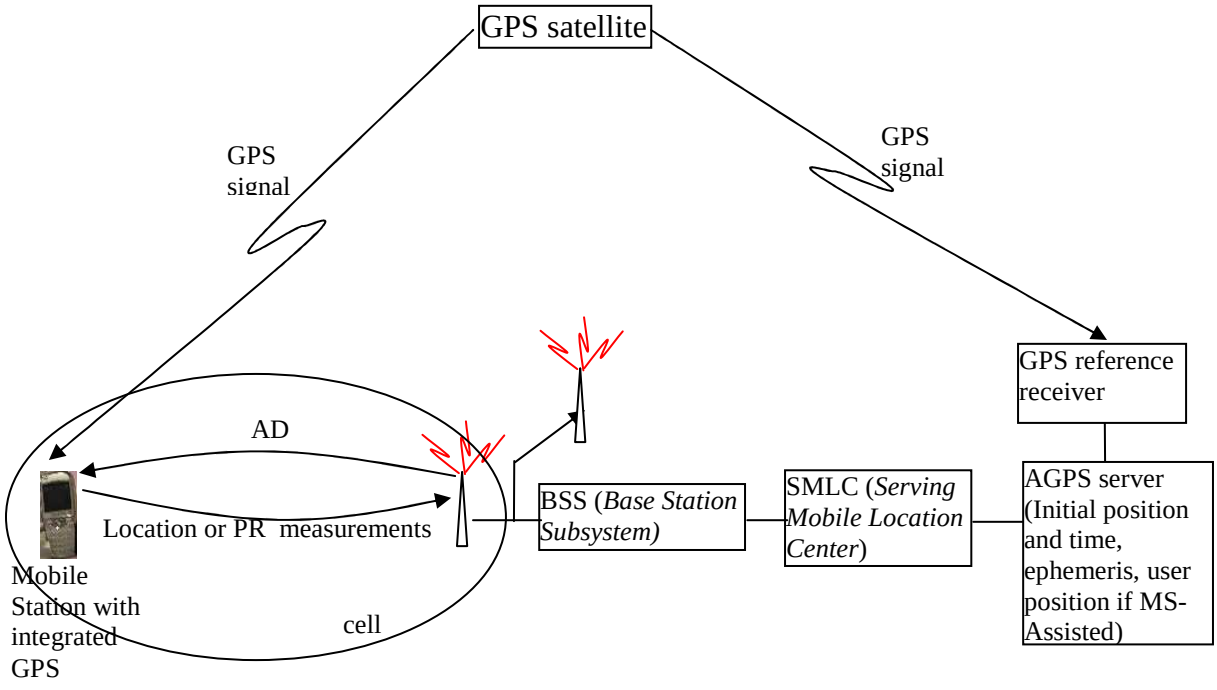

Fig IV-5 : General AGPS functioning process

In the AGPS system, the functions normally performed by a standalone GPS receiver, namely determining the code phase, demodulating the navigation message, calculating the PR (*Pseudo Range*) measurements and computing the user's position are distributed among the GPS enabled MS and the AGPS server. This distributed approach leads to high performance levels.

The server collects satellite almanac, ephemeris, approximate user position (which is defined by the initial reference position and its associated uncertainty) and timing assistance data from the reference receiver, computes the assistance information and sends it to the MS. The receiver uses this information to speed up the acquisition process.

AGPS methods can be divided into two categories, depending on where the user GPS position calculation is performed. If the position is calculated at the user MS, the method is called MS-based GPS. Alternatively, if the network calculates the position, it is called MS-assisted GPS. The use of one of these methods depends on the application type.

The received GPS signals are shifted in frequency (Doppler frequency shift). The receiver must find the approximate frequency of the received signal carrier before it can lock onto its phase. Knowledge of the satellite position and velocity data and the approximate receiver position (with an accuracy that depends on the cellular network based location technique used, Cell ID in our case) reduces the frequency range to be searched because the receiver can better predict the Doppler frequency shift instead of searching over a large possible frequency range. Reducing the number of frequency bins to be searched reduces the TTFF, and thus the power consumption. For applications where weak signals must be acquired, this allows the receiver to dwell in each bin for longer periods of time for example. But increasing the coherent integration results in smaller Doppler bins, and thus more Doppler bins to be explored within the considered Doppler range. This additional dwell time increases the sensitivity of the receiver, so that it can use signal strengths below the conventional thresholds. But increasing the coherent integration results in smaller Doppler bins, and thus more Doppler bins to be explored within the considered Doppler range. Therefore, a compromise must be set between the TTFF and the receiver sensitivity that are needed. Figure IV-6 illustrates the reduction in AGPS search space.

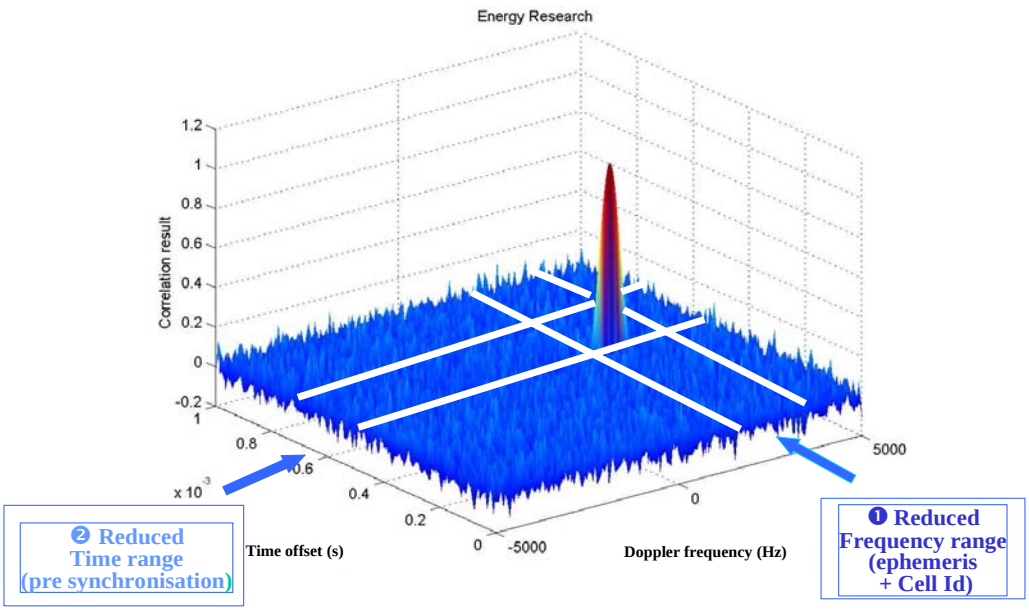

Fig IV-6 : Reduction in the search space using the AGPS Assistance Data

The sensitivity can be enhanced if the AGPS server communicates to the handset the time information with an accuracy of several microseconds. This is relatively straightforward in synchronous CDMA systems, because base stations and mobiles are in synchronization with the GPS time. However, this is not the case for the GSM and UMTS networks, and time transfer uncertainty is of about a few seconds, due to unpredictable delays in network signalling layers. Thus novel approaches are required to satisfy this stringent timing requirement.

At present, the AGPS is being standardized for all air interfaces. The Assistance Data standardized at 3GPP level is described in the TS44.031 standard for GSM and replicated in TS23.371 for UMTS [*3GPP, 2006*]. It is summarized in table IV-1 below.

Assistance data type	**Comments**
Reference location	Pre location of the mobile generally deduced from cellular information. It is a pre-location for the receiver to initiate its computation.
Reference time	Reference time relative to the GPS time. It is destined to pre-synchronise the receiver to make easier the acquisition
Navigation model	Visible satellites ephemeris and clock corrections
Ionosphere corrections	Klobuchar model broadcast by the GPS signal in space
Differential correction	Standard differential corrections
Real time integrity	List of bad satellites
Almanacs	Almanacs of the GPS constellation
UTC model	UTC model broadcast by the Signal in space
Acquisition assistance	List of assistance to improve the acquisition in particular in MS-Assisted. Indeed in MS-Assisted, the mobile does not compute its own location. In this case, the processing of the mobile is limited to the acquisition and the pseudorange measurement. In this case, it has no need to get the ephemeris and various correction. This packet of assistance data contains only - the list of satellite in view from the user point of view (deduced from the cell location of the user) - the Doppler of the satellites, so that the mobile can directly search the PRN in an appropriate frequency slot - a code phase search window for all the satellites so that the mobile can directly scan the signal over a specific time span, instead of scanning an entire 1ms. The mobile phone can then acquire the signal, measure the code delays of the signals and send them back to the server to compute the location. The server then - deduces the pseudoranges from the code delays, the GPS time, and the cell location of the users - applies corrections (sat. Clock, ionnosphere, troposphere, differential etc…) - computes the accurate position of the mobile

Tab IV-1 : List of AGPS Assistance Data

Sending this data to the receiver can be achieved using one of the following two methods:

- **Control plane implementation**: this implementation uses the signalling layers of the communication network to convey the AD to the mobile phone and to retrieve position information from the telephone. The protocol is standardised in the TS44.031 (RRLP) for GSM and the TS23.371 (RRC) for UMTS. The advantage of the control plane implementation is precisely that it uses the low layers of the communications which means that AD can be conveyed to the users even if they have no SIMM cards. Any E112 (emergency call) shall be supported by the operator even if the user has not subscribed. Since emergency calls have to be located, AD shall be conveyed to the user even if he has not subscribed. This is possible in the Control Plane implementation. The other advantage is that the operator is completely master of the process and then can vouch for the service.

The main drawback is that the signalling layers have a very low data rate, which leads to problems when many users want to locate.

- **Secure User plane Implementation**: this implementation uses the high level layers of the communication network, i.e. the applicative layers. This is dealt with by the OMA standardisation group. Nevertheless the protocol used for assistance data transmission is the protocol defined at 3GPP level (RRLP for 2nd generation cellular networks, RRC for 3rd generation cellular networks). The data are then exchanged through IP. The advantage of such a solution is that the applicative layer has a much higher data rate. Nevertheless, the user can access to this layer only if it has subscribed, which raises an issue when it is question to deal with emergency calls. On the other hand, the standardisation of this protocol appears to be quite long for the simple reason which is that if it is standardised, then operators could possibly loose control on this location business.

IV.2.2 AGPS test results

An AGPS test has been conducted in urban, light indoor and deep indoor environments using an Alcatel demonstrator designed to be used in cellular phones, Smart Phones or PDAs. It is an A-GNSS software receiver. The AD is delivered to the receiver from an AD sever through a modem. This receiver allows for the acquisition of satellites with power levels lower than can acquire a conventional receiver. The results are compared to those obtained with a mono frequency Haicom HI-204E conventional receiver. This receiver is also destined to be connected to PDAs or pcs. It provides data in the NMEA format. It is not supposed to have desirable performances under weak signal conditions. The two receivers used are shown in figures IV-7 and IV-8.

Fig IV-7: Haicom HI-204E standalone GPS receiver

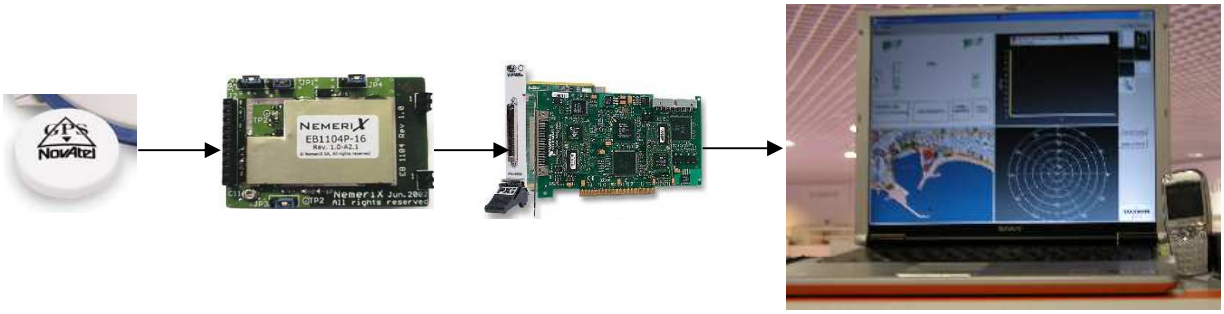

Fig IV-8 : Alcatel AGPS solution

The graphical interfaces for each of the two receivers are depicted in figures IV- 9 and IV-10.

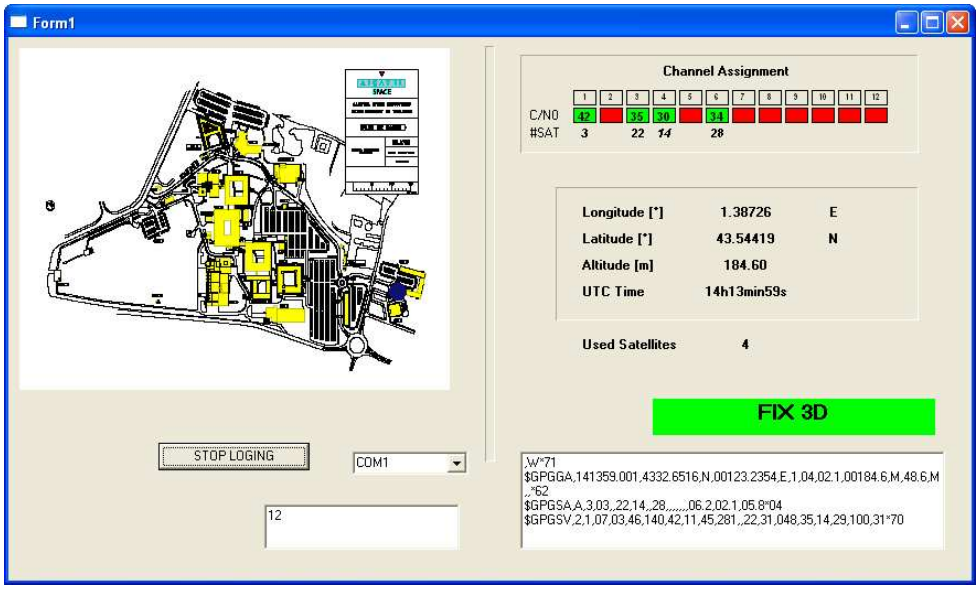

Fig IV-9 : Graphical interface of the Haicom receiver

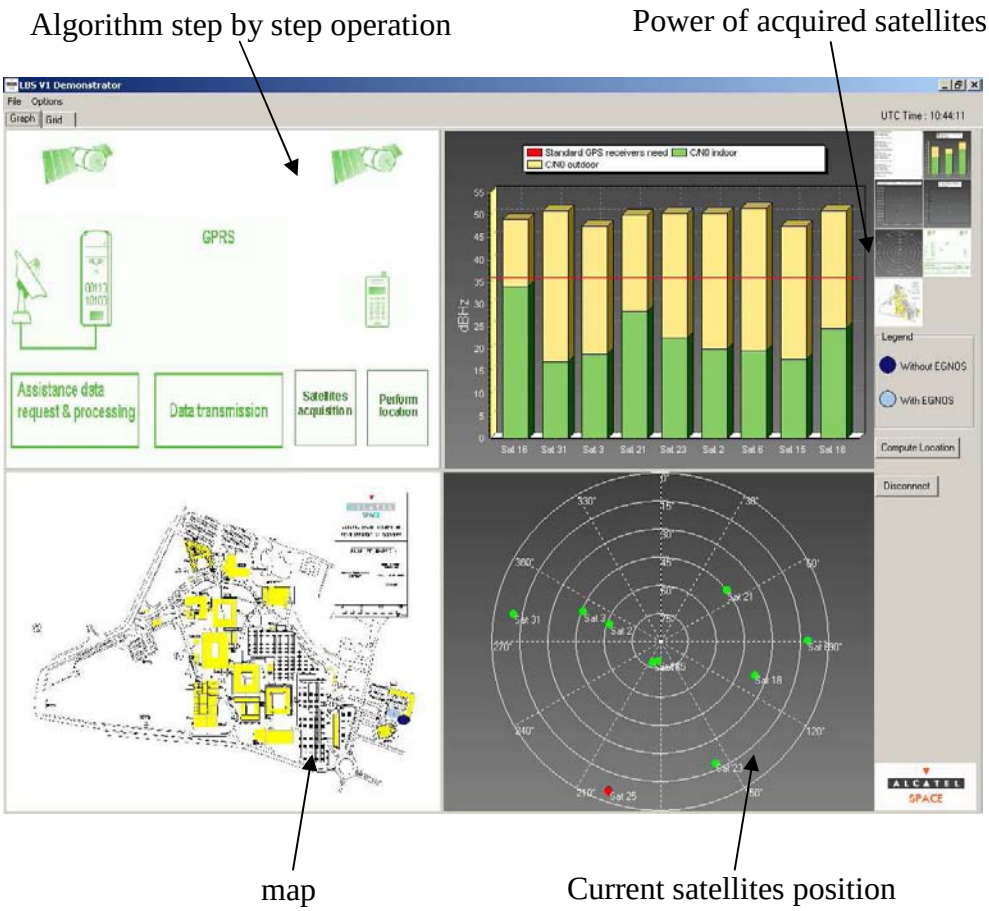

Fig IV-10 : Graphical interface of the Alcatel AGPS receiver

The Alcatel solution used here is the first version of this demonstrator. New more robust versions are now available.

For both receivers raw measurements are recorded for subsequent analysis. The following assumptions are made for the AGPS receiver:

- GSM time transfer uncertainty of $\pm 2\ s$ (new synchronisation methods exist which allow for much lower uncertainty on time synchronisation)
- Position uncertainty depending on the concerned cell size
- Static receiver (optimistic assumption, but a good first approximation)
- Doppler range of $\pm 2\ kHz$ (The satellite motion induced Doppler is easily predicted using the AD, the only Doppler components that has to be searched for corresponds to the receiver clock frequency drift and the user motion induced Doppler. In this case it is null)

The experiments outputs are:

- The number of satellites used for position computation, and the availability percentage
- The position 2D and 3D errors
- The mean received C/N_0 levels

The receivers were compared in either acquisition or tracking modes. The difference between the two modes is that for the acquisition tests, the receivers are set to a cold start mode. In cold start mode, the receiver has no acquisition aiding information available, meaning it has no information about the current time, the orbits of the satellites or its current position; therefore, it has to perform a full search. However, for tracking, the receivers are initialised, that is they were first switched on in a strong signal environment and kept for a while in order to be sure that the ephemeris data is completely demodulated.
Only a 3D position fix was reported in the results. In other words, the cases where the number of satellites tracked is lower than 4 are not reported. A comparative table is presented at the end of this section, which summarizes all the results, with an analysis following.

IV.2.2.6 Light indoors results

This test was conducted in one of Alcatel offices situated at the 2nd and last floor of a two floors building with large windows. The office is shown in figure IV-11.

Fig IV-11: Alcatel office in deep indoors

In tracking mode, the receivers showed a 100% availability. Only the results of the acquisition mode in terms of number of satellites acquired, 2D and 3D position errors, and C/N_0 ratios, are reported here.

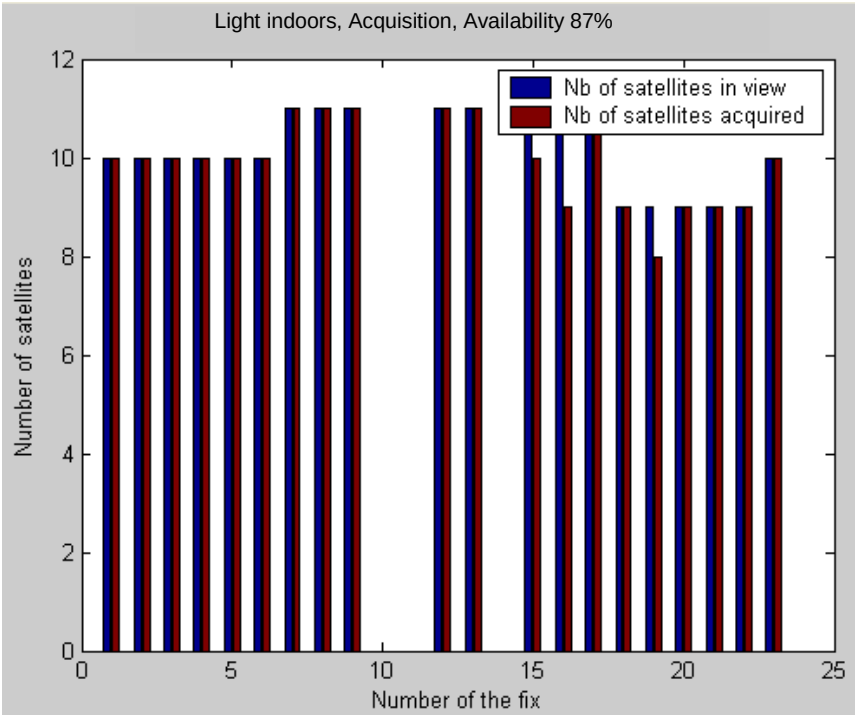

Fig IV-12 : Number of satellites acquired with Alcatel demonstrator and availability percentage

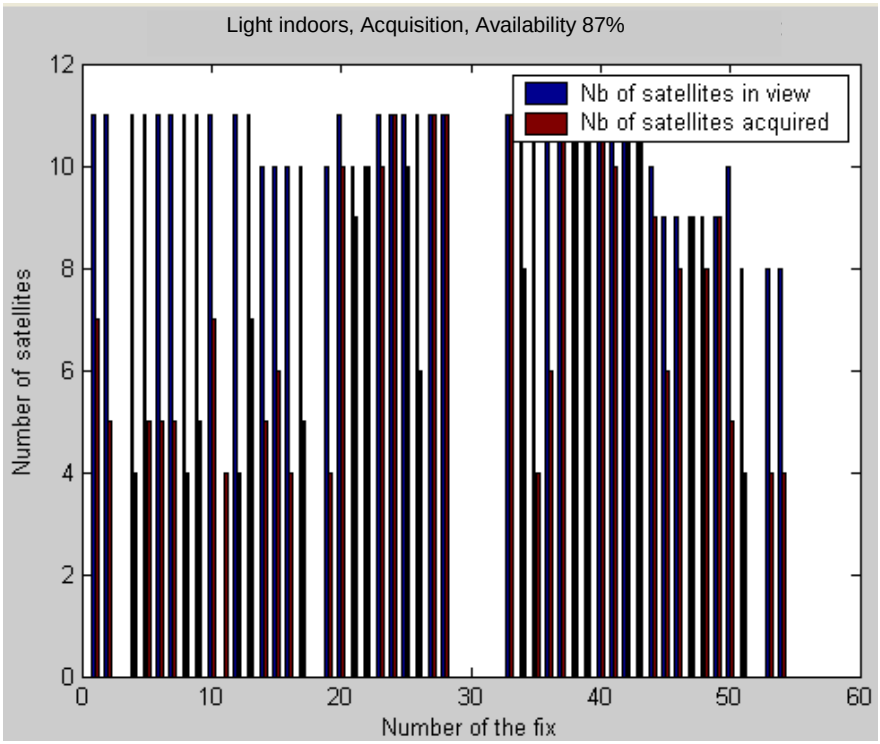

Fig IV-13 : Number of satellites acquired with the Haicom receiver and availability percentage

As illustrated in the figures IV-12 and IV-13 above, the two receivers had the same availability percentage in this test. But the number of satellites acquired compared to the

number of satellites in view is much higher for the AGPS Alcatel solution than to the Haicom receiver.

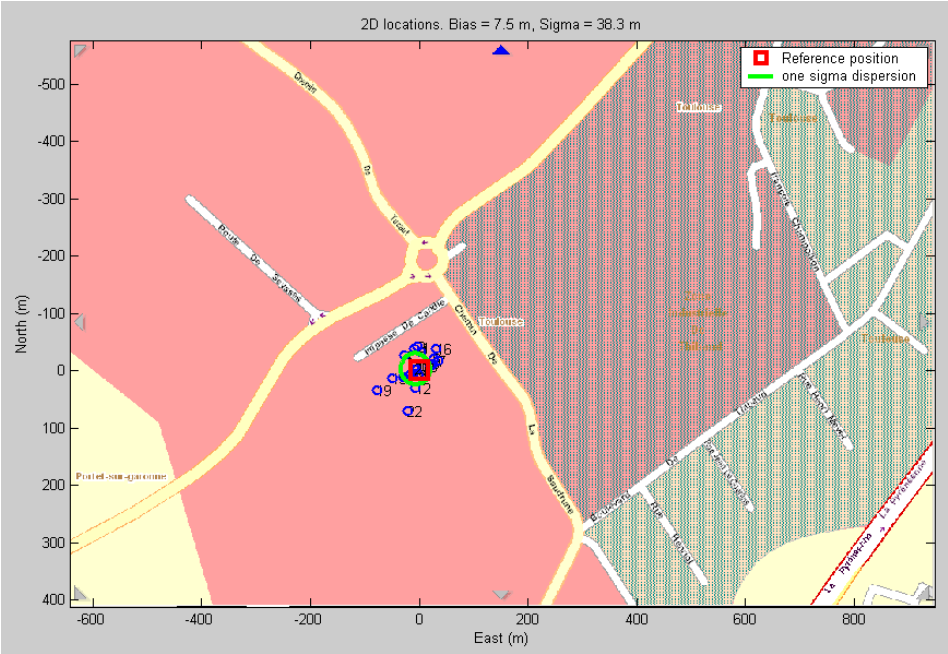

Fig IV-14 : Alcatel demonstrator 2D position error

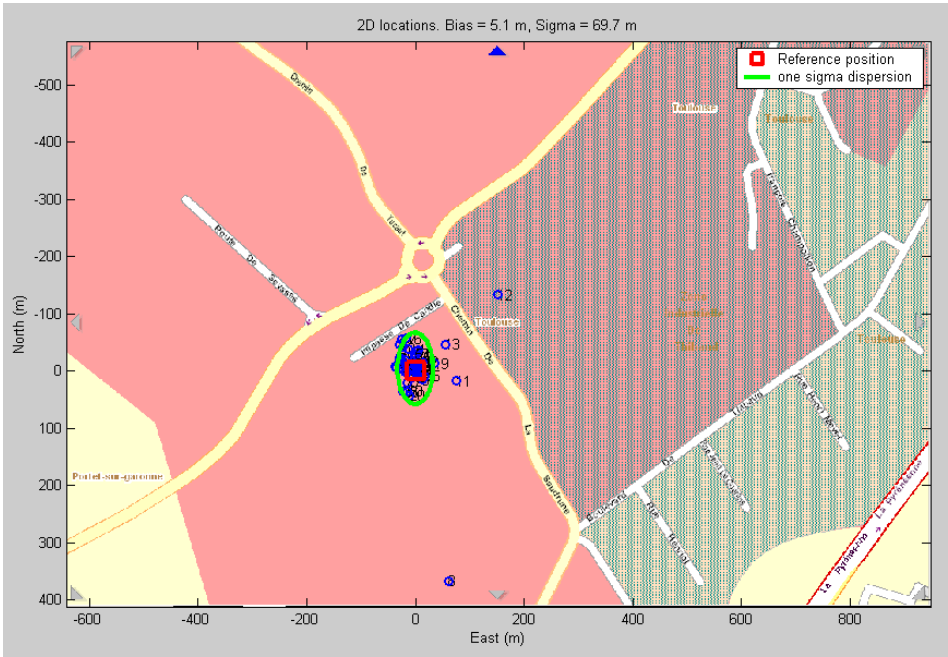

Fig IV-15 : Haicom 2D position error

As for the 2D position error, the Alcatel demonstrator performance (figures IV-14) is better than that of the Haicom (figures IV-15) in terms of maximum error (sigma of 38.3 *m* for the Alcatel solution versus 69.7 *m* for the Haicom), but not in terms of mean error (7.5 *m* for the Alcatel solution versus 5.1 *m* for the Haicom).

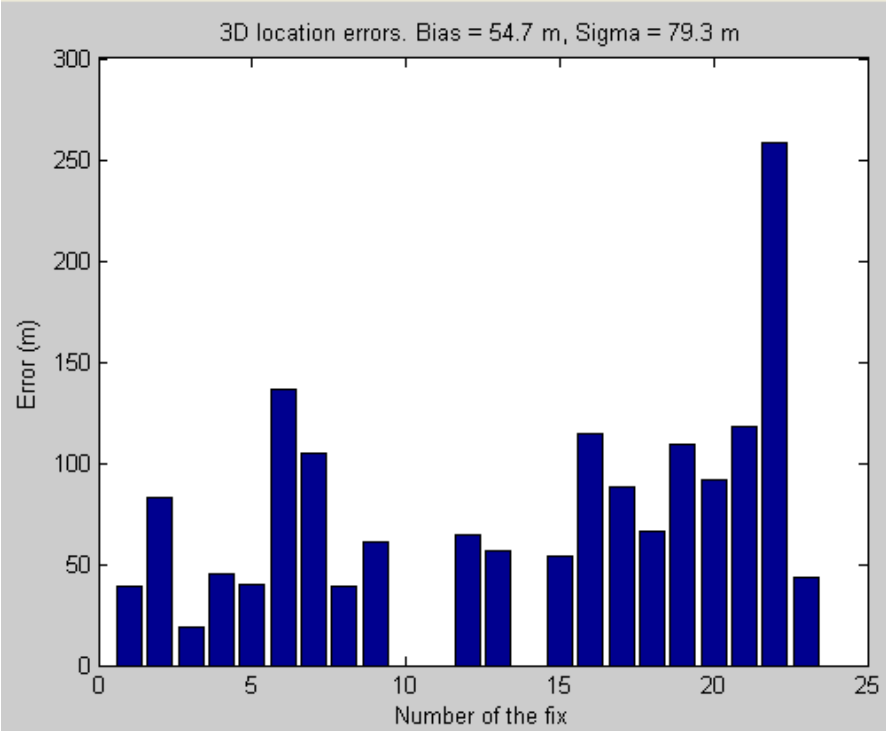

Fig IV-16 : Alcatel demonstrator 3D error

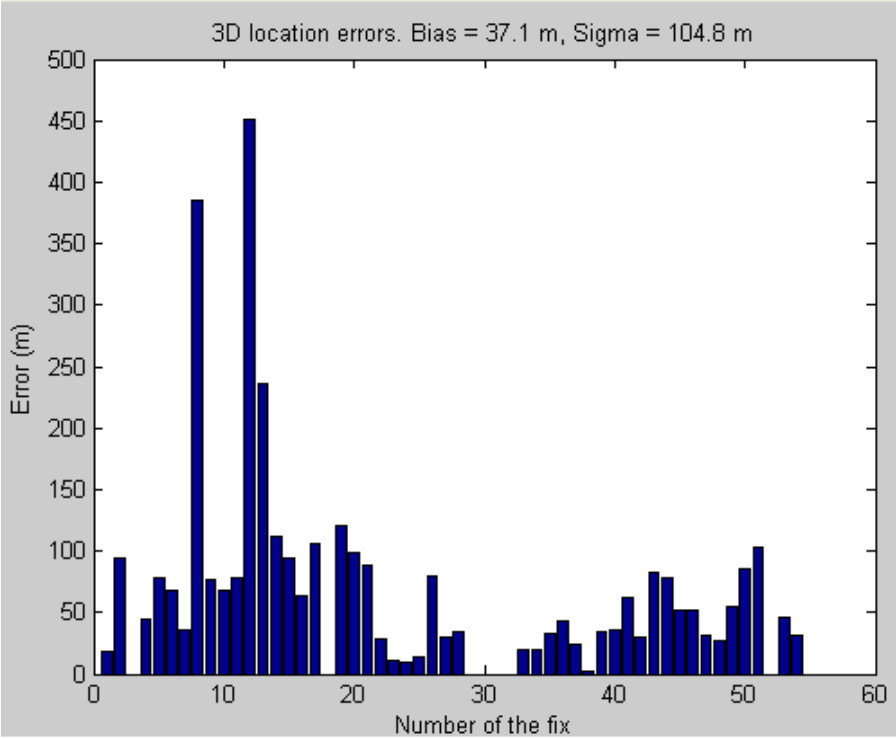

Fig IV-17 : Haicom 3D position error

The result of the 3D position error echoes that of the 2D error position: the Haicom provided better mean error value, but worse sigma error value, as illustrated in figures IV- 16 and V-17.

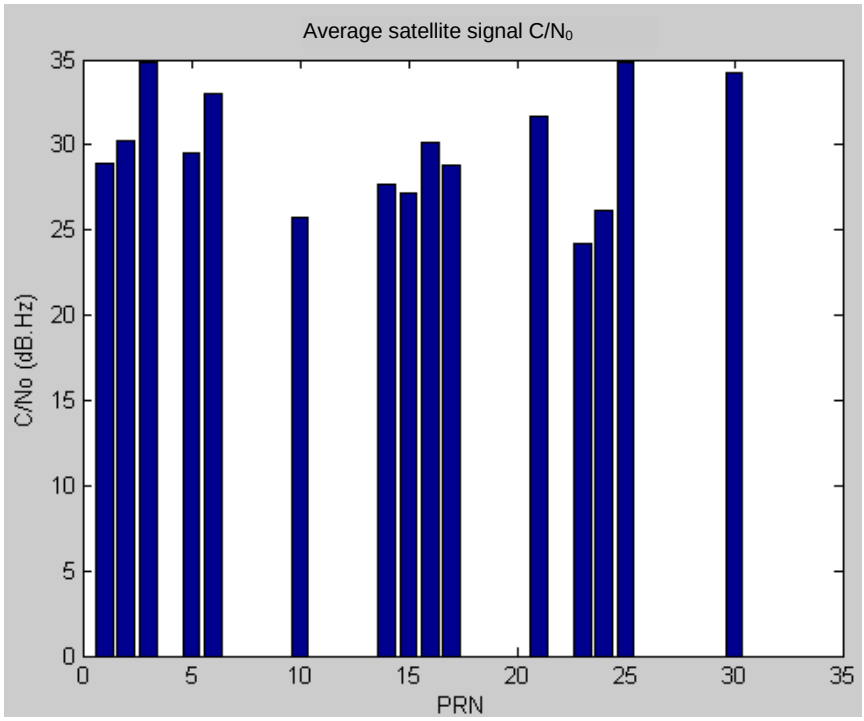

Fig IV-18 : Alcatel demonstrator average satellite signal C/N_0

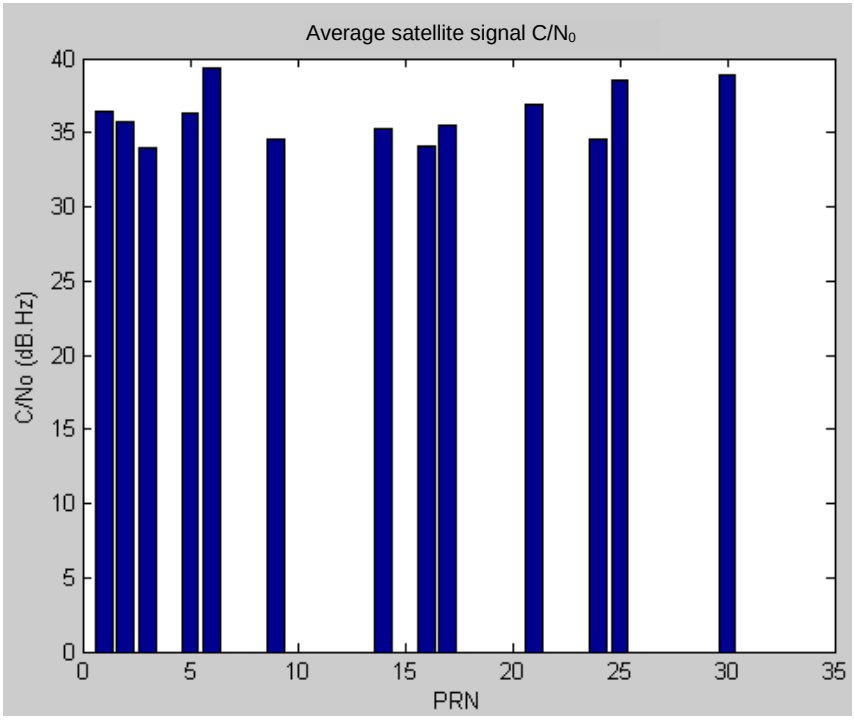

Fig IV-19 : Haicom average satellite signal C/N_0

Figures IV-18 and IV-19 above illustrate the average satellite signal C/N_0 . It is higher for the Haicom. However the number of satellites acquired are higher using the Alcatel AGPS receiver.

IV.2.2.7 Deep indoor environments

The experiments were conducted in an Alcatel Space office, on the ground floor of a 2 stores building this time. The receiver was placed in the middle of the office, at 1.5m from the window. None of the receivers could provide a solution with a cold start: acquisition could not be realized. This is why only the tracking test is reported. For the tracking test, the acquisition was first realised in an open space. All through this test, the Haicom receiver was not available neither.

The results obtained with the Alcatel demonstrator are illustrated next.

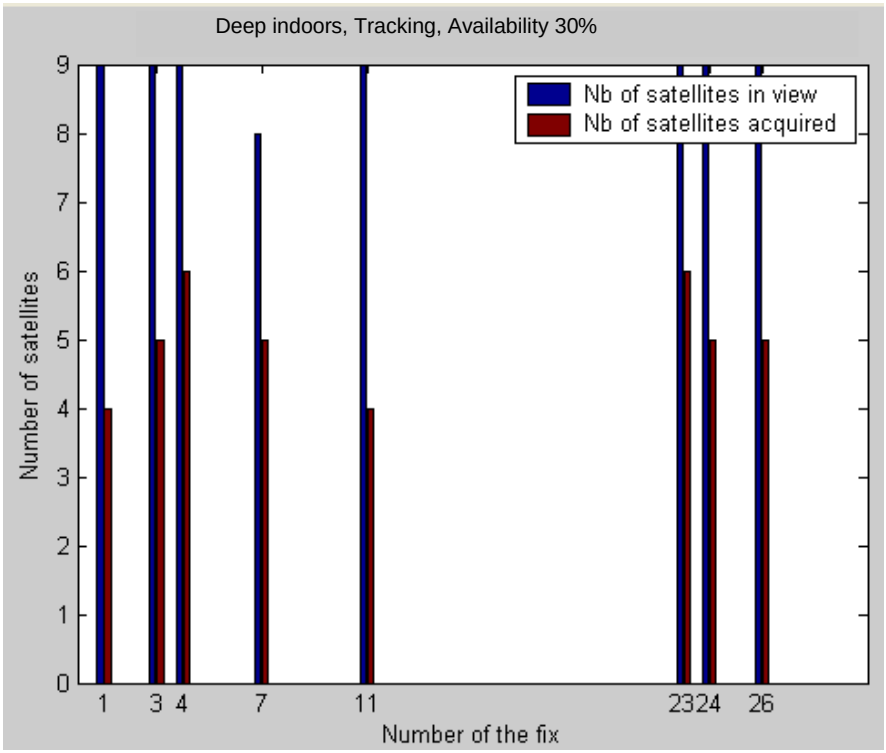

Fig IV-20 : Number of satellites tracked by the Alcatel demonstrator and availability percentage

As it could be expected, the availability in such environment is lower than for light indoor environments, but the receiver could still provide a solution (see figure IV-20 above).

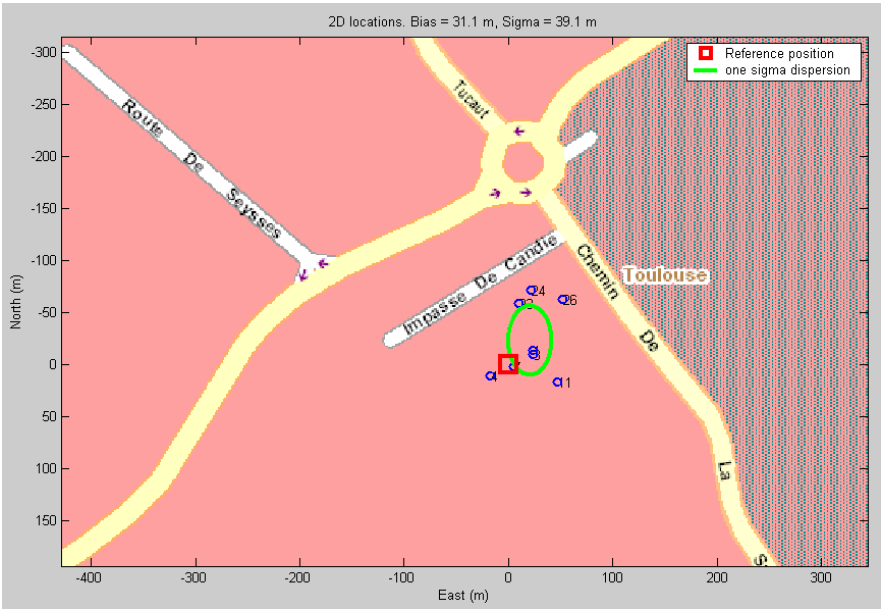

Fig IV-21 : Alcatel demonstrator 2D position error

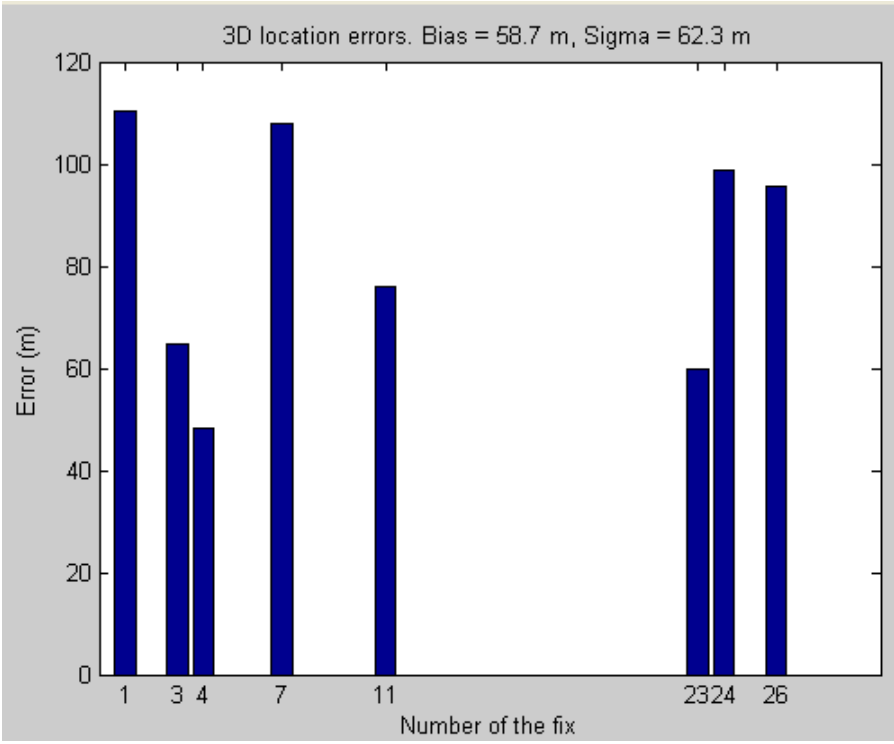

Fig IV-22 : Alcatel demonstrator 3D position error

The resulting 2D and 3D errors are illustrated in figures IV-21 and IV-22 above; they are significant in this case: 31.1 and 58.7 meters respectively versus 7.5 and 54 meters. Last, the following figure illustrates the average satellite signal C/N_0 observed.

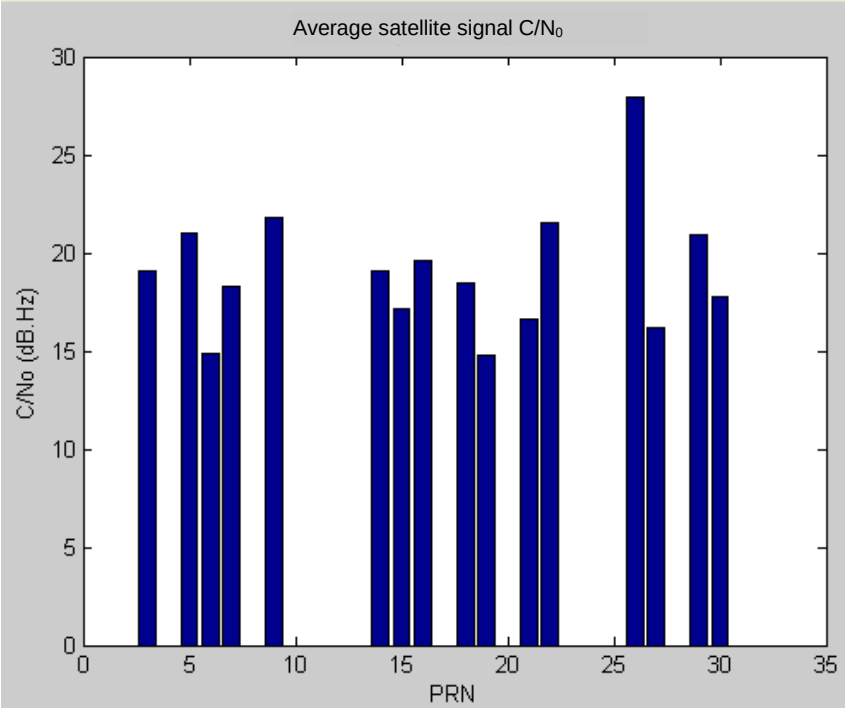

Fig IV-23 : Alcatel demonstrator average satellite signal C/N_0

Other test experiments were conducted in the next office. The results, summarized in table IV-2, were better, meaning that the GPS availability and performance greatly depend on the epoch the tests were conducted. This is mainly explained by the fact that for the two experiments the corresponding satellites constellations were not the same.

Number of fixes	Availability	Mean 2D position error	2D error standard deviation	Mean 3D error	3D error standard deviation
16	81 %	28 *m*	31 *m*	48 *m*	48 *m*

Tab IV-2 : Results obtained with another test series for this type of environments

IV.2.2.8 Urban environments

The tests were conducted in Toulouse downtown, with narrow streets. They were repeated in two different locations at different times, with an acquisition test in the first street and a tracking test in the other street (because the second street is more constrained than the first one).

Croix Baragnon street results (acquisition performance)

The Haicom standard receiver could not deliver a solution in this street.

Fig IV-24 : Croix baragnon street in the West and the East directions

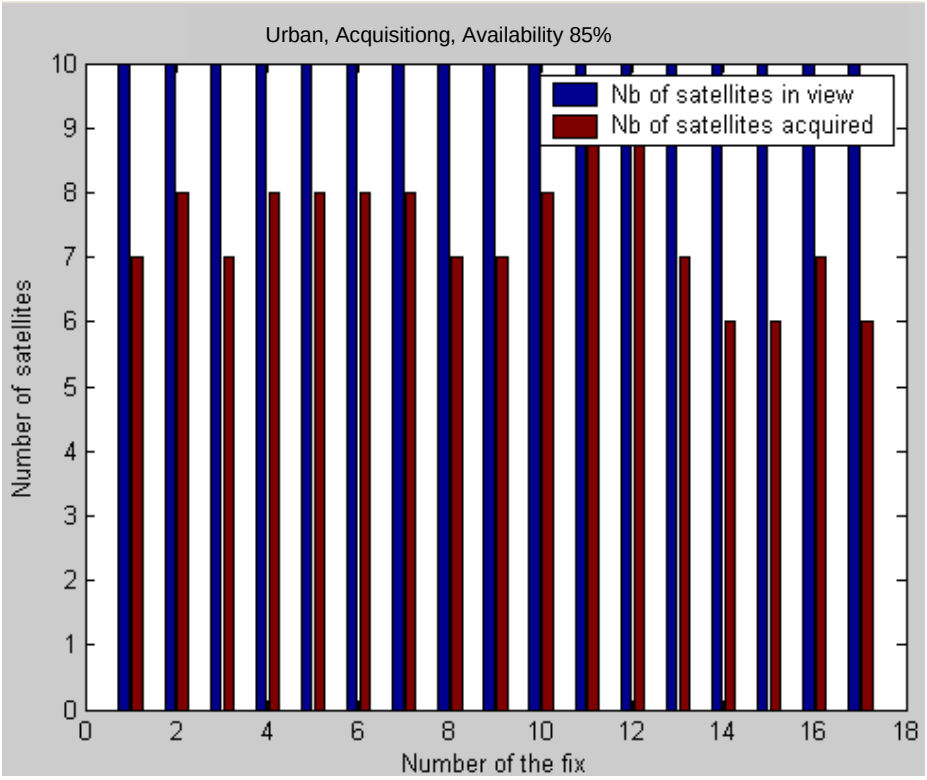

Fig IV-25 : Alcatel demonstrator number of satellites and availability percentage

The availability of the AGPS receiver in this street (figure IV-25) is close to its availability in light indoors (figure IV-20).

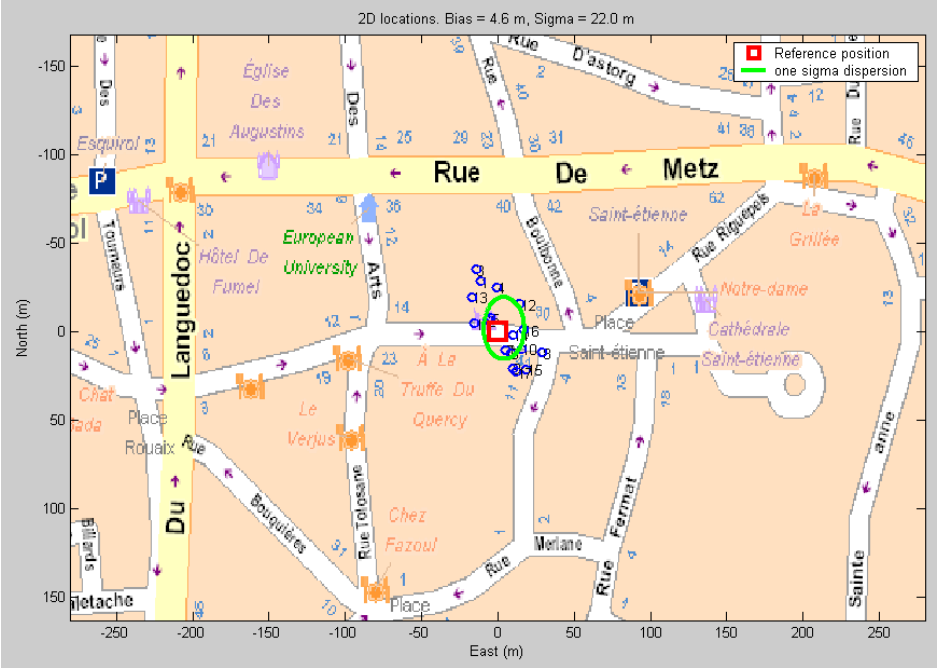

Fig IV-26 : Alcatel demonstrator 2D error

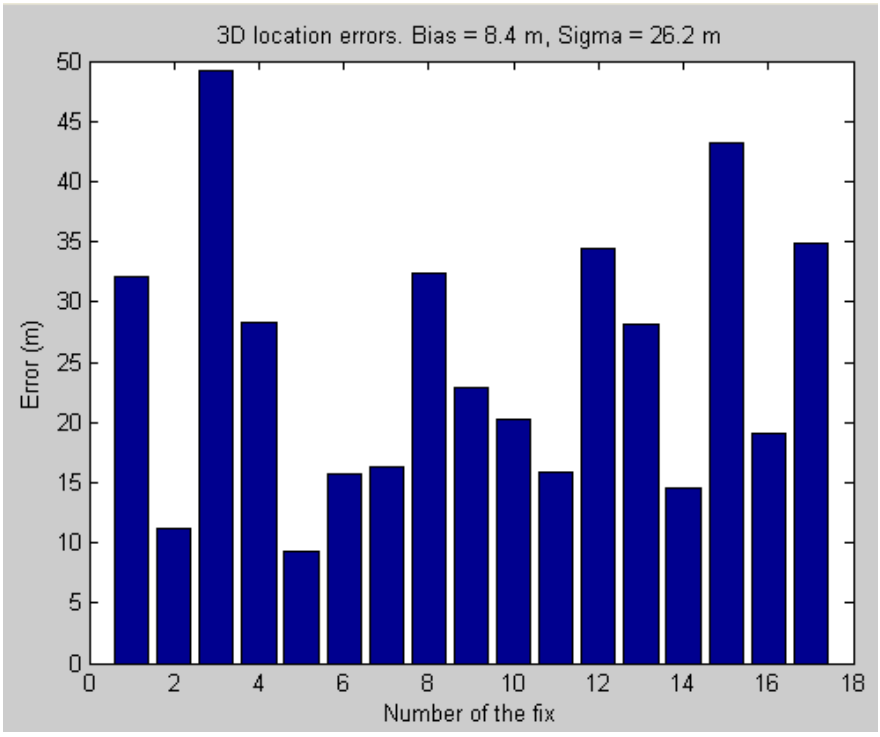

Fig IV-27 : Alcatel demonstrator 3D error

The 2D and 3D errors illustrated in figures IV-26 and IV-27 are also close to those obtained in light indoors environments. The same goes for the average satellites power as depicted in figure IV-28 next.

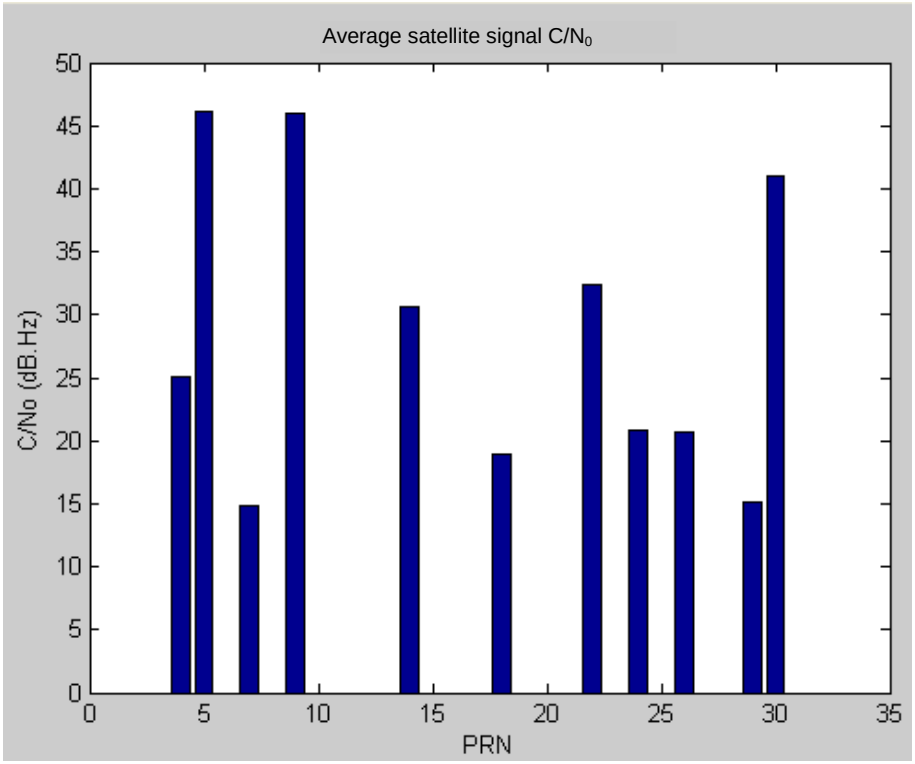

Fig IV-28 : Alcatel demonstrator average satellite signal C/N_0

Impasse du canard street results (Tracking mode)

Even in tracking mode, the Haicom standard receiver was not available in such urban streets (figure IV-29).

Fig IV-29 : Impasse du canard street in the North and the South directions

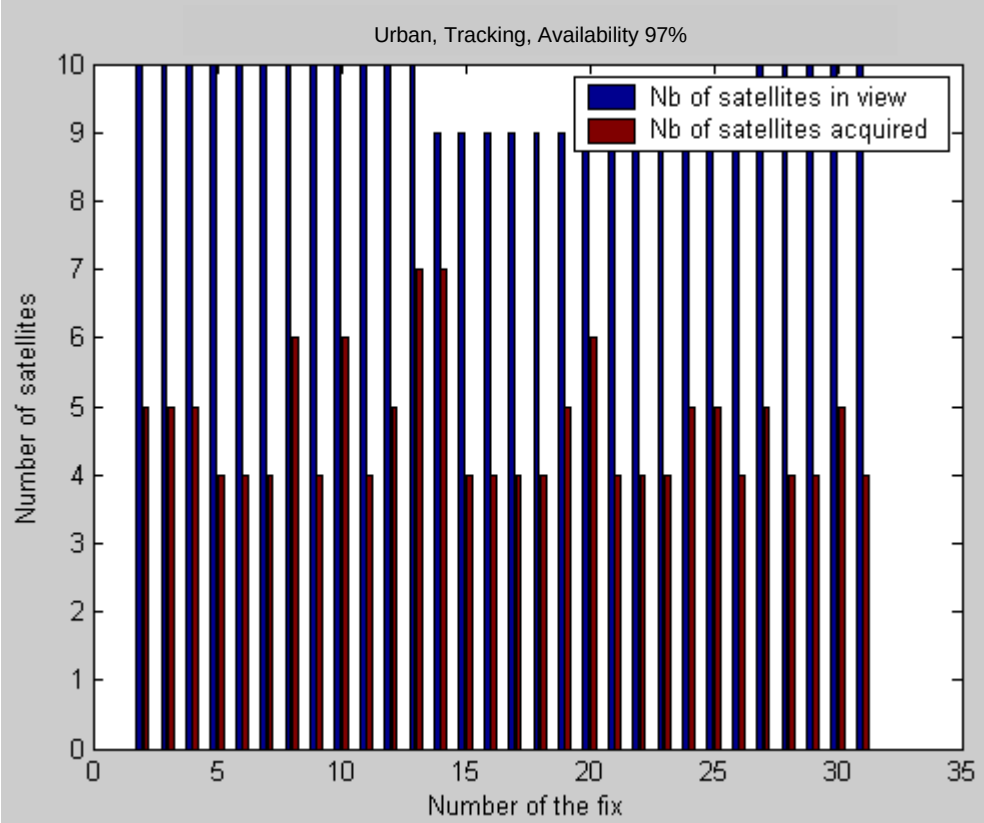

Fig IV-30 : Number of satellites tracked by the Alcatel demonstrator and availability percentage

The Alcatel solution provided a quasi 100% percent availability (figure IV-30). But the average number of satellites tracked is approximately 4 to 5 satellites. With only 4 satellites successfully tracked, the receiver is forced to use these satellites to compute the final solution, either they have a good geometry or not; in other words, there is no redundancy to compute the solution. Such a situation is very frequent in urban or indoor environments, leading to lower accuracy in the final position.

Fig IV-31 : Alcatel demonstrator 2D error

The 2D errors characteristics (mean and standard deviation) are quite the same as those obtained in the Croix Baragnon street (figure IV-26). This is not the case for the 3D error as it can be seen on the following figures IV-32 and IV-33. The difference is mainly due to the satellites geometry available for this test.

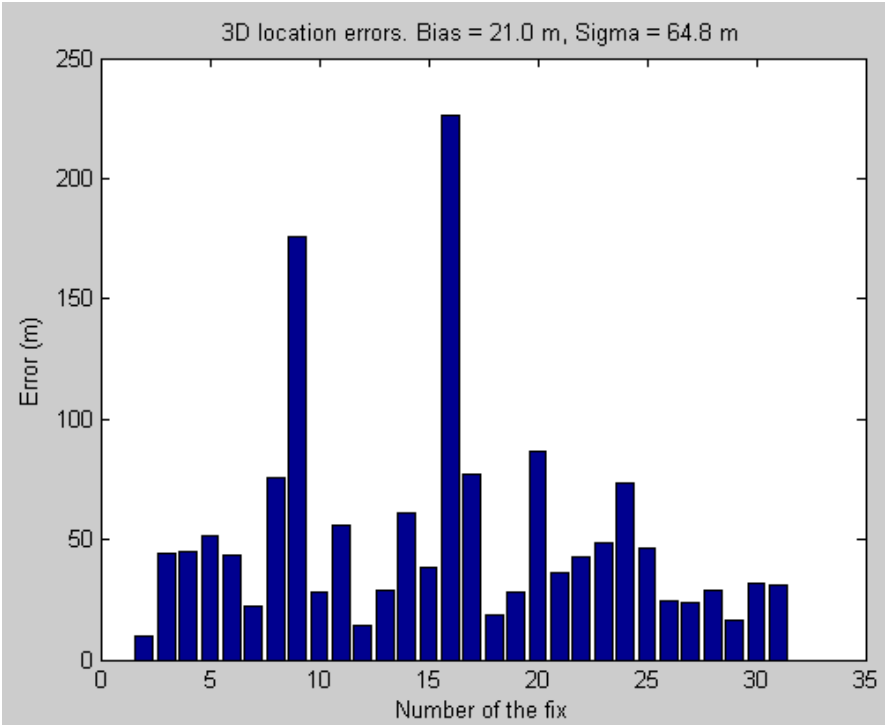

Fig IV-32 : Alcatel demonstrator 3D error

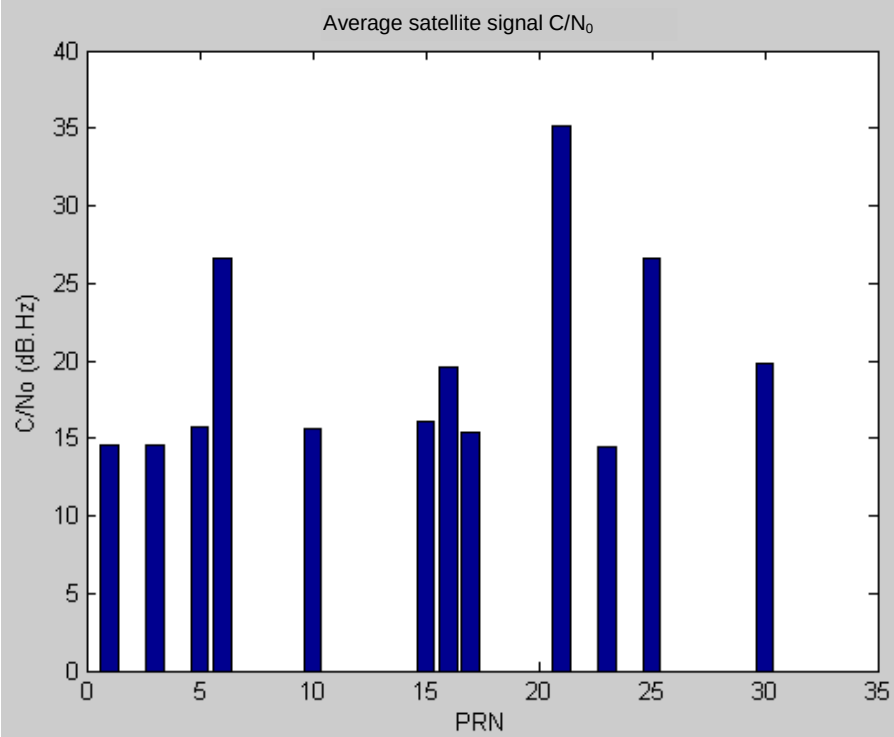

Fig IV-33 : Alcatel demonstrator average satellite signal C/N_0

The former results are all summarized in the following table.

	Availabili-ty		**Mean 2D position error**		**2D error standard deviation**		**Mean 3D error**		**3D error standard deviation**		**Minimum acquired satellite power**	
	Hai-com	Alcatel demonstra-tor	Hai-com	Alcatel demonstra-tor	Hai-com	Alcatel demonstra-tor	Hai-com	Alcatel demonstra-tor	Hai-com	Alcatel demonstra-tor	Hai-com	Alcatel demonstra-tor
Light Indoors (acq)	87 %	87 %	7.5 *m*	5.1 *m*	38.3 *m*	69.7 *m*	54.7 *m*	37.1 *m*	79.3 *m*	104.8 *m*	33*dB Hz*	24 *dBHz*
Urban: Croix Baragnon (acq)		85 %		4.6 *m*		22.0 *m*		8.4 *m*		26.2 *m*		15 *dBHz*+5 *dBHz*=20 *dBHz*
Deep Indoors (track)		87 %		31.1 *m*		39.1 *m*		58.7 *m*		62.3 *m*		*14 dBHz*+5= 19 *dBHz*
Urban: Impasse du canard (track)		97 %		4.7 *m*		23.7 *m*		21.0 *m*		64.8 *m*		~14 *dBHz*+5 *dBHz*=19 *dBHz*

Tab IV-3 : Summary of AGPS tests in indoor and urban environments

According to this table, in the acquisition mode, the standalone GPS receiver proved to have better error standard deviation performances than those of the AGPS receiver: 38 *m* versus 69

m for the AGPS as standard 2D error deviation, 79 *m* versus 104 *m* as standard 3D error deviation. However, the AGPS was better in terms of mean error values. But the availability of the Haicom receiver is very limited. Indeed, according to its technical specifications, its acquisition threshold is at 33 *dBHz*.

In further tests, a Garmin e-trex Venture conventional receiver was used by Alcatel. The results showed that it has comparable sensitivity and accuracy performance as the Haicom, but exhibits enhanced availability in light indoors.

In summary, these results show that the AGPS receiver could acquire signals as low as 19 *dBHz*, compared to a minimum of 32 *dBHz* for the HSGPS. This value for the AGPS receiver limit C/N_0 for acquisition are in accordance with the result provided by [*Karunanayake et al., 2004*]. He found an acquisition threshold of 19 *dBHz* approximately if one of the signals present is strong enough, for the AGPS receiver, and 27 *dBHz* if all the satellites have the same received power.

For the tracking mode, the tests conducted here could not be conclusive since the conventional receiver did not provide a 3D solution in any of the tracking tests. However, a tracking test conducted by [*Karunanayake et al., 2004*] showed that when the conventional receiver is available, it delivers better solution accuracy, but cannot provide a position for C/N0 ratios lower than 32 *dBHz*. We conducted a tracking test using an OEM4 conventional receiver (the Haicom receiver was not available then) confirmed this value. The signals used are generated by a Spirent STR4500 generator. This tracking test was carried with all the satellites initially at –130 *dBm*. The receiver was first given these constant power satellite signals for approximately 20 minutes so that we are sure that it was able to acquire and track the signals. Next, the power level of the satellites is decreased by 1 *dB* every one minute, until no position fix could be reached anymore. During this test we saved the C/N_0 values computed by the receiver, the number of satellites tracked, and the receiver computed position in order to assess the height error and the two-dimensional error respectively. The results are summarized in figure IV-34. The y axis of the power level curve represents the relative power with respect to –130 *dBm*. Its limits are: –130 *dBm* which corresponds to 0, and –142 *dBm* which corresponds to –12.

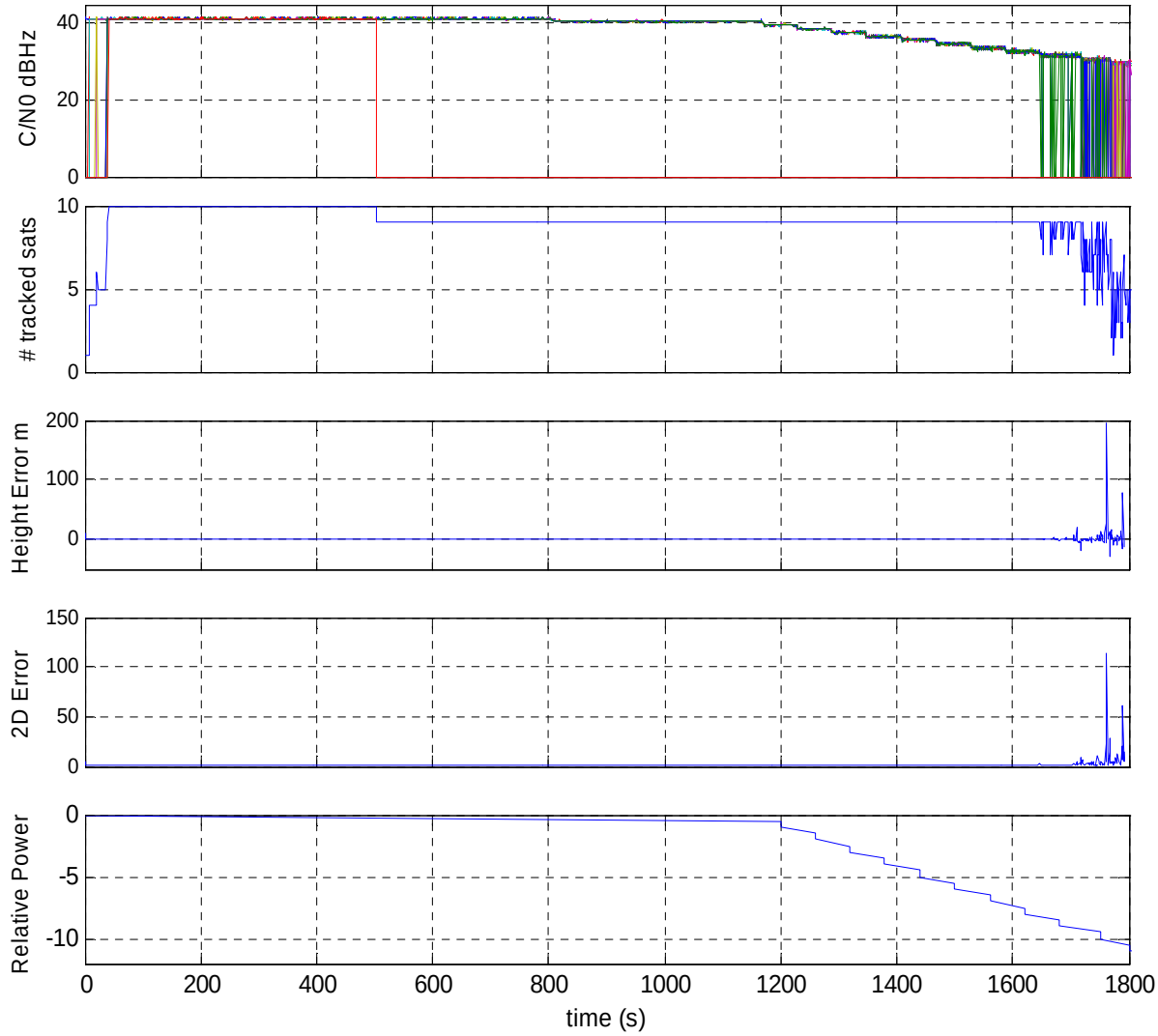

Fig IV-34 : Tracking performance of a standalone receiver (OEM4)

It can be seen on these figures that at –138 *dBm* the receiver begins to loose track of some satellites consecutively, however a position fix could still be obtained till –140 *dBm*, that is approximately 32 *dBHz* with N_0=–202 $dBHz^{-1}$. At this level a position could be computed but not all of the time. And the position errors are very important.

As for the AGPS receiver tracking threshold, it was found in [*Karunanayake et al., 2004*] that it could track signals down to 17 *dBHz*. This value is congruent with the tracking threshold found in the course of this thesis (19 *dBHz*). In the same paper, the HSGPS tracking threshold was found at 17 *dBHz* also. The test conducted with the HSGS in the course of thesis yielded tracking thresholds of 10 *dBHz*, but it is thought that the C/N_0 was not well estimated. But in generally, the HSGPS and the AGPS systems tracking thresholds are quite the same. The main difference between AGPS and HSGPS is in the acquisition performance. Indeed, the coarse estimates provided by the AD are very beneficial for acquisition, but do not impact the tracking mode where the receiver has a much more precise GPS time and location.

IV.2.3 Conclusion on AGPS

The AGPS is a promising technique which presents many advantages. It essentially enhances the acquisition sensitivity of the receiver, thus enabling GPS positioning in difficult conditions. It also has good accuracy performance compared to the HSGPS technique. Moreover, it dramatically decreases the TTFF which is very important for beneficial real time commercial applications.

Yet, due to lack of time, the AGPS TTFF was not studied in the frame of the tests performed. However this was done by Karunanayake et al. [*2004*] who found that the TTFF is considerably lower in the case of AGPS owing to the AD.

It can be concluded that the "coarse" estimates provided by the Assistance Data mainly enhance acquisition not tracking performance because when the receiver is in tracking mode, it has a much more precise GPS time and location.

In short, AGPS provides greater acquisition sensitivity and similar tracking performance as HSGPS receivers.

IV.3 Conclusion

The table below gives a quick view over the advantages and drawbacks of the three basic types of wireless satellite based location technologies:

	Advantages	Drawbacks
Standalone GPS	- Little or no additional network equipment - Works with all mobiles - Privacy not an issue (user controlled) - Location capability remains in absence of wireless coverage or network assistance - No air interface traffic overload	- New handsets - No indoor or urban coverage (<32 or even 38 *dBHz*) - Considerable increase in handset cost and complexity - Additional battery consumption - Long TTFF - system upgrades limited by deployed handset base
HSGPS	- Superior availability and coverage (tracking down to 18 *dBHz*), therefore avoids repeated signal loss and reacquisition - Little or no additional network equipment - Works with all mobiles - Location capability remains in absence of wireless coverage or network assistance - No air interface traffic overload	- Lower accuracy - Long TTFF - Acquisition threshold of 32 *dBHz* , therefore, not efficient if the receiver is launched in an indoor environment - Additional Battery consumption - New handsets - System upgrades limited by deployed handset base
AGPS	- Superior accuracy, availability and coverage (acquisition and tracking down to 18 *dBHz*) - Short TTFF - Maps and databases increase location accuracy if processing in network - Minimal impact on battery life - Implementation cost shared by mobiles and the network - System evolves with network upgrades - Location data shared between users and network operator (users can withhold data for privacy reasons, and operator can restrict assistance data for privacy reasons, and operator can restrict assistance data to subscribers of service) - Air-interface traffic optimized by distributing data and processing between network and mobiles	- Network assistance increases signaling load - Interoperability between network and mobiles requires standards, delaying deployment - New upgraded handsets needed for initial deployment - Needs a communication fee - Positioning service not available outside of the GSM service area

Tab IV-4 : Comparison between Standalone GPS, HSGPS and AGPS

According to the previous table, AGPS seems to be the best solution, especially in the frame of this thesis where the focus is brought on the acquisition stage. Besides, since it uses the wireless network to supply assistance data to handset GPS receivers, it is an inherent

solution for hybrid techniques. In addition, AGPS can easily integrate high sensitivity issues. Indeed, recent developments of AGPS have enabled the use of long coherent integrations by providing the navigation message, timing information, almanac, and approximate position through alternate communications channels. This assistance may improve receiver timing to lessen the limitations caused by Doppler mismatch. Current timing accuracy is sufficient to increase integration times to hundreds of milliseconds, but not yet past 1 second and beyond [*Karunanayake et al., 2004*]. This means that AGPS and HSGPS are compatible technologies and can be used together to enhance the overall system acquisition and tracking TTFF, availability and accuracy.

The next chapter describes different advanced acquisition algorithms to be used in conjunction with the AGPS in order to further enhance the acquisition performances.

Résumé du chapitre V

Ce chapitre présente plusieurs techniques avancées de traitement du signal. De façon générale, l'amélioration des performances de l'acquisition implique l'amélioration de la sensibilité du récepteur aux signaux faibles, classiquement via des intégrations longues, comme c'est le cas pour l'HSGPS. Mais ceci est généralement réalisé au prix d'un temps de calcul beaucoup plus long et dans certains cas d'une précision réduite. Ainsi, améliorer la sensibilité du récepteur et le temps de calcul sont deux objectifs opposés. Le meilleur compromis serait de réduire le temps de calcul pour pouvoir acquérir pendant longtemps afin de détecter des signaux faibles, sans pour autant augmenter le temps global observé dans les méthodes conventionnelles.

Les algorithmes décrits dans ce chapitre visent surtout à diminuer le temps de calcul, tout en garantissant une perte nulle ou minimale. Ces algorithmes sont comparés à l'algorithme d'acquisition de base, utilisant la FFT pour réaliser la corrélation.

Le premier algorithme permet de réaliser l'intégration cohérente en sommant après le couple d'opération FFT-IFFT, donc en d'autres termes en sommant après la corrélation. Cette méthode permet de réaliser des intégrations plus longues sans augmenter la taille du signal utiliser pour réaliser la FFT ; ce qui très avantageux vu que la FFT est une opération très couteuse en temps, et sa complexité augmente non-linéairement avec la taille du bloc de données traité. Ainsi, seuls des blocs d'$1\,ms$ sont utilisés, et l'intégration cohérente est réalisée en sommant ces blocs.

Le deuxième algorithme permet d'accomplir l'intégration cohérente en sommant avant la corrélation. Ainsi, l'intégration cohérente a lieu avant de convertir le signal dans le domaine fréquentiel. La sommation a lieu cependant après la compensation Doppler. En d'autres termes, T_p ms de signal sont sommés ensemble après compensation Doppler, puis convertis dans le domaine fréquentiel pour être corrélé avec le code à l'aide de la FFT.
Cette méthode permet de réduire le temps de calcul. Cependant théoriquement, elle pourrait engendrer des pertes liées au Doppler du code qui n'est pas compensé correctement, car une seule ms de code est utilisée pour plusieurs ms de signal. Pour une intégration cohérente sur $2\,ms$ cette erreur est de l'ordre de $0.06\,dB$, ce qui est négligeable dans ce cas.

Le principe de l'algorithme de la FFT shift est de réaliser la compensation en Doppler non pas en multipliant par une exponentielle complexe comme cela a été le cas pour les algorithmes précédents, mais plutôt de déplacer les composantes fréquentielles du signal d'une valeur équivalente à la compensation Doppler. Cependant cet algorithme induit des pertes au niveau de la corrélation et résulte en un pic de corrélation dont la forme serait déformée, induisant ainsi quelques erreurs.

L'algorithme de la FFT transverse réduit dramatiquement le temps de calcul de la FFT. L'idée principale est de supposer que la phase résiduelle du signal est constante sur des intervalles d'$1\,ms$ et pour des cases Dopplers très petites.

Le principe consiste à ne pas utiliser la technique de recherche séquentielle sur les cases des fréquences Doppler, mais d'utiliser un autre schéma. Le domaine fréquentiel est décomposé en deux types de cases : des cases larges avec des pas de $500\,Hz$, ce qui correspond à un temps d'intégration d'$1\,ms$. Puis des cases plus petites sont définies à l'intérieur de ces cases. L'intégration cohérente elle est réalisée en sommant $T_p\ ms$ de signal comme dans le cas de la FFT classique. Par la suite, une sorte de transformée de fourrier est effectuée dans le sens transverse.

Finalement, l'algorithme somme des répliques, ou SOR, permet de rechercher en parallèle plusieurs satellites, au lieu de réaliser une recherche séquentielle de ceux-ci. Ceci est possible en corrélant le signal reçu avec une somme de codes C/A compensés en Doppler au lieu de faire la corrélation avec un seul code. Cette opération permet de gagner du temps au niveau de la recherche de plusieurs satellites, mais résulte en une augmentation du niveau de bruit total, réduisant ainsi la sensibilité du récepteur aux signaux faibles.

Ces algorithmes ont été implémentés sous matlab, et ont fait l'objet de plusieurs tests de comparaison rapporter au chapitre VI.

Chapter 5

Advanced AGPS acquisition techniques

Contents

In the previous chapter we described the HSGPS and AGPS principles in details. It was found that the AGPS improves the GPS signal acquisition. Not only the receiver acquisition sensitivity is enhanced, but also the TTFF is decreased. Indeed, using the AGPS, the AD (*Assistance Data*) reduces the visible PRN, each code delay and carrier Doppler frequency search spaces. Further improvement to the acquisition mode of the receiver is considered in this chapter. Usually, improving the acquisition performance implies enhancing the receiver sensitivity to weak signals, classically through the use of extended dwell times as for the HSGPS technique; but this is generally done at the cost of longer computation time, and reduced accuracy as was evidenced in Chapter IV. In short, improving the receiver sensitivity and the computation time are competing objectives. A good compromise would be to decrease the computation time such that longer signal blocks can be processed to compensate for the loss in sensitivity while keeping an overall computation time lower than in conventional methods.

In this chapter, different algorithms aiming at improving the acquisition performance are described. Their performances are assessed in the next chapter. All of the algorithms mainly cope with means to decrease the computation time, with a minimum or no loss in sensitivity performance. Note that all of these methods assume an AGPS context, implying a

prior estimation of the Doppler frequency to within 2 *kHz*, the time information to within 2 *s*, and the reference position depending on the transmitting GSM cell. The use of the AGPS allows for a reduction of cross-correlation peaks as it is explained in the first paragraph. For the sake of simplicity, the AGPS scenario is exposed once at the beginning since it is common to all algorithms. Then, the algorithm of the classical acquisition scheme based on FFT is recalled, before describing the advanced acquisition techniques.

The task of proposing innovative algorithms for acquisition in constrained environments was very difficult in the frame of the PhD. thesis because this was a totally new subject in the laboratory when this study started, and a period of learning has been needed to correctly seize this issue. Second, too many acquisition techniques are patented or published, this has had as a consequence to limit the possibilities to explore new techniques. That is why, in this chapter, we describe some of the most performant algorithms in the frame of our application, and we introduce a new one, namely the SOR algorithm.

V.1 Brief recall of AGPS and way of reducing cross-correlation

As described in Chapter II, the AGPS technique aims at combining a satellite positioning receiver and a cellular system enabled mobile station in such a way that the positioning receiver can benefit from AD disseminated by the telecommunication channel in order to improve the sensitivity of the positioning solution and to decrease the TTFF.

Typically in cold start, the AD set required is composed of:

- The reference time,
- The reference location,
- The navigation model (ephemeris and various corrections),
- The ionosphere correction

The receiver is provided information on its reference location (using the cell id technique described in appendix D), the satellites ephemeris and clock data, and visible PRNs (using the ephemeris data). With this information, the receiver can compute estimates of each satellite signal Doppler frequency and code delay by applying $\hat{\tau} = \frac{Satellite\ to\ \text{Receiver}\,\text{distance}}{\text{c}}$ for delay, and $f_d = -L_1.\frac{v_d}{c}$, with L_1 the carrier frequency, v_d the satellite radial velocity at the reference time, and c the speed of light in vacuum.

The satellite to receiver distance and the satellite radial velocity are computed using the Assistance Data. But this Doppler-Delay estimation is not accurate since the following hypotheses are taken into account in the AGPS context (refer to Chapter IV, paragraph IV.2.2):

- The Assisted server is able to provide timing information with an accuracy of only $\pm 2\ s$,

- The reference location of the receiver is provided with a minimum accuracy of 1, 10 or 30 km depending on the studied environment, either if it is a rural, an urban or an indoor environment.

With these uncertainties, code delay and Doppler frequency estimates are affected by errors. The overall peak range P_R of a satellite due to uncertainties on the reference time and the reference location is given as (refer to figure V-1):

$$P_R(k) = P_k \pm \left[\frac{2\Delta x \cos(\gamma)}{c} + \frac{[v_d * \Delta t]}{c} \right] R_c \quad (in\ chips) \qquad \textbf{(V-1)}$$

where P_k is the estimated code delay using ephemeris data (taking into consideration the time synchronisation error), γ the satellite elevation angle, Δx the cell radius (user position uncertainty), v_d the satellite radial velocity, Δt the GSM time transfer uncertainty, and $v_d * \Delta t = \delta d$ the travelled distance estimation error (resulting in code delay estimation error).

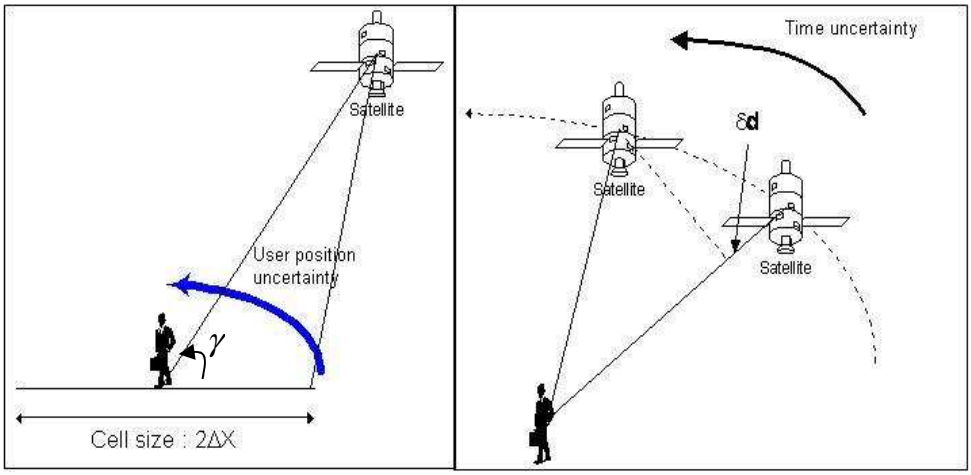

Fig V-1 : Illustration of time and the user position uncertainties

In the worst case where a satellite is on the horizon, with an elevation of $0°$, a Doppler velocity of approximately $924\ m/s$, a cell radius of $30\ km$, and a reference time uncertainty of $\pm 2\ s$, the peak window is of about $211\ chips$ (the worst case). This means that a correlation peak needs to be searched for only within this window, and all peaks falling outside these boundaries are not considered. Such correlation peak identification process reduces the probability of false detection due to eventual cross-correlation peaks.

In terms of Doppler frequency, the Doppler frequency induced by the satellite motion is easily determined using the AD which enables to compute the satellite position (ephemeris Data) and the user position (estimated using the GSM network). But the time and position uncertainties result in an overall Doppler range of about $28\ Hz$ over the satellite induced Doppler (refer to appendix C). This is not very significant especially for coherent integrations lower than $10\ ms$ where the Doppler frequency error must not exceed 25 *Hz*. For such coherent integrations, only one or two Doppler cases need to be explored. But for longer coherent integrations, the tolerated frequency error is lower than 25 *Hz* and more Doppler cases need to be explored. Note however that there is still the uncertainty on the receiver

clock stability which may lead to a Doppler uncertainty of about $\pm 1\,kHz$ (depending on the receiver clock oscillator performance measured in *ppm* where 1 *ppm* induces an error of $10^{-6} \times 1.57542 \times 10^{9} = 1.57542 \times 10^{3}\,Hz$), and that resulting from a user motion. Yet, the latter can be neglected in the case of a pedestrian user. The receiver clock instability and user motion induced Doppler are common to all the received signals since they only depend on the receiver. Hence, once a first satellite is successfully acquired, there is no more uncertainty on the Doppler frequency (the frequency drift of the local oscillator is supposed to be precisely known, otherwise a search over a range of ± 1 *kHz* must be performed as explained in Chapter II), and only one Doppler case needs to be explored for all the other satellites. This scenario is used in all the subsequent acquisition strategies: A first satellite is acquired while searching for all the Doppler cases to be explored; the estimation error on the Doppler frequency due to user clock drift is then removed for all the other satellites before acquiring them. This method is detailed in [*Camp et al., 2000*].

The principle of the AGPS is illustrated in figure V-2. This part of the signal processing is common to all the AGPS algorithms presented in this chapter.

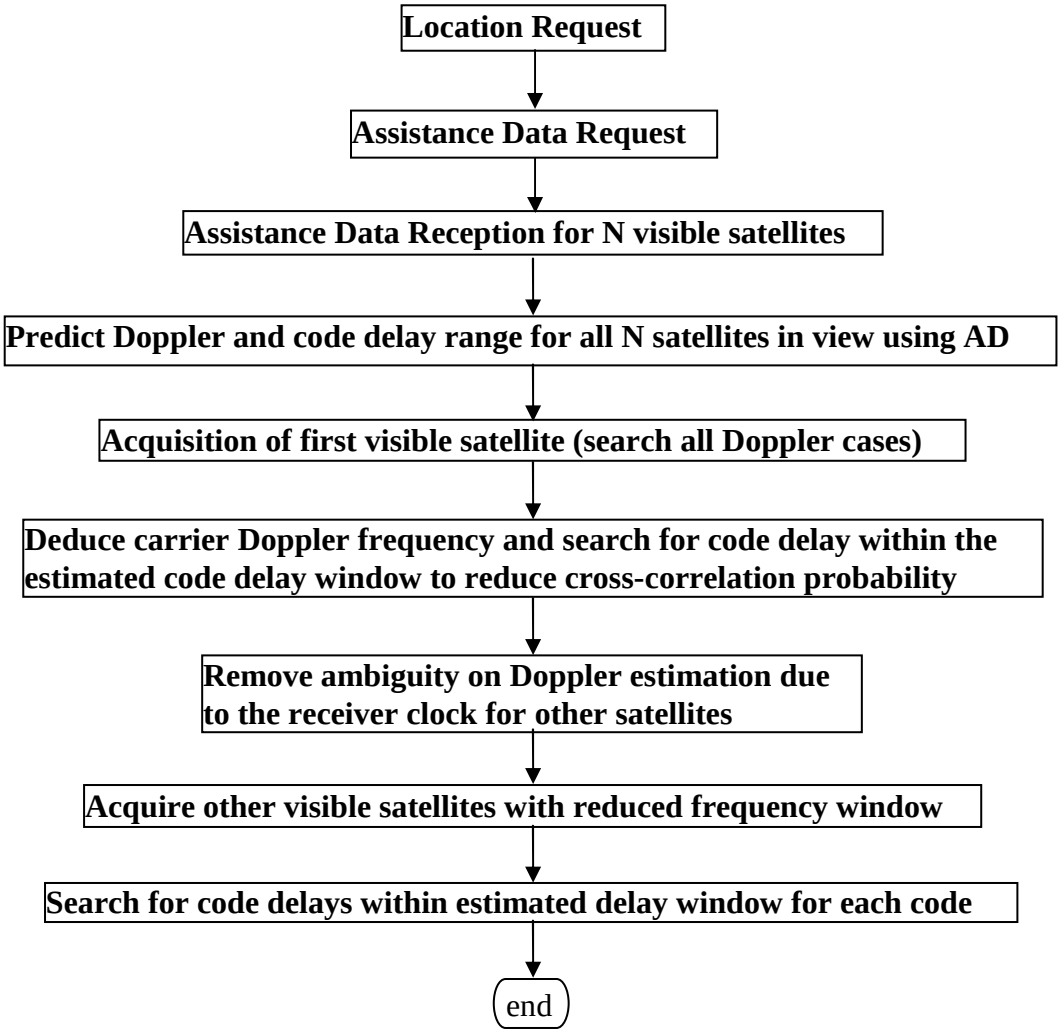

Fig V-2 : AGPS scenario

In the algorithms presented next, only the acquisition part of this scenario is described in each case. All of these algorithms process the satellites one by one, except for the SOR algorithm.

V.2 Classical acquisition scheme using FFT

Recall that the FFT is an efficient algorithm to compute the DFT, but since the FFT algorithm is so commonly employed to compute the DFT, the two terms are often used interchangeably. It was shown in Chapter II, paragraph II.5, that the DFT can be used to replace the classical temporal correlation. The following flow chart illustrates the classical acquisition scheme using FFT.

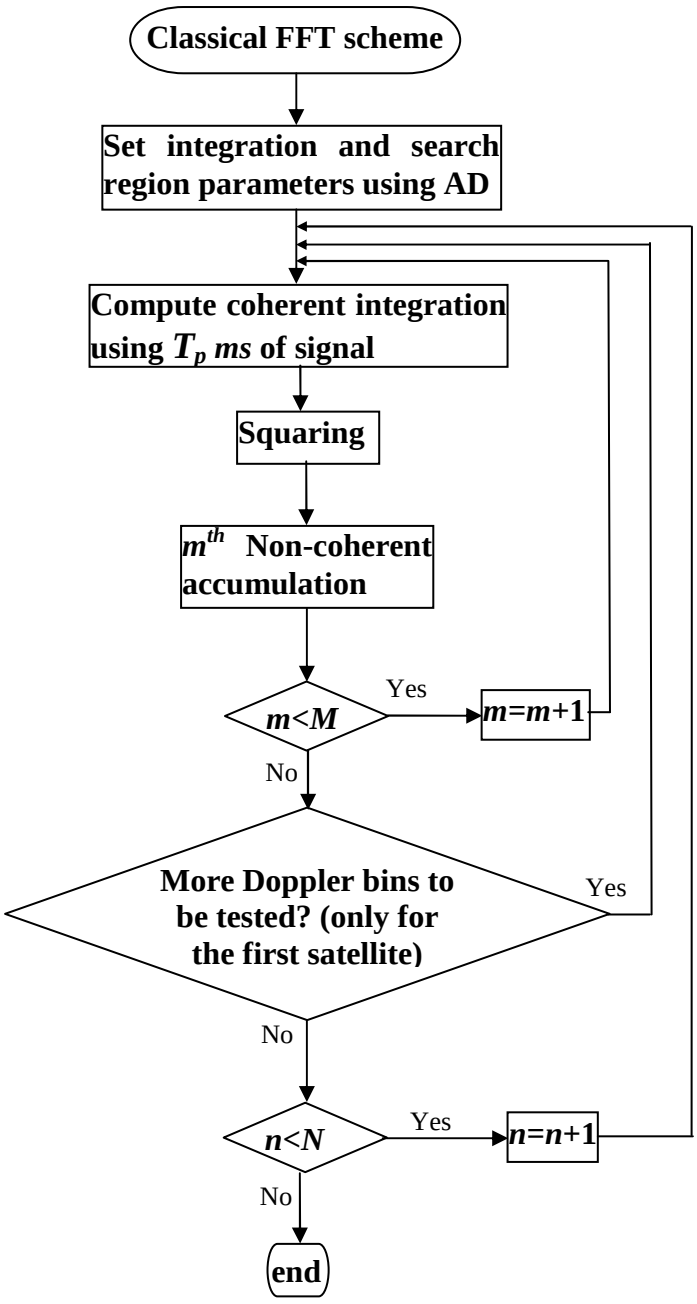

Fig V-3 : Classical acquisition algorithm flowchart

Recall that M and T_p stand for the number of non-coherent accumulations and the duration of the coherent integration in ms. The size of the frequency bins is $\Delta f_{DOP} = 1/2T_p$. N is the number of visible satellites.

The FFT technique is used to compute the coherent integration illustrated in the block diagram of figure V-4.

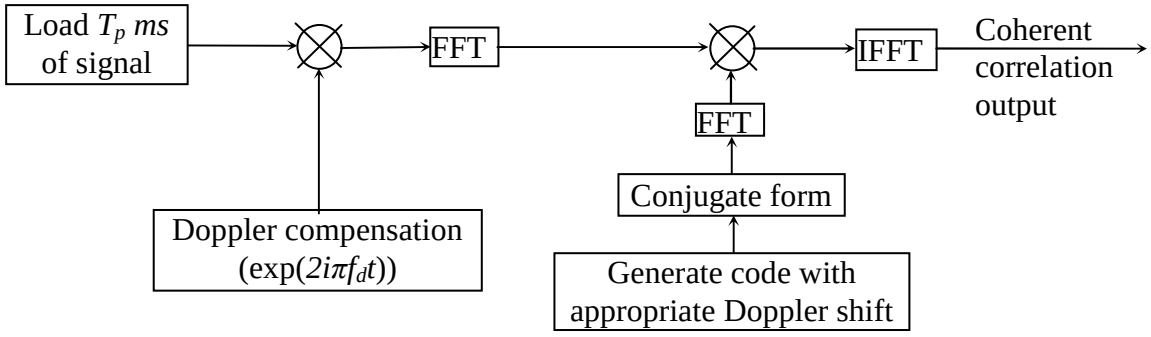

Fig V-4 : General coherent correlation synoptic

As explained in Chapter II, the FFT algorithm covers all possible code delays for a given Doppler estimate in a single step, instead of the linear search of each possible code delay performed using the classical acquisition scheme presented in paragraph II.4. However it has more stringent requirements in terms of memory availability since it processes all the samples at once, thus these samples need to be stored in memory. Note that the linearity of the FFT operator allows for more optimisation of algorithm complexity. The Sum after FFT-IFFT and Sum before FFT-IFFT described in paragraphs V.4 and V.5 take advantage of the FFT linearity to reduce the algorithm complexity.

For weak signal acquisition, extended dwell times are needed. Increasing the dwell time is possible through the use of higher non-coherent and/or coherent accumulations. Extending the non-coherent integration period leads to what is called squaring losses. This is not the case when the coherent integration is increased. Nevertheless, extending the coherent integration classically implies that longer signal blocks are processed at once. This leads to higher memory needs since the FFT has to be computed on a higher number of points, and dramatic increase in computation time, thus more power consumption. All of these parameters should be minimized for small devices like cellular phones.

Figure V-5 depicts the correlation function resulting from a $10ms$ coherent integration duration for example:

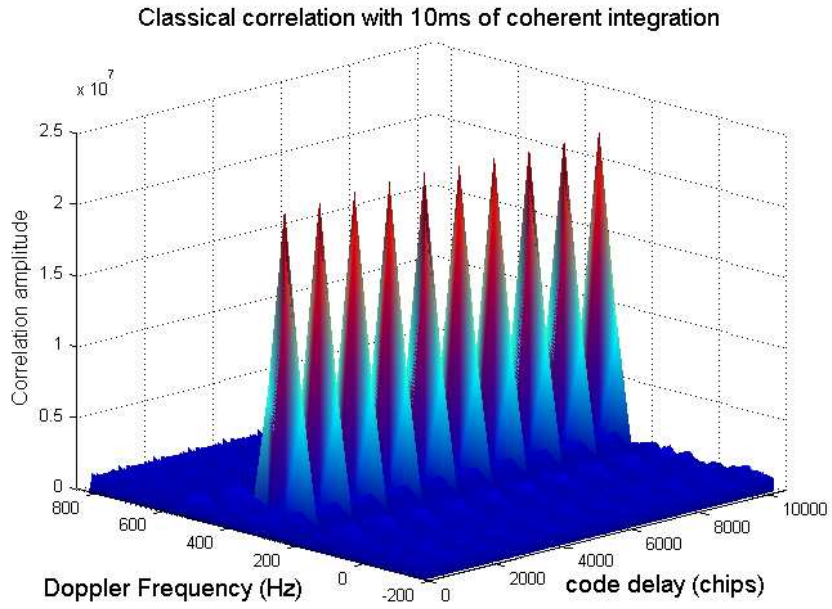

Fig V-5 : Classical correlation with a $10\ ms$ **coherent correlation**

This result corresponds to a sufficiently high C/N_0 (45 *dBHz*). The presence of 10 peaks is due to the C/A code periodicity ($1\ ms$). The peaks have approximately the same amplitudes since the code Doppler is compensated.

V.3 Average correlation algorithm

This algorithm was the object of different studies, such as in [*Djebbouri et al., 2003*] and [*Starzyk et al., 2001*] for example. These studies use a sampling frequency of 5 *MHz*, thus yielding 5000 samples per C/A code period (periodic with period $1\ ms = 1023$ chips). The FFT is not directly applied to the 5000 point observation vector, instead, the 5000 point vector is downsampled to form 5 1023-point vectors, and only 1023 points FFTs are used instead of 5000-point FFTs, by averaging. The down sampling is carried out because it is much easier in hardware to implement five 1023-point FFTs than a single 5000 FFT, as pointed out by the authors.

The correlation is carried out by frequency transforming the 1023 averaged (or down sampled) GPS signal using 1023-points FFT. This is performed on both the in-phase and the quadrature-phase by considering the in-phase values as the real input components, while the quadrature-phase values are used as the imaginary input components. First, 1023-points FFT is applied to the local code and the conjugate operation to the FFT output is performed. The next step is to multiply the complex outputs of the FFTs. The results are then changed back to the time domain using 1023-points IFFT.

The received signal needs to be reduced back to 1023 chips per millisecond by averaging consecutive 4 or 5 points into one chip. The averaged chip is similar to a chip of C/A code. Since the signal cannot be observed in forms of square waves, there is not enough information to determine which 4 or 5 points should be grouped together and averaged, unless there can be an approach to know the relative position of the samples and the chips; this

relative position can be found out from several attempts of averaging with different assumption of the relative position, as displayed below.

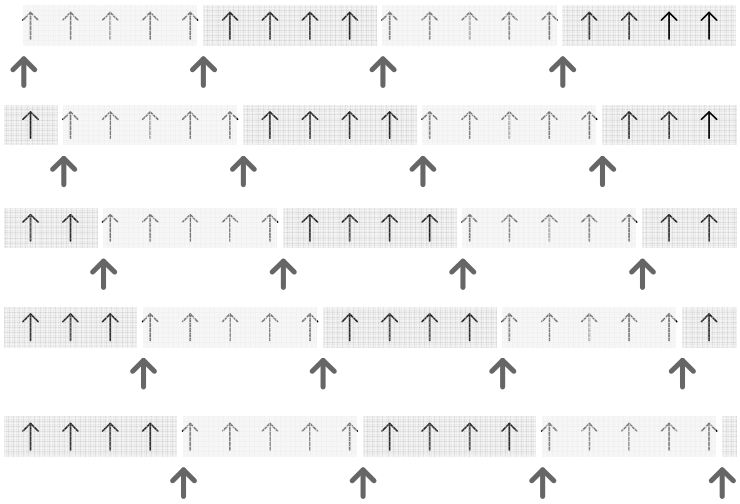

Fig V-6: The 5 sequences of averaged steps

In figure V-6, consecutive chip periods are represented in dark and light grey colours respectively, with inside arrows corresponding to samples obtained after down sampling from 5000 samples per C/A code period to only 1023 per code period. The outside arrows mark the beginning of each chip.
Among the first consecutive 5 samples, one of them must be the first sample of a chip, since no chip contains more than 5 samples. Assuming this sample is regarded as the beginning of the first chip, the relative position of the 1023 chips and all the samples can be determined and the chips can be recovered completely. Thus 5 averaged sequences, each containing 1023 chips, are generated and their correlation functions with local C/A code are computed respectively. Knowing the correlation peak indicates the signal energy, the sequence with the largest correlation peak is chosen as the best candidate for acquisition. With the 5 averaged sequences and 1023 chips C/A code, the correlation must be performed 5 times. For further reduction in computation time, the signal is down sampled to 1024 samples rather than 1023, since the FFT algorithm is much more efficient when it operates on powers of 2 points blocks using a butterfly structure for example.

The results conducted using this method did not show a net improvement of the acquisition time, and induced a great loss in the output signal power. Consequently, no further analysis was carried out using this method.

V.4 Coherent integration by summing after FFT-IFFT

This method allows for using longer coherent integrations for enhanced sensitivity, without increasing the signal block size used to compute FFT. Only $1\,ms$ signal blocks are processed at once, and the coherent integration is performed by summing these blocks. This is possible since the correlation and the coherent accumulation are linear operators.

Assuming that the received signal is modelled as:

$$r(t-\tau) = A \cdot d(t-\tau) \cdot c(t-\tau) \cdot \cos[2\pi L_1 (t-\tau)]$$
$$\cong A \cdot d(t-\tau) \cdot c(t-\tau) \cdot \cos[2\pi (L_1 + f_d)t - \theta]$$

with A the signal amplitude, $d(t)$ the data bit train, $c(t)$ the C/A code chip representation, τ the signal delay, L_1 the carrier frequency, and f_d the Doppler frequency.

For a coherent integration over T_p ms for example, the Doppler bins tested are of size $\Delta f_{DOP} = 1/2T_p$. The classical correlation is represented by:

$$R(\hat{\tau}, \hat{f}_d) = \int_0^{T_p ms} r(t-\tau).c(t-\hat{\tau}).e^{i[2\pi(L_1+\hat{f}_d)t+\hat{\theta}]}.dt \qquad \textbf{(V-2)}$$

where $r(t)$ is a T_p ms section of the received signal. The same goes for $c(t)$. $\hat{\tau}$, $\hat{f}_d$ and $\hat{\theta}$ are the estimated code delay, the Doppler frequency and phase respectively.
In equation V-2 the inphase and quadrature signal components are calculated by using a complex exponential as explained in Chapter II, paragraph II.5.

For the first satellite, this function is calculated repeatedly for all the possible values of the code delay over the integration duration, and of the Doppler bins to be tested over the predefined Doppler frequency range. Globally, *N* points are used to calculate this correlation for each value of the code delay and the Doppler frequency. In the classical process, a coherent integration through the use of the FFT, over T_p ms produces a correlation function with $N_c = T_p \cdot 10^3$ peaks, where N_c is the number of C/A code periods coherently accumulated; in figure V-5 for instance, 10 peaks can be observed for $T_p = 10\,ms$. As explained, these peaks are the result of the code periodicity of $1\,ms$. Obviously with these assumptions, these peaks have approximately the same amplitude, thus inducing a kind of redundancy on the output correlation function. To reduce this redundancy, longer coherent integrations are carried out by coherently summing successive $1\,ms$ coherent correlation results, before squaring them. $R(\hat{\tau}, \hat{f}_d)$ becomes:

$$R(\hat{\tau}, \hat{f}_d) = \sum_{k=1}^{N_c} \int_{(k-1).1ms}^{k.1ms} r(t-\tau).c(t-\hat{\tau}).e^{i[2\pi(L_1+\hat{f}_d)t+\hat{\theta}]}.dt \qquad \textbf{(V-3)}$$

In this expression $1\,ms$ blocks of the received signal $r(t)$ and the code replica $c(t)$ respectively. Globally, *N* points are used to calculate this correlation for each value of the code delay.

Using the FFT, the expression of the correlation of equation V-2 becomes:

$$R(\hat{f}_d) = IFFT\left\{FFT[r(t)].FFT\left[c(t).e^{i[2\pi(L_1+\hat{f}_d)t+\hat{\theta}]}\right]\right\} \qquad \textbf{(V-4)}$$

With $r(t)$ and $c(t)$ of T_p ms duration. $R(\hat{f}_d)$ is computed for all the possible values of the code delay $\hat{\tau}$.
Similarly, applying the FFT to equation V-3 gives:

$$R\left(\hat{f}_d\right)=\sum_{k=1}^{N_c} IFFT\left\{FFT\left[r(t_k)\right].FFT\left[c(t_k).e^{i\left[2\pi(L_1+\hat{f}_d)t_k+\hat{\theta}\right]}\right]\right\} \quad \textbf{(V-5)}$$

Where $r(t_k)$ and $c(t_k)$ are $1\,ms$ blocks (t_k is the k^{th} time vector of $1\,ms$ duration). They represent the k^{th} section of signal of duration $1\,ms$. Obviously in this case also the result of the IFFT is correlation vector computed for all possible values of $\hat{\tau}$.

This algorithm is illustrated with the flow chart of figure V-7

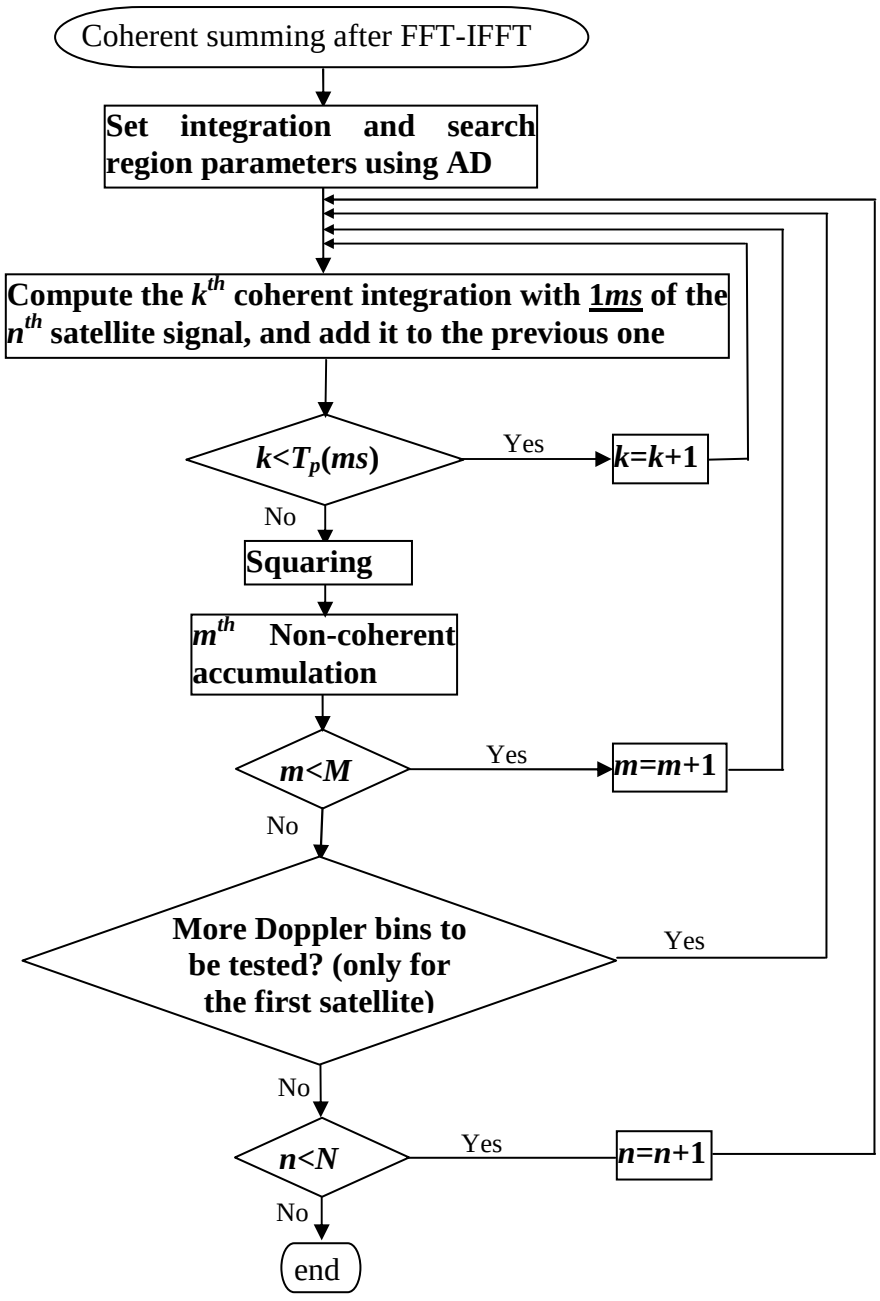

Fig V-7 : Coherent summing after FFT-IFFT algorithm flowchart

The advantage of this algorithm is that it is faster than the classical one since computing a Fourier Transform with N points, as in the classical case, is slower than

computing k Fourier Transforms with $\frac{N}{k}$ points [*Akopian et al., 2005a]*, [*Agarwal et al., 2002*]. Indeed, an FFT with N points requires $N.\log_2 N$ arithmetic operations, whereas k FFT with $\frac{N}{k}$ points each one for example require $N.\log_2 \frac{N}{k}$ arithmetic operations. The reduction in operations needed is of $N.\log_2 k$. This reduction in computation complexity is done twice, first when converting to the frequency domain using FFT, and second when converting back to the time domain using IFFT.

In addition, processing only $1\,ms$ blocks of received signal at once allows for the implementation of a sensitivity improvement technique by avoiding a possible phase jump or shift due to bits transitions for the correlation result within $1ms$. This is done by performing a circular correlation over $2\,ms$ of signal and a zero padded $2\,ms$ version of the replica code ($1ms$ of code, and $1ms$ of zeros) to produce a linear correlation over $1ms$ (the $2\,ms$ correlation result is truncated to half its size). This is not possible in the classical sequential algorithm since it introduces a large computation charge and large memory needs in order to be able to double the signal block size to be processed by each FFT-IFFT operations. This optimisation is considered in all of the following algorithms. However this technique does not prevent energy loss due to data bit transitions occurring within a total coherent integration time larger than , because it is only used for 1ms blocks, not for longer blocks. Indeed, using such technique for longer blocks of data requires processing each time twice the number of points needed in the standard case. For longer blocs this results in high complexity.

The Sum after FFT-IFFT algorithm also reduces the memory needed to carry out the correlation, since only blocks of the minimum size for correlation over one C/A code period of $1ms$ are kept in memory at once. It essentially does not affect the sensitivity because correlating is equivalent to summing the signal. Knowing that the summing operation is associative and that the FFT operator is linear, this operation is possible. Note however that since the code Doppler is compensated, the 10 correlation peaks have the same amplitude.

V.5 Coherent integration by summing before FFT-IFFT

The principle of the summing before FFT-IFFT method, [*Krasner, 1998*], is the same as that of the previous method: processing $1\,ms$ (in practice $2\,ms$) data blocks at once. According to O'Driscoll [*2006*], although it would appear that this algorithm was first observed by Krasner, it is also implicit in [*Coenen et al., 1992*]. The difference here is that the coherent integration is performed before converting the signal to the frequency domain in order to correlate it with the code. The summation is carried out after removing the signal Doppler. In other words, $T_p\,ms$ of the signal are summed together after code (f_{d_c}) and carrier (f_d) Doppler compensation, then converted to the frequency domain. The subsequent steps are the same as in the previous method. In this case, the correlation function can be written as:

$$R\left(\hat{f}_d\right) = IFFT\left\{ FFT\left[\underbrace{\sum_k r(t_k) \cdot e^{i\left[2\pi\left(L_1+\hat{f}_d\right)t_k\right]}}_{Doppler\ \ compensation} \right] \cdot FFT\left[c(t_1)\right] \right\} \quad \textbf{(V-6)}$$

The use of $c(t_1)$ implies that the accumulation of k $1\,ms$ correlation results are correlated with only one $1\,ms$ of C/A code with code Doppler compensation for only this ms.

Figure V-8 next depicts the flow chart of this algorithm.

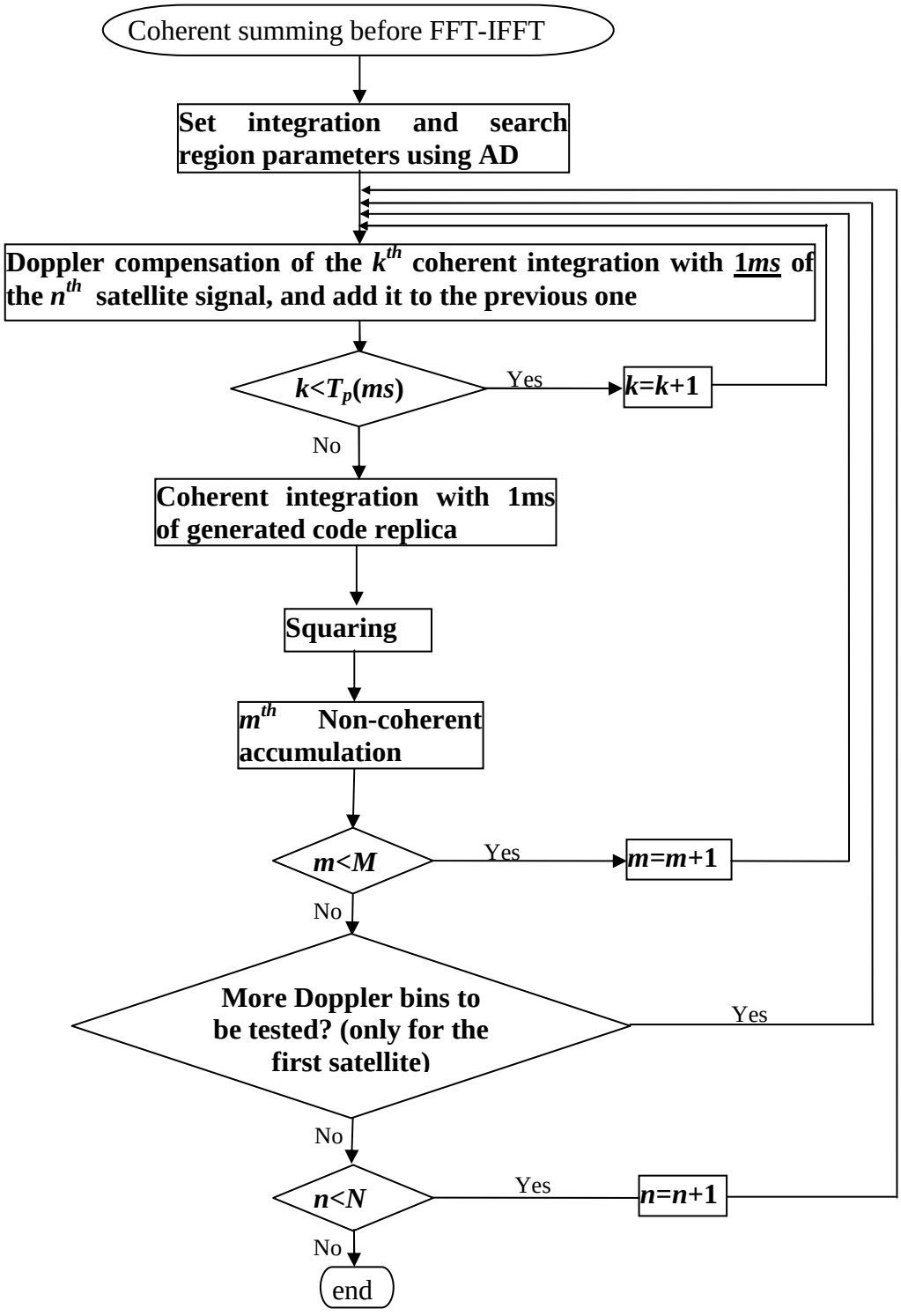

Fig V-8 : Coherent integration by summing before FFT-IFFT algorithm flowchart

Coherently summing the signal before applying FFT-IFFT transform is possible since both the coherent integration is a linear operation, and so any coherent accumulation carried out after the correlation function can equally well be performed prior to FFT [*O'Driscoll, 2006*].

This method allows for reducing the number of FFT performed by a factor depending on the coherent integration duration needed (a factor of 4 for a coherent integration over 4ms for instance). However, theoretically some losses may appear due to code Doppler which is not accurately compensated during the pre-integration phase, because the total signal is summed onto a $1ms$ block, and therefore the local code replica is only $1ms$ long, versus T_p ms of signal. This means that a code Doppler compensation of only $1ms$ is performed, instead of a code Doppler compensation of T_p ms. The code error in chips resulting from a coherent integration over t seconds in the absence of code Doppler compensation, is:

$$E_c = f_{d_c} \times t \qquad \textbf{(V-7)}$$

where f_{d_c} is the code Doppler frequency (refer to appendix C for more details).
The error E_c is illustrated in figure V-9 as a function of coherent integration duration, for a maximum carrier Doppler frequency of $f_d = 5\,kHz$, that is for $f_{d_c} = 3.2467\,Hz$ (worst case). The plot shows that for a coherent integration of up to 150 ms approximately, the code delay error is lower than 0.5 code chip which is the limit on code delay error acceptable in acquisition.

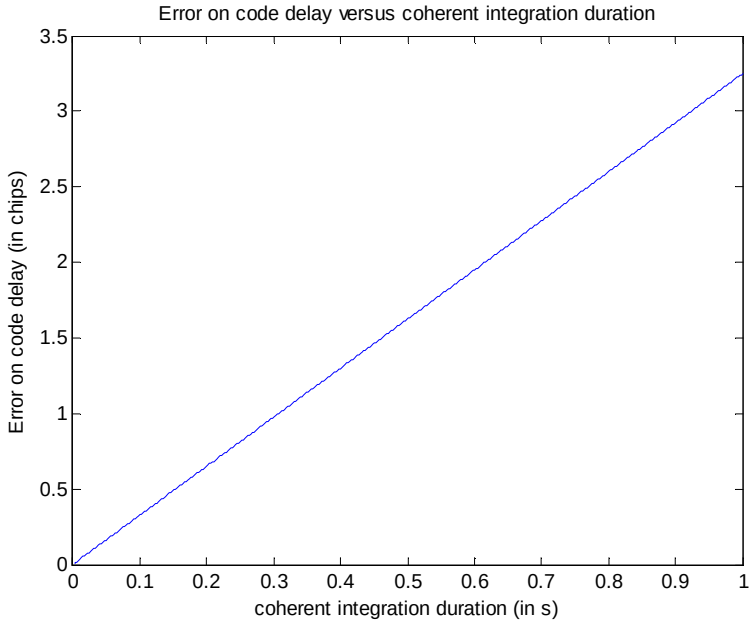

Fig V-9 : Code delay error versus coherent integration duration for a maximum Doppler frequency ($5\,kHz$)

The resulting signal power degradation in each $1\,ms$ correlation block output is given as: $D_c = 20\log(1 - E_c)$ (refer to figure II-8). For a coherent duration lying in $[0;1\,s]$ with $1\,ms$ steps and an f_{d_c} of $3.2467\,Hz$, figure V-10 illustrates the signal degradation as a function of the coherent correlation duration.

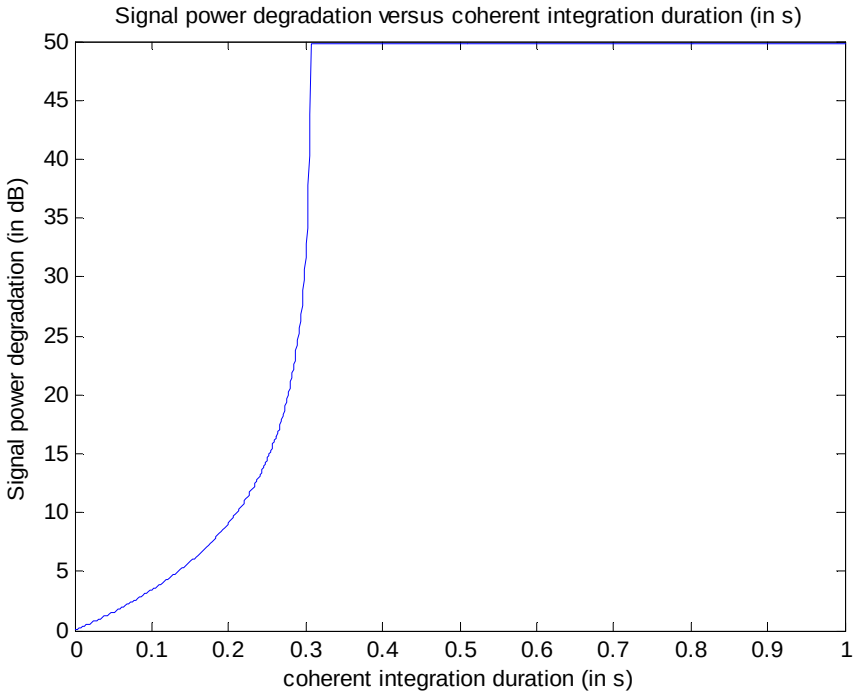

Fig V-10 : Signal power degradation due to code Doppler error versus coherent integration duration for a maximum Doppler frequency ($5\ MHz$)

For a coherent integration of 2 *ms*, the resulting signal power degradation is 0.06 *dB* which is negligible. This will be verified in the performance results presented in Chapter VI.

V.6 FFT shift algorithm

This method presented amongst others in [*Akopian et al., 2005b*], and [*Sorrells et al., 2000, 2002*], allows for speeding up the signal Doppler removal phase of the acquisition algorithm. In all of the former algorithms, the signal Doppler removal is done by multiplying the time domain signal by a complex exponential having a frequency equal to the Doppler frequency to be tested. Alternatively, this can be performed by shifting all bins in the frequency representation of the input GPS signal or Gold code one way or the other by a predetermined number of bins. This is possible thanks to the frequency shift theorem, a useful property of the Fourier Transform. It states:

$$FT\{\exp(-j2\pi f_d t)\cdot f(t)\} \Leftrightarrow F[(f+f_d)] \text{ with } F(f)=FT[f(t)]$$

Thus the FT of a product of a function by a complex exponential is simply a shifted version of the FT of the function.

The frequency shift applied is an integer number of the FFT frequency resolution: shifting to the left decreases frequency, while shifting to the right increases frequency. No flow chart will be presented for this algorithm, since it only acts on a small part of the overall acquisition algorithm and can be incorporated in all of the previous ones to replace the classical Doppler removal.

This algorithm enhances the acquisition time because it enables to avoid multiplying by a complex exponential which is more time consuming then simply shifting the vector indices. Using the frequency shift theorem, only one FFT operation needs to be performed for all Doppler bins.

The main problem of this algorithm is the final frequency resolution. In fact, when integrating over T_p *ms*, the FFT frequency step is twice the Doppler bin size. Indeed; the FFT resolution is given as [*Proakis, 1995*]:

$$\Delta f_{FFT} = \frac{f_s}{N} = \frac{f_s}{T_p / T_s} = \frac{f_s}{T_p \cdot f_s} = \frac{1}{T_p}$$

With F_s the sampling frequency, T_s the sampling period, T_p the coherent integration time, and *N* the length of the considered signal block.

The usual Doppler bin size is : $\Delta f_{DOP} = \frac{1}{2T_p}$, that is half the FFT step. Therefore, the actual Doppler bin size will be $\Delta f_{DOP} = \Delta f_{FFT} = \frac{1}{T_p}$. The correlation output in this case is given in figure V-11:

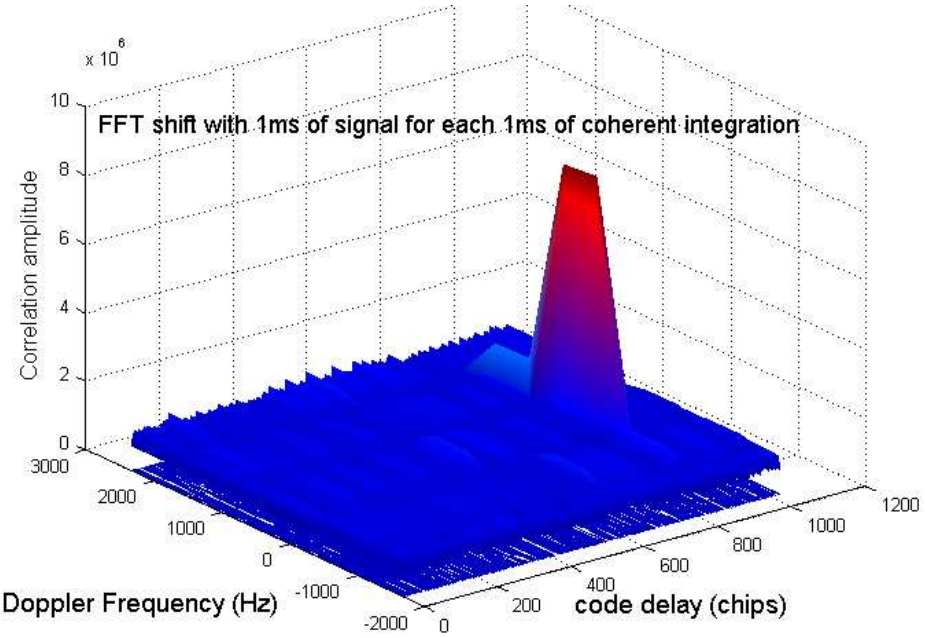

Fig V-11 : FFT shift correlation with 1ms of signal per $1ms$ of coherent integration

As we can see in figure V-11, the correlation peak rather has a rectangular shape, not a triangular shape as is the case for the conventional algorithms. This problem can be solved in the case of a 1ms coherent integration since 2ms of signal are used to compute a 1ms integration, as explained before. In this case, the FFT and Doppler resolution are equivalent, and the result is depicted in figure V-12 below. The same strategy can be used for longer coherent durations but memory requirements become in this case more stringent and the increase in the algorithm complexity cannot anymore be compensated by the reduction induced by the FFT shift technique.

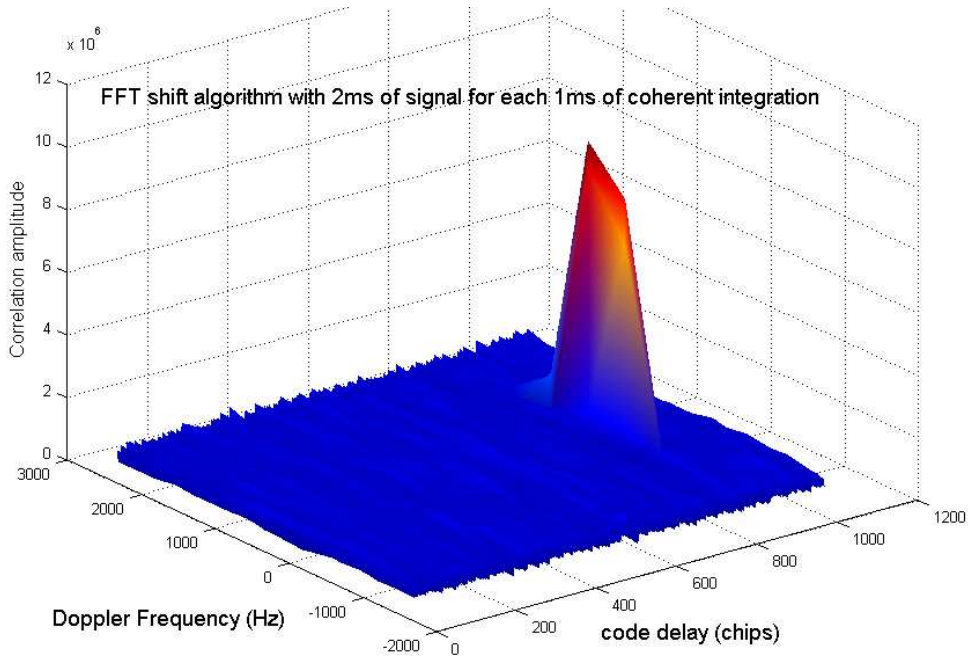

Fig V-12 : FFT shift correlation with $2ms$ of signal per $1ms$ of coherent integration

Another way to solve this problem for coherent integrations of more than 1ms is to compute in a first iteration the FFT for Doppler bins equal to the FFT resolution. For example, assuming a signal with an estimated Doppler frequency of 200 *Hz* (from the AD), a true Doppler frequency of 1000 *Hz*, and a 4000 *Hz* frequency range $[-1800\ Hz; 2200\ Hz]$; with a coherent integration over 2 *ms*, that is a usual Doppler resolution of 250 *Hz*, the first iteration of the algorithm with a 500 *Hz* FFT resolution computes Doppler compensations at $-1800\ Hz$, $-1300\ Hz$, $-800\ Hz$,…$1200\ Hz$, $1700\ Hz$, and $2200\ Hz$. Next, the signal frequency is translated by 250 *Hz* using a complex exponential; the second iteration of the algorithm thus yields Doppler compensations at $-1550\ Hz$, $-1050\ Hz$,…, 950 *Hz*, 1450 *Hz*, 1950 *Hz*. This technique is described in details in [*Psiaki et al., 2001*]. The issue is to bear out the resulting reduction in algorithm complexity. This is done in the next chapter.

The frequency shift theorem can equally be applied to the local code replica as explained in [*Akopian, 2001*]. But the same problems as before arise also in this case.

V.7 Transverse FFT algorithm

This method dramatically reduces the number of FFT-IFFTs to be carried out. The main idea is to consider the residual signal phase to be constant over 1ms intervals and for small Doppler bins.

The principle is not to use the classical linear search over the different Doppler frequency bins (refer to figure II-16), but rather use another scheme. The frequency domain is first divided into large steps of $500\ Hz$ which corresponds to $T_p = 1\ ms$. Then, small bins, according to the coherent duration needed, are defined within the large bins. Therefore, the frequency bins are defined as: $f_d(i,n) = f_i + j \cdot \delta f$, and $f_i = f_1 + i \times 500$, with i the

number of 500 *Hz* bins to be tested, j the number of smaller bins ($\frac{1}{2T_p}$) to be tested within each 500 *Hz* Doppler bin, and f_1 the first frequency to be tested. Thus f_i sweeps all the large bins to be tested, and $j \cdot \delta f$ sweeps the small bins to be tested within each large bin. As an example, for a Doppler window of 1000 *Hz*, [-500 *Hz*;+500 *Hz*], and a coherent integration of $T_p = 4\,ms$, the usual Doppler bin is in this case of 125 *Hz*. We have, $f_d(i,n) = f_i + j \times 125\ Hz$, with $f_i = \{-500Hz; 0Hz; +500Hz\}$, and $j = \{0;1;2;3\}$

The idea of processing $1\,ms$ of signal at once is preserved. The coherent integration is accomplished by summing $T_p\ ms$ of signal after FFT-IFFT, as in the first method.

This method would be equivalent to the sum after FFT-IFFT algorithm if the signal phase was constant over $1\,ms$ steps. But this is not the case in reality, and such approximation may result in a small loss due to error on code Doppler. This error is however smaller than that of the sum before FFT-IFFT algorithm since it corresponds to only $1\,ms$ interval and for small residual Doppler values.

Consequently, the signal can be rewritten as:
$r(t) = Ad(t-\tau) \cdot c(t-\tau) \cdot \cos[2\pi(L_1 + f_I)t] \cdot \cos(2\pi j \delta f t)$
The corresponding correlation result is expressed as:

$$R(f_i + n \cdot \delta\hat{f}) = \sum_{k=1}^{N_c} IFFT\left\{FFT\left[s(t_k)\right].FFT\left[c(t_k)\right].e^{i[2\pi(L_1 + f_i + j\delta\hat{f}).t]}\right\}$$

This correlation must be computed for each frequency bin for the first satellite. With the transverse FFT the phase $2\pi j \delta f.t$ is supposed to be constant over one code period of $1\,ms$ and the signal is approximated by:

$$r(t) = A.d(t-\tau).c(t-\tau).e^{i[2\pi(L_1 + f_i).t]}.e^{i[2\pi j \delta f \cdot floor\ (t/1ms)]}$$

Thus the local counterpart is generated such that the phase is constant over $1ms$ steps. The correlation becomes:

$$R(f_i + j \cdot \delta\hat{f}) = \sum_{k=1}^{N_c} e^{i\left[2\pi j \delta\hat{f} \cdot floor\ (t/1ms)\right]}.IFFT\left\{FFT\left[r(t_k)\right].FFT\left[c(t_k)\right].e^{i[2\pi(L_1 + f_i).t]}\right\} \quad \textbf{(V-8)}$$

This expression of the correlation function recalls a Fourier transform function, which would be in this case applied column wise to the IFFT result. This is why this algorithm is referred to as the Transverse FFT.

This algorithm essentially speeds up the correlation over different Doppler bins. Thus it is only beneficial in the case of the first satellite acquisition where a Doppler search is necessary.

The flow chart which better explains this method is illustrated in figure V-13.

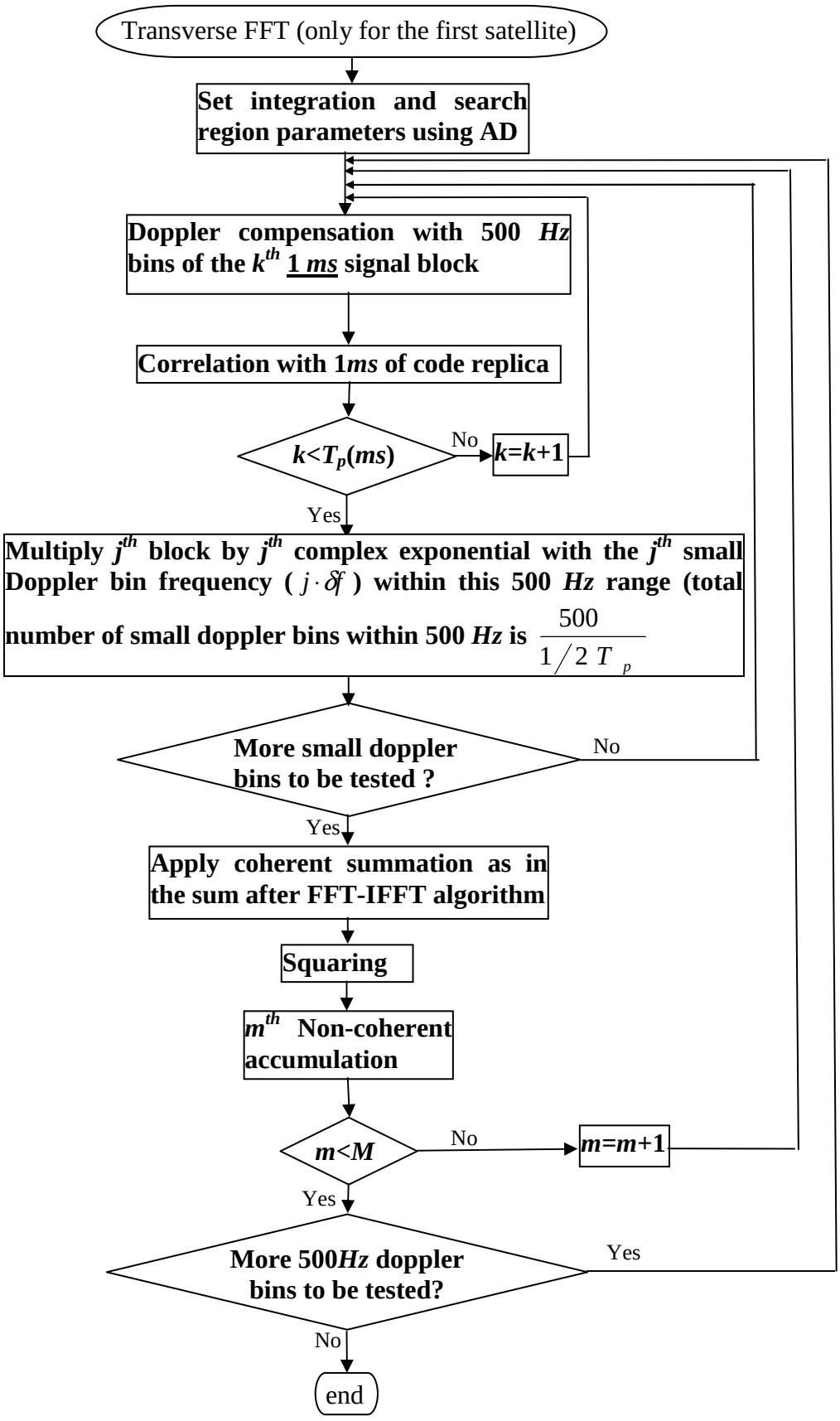

Fig V-13 : Transverse FFT algorithm flowchart

This way, the correlation is computed only for large bins and the results corresponding to smaller bins are obtained by multiplying and summing the correlation outputs of large bins by complex exponentials as in the former equation.

The advantage of this algorithm is to further reduce the TTFF, since it reduces the number of FFTs and IFFTs needed to be performed compared to a classical FFT algorithm. For a coherent integration of 10 *ms* for example, the Doppler resolution is of 50 *Hz*. If a Doppler range of 2 *kHz* needs to be tested, the number of FFT-IFFTs carried out is 10*2000/50=400, whereas with the transverse FFT algorithm only 10*2000/500=40 FFT-IFFTs couples are needed! But in our case, the transverse FFT algorithm does not induce a reduction by 10 of the acquisition time, since we use 2 *ms* of signal for a 1ms correlation. The reduction in complexity resulting from the use of such algorithm and other related issues will be the object of Chapter VI.

However this method requires more memory storage capacities compared to the Sum after FFT-IFFT and the Sum before FFT-IFFT algorithms. This is because the coherent summation is made after computing all necessary 1ms vectors. Whereas in the preceding algorithm the summation is done progressively as the 1ms vectors are computed, and only 1ms is stored in the memory at once. Thus the requirements of the transverse FFT algorithm in terms of memory are similar to the classical case.

Assuming that the phase $2\pi j\delta f.t$ is constant over one C/A code period may introduce some errors or attenuation of the correlation peak. This error is expected to have only a minor effect on the resulting correlation function, and the impact of this assumption will be tested through simulations tests which are presented in the next chapter.

V.8 Sum Of Replicas algorithm

This algorithm differs from all the previous ones, since it rather focuses on speeding up the acquisition of many satellites rather than speeding up the acquisition of one satellite. It can be viewed as a “multiple-satellites” acquisition improvement rather than the “mono-satellite” acquisition improvements previously proposed.

All of the previous algorithms perform acquisition of the different satellites in view sequentially, i.e., the satellites are acquired one by one. A joint search of several satellites would allow a reduction of the time allocated to the acquisition of the different satellites. This is the base of the sum of replicas algorithms which acquires different satellites at once by correlating the incoming signal with a sum of different replicas corrected by their respective Doppler. This yields to a software parallel search for all visible satellites rather than searching for them sequentially. The output is a sum of autocorrelation and cross-correlation functions. The resulting correlation function has as many useful correlation peaks as there are replicas added together.

The acquisition is realized according to the scheme presented in figure V-14:

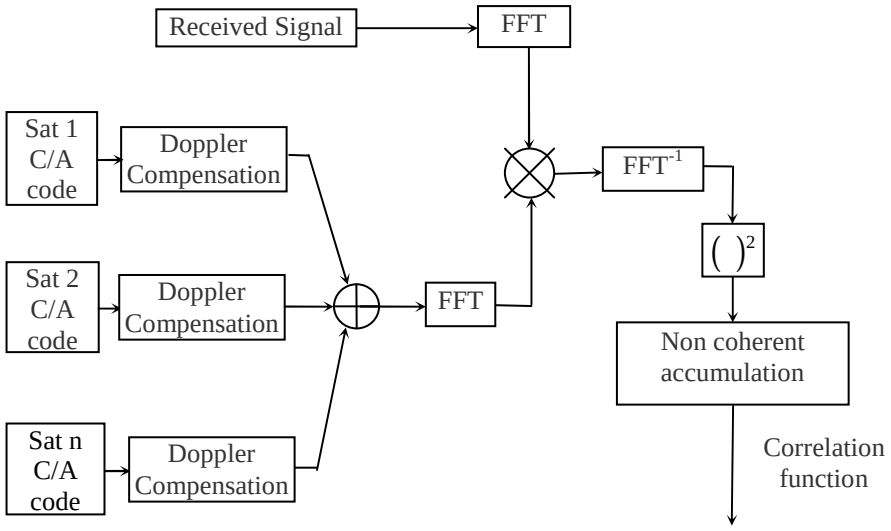

Fig V-14 : SOR algorithm principle

The resulting correlation function in each explored Doppler cell is equal to the sum of the correlation function which would have been obtained if satellites were individually correlated.

Figure V-15 illustrates an example of such a correlation function for a composite signal comprising 4 satellite signals, all at 30 *dBHz* . The four of them are acquired at once. This figure shows the correlation function at a given Doppler bin (the right one).

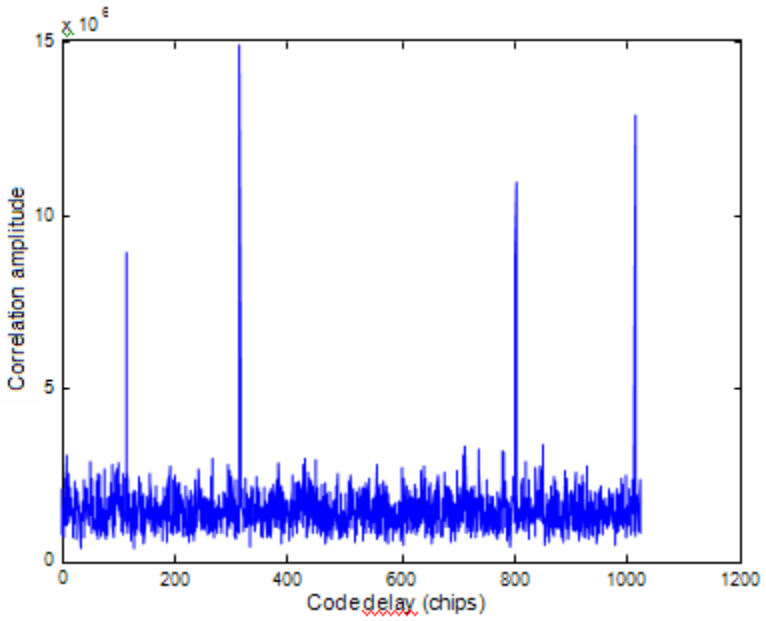

Fig V-15 Example of the output correlation function of the SOR algorithm with 4 satellites acquired together at the right Doppler bin

Each satellite PRN code has its own delay, and hence corresponds to one of the acquisition peaks detected in this correlation function. At this stage, the issue is to determine the proper relation between satellite PRNs and acquisition peaks. This correspondence is done

first by trying to locate each acquisition peak within a code delay window. Indeed, as explained previously, assuming that the reference location, the reference time and the navigation model are known thanks to AD, the receiver can compute the differential time of arrival between the satellites. This information can be used to identify the correlation peak pattern. The correspondence is then possible since each code delay window is already assigned to a satellite PRN code as it is shown in figure V-16 below.

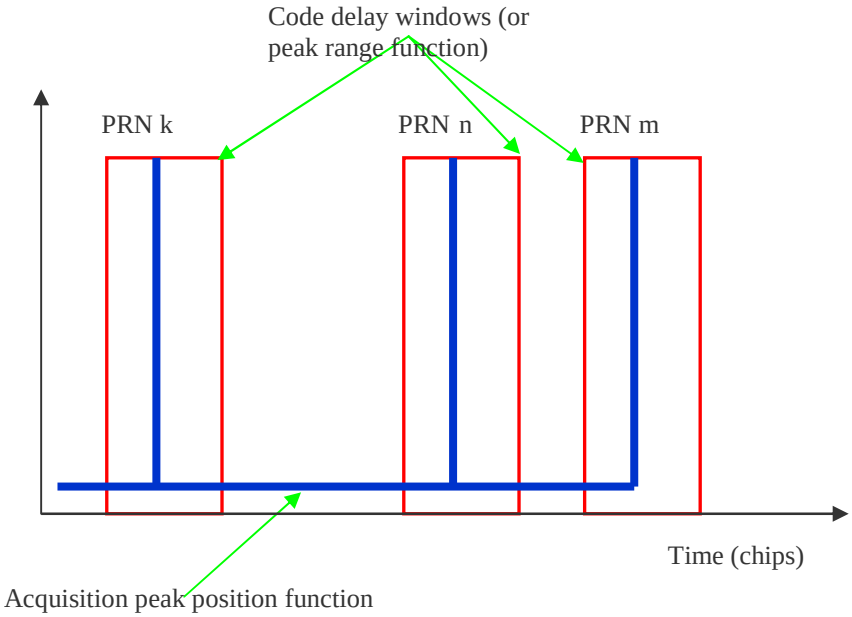

Fig V-16 : Satellites identification process using the code delay ranges function (red plot) estimated by the AD. The blue plot corresponds to the acquisition code delay positions

However, this identification process is not possible if for example, two or more satellites have the same or close code delays. Thus a discrimination process should first be undertaken to detect whether the possible delay of different satellites are intersecting or not. If it is the case, then the satellites cannot be part of the same composite replica. It comes out that a classification in groups of the visible satellites according to their respective expected code delays is first carried out to avoid correlation peak collisions. The result is that satellites of the same group are such that their respective code delay windows do not intersect with each other. This is shown in figure V-17.

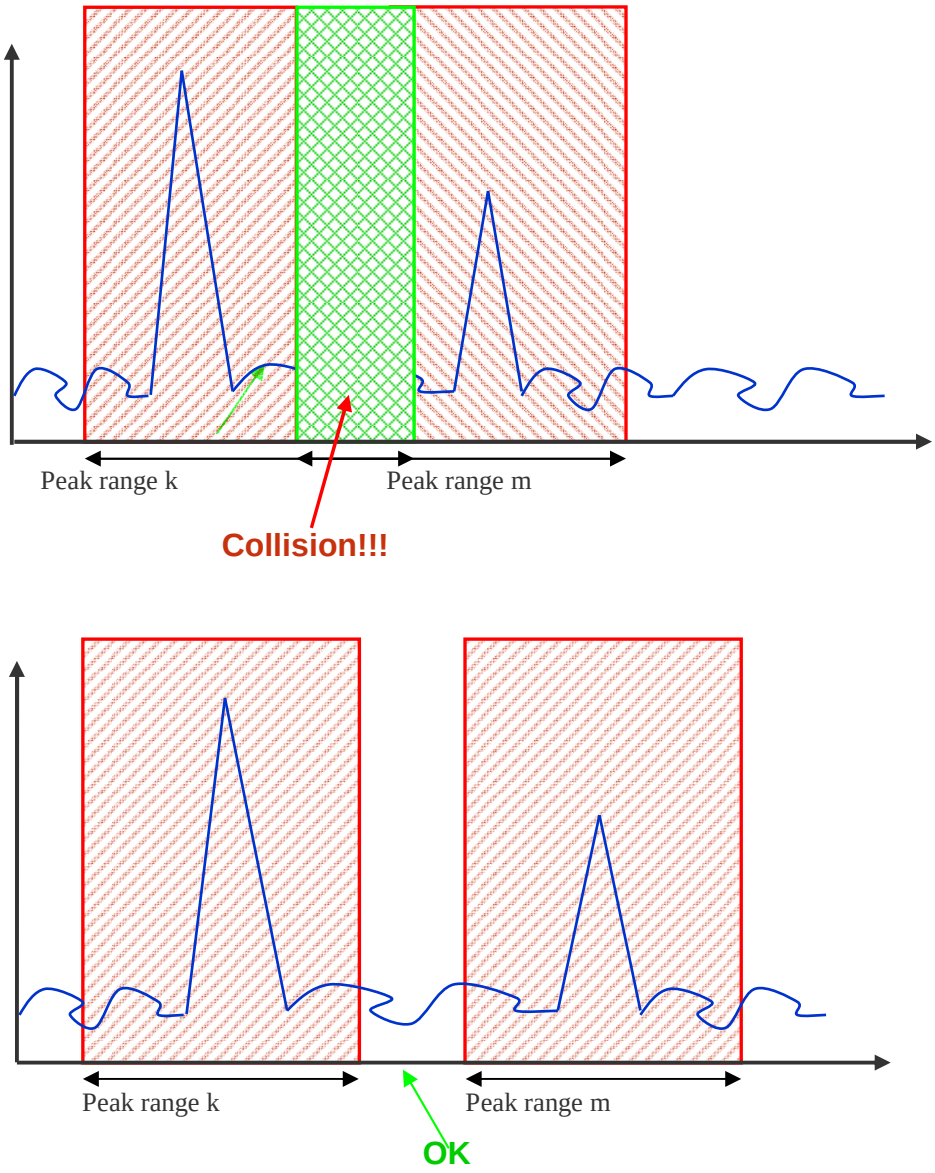

Fig V-17 : Collisions between satellites having close code delays

The uncertainties on the reference position and on the time information have a direct influence on the code delay range width computed using the AD. The greater the uncertainty, the wider the code delay windows, the lower the separation between the satellites, and the lower the number of satellites per group. The maximum reference position uncertainty is that of the maximum GSM cell radius, about $30\ km$ for rural areas. This parameter is considered as variable according to different types of environments. Three different values are studied: $30\ km$, $10\ km$ and $1\ km$, reflecting different GSM cell sizes ranging from rural to urban areas.

We conducted some tests which provide statistical values of the mean width of the code delay windows, the number of subset of satellites used in the algorithm, and the mean number of satellites per group. Note that for a satellite in the horizontal plane, i.e., with a maximum Doppler frequency of 5 *kHz* and an elevation of 0° (generally the mask angle is of 5°), the range width values due to uncertainties on the reference position and the GPS time add together. Thus, for the time uncertainty of 2 *s*, the approximate code delay window is of 273 chips, 136 chips and 75 chips for GSM cell radii of 30, 10 and 1 *km* respectively. At the

zenith, i.e., with a null Doppler frequency and an elevation of 90° the code delay range width is equal to 0, which means that we have no uncertainty on the code delay in this case. In other words, in this case the code delay for a user located at the Base Station or anywhere else within the considered cell is approximately the same. Figure V-18 depicts the code delay window (the total width from minimum to maximum) variation for elevations lying between 0 and 90°, and Doppler frequencies ranging from 5 *kHz* to 0 correspondingly.

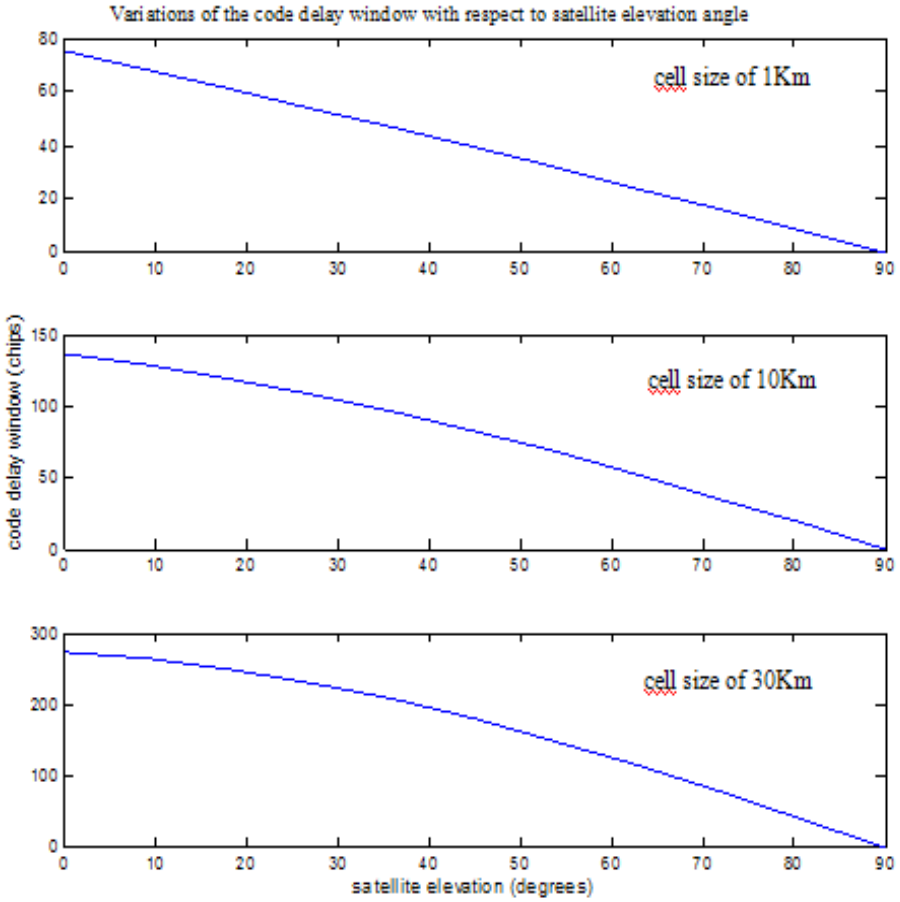

Fig V-18: Variations of the code delay windows with the satellites elevation for three different reference position uncertainties: 1 *km* **,** 10 *km* **, and** 30 *km*

Next, we present the results for the average number of groups of satellites, the average number of satellites per group and the average width of AD code delay ranges as a function of the user position uncertainty (the considered GSM cell radius). These three parameters are related to each other. The results of figures V-19, V-20 and V-21 correspond to averaged results obtained with different real GPS signals collected using a GPSBuilder 2.1 receiver and with different simulated signals using a Spirent STR4500. Note that results obtained using simulated signals were similar to those obtained with real signals; this is why the respective results could be averaged all together.

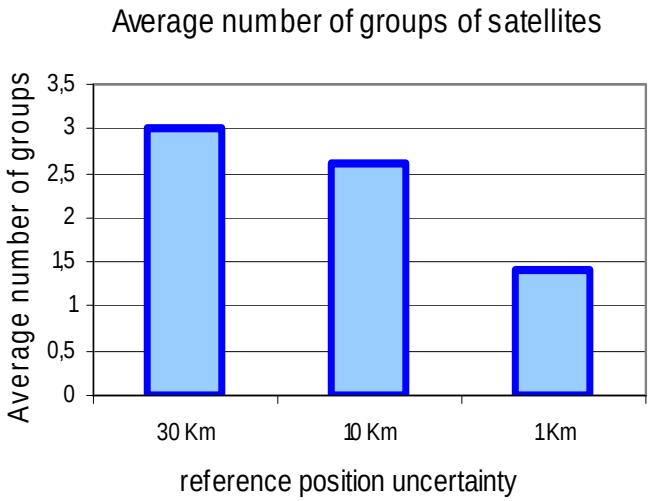

Fig V-19: The average number of groups of satellites for 3 reference position uncertainties

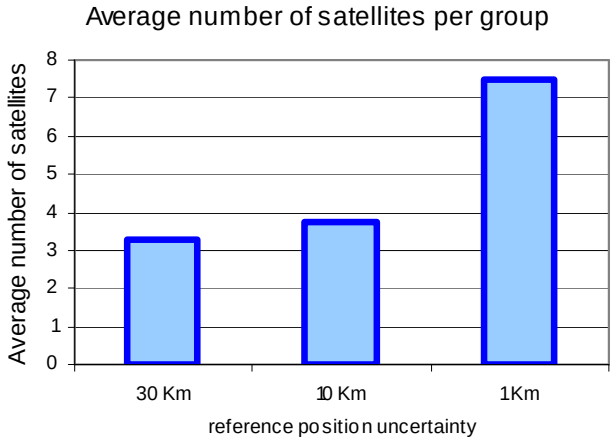

Fig V-20: The observed average number of satellites per group for 3 reference position uncertainties

Figures V-19 and V-20 clearly show that the number of groups of satellites has unsurprisingly opposite variations compared to the code delay windows.

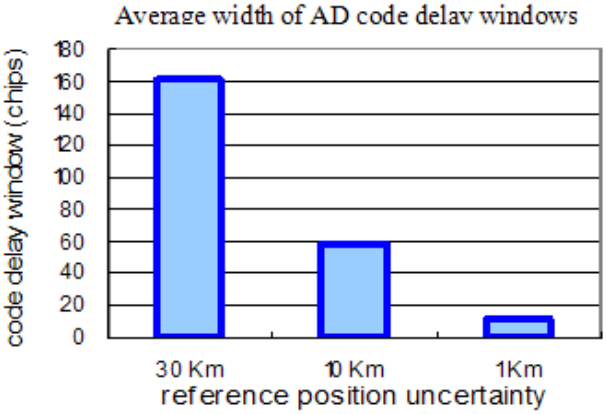

Fig V-21: The average width of AD ranges for 3 reference position uncertainties

Thus, the number of satellites per group increases when the reference position uncertainty decreases. For an uncertainty of 10 *km* for example, the average number of satellites per group is approximately 3. Obviously, the more satellites per group, the greater the complexity reduction compared to a conventional algorithm.

Once the satellites are grouped according to their code delays, each group goes through an acquisition process by correlating the incoming signal with the sum of the corresponding replicas. The correlation is performed using one of the previous "mono-satellite" algorithms. The output is a correlation function similar to that shown in figure V-15 with as many peaks as there are satellite signals in the considered group.

There still remains the satellites identification issue. In fact, the peak position returned by the function is affected by the sum of two time offsets: the propagation delay and the receiver clock offset which causes the peak configuration computed by the grouping function to be shifted. The receiver clock offset cannot be determined precisely due to its time uncertainty with respect to GPS time. The time uncertainty is due to the time transfer through the GSM network. Note that this time uncertainty is the same for all the satellites, which implies that the differential code delays (the separation between code delays in chips) are accurate. This has no impact on the previous processing (correlating the signal with code replicas, grouping the satellites in order to avoid collisions between their code delays), but has an impact on the identification of the peaks: Indeed, the peaks of the correlation function may not correspond to the right code delay window. A solution to this problem is to correlate the code delay windows function and the acquisition peaks position function (resulting from correlation) defined as:

- Peak range function

$$\begin{cases} \chi(t) = 1 \ if \ \ t \in PRN \ \ code \ \ delay \ \ windows \\ \chi(t) = 0 \ \ elsewhere \ \ \ on \ the \ 1 \ ms \ \sup \ port \end{cases}$$

- Acquisition peaks position function

$$\begin{cases} \eta(t) = 1 \ if \ \ t \in \{\det ected \ \ acquisitio \ \ n \ \ peaks \ \ \} \\ \eta(t) = 0 \ \ elsewhere \ \ \ on \ the \ 1 \ ms \ \sup \ port \end{cases}$$

This correlation is carried out using the FT technique. The maximum of the resulting correlation function provides the most likely configuration and in the same time provides the relationship between the peaks and the PRN number (figure V-22).

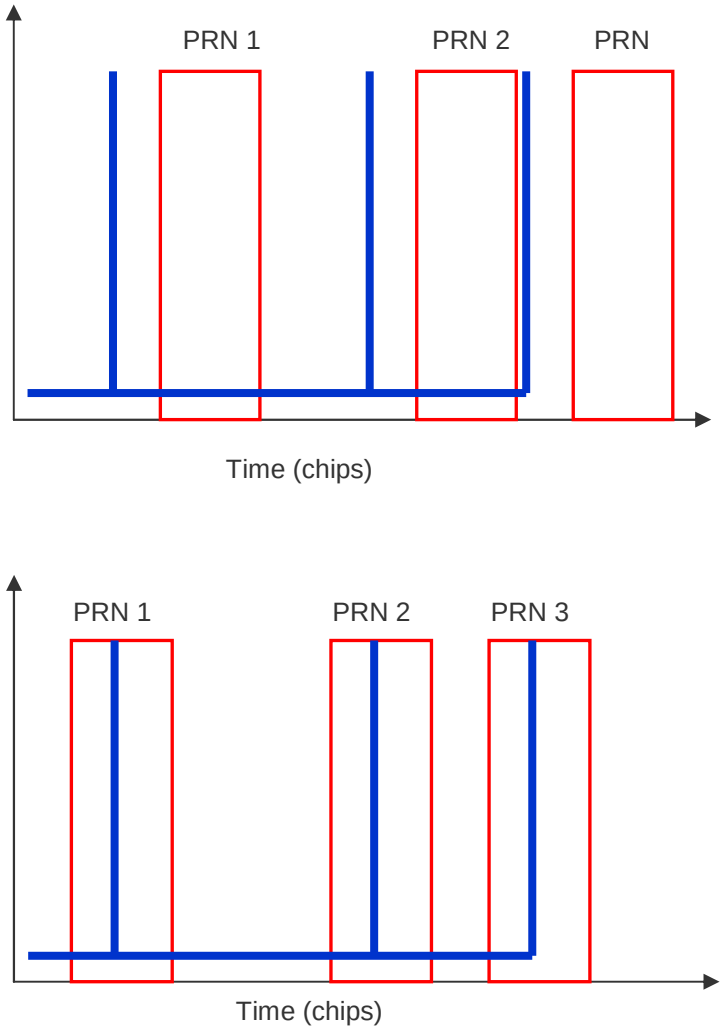

Fig V-22 : Satellites identification by correlating the ranges function (in red) and the acquisition code delay ranges function (in blue)

In practice, even if the satellites were grouped a priori such that collisions are avoided between their code delays, collisions are still possible. The reason is that the code delays detected by the acquisition process do not have necessarily the same pattern as that of the windows estimated by the AD. This is due to possible cross-correlation peaks which may mask those of weak signals or even multipath peaks. Indeed, correlating with the sum of different replicas results in a final correlation function with more cross-correlation peaks than in the standard case where one satellite is processed at once. These peaks have random delays. In this case, some of the output correlation function peaks are wrong. However, while the SOR algorithm increases the probability of cross-correlation peak detection, the use of AGPS enables to reduce this probability as already explained, since the code delay window for each of the satellites is pre-estimated by the AD. Accordingly, each code delay is searched for only within the boundaries of the corresponding code delay window, and the peaks which are not included in any code delay window are not accounted for since code delays are searched for only within the precalculated windows. Whereas if two peaks are included in the same code delay window, one of them obviously does not correspond to the proper correlation peak, i.e., it does not correspond to a PRN code delay.

This situation is illustrated in the next figure:

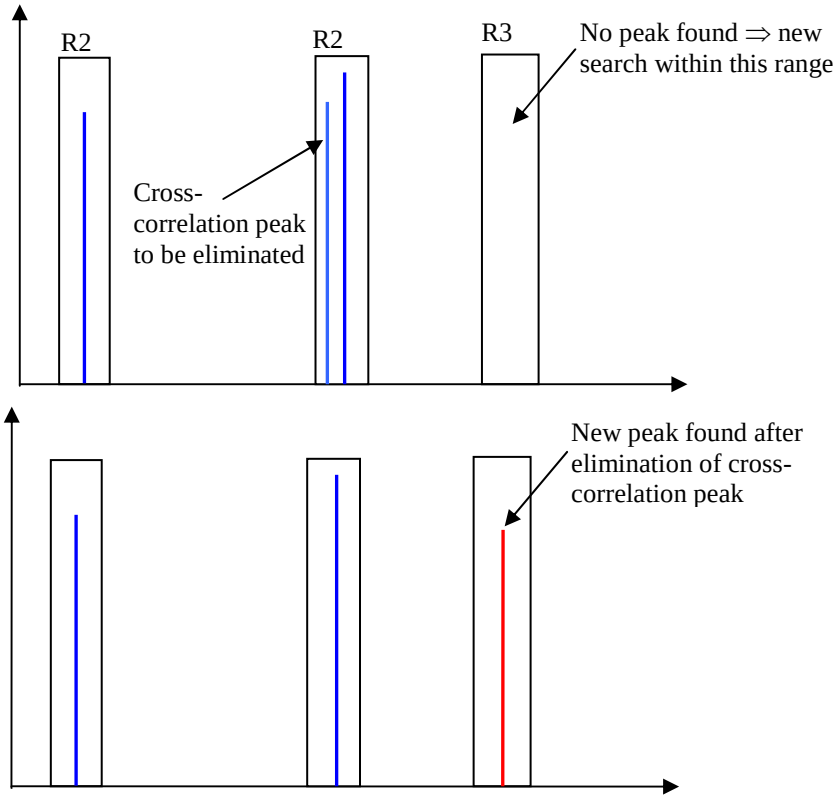

Fig V-23 : in red : peaks detected after acquisition ; in blue : New maximum searched for within the first range

In such cases, the lower peak is eliminated and only the higher one is taken into consideration; indeed, it is assumed that the stronger peak is more likely to be a right peak, not a multipath or a cross-correlation peak. This is also applied if more than two peaks coincide within the same code delay window.

In figure V-23, three peaks (satellites) were searched for. Two of them correspond to accurate code delays and the third is a cross-correlation one. In the window R2 where the 2 delays coincide, the higher maximum is considered. The other one is eliminated, and another maximum is searched for within the R3 window.

Using this identification method is not always possible. In fact, by correlating the acquisition peaks function with the code delay ranges function, the resulting correlation function has many maximums corresponding to different circularly shifted versions of the chi square function. The proper correlation maximum, or in other words the right code delay range shift, corresponds to that of the receiver clock offset. But finding this value is not obvious. This is the case since the searched delay is not always a maximum of the correlation function due to a possible presence of cross-correlation peaks. Another mean of identification could be a correlation of the signal with all the PRN codes corresponding to this first group one by one. The maximum correlation result allows for identifying the proper PRN of the considered acquisition peak. This is possible because the exact location of the code delay is known, thus a classical sequential correlation can be used rather than using the FFT.

Other constraints may be considered while pre-grouping the satellites, such as considering Doppler frequencies and/or bit transition positions. But tests showed that adding these constraints results in many groups of 1 satellite. It also introduces a reduced sensitivity since a Doppler error is inevitable in this case.

The SOR algorithm flowchart is depicted in figure V-24 next:

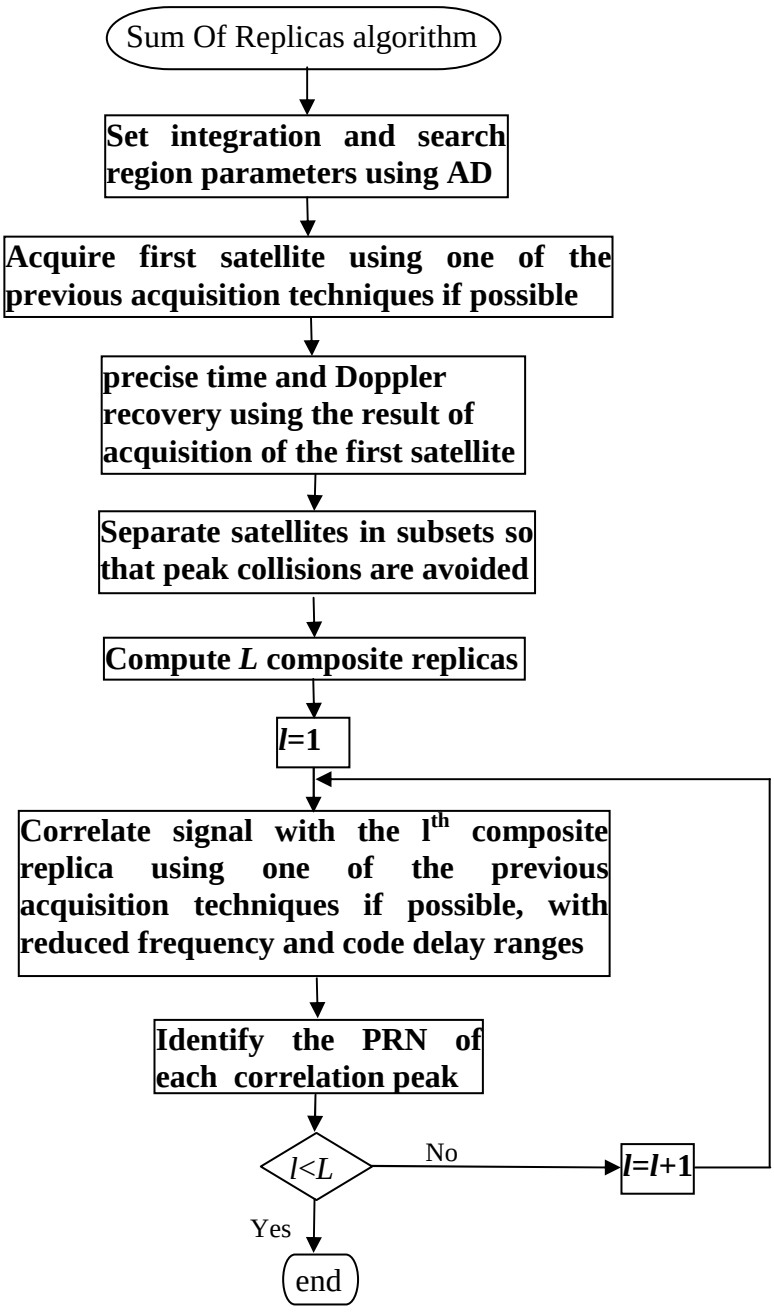

Fig V-24 : SOR algorithm flowchart

The main advantage of the SOR algorithm is to reduce the TTFF by reducing the complexity in comparison to a conventional algorithm, since it allows the acquisition of more than one satellite at once, or in other words, it allows for a parallel processing of the satellites. This reduction depends on the number of satellites processed together. Thus the more satellites per group, the lower the complexity and the lower the TTFF.

Conversely, having more satellites per group induces a reduction in sensitivity, since the global noise level in the total correlation output is increased. Consider for example, a composite GPS signal comprising the signals coming from N_{rec} satellites, where N_{rec} is the number of satellite signals present in the composite received signal. Using a conventional algorithm to search for one satellite signal results in one autocorrelation function added to $N_{rec}-1$ cross-correlation functions. The additive noise is correlated with only one code. Using the SOR algorithm, and assuming a group of N_{loc} satellites for example, with N_{local} the number of locally generated replicas summed together, the incoming signal is correlated with N_{loc} Doppler compensated replicas. The result is the sum of N_{loc} autocorrelation functions and $N_{loc}\cdot(N_{rec}-1)$ cross-correlation functions. In this case, the noise is correlated with the sum of the 3 codes. As a result the final noise level is increased. This increase in the noise level is derived here for the conventional and the SOR acquisition algorithms respectively.

- In the case of a conventional algorithm, after code and Doppler removal the signal can be written as (considering only the Inphase channel, and assuming no code delay and no front end filtering errors, with a large rectangular double sided bandwidth, *B*):

$$\left\{c_1\cos\left[2\pi(f_I+f_{d1})t\right]+\sum_{n=2}^{N_{rec}}c_n\cos\left[2\pi(f_I+f_{dn})t\right]\right\}\cdot\left\{c_1\cos\left[2\pi\left(f_I+\hat{f}_{d1}\right)t\right]\right\}$$
$$+n_f\cdot c_1\cdot\cos\left[2\pi\left(f_I+\hat{f}_{d1}\right)t\right]$$
$$=c_1\cdot c_1\cdot\cos\left\{2\pi\left[f_I+\left(f_{d1}-\hat{f}_{d1}\right)\right]t\right\}+c_1\cdot\sum_{n=2}^{N_{rec}}c_n\cos\left\{2\pi\left[f_I+\left(f_{dn}-\hat{f}_{d1}\right)\right]\right\}$$
$$+n_f\cdot c_1\cdot\cos\left[2\pi\left(f_I+\hat{f}_{d1}\right)t\right]$$

  With $c_1\cos[2\pi(f_I+f_{d1})t]+\sum_{n=2}^{N_{rec}}c_n\cos[2\pi(f_I+f_{dn})t]+n_f$ the composite received signal with band pass filtered noise (n_f), $\hat{f}_{d1}$ the estimated Doppler frequency of C/A PRN code 1. The double frequency terms are not considered since they are supposed to be filtered by the low pass coherent integration.
  The useful component of the signal before coherent integration is $\frac{1}{2}c_1\cdot c_1\cdot\cos\left[2\pi\left(f_{d1}-\hat{f}_{d1}\right)t\right]$. The other component $\frac{1}{2}c_1\cdot\sum_{n=2}^{N_{rec}}c_n\cos\left[2\pi\left(f_{dn}-\hat{f}_{d1}\right)\right]$ imply secondary peaks which correspond to the cross-correlation between code 1 and the other $N_{rec}-1$ codes of the composite replica.
  The cross-correlation peaks are negligible if the power difference between code 1 and the other codes is not very significant. For the sake of simplicity, they will not be considered herein, since they are very difficult to be theoretically evaluated. These cross-correlations are however expected to be negligible compared to the impact of additive noise. This will be checked out through out the simulation results. The noise power is $P_{n_i}=\frac{N_0}{4T_p}$, as computed in Chapter II, equation II-12

- With the sum of replicas algorithm, in the case of a composite replica with N_{loc} satellites being acquired together, the signal after code and Doppler removal is (again

considering only the Inphase channel, and assuming no code delay and no front end filtering errors, with a large rectangular double sided bandwidth, *B*):

$$\left\{\sum_{n=1}^{N_{loc}} c_n \cos\left[2\pi\left(f_I + f_{dn}\right)t\right] + \sum_{n=N_{loc}+1}^{N_{rec}} c_n \cos\left[2\pi\left(f_I + f_{dn}\right)t\right]\right\} \cdot \sum_{n=1}^{N_{loc}} c_n \cos\left[2\pi\left(f_I + \hat{f}_{dn}\right)t\right]$$

$$+ n_f(t) \cdot \sum_{n=1}^{N_{loc}} c_n \cos\left[2\pi\left(f_I + f_{dn}\right)t\right]$$

$$= \sum_{n=1}^{N_{loc}} c_n \cos\left[2\pi\left(f_I + f_{dn}\right)t\right] \cdot \sum_{n=1}^{N_{loc}} c_n \cos\left[2\pi\left(f_I + \hat{f}_{dn}\right)t\right]$$

$$+ \sum_{n=N_{loc}+1}^{N_{rec}} c_n \cos\left[2\pi\left(f_I + f_{dn}\right)t\right] \cdot \sum_{n=1}^{N_{loc}} c_n \cos\left[2\pi\left(f_I + \hat{f}_{dn}\right)t\right]$$

$$+ n_f(t) \cdot \sum_{n=1}^{N_{loc}} c_n \cos\left[2\pi\left(f_I + \hat{f}_{dn}\right)t\right]$$

$$= \left\{c_1 \cdot c_1 \cdot \cos\left[2\pi\left(f_{d1} - \hat{f}_{d1}\right)t\right] + c_2 \cdot c_2 \cdot \cos\left[2\pi\left(f_{d2} - \hat{f}_{d2}\right)t\right] + \ldots\ldots + c_{N_{loc}} \cdot c_{N_{loc}} \cdot \cos\left[2\pi\left(f_{dN_{loc}} - \hat{f}_{dN_{loc}}\right)t\right]\right\}$$

$$+ \sum_{k=1}^{N_{loc}} c_k \sum_{\substack{n=1 \\ n\neq k}}^{N_{loc}} c_n \cos\left[2\pi\left(f_{dn} - \hat{f}_{dk}\right)t\right] + n_f(t) \cdot \sum_{n=1}^{N_{loc}} c_n \cos\left[2\pi\left(f_I + \hat{f}_{dn}\right)t\right]$$

It can be seen in the previous expression that in the case of the SOR, the resulting correlation function is the sum of different auto-correlation and cross-correlation peaks. Assuming that the cross-correlation peaks are negligible, the noise correlation function is computed in order to calculate its power. First we set,

$$n(t) = n_f(t) \cdot \sum_{n=1}^{N_{loc}} c_n \cos\left[2\pi\left(f_I + \hat{f}_{dn}\right)t\right]$$

$$R_n(\tau) = E\left[n(t).n(t-\tau)\right]$$

$$= E\left\{n_f(t) \cdot \sum_{n=1}^{N_{loc}} c_n \cos\left[2\pi\left(f_I + \hat{f}_{dn}\right)t\right] \cdot n_f(t-\tau) \cdot \sum_{n=1}^{N_{loc}} c_n \cos\left[2\pi\left(f_I + \hat{f}_{dn}\right)\cdot(t-\tau)\right]\right\}$$

$$= R_{n_f}(\tau) \cdot$$

$$\left\{\begin{array}{l} \sum_{n=1}^{N_{loc}} R_{c_n}(\tau) \cdot \cos\left[2\pi\left(f_I + \hat{f}_{dn}\right)\cdot\tau\right] \\ + \sum_{n=1}^{N_{loc}} \sum_{\substack{k=1 \\ k\neq n}}^{N_{loc}} R_{c_n c_k}(\tau) \cdot E\left\{\cos\left[2\pi\left(\hat{f}_{dn} - \hat{f}_{dk}\right)t + 2\pi\left(f_I + \hat{f}_{dk}\right)\tau\right]\right\} \end{array}\right\} \cdot \frac{1}{2}$$

The PSD of $n(t)$, which is the FT of its autocorrelation function (Wiener-Kintchine theorem), can be written as:

$$S_n(f) = \frac{1}{4} S_{n_f}(f) * \sum_{n=1}^{N_{loc}} S_{c_n}(f) * \left\{\delta\left[f + \left(f_I + \hat{f}_{dn}\right)\right] + \delta\left[f - \left(f_I + \hat{f}_{dn}\right)\right]\right\}$$

The bandwidth *B* (>2 *MHz*) of the signal n_{int} being very large compared to $\hat{f}_{dn}$ (of the order of a few *kHz*), leads to:

$$S_n(f) \cong \frac{1}{4} S_{n_f}(f) * \sum_{n=1}^{N_{loc}} S_{c_n}(f) * \left\{\delta\left[f + f_I\right] + \delta\left[f - f_I\right]\right\}$$

Where $S_{c_n}(f)$ are the respective power spectral densities of the N_{loc} C/A codes used in the composite replica.

Recalling that $S_{n_f}(f) = \frac{N_0}{2}\left|H_{FE}(f)\right|^2 * [\delta(f + f_I) + \delta(f - f_I)]$, from equation II-11, the noise PSD becomes:

$$S_n(f) = \frac{N_0}{4}\left|H_{FE}(f)\right|^2 * \sum_{n=1}^{N_{loc}} S_{c_n}(f)$$

After demodulation, dispreading and correlation, the resulting noise DSP is:

$S_{ni}(f) = S_n(f) \cdot \left|H_{CI}(f)\right|^2$ (Wiener Lee)

Where $n_I(t)$ is the noise component on the Inphase channel, $h_{CI}(t)$ represents the low pass filtering throughout the correlator.

Knowing that $S_n(f)$ with large bandwidth B compared to that of the integrator bandwidth $(1/T_p)$, $S_n(f)$ is assumed to be constant over the integrator bandwidth and $S_{ni}(f)$ becomes:

$$S_{ni}(f) = \left|H_{CI}(f)\right|^2 \cdot S_n(0)$$

With $S_n(0) = \frac{N_0}{4}\int_{-\infty}^{+\infty}\left|H_{FE}(f)\right|^2 \cdot \sum_{n=1}^{N_{loc}} S_{c_n}(f) \cdot df \times \left|H_{CI}(f)\right|^2$

Finally, the noise power is:

$$P_{n_I} = \frac{N_0}{4}\int_{-\infty}^{+\infty}\int_{-\infty}^{+\infty}\left|H_{FE}(f_1)\right|^2 \cdot \sum_{n=1}^{N_{loc}} S_{c_n}(f_1) \cdot df_1 \times \left|H_{CI}(f)\right|^2 \cdot df$$

$$= \frac{N_0}{4}\int_{-\infty}^{+\infty}\left|H_{FE}(f_1)\right|^2 \cdot \sum_{n=1}^{N_{loc}} S_{c_n}(f_1) \cdot df_1 \times \int_{-\infty}^{+\infty}\left|H_{CI}(f)\right|^2 \cdot df$$

$$= \frac{N_0}{4T_p}\int_{-\infty}^{+\infty}\left|H_{FE}(f)\right|^2 \cdot \sum_{n=1}^{N_{loc}} S_{c_n}(f) \cdot df$$

In the case of a rectangular front end filter, the noise power becomes:

$$P_{n_I} = \frac{N_0}{4T_p} \times N_{loc} \qquad \textbf{(V-9)}$$

The result in equation V-9 shows that theoretically the noise level linearly increases with the number of satellites processed together. However, the algorithm introduces more marginal, although may be still significant, cross-correlation and autocorrelation off-peaks compared to the conventional algorithm which may lead to more false alarms. The impact of these peaks is very difficult to be theoretically derived here, and performance tests will show if they have a real impact or not. Let us recall however that using the AGPS provides a partial solution to this problem. Indeed, the correlation peaks are searched for within predetermined code delay windows. Thus all cross-correlation peaks which occur outside the boundaries of these windows are eliminated. Hence, the smaller the windows width, the lower the probability of false alarm.

This increase in the noise level was simulated using Matlab. We conducted a test where sums of 1, 2, 3, 4 or 5 PRN codes are formed. An AWGN is correlated with these sums. All possible PRN combinations out of 30 PRN codes were tested. The number of combinations of *n* PRN codes out of 30 PRN codes is given by: C_n^{30}. In other words, all possible sums of 2, 3, 4, or 5 PRN codes out of the 30 PRN codes used in GPS civil signal,

were tested in order to assess possible affinities between codes. Figure V-25 shows the result obtained. A Doppler range of ±5 *kHz* was considered. In other words, each PRN code is supposed to be affected by a code Doppler within ±5 *kHz*.

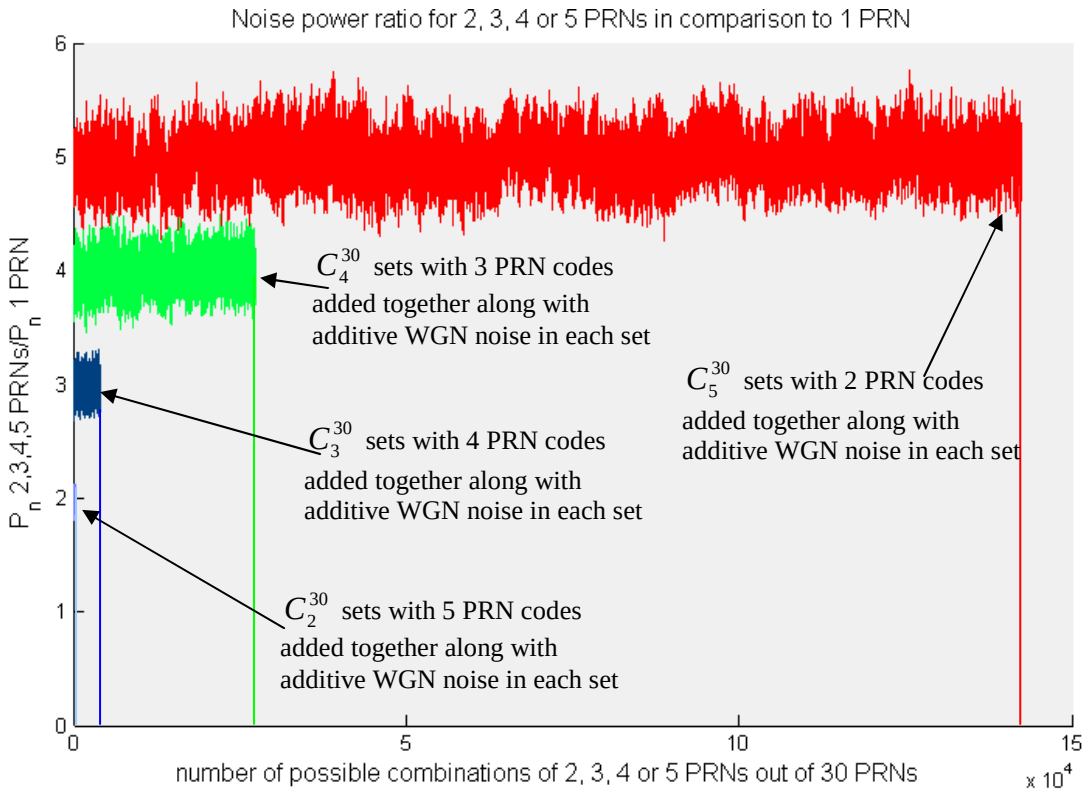

Fig V-25: Noise level (P_n) for all sets of 2, 3, 4 or 5 satellites, represented by pseudo noise sequences. Doppler between $\pm 5kHz$

The first thing to be noted in figure V-25 is that the number of sets of codes added together depends on the number of satellites per set. With 5 satellites per set, the number of sets is maximum.

This figure also shows that the mean value of the despreaded noise level increases linearly with the number of codes. Besides, it shows that this is approximately the case for all possible PRN sets, and whether the codes are affected with Doppler frequencies or not. In fact, another test was conducted with C/A code not affected by Doppler, and the results obtained were similar to those presented in figure V-25 above.
The mean noise level is in average multiplied by 2.999 ± 0.309 (4.75 *dB* ± 0.358 *dB*) for groups of 3 satellites, by 3.998 ± 0.5 (6 *dB* ± 0.13 *dB*) for groups of 4 satellites, and by 4.996 ± 0.75 (6.98 *dB* ± 0.655 *dB*) for groups of 5 satellites.

Signals at 41.5 and 26.5 *dBHz* respectively, obtained with a Spirent STR4500 generator were used to validate these theoretical values of the reduction in C/N_0 using the SOR algorithm. The results are illustrated in figure V-26 next.

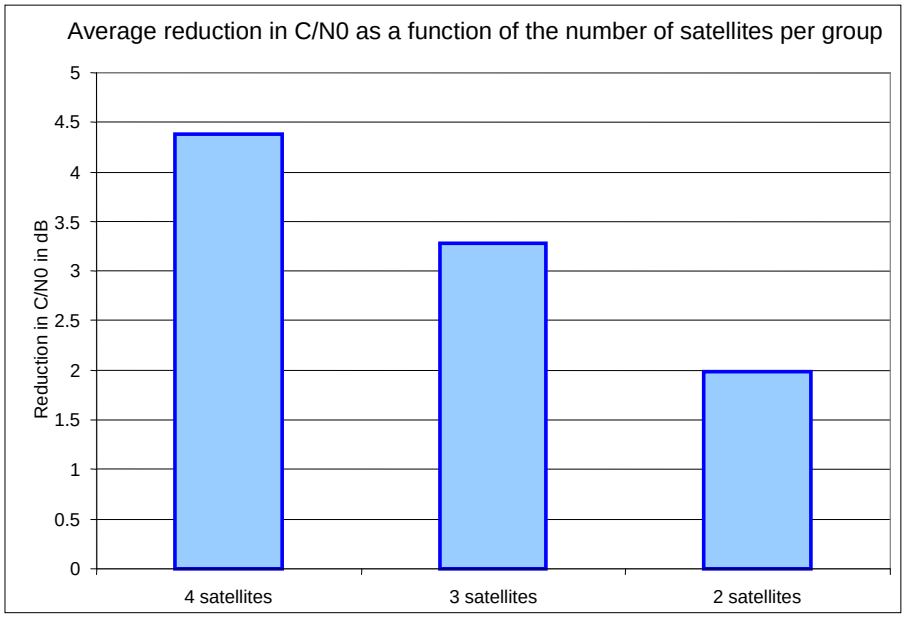

Fig V-26: Reduction in C/N_0 as a function of the number of satellites per group

In conclusion, the performances of the SOR algorithm are expected to depend on the number of satellites processed in parallel. In fact it introduces some losses in the C/N_0 which greatly depend on the number of satellites per group: these losses increase for increasing number of satellites per group. Thus a compromise must be set in order to have the best correspondence between the reduction in sensitivity and that of the TTFF. An upper limit for the number of satellites per group may be adopted in order to limit the loss in C/N_0 ratio.

An implementation of the SOR algorithm based on the classical FFT algorithm is shown in figure V-14. The Sum after FFT-IFFT algorithm can also be used. A further optimisation consists in introducing the transverse FFT algorithm as the acquisition method. This significantly enhances the SOR performances compared to the classical SOR algorithm as will be shown in the next chapter.

The Sum before algorithm cannot be implemented within the SOR algorithm since the signal must be Doppler compensated before coherent summing. But with the SOR different Doppler compensations must be made since it deals with many satellites at once. Thus it is not possible to use the Sum before. Results obtained with the SOR based on a classical FFT scheme were not quite satisfactory. A further optimisation was considered: as for the “mono-satellite” algorithms, a first satellite is acquired at the beginning. Precise time and Doppler info are computed. And the other satellites are acquired as described here but without Doppler search. Such implementation of the SOR algorithm avoids searching for the right satellites code delay pattern, since the first group only contains one satellite.

V.9 Conclusion

This chapter focused on describing different software techniques to improve the classical GPS acquisition process. The improvement essentially deals with the TTFF, while trying not to dramatically affect the receiver sensitivity. Each enhancement was theoretically described, and analysed through the presentation of its advantages and drawbacks.

The first algorithms acquire the satellites one by one and enhance the acquisition of each satellite, whereas the last method, SOR, acquires more than one satellite at once thus allowing for reduction of complexity by eliminating redundancy between the iterations needed to acquire different satellites. This implies that there are possibilities for mixing between these methods and the last one, as it is the case for the optimised SOR algorithm.

A small optimisation can be introduced to the "mono-satellite" algorithms compared to their basic implementation. It consists in generating the code replica once and for all at the beginning of the acquisition process, instead of generating it at each iteration, i.e. for each frequency bin and each non-coherent accumulation. Classically this is done in order to compensate for the code Doppler. But this may rather be performed in the frequency domain in the advanced algorithm. Thus the code is generated and translated to the frequency domain at the beginning, and only a multiplication by a complex exponential is performed within the loops to compensate for the code Doppler. This optimisation is a result of the time shift property of the FT [*O'Driscoll, 2006*].

According to the operational environment, one of these methods may be more efficient than the other. Namely, in open areas, the GPS signal is generally strong enough, that the receiver sensitivity is not the main issue, but it is the complexity and hence the TTFF which is of primal importance. In such cases sensitivity may be sacrificed on behalf the computation speed.

Note that an advantage of the FFT is to compute the correlation for the possible code delays at once. However in the context of a better time synchronisation between the GPS receiver and the GSM base stations, the FFT would not be needed, since very few chips would have to be explored.

The next chapter reports on a specific set of experiments conducted to compare these algorithms with each other while highlighting their respective advantages and drawbacks. The results will lead to pointing out the algorithm(s) which represent the best compromise between sensitivity and complexity issues for the different GPS operational environments.

Résumé du chapitre VI

Les performances des différents algorithmes présentés précédemment au chapitre V, sont comparées en termes de sensibilité et de temps de calcul.
Ces performances ont été évaluées à l'aide des paramètres suivants : la durée d'intégration cohérente (T_p) , le nombre d'accumulations non-cohérentes (M), le rapport C/N_0 du signal entrant, les cases Doppler à tester, et l'incertitude sur la position de récepteur (déterminée à l'aide des données d'assistance).

Trois types de tests ont été réalisés pour étudier l'impact de ces paramètres : les deux premiers tests comparent la complexité des algorithmes (en termes du nombre d'opérations arithmétiques et du nombre de cycles du processeur) et leur sensibilité (en termes du rapport C/N_0), respectivement pour une les mêmes valeurs de T_p, M, et des incertitudes sur la position et le l'information temporelle fournies par le réseau cellulaire.
Le troisième test se focalise sur les limites de sensibilité des algorithmes, tout en évaluant à chaque fois le temps de calcul.

Pour les tests de sensibilité, les signaux utilisés ont été générés à l'aide du générateur de signal GPS Spirent STR4500, à une fréquence d'échantillonnage de $2.046\ MHz$. Chaque signal étant compris de 9 satellites visibles ayant le même rapport C/N_0. Plusieurs signaux avec des rapports C/N_0 différents ont cependant été générés pour établir l'impact de ce paramètre sur les performances de l'acquisition.

Dans tous les tests, les satellites ont été classés suivant leurs angles d'élévation. Pour des signaux relativement forts ($42\ dBHz$ et $27\ dBHz$), les satellites ont été classés par ordre d'angle d'élévation décroissants. De cette façon, la probabilité d'acquérir en premier un satellite fort est plus élevée, pour garantir une solution plus rapide. Pour les signaux faibles ($17\ dBHz$), concernant par exemple des environnements indoors, les satellites ont été classés de sorte que le satellite ayant un angle d'élévation autour de 60° soient les premiers à être acquis. Les autres sont choisis aléatoirement.

Les résultats des tests réalisés montrent que la classification des algorithmes suivant leurs performances dépend principalement de la durée d'intégration cohérente, T_p. Cela signifie que cette classification ne dépend pas du nombre d'accumulations non-cohérentes, M. En effet, la complexité des algorithmes est globalement linéaire en fonction de M, mais non linéaire en fonction de T_p. Un T_p plus grand induit un plus grand nombre de blocs de données à traiter pour l'intégration cohérente, ou en d'autres termes le couple d'opération FFT-IFFT ; et en parallèle, plus de cases Doppler à explorer, résultant ainsi en une complexité accrue. Mais un M plus grand induit uniquement un plus grand nombre de blocs de données à traiter.

Pour un $T_p \geq 7\ ms$ - nécessaire pour des environnements sévères, les résultats ont montré un avantage net de la FFT transverse sur les autres algorithmes, car elle présente une complexité minimale, et en même temps ne conduit pas à des pertes en sensibilité.
L'algorithme de la FFT transverse est suivi par l'algorithme de la sommation avant corrélation.

Pour un $T_p \leq 7\ ms$, l'algorithme de la sommation avant corrélation est le plus performant, suivi par la FFT transverse.

Pour un $T_p = 1\ ms$, l'algorithme de la FFT shift est le plus efficace. Il est suivi de l'algorithme de la sommation avant corrélation. La FFT transverse n'est plus que le 5^{eme} algorithme en termes de performances en acquisition. L'algorithme de la sommation après corrélation a des performances comparables à l'algorithme de la FFT classique, voire même pires dans certains cas.

En ce qui concerne l'algorithme SOR introduit dans ce manuscrit, il peut être relativement plus intéressant quand M et T_p sont présélectionnés indépendamment de la valeur du rapport C/N_0 , donc en d'autres termes si ces deux paramètres sont légèrement surestimés.

Finalement, en termes d'occupation mémoire, les algorithmes de la sommation après et avant corrélation ont des besoins en mémoires assez faibles, alors que l'algorithme de la FFT transverse est plus contraignant en termes de mémoire. Il est à noter que l'algorithme SOR est basé sur la FFT transverse pour l'acquisition du premier satellite, et l'algorithme de la sommation après corrélation pour l'acquisition des autres satellites. Ceci rend cet algorithme aussi contraignant qu'en mémoire que la FFT transverse.

Chapter 6

Performance Evaluation of AGPS Acquisition Techniques

Contents

This chapter reports on a set of experiments conducted to evaluate and compare the performance of the algorithms described in Chapter V. The algorithms performance analysis will be conducted in terms of both sensitivity and processing time (directly related to the TTFF). As explained previously, these two parameters are the key drivers for acquisition performance analysis, and their importance depends on the considered operational environment. For rural environments, the main objective is the reduction of the TTFF, since there are no sensitivity problems: a suitable solution must essentially reduce the TTFF, even if it introduces some tolerable losses in the final C/N_0 (since in such environments the signals are rather strong). On the other hand, for urban and indoor environments, the solution to be adopted attempts to find the best compromise between the TTFF and sensitivity, thus providing a fast solution without penalising sensitivity. The TTFF being directly related to the algorithm complexity, and since the algorithms are implemented using Matlab, the TTFF is not directly estimated, and the algorithms are rather compared in terms of complexity.

One of the proposed algorithms presented in Chapter V is the SOR (*Sum Of Replicas*) algorithm [*El Natour et al., 2006a*]. We recall that this "multi-satellites" algorithm enhances the TTFF by computing more than one satellite at once: the received signal is correlated with a sum of locally generated replicas rather than being correlated with only one. The other algorithms are all "mono-satellite" algorithms, meaning that the satellites are searched for one after another. They involve enhancements in the TTFF that depends on the algorithm complexity, compared to the conventional algorithm, with no or negligible loss in sensitivity. The main idea behind these algorithms complexity reduction is to carry out coherent integration by coherently summing 1 *ms* correlation results regardless of the total coherent integration duration instead of processing $T_p ms$ of signal at once as is the case for the classical FFT algorithm. The Transverse FFT algorithm introduces further optimisation by considering the signal phase to be constant over a period of 1 *ms* and for small Doppler shifts to further reduce the complexity. The SOR was basically implemented using the sum after FFT-IFFT algorithm. Yet, it can be optimised by rather applying the transverse FFT algorithm as acquisition process to optimise the acquisition of the first satellite; the other satellites still being acquired using the sum after FFT-IFFT algorithm. Only the results obtained with the optimised SOR algorithm are presented here, since the non-optimised one yielded very bad performances. (Recall that the transverse FFT is only used to optimise the acquisition of the first satellite, since no Doppler search is used to acquire the other satellites.)

Let us note that, the results obtained with the average correlation algorithm were not satisfying, especially in terms of sensitivity as explained in Chapter IV; so they will not be presented here neither.

Besides, recall that all of these algorithms are based on the Assisted GPS concept to improve their false detection ability. Thus, the reference time is known with a $\pm 2\,s$ uncertainty, the reference position uncertainty depends on the transmitting GSM cell size, and the Doppler search range is of $\pm 2\,kHz$ (refer to Chapter IV § IV.2.2). This uncertainty on the Doppler search range is due to the receiver clock drift and user motion induced Doppler (the satellite motion induced Doppler is accurately calculated using the AD). The remaining Doppler component is the same for all of the satellites comprised in a particular signal. Consequently, the acquisition of the first satellite is enough to remove this uncertainty. Thus no frequency search is required for the other satellites.

The algorithm performances were evaluated based on different parameters: the duration of the coherent integration (T_p), the number of non-coherent accumulations (M), the incoming signal C/N_0, the Doppler frequency bins to be tested, and the uncertainty on the receiver position (determined using the Assistance Data).

Three types of tests were conducted to study the impact of these parameters: the first two tests compare the algorithms complexity (in terms of number of arithmetic operations and number of processor cycles) and sensitivity (in terms of loss in C/N_0), respectively, for the same T_p, M, position and time uncertainties. The third one rather focuses on the sensitivity limits of the algorithms, while evaluating the resulting processing time. These tests are explained in detail in the subsequent sections. The best compromise solutions are derived based on the results, with some concluding remarks following.

For sensitivity tests, the signals used were generated using a SPirent STR4500 GPS signal generator and an NI-6534 acquisition card with a sampling frequency of $2{,}046\ MHz$. Each signal is comprised of 9 visible satellites at the same C/N_0 ratio. The overall C/N_0 is different from one signal to another in order to assess the impact of this ratio. We have considered a static user only.

In all of the tests, the visible satellites are sorted based on their elevation angles. For relatively strong signals (typical of rural and urban environments: $42\ dBHz$ and $27 dBHz$), the satellites are sorted and searched for from the highest down to the lowest. This is a way to increase the probability of having the strongest signals processed at first to guarantee faster solution availability, which is in accordance with results obtained in Chapters III and IV. For weak signals, referring to indoor environments, the satellites were rather sorted such that the first satellites to be acquired are those having elevation angles around 60°, once again according to results obtained before. The others are randomly chosen.

Part of the results presented in this chapter was the object of a paper [*El Natour et al., 2006c*] presented at the GNSS ION 2006 meeting.

VI.1 Complexity evaluation and comparison

The TTFF is evaluated using similar conditions for all of the algorithms. Different values of coherent and non-coherent durations are considered: $M = 10, 20, \ldots 500$, $T_p = 0.001, 0.002, \ldots 0.02$ (sec). The Doppler frequency search range is $[-2\ kHz; 2\ kHz]$. For each algorithm, the number of arithmetic operations, multiplications and additions, to be carried out through out the acquisition were counted. The complexity was also quantified in number of cycles needed using a TM 320 C64x processor for illustration purposes. Nine satellites are assumed to be visible to the receiver during simulations. The SOR algorithm complexity was evaluated for different numbers of satellites per group: 2, 3 or 4 satellites per group. Recall that a first satellite is always acquired alone at the beginning. Figures VI-1, VI-2, VI-3, and VI-4 illustrate the number of additions, multiplications, the joint number of additions and multiplications and the number of cycles needed for the "classical FFT" algorithm, the "sum after FFT-IFFT", "sum before FFT-IFFT", "Transverse FFT", "FFT shift", and the optimized SOR algorithm with either 2, 3 or 4 satellites per group. The number of operations and cycles are represented on the z-axis in a logarithmic scale: the unit represented on the z-axis is the power of 10 of the true number (of operations or cycles). In all these figures, the higher the curve, the higher the number of operations or processor cycles needed, the higher the algorithm complexity and the higher the time needed for acquisition. Following each figure, that is for each comparison, a classification of the algorithms in terms of complexity is proposed.

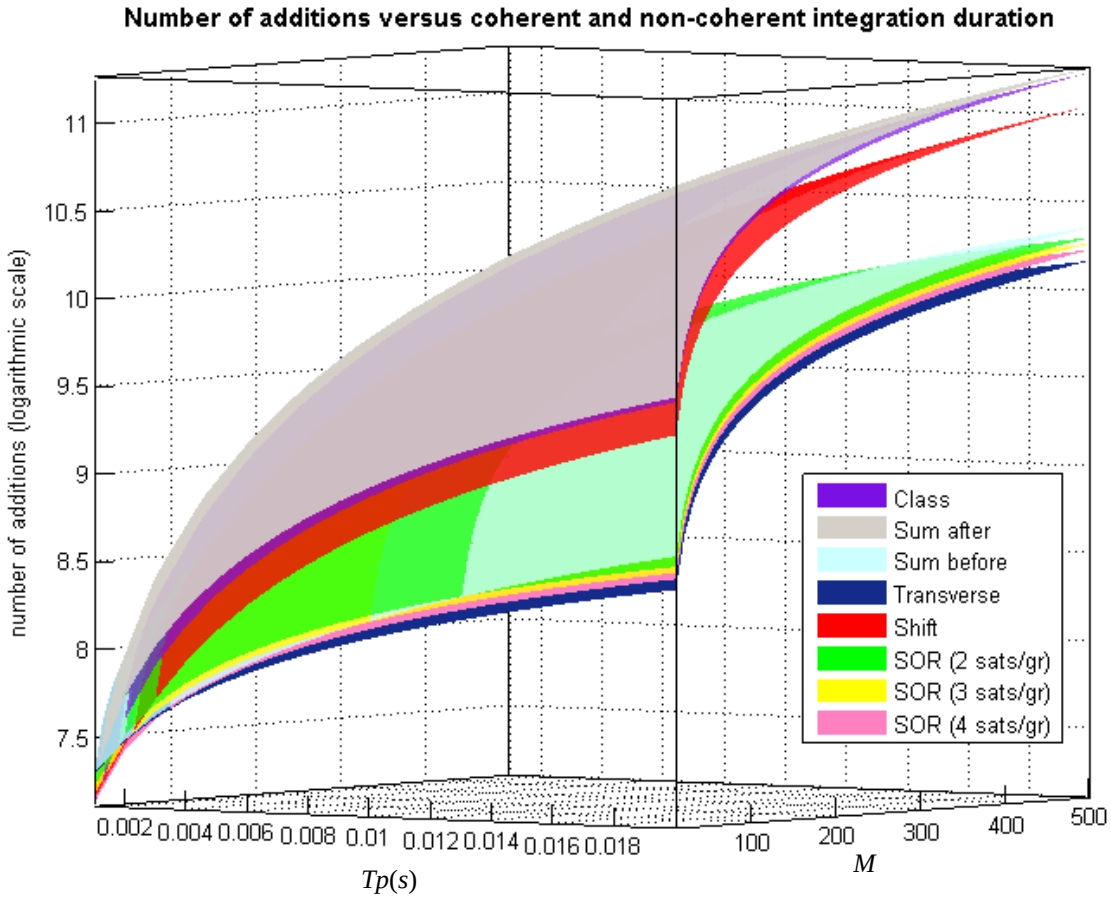

Fig VI-1 : Number of additions carried out during acquisition for the different algorithms, with 9 satellites in view

As for the number of additions, for high values of T_p, the algorithms can be classified in the following order in terms of number of additions (from the best to the worst): transverse FFT, SOR with 4 satellites per group, 3 satellites per group, 2 satellites per group, sum before, FFT shift, classical algorithm, sum after algorithm.

Transverse FFT (best)
SOR (4 satellites per group)
SOR (3 satellites per group)
SOR (2 satellites per group)
Sum before
FFT shift
Classical algorithm
Sum after algorithm (worst)

Tab VI-1 : algorithms classification in terms of number of additions for high T_p, from the best to the worst

For lower values of T_p, this classification is not the same. The Sum before FFT-IFFT for example, is better than the SOR (for lower values of T_p): it is better than the SOR with 3 satellites per group for $T_p \leq 10\,ms$, and better than the SOR with 2 satellites per group for $T_p \leq 12\,ms$. Details on the algorithms classification for low values of T_p will be provided later on, using zoomed in curves.

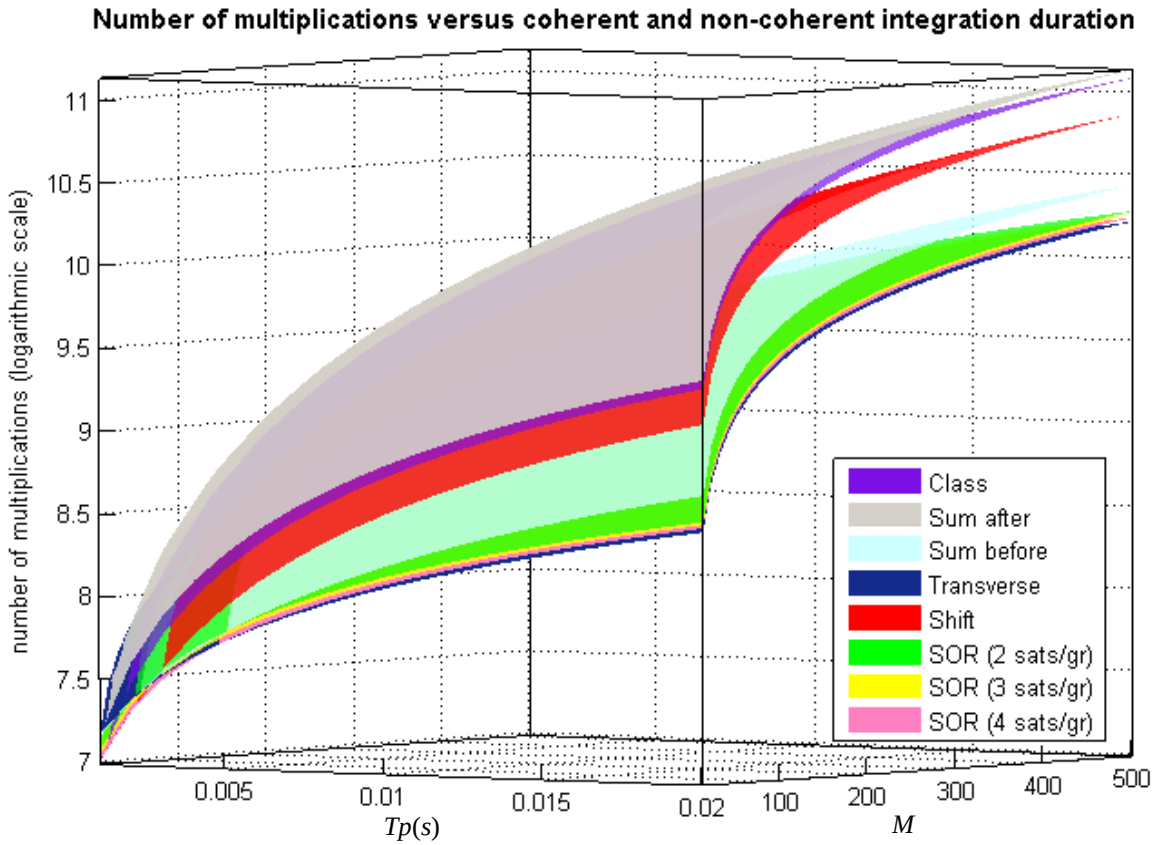

Fig VI-2 : Number of multiplications carried out during acquisition for the different algorithms, with 9 satellites in view

In terms of number of multiplications also the algorithms can be classified as before for high values of T_p. But for lower values of T_p, the Sum before algorithm becomes better than the SOR algorithm only for $T_p \leq 5\ ms$ compared to $T_p \leq 12\ ms$ in terms of number of additions.

The curves of figures VI-1 and VI-2 have approximately the same shape. Globally, the SOR algorithm is more comparable to the Sum before and the transverse FFT algorithms; whereas the Classical, the Sum after and the FFT shift algorithms are more comparable to each other. These differences may be accentuated or decreased according to the implementation of addition and multiplication operations in a given processor. In the TM 320 C64x processor for example, an addition needs more cycles than a multiplication. Hence the differences shown in these figures between the algorithms may be more or less important when the number of operations is translated in number of processor cycles which provides a more uniform and coherent view of the algorithms complexity than the total number of arithmetic operations. For this reason, the next results are conducted using this parameter.

Figure VI-3 next, shows a comparison of the algorithms performance evaluated in terms of number of cycles needed by a TM 320 C64x processor to perform the acquisition of 9 visible satellites, for different values of M and T_p.

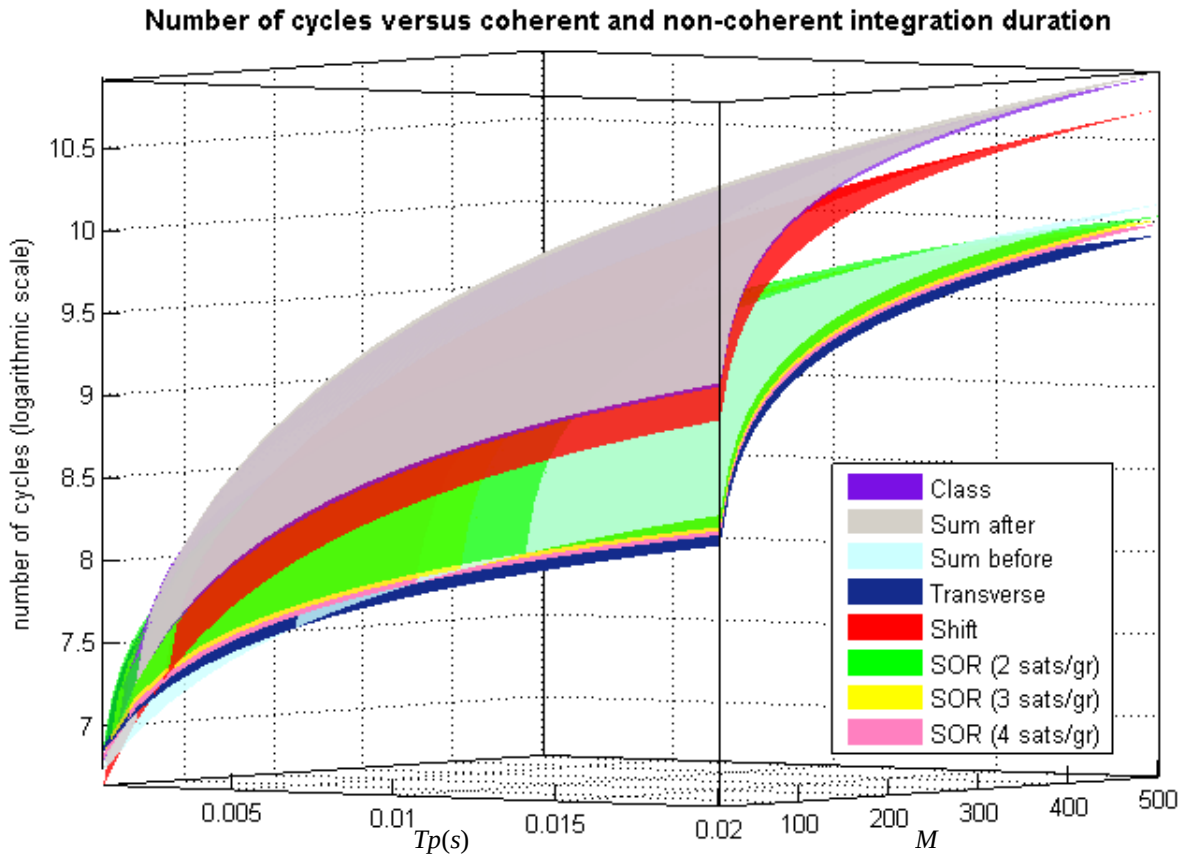

Fig VI-3 : Number of cycles needed during acquisition for the different algorithms, with 9 satellites in view

According to figure VI-3, the algorithms overall classification for high values of T_p is also as before: transverse FFT, optimised SOR with 4 satellites per group, 3 satellites per group, and 2 satellites per group, Sum before, FFT shift, Classical algorithm, and Sum after algorithm. As for the SOR algorithm, the difference in complexity between having 2, 3, or 4 satellites per groups is not very significant in this figure. It is however faster than the Sum after and the Classical algorithms, but it is still slower than the transverse FFT, and the Sum before algorithms for $T_p \geq 14\,ms$.

A closer view of figure VI-3 shows different intersections of the different algorithms curves edges especially for relatively small coherent durations. To best view these intersections, we plotted the number of cycles needed for each algorithm as a function of M for a given value of T_p, and as a function of T_p for a given value of M respectively.

Figures VI-4 and VI-5 illustrate the number of cycles needed for $M = 10$ and $M = 500$ as a function of T_p.

Fixed M : 10 or 500, variable T_p

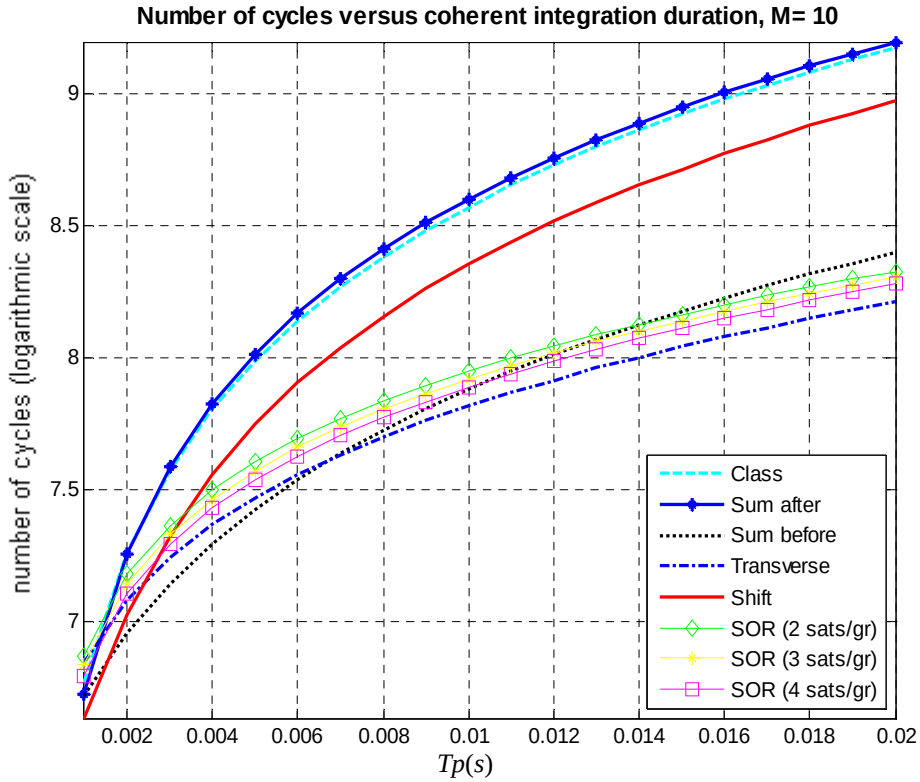

Fig VI-4 : Number of cycles (represented in logarithmic scale) versus coherent integration for $M = 10$

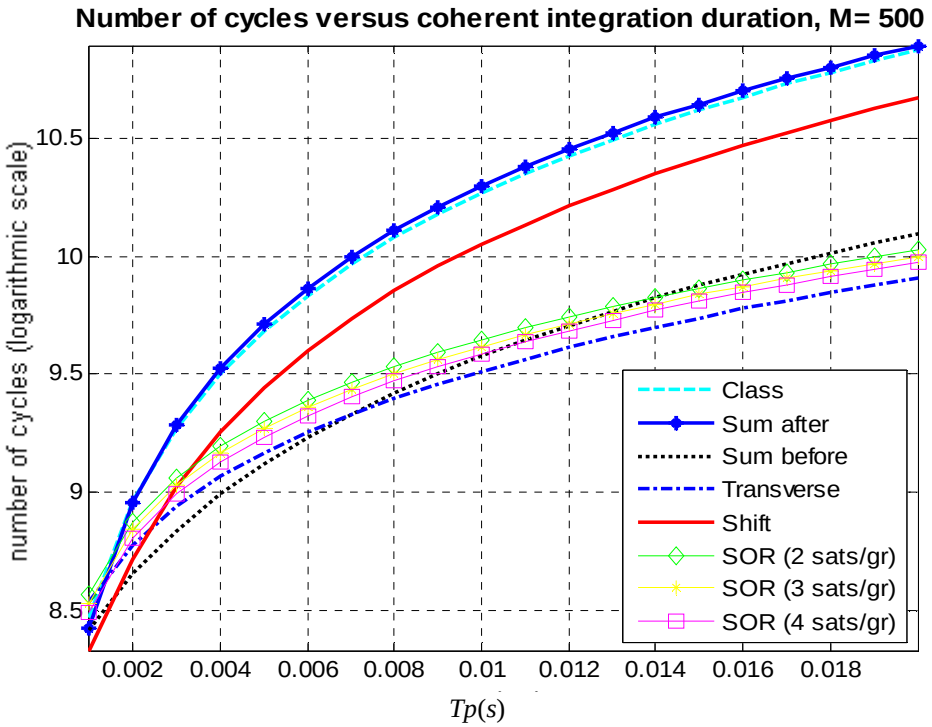

Fig VI-5 : Number of cycles versus coherent integration for $M = 500$

Both figures VI-4 and VI-5 have the same shape meaning that the algorithms complexity classification is the same whatever the value of M . The complexity variations, or in other words the algorithms complexity classification only depends on the coherent integration duration. In these figures, we can find again that the Sum before starts to be worse than the

SOR algorithm for $T_p \geq 10\,ms$. It is worse than the SOR with 2 satellites per group for $T_p \geq 14\,ms$. Another interesting intersection can be seen between the Sum before and the Transverse FFT algorithms at $T_p = 7\,ms$. In fact below this value, the Sum before is more beneficial, whereas the transverse algorithm is more interesting for coherent integrations higher than $7\,ms$. The FFT shift algorithm has complexity closer to the classical and the sum after algorithms than to the other algorithms.

Many other intersections appear for low values of T_p. Figure VI-7 next shows a zoom of figure VI-6 at low values of T_p.

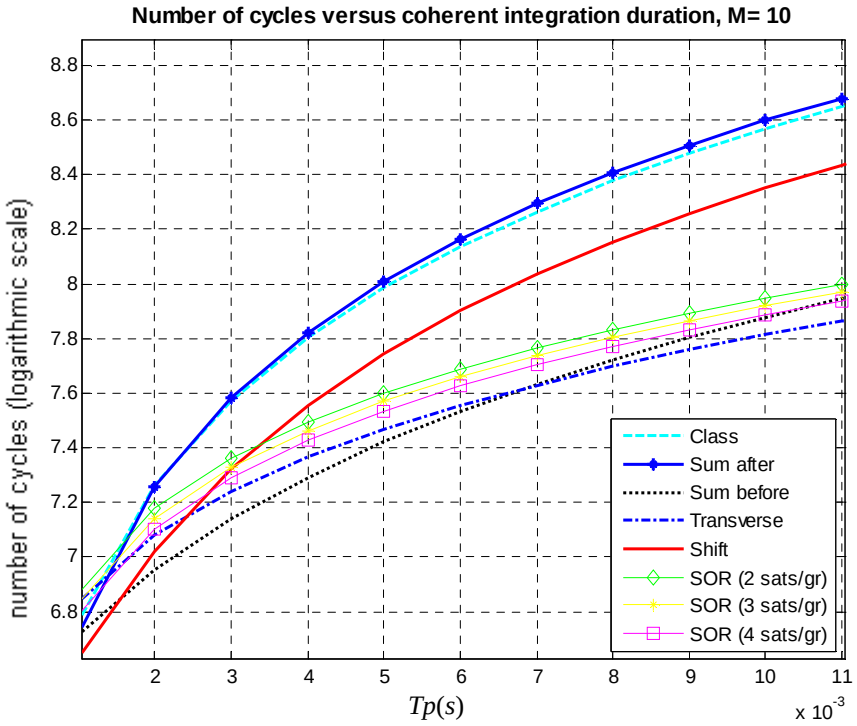

Fig VI-6 : zoom on figure VI-5

As it can be seen in figure VI-6, for $T_p = 1\,ms$, the Classical and the Sum after algorithms have performances comparable to the Sum before algorithm, and are slightly better than the SOR and the transverse FFT algorithms. However, the other algorithms (Sum before, Transverse FFT and optimised SOR) start to be beneficial for $T_p \geq 2\,ms$. The FFT shift has the lowest complexity for $T_p = 1\,ms$. As T_p becomes higher, the algorithm performances are gradually degraded, and for $T_p \geq 4\,ms$, it is only better than the Classical and the Sum after algorithms, and worst than all the others.

Fixed T_p : $1\,ms$ and $20\,ms$, variable *M*.

According to figures VI-4, VI-5, and VI-6, the algorithms complexity variations are the same for all values of M, but not for all values of T_p. Consequently, figures VI-7 and VI-8 depict the number of cycles needed as a function of M for given values of T_p. Figure VI-7 is plotted for $T_p = 1\,ms$ while figure VI-8 gives the results for $T_p = 20\,ms$.

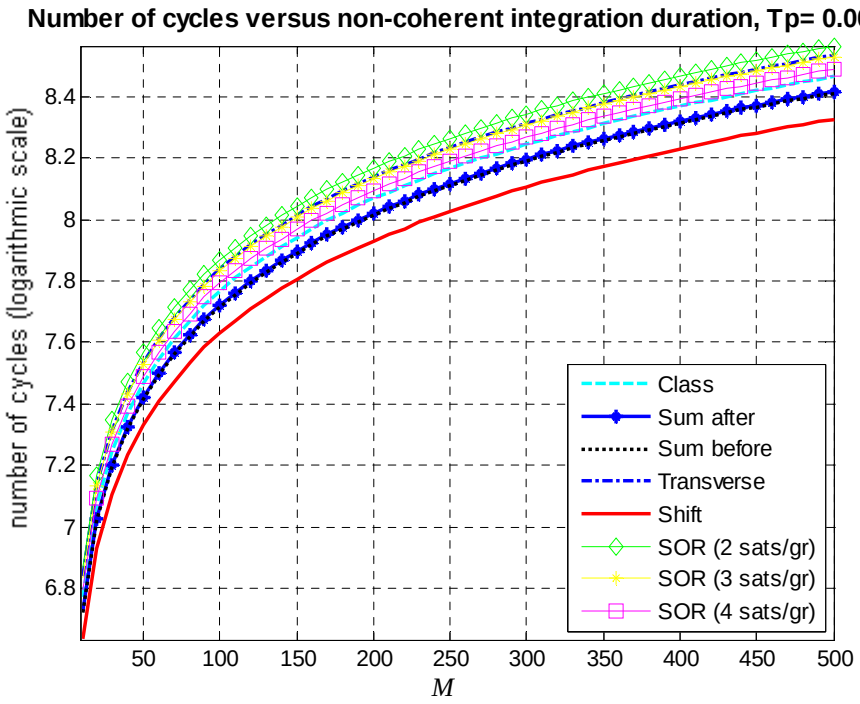

Fig VI-7 : Number of cycles versus non-coherent integration for $T_p = 1\ ms$

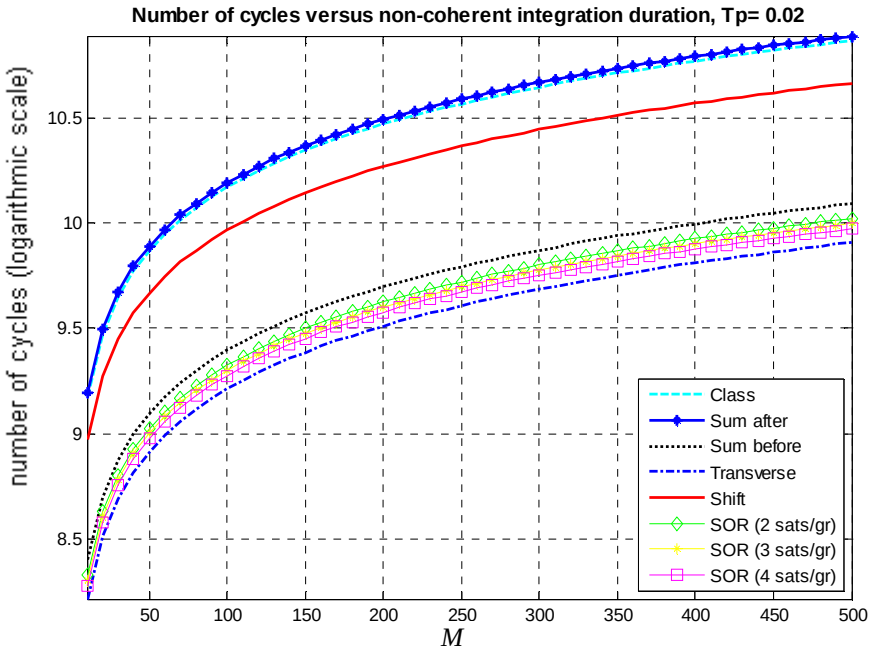

Fig VI-8 : Number of cycles versus non-coherent integration for $T_p = 20\ ms$

Figures VI-7 and VI-8 have completely different shapes, as opposed to figures VI-4 and VI-5. In figure VI-7, the FFT shift algorithms have the lowest complexity. It is followed by the Classical and the Sum after algorithms. Indeed, the advanced algorithms are essentially optimised to speed up the coherent integration process. The Classical algorithm complexity increases with the coherent integration duration, since the number of samples processed by the FFT-IFFT couple, is greater. This is not the case for the other algorithms since they all process only $2\ ms$ of signal at once regardless of the coherent integration duration. For a

coherent integration over $1\,ms$ their complexities are worse than that of the Classical algorithm since they induce more complex processing, while trying to shorten the coherent integration time. This also explains the global increase of the differences between the algorithms with increasing values of the coherent integration duration. Note that in this case the SOR algorithm has the worst performance. For $T_p = 20\,ms$, the transverse FFT has the lowest complexity, followed by the SOR and the Sum before algorithms respectively. The Classical and the Sum before algorithms have the worst performances.

The Sum after FFT-IFFT algorithm is surprisingly not faster than the Classical one: it is comparable and even slightly worse in some cases. This can be explained by the fact that for each correlation result of $1\,ms$, $2\,ms$ of signal are considered for the Sum after algorithm ($2\,ms$ of signal are used to emulate a $1\,ms$ linear correlation by performing a $2\,ms$ circular correlation using the FFT technique, refer to Chapter V for more details), compared to $1\,ms$ for the Classical algorithm; this means that the Sum after algorithm processes twice more signal samples than the Classical one. The difference in computation is not however twice between the two algorithms implying a reduction in complexity using the Sum after algorithm, else it should need twice more time. But this complexity reduction is not enough for the Sum after algorithm to be better than the Classical algorithm. Yet, as explained in chapter V, this linear correlation is important to avoid data bits edges within a $1\,ms$ of signal, and simulations showed that it was harder to acquire signals without using this technique (in some cases, signals could not be acquired at all).

Conclusions

- Globally, the SOR algorithm is more comparable to the Sum before and the transverse FFT algorithms; whereas the Classical, the Sum after and the FFT shift algorithms are more comparable to each other.
- The increase in complexity is as expected more sensitive to the increase of the coherent integration duration, than to the non-coherent accumulation increase.
- The largest difference in complexity performance is seen between the Classical FFT, the FFT shift and the Sum after algorithms on one side, and the other algorithms on the other side, where the Classical, the FFT shift and the Sum after algorithms are always less performant, except for a $1\,ms$ coherent duration.
- No algorithm was found to have the best performances in terms of processing cost in all cases. The latter mainly depended on the value of the coherent integration.

The algorithms complexity classification as a function of the coherent integration is summarized in table VI-2 below from the best to the worst (according to the results obtained before). Recall that this classification is the same for all values of *M*.

$T_p = 1ms$	$2ms \le T_p \le 7ms$	$7ms \le T_p \le 11ms$	$11ms \le T_p \le 12ms$	$12ms \le T_p \le 14ms$	$T_p \le 14ms$
FFT shift	Sum before	Transverse FFT	Transverse FFT	Transverse FFT	Transverse FFT
Sum before	Transverse FFT	Sum before	SOR (4 satellites per group)	SOR (4 satellites per group)	SOR (4 satellites per group)
Classical, Sum after	SOR (4 satellites per group)	SOR (4 satellites per group)	Sum before	SOR (3 satellites per group)	SOR (3 satellites per group)
SOR (4 satellites per group)	SOR (3 satellites per group)	SOR (3 satellites per group)	SOR (3 satellites per group)	Sum before	SOR (2 satellites per group)
Transverse FFT	SOR (2 satellites per group)	SOR (2 satellites per group)	SOR (2 satellites per group)	SOR (2 satellites per group)	Sum before
SOR (3 satellites per group)	Classical	Classical	Classical	FFT shift	FFT shift
SOR (2 satellites per group)	FFT shift	FFT shift	FFT shift	Classical	Classical
	Sum after	Sum after	Sum after	Sum after	Sum after

Tab VI-2 : algorithms complexity classification as a function of T_p from the best to the worst

The threshold values of T_p given in this table may differ from one processor to another. But they still give an order of magnitude of these values.

VI.2 Sensitivity evaluation and comparison

In this test, 3 signals with different C/N_0 are studied: 42, 27 and 17 *dBHz* characteristic of a rural, an urban or an indoor environment, respectively. For each C/N_0, values of T_p and M are chosen large enough such that all of the satellites can be successfully acquired, i.e., there is no acquisition problems. The focus is only brought on the reduction of the C/N_0 value induced by each algorithm in the context of a successful acquisition. A signal is said to be successfully acquired if the correlation maximum corresponds to the right code delay and Doppler values (found using an OEM receiver).

The algorithms are implemented with Matlab®. The values of T_p and M are set to be the same for all of the algorithms, for the sake of comparison. Table VI-3 shows the values of T_p and M chosen for each value of the C/N_0; accordingly a value of the GSM cell radius was chosen also depending on the corresponding environment type. The user position uncertainty (Δx) is in each case equal to the considered GSM cell radius [*Changlin Ma, 2003*].

C/N_0 $(dBHz)$	42	27	17
T_p (ms)	4	10	10
M	5	15	230
Δx (km)	30	10	1

Tab VI-3: parameters used for the sensitivity evaluation test

Depending on the value of the C/N_0 , all or some of the visible satellites are assumed to be needed in order to compute a position. In other words, in rural areas all the satellites viewed by the signal generator as visible (with elevation angle between 5° and 175°) are acquired since they are all supposed to be visible to the receiver. (However, in) In urban or indoor environments, not all the satellites visible in the sky are visible to the receiver due to the presence of obstacles such as buildings. In these cases only part of the satellites are acquired. The number of satellites acquired is chosen based on results obtained in Chapter IV.

The time uncertainty is kept at $\pm 2\ s$. The results obtained are presented next.

VI.2.1 Rural environments

In this case, we assume the received signal to be sufficiently strong, with a $C/N_0 \cong 42\ dBHz$. T_p and M are such that $T_p = 4\ ms$, and $M = 5$ respectively. The cell size, or in other words the initial position uncertainty, is $\Delta x = 30\ km$

The estimated C/N_0 ratios obtained in this case for each of the algorithms are illustrated in figure VI-9 next.

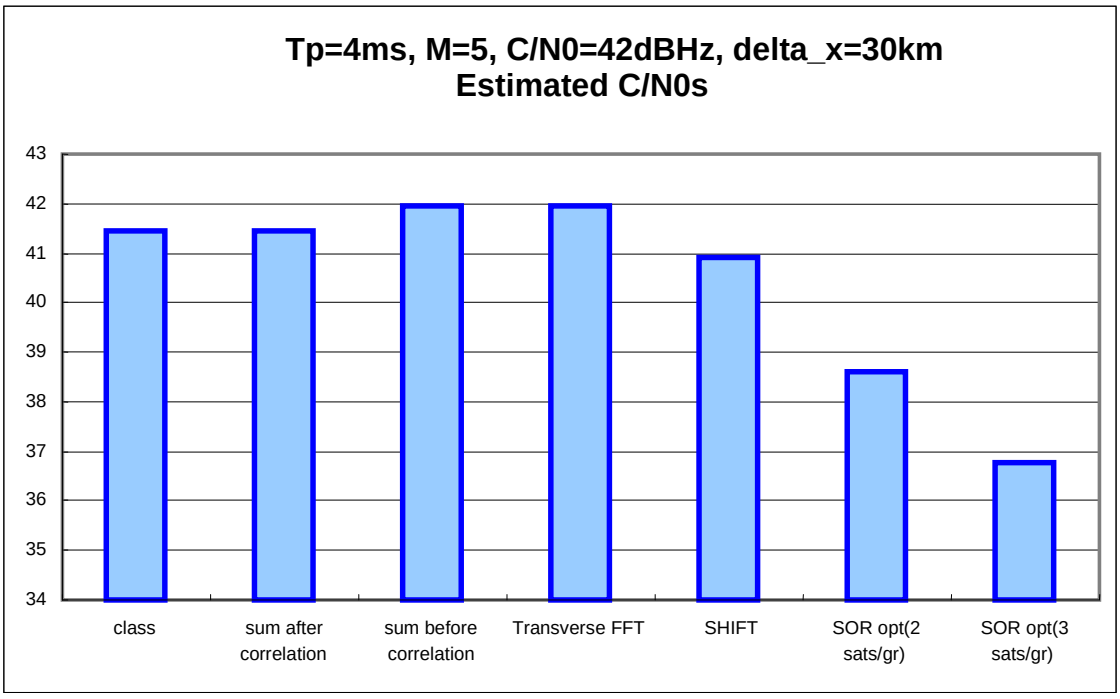

Fig VI-9: Estimated C/N_0 for a signal of $42\ dBHz$, with fixed M and T_p

Figure VI-10 below illustrates the number of arithmetic operations and cycles needed for each algorithm, normalized with respect to the classical algorithm.

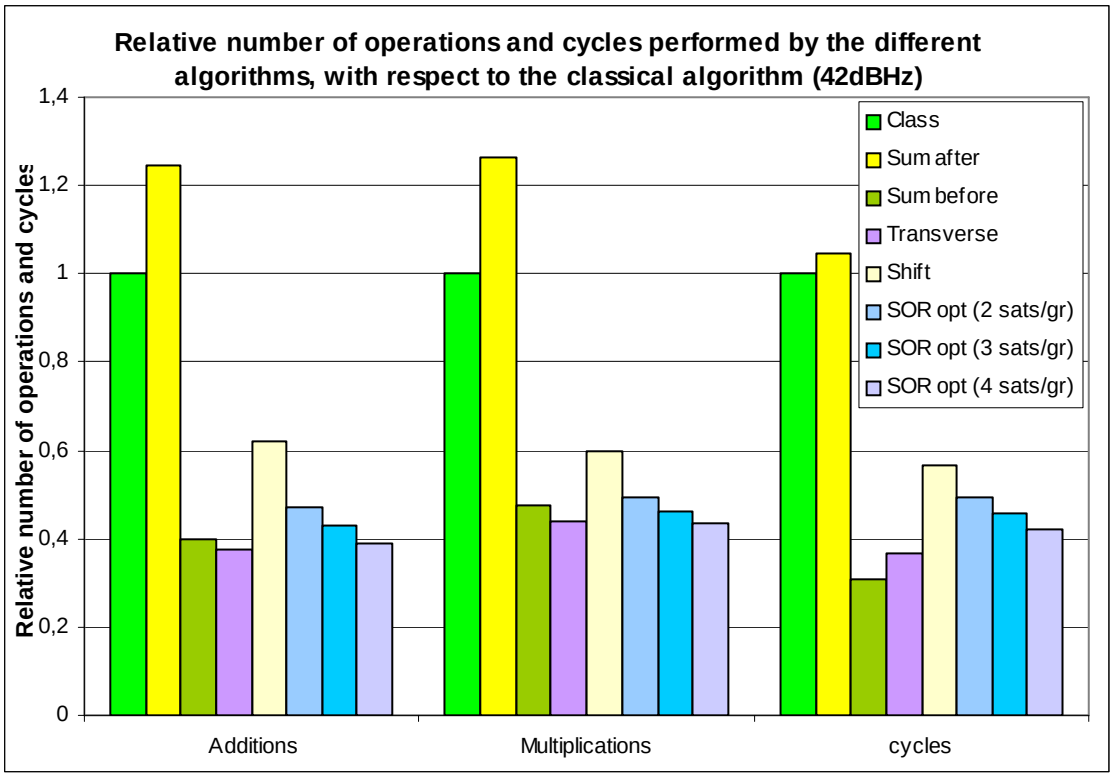

Fig VI-10 : Number of operations and cycles needed for the values of M and T_p used here

Figure VI-10 shows that the Sum after correlation, Sum before correlation and transverse FFT algorithms have approximately the same performance as the Classical algorithm (the small increase in sensitivity noticed in the case of the Sum before correlation and the transverse FFT algorithms is due to C/N_0 estimation errors because the signal used for this estimation is very short). An average power loss of lower than 1 *dB* is noticed for the FFT Shift algorithm compared to the Classical algorithm.

As for the optimised SOR algorithm, it introduces a significant loss in the estimated C/N_0 which increases with the number of satellites per group, as was expected in chapter V. The average in the case of 2 satellites per group is approximately 3 *dB* which is in accordance with the theoretical value predicted in Chapter V. For 3 satellites per group the average loss is approximately 5 *dB* compared to the theoretical value of 4.75 *dB*. The small differences between the values of the loss in the C/N_0 ratio found here and their theoretical values, is due to the presence of cross-correlations which may randomly have a negative or a positive effect. However, it can be concluded that the thermal noise is the most important parameter for the estimation of the final C/N_0 value. Cross-correlations only play a negligible role.

The same test is repeated next with a signal at $27dBHz$.

VI.2.2 Urban environments

In this case, the signal parameters are: $C/N_0 \cong 27\,dBHz$, $T_p = 10\,ms$, $M = 15$, $\Delta x = 10\,km$

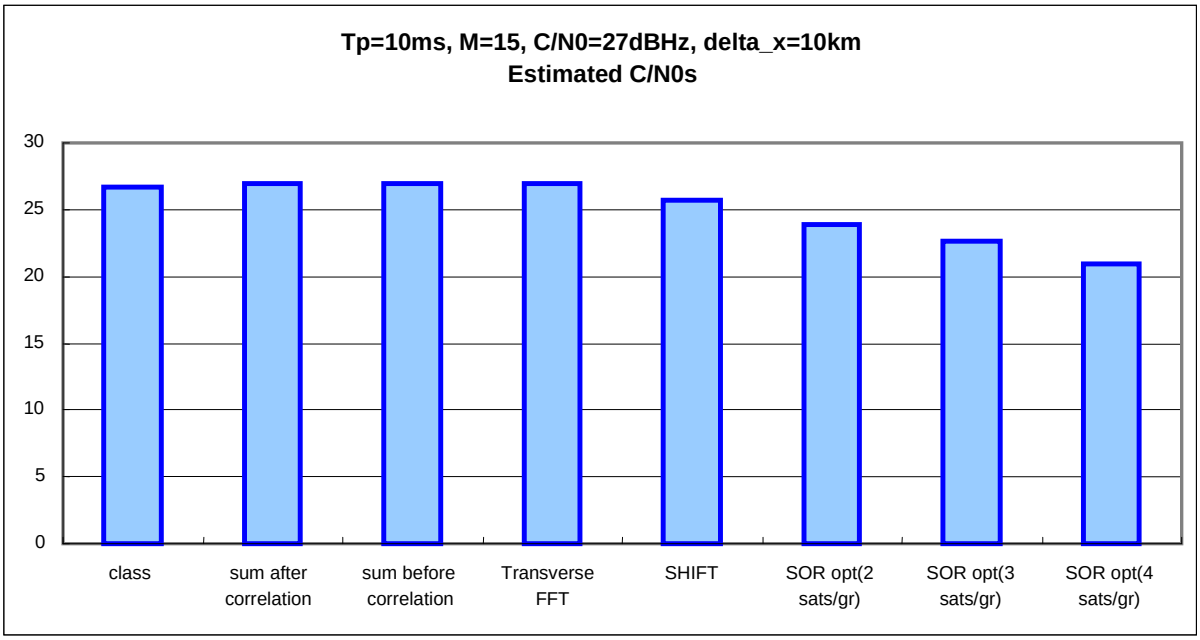

Fig VI-11: Estimated C/N_0 for a signal of $27dBHz$, with fixed M and T_p

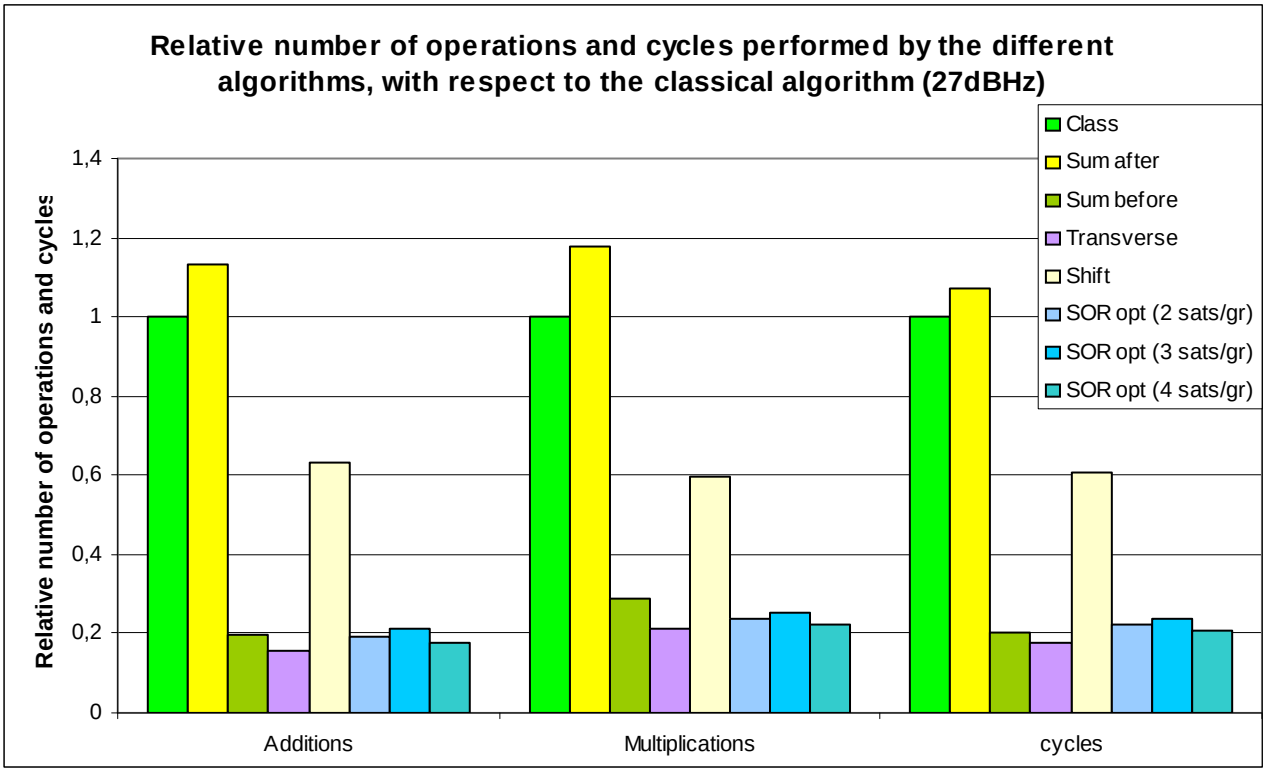

Fig VI-12 : Number of operations and cycles for the values of M and T_p used here

It can be noticed here that more satellites per group were tested for the SOR algorithm, namely 4 satellites per group. In fact, for a lower uncertainty on the user position more satellites can be grouped together since the code delay windows estimated using the AD are narrower and more satellites can be treated at once without intersection between these windows. This is why groups of up to 4 satellites can be formed.

The results of this test meet with those of the previous test: the "mono-satellite" algorithms have sensitivities comparable to the classical algorithm except for the FFT shift algorithm (loss of $\cong 1\,dB$). With the optimized SOR algorithm, losses in the C/N_0 ratio also increase with the number of satellites per group. The average loss is again approximately the same as that predicted in theory.

VI.2.3 Indoor environments

The signal parameters for this case are: $C/N_0 \cong 17\,dBHz$, $T_p = 10\,ms$, $M = 230$, and $\Delta x = 1\,km$.

The results obtained for a signal at $17 dBHz$, echoed those obtained previously, except for the FFT shift. They are illustrated in figure VI-13 below.

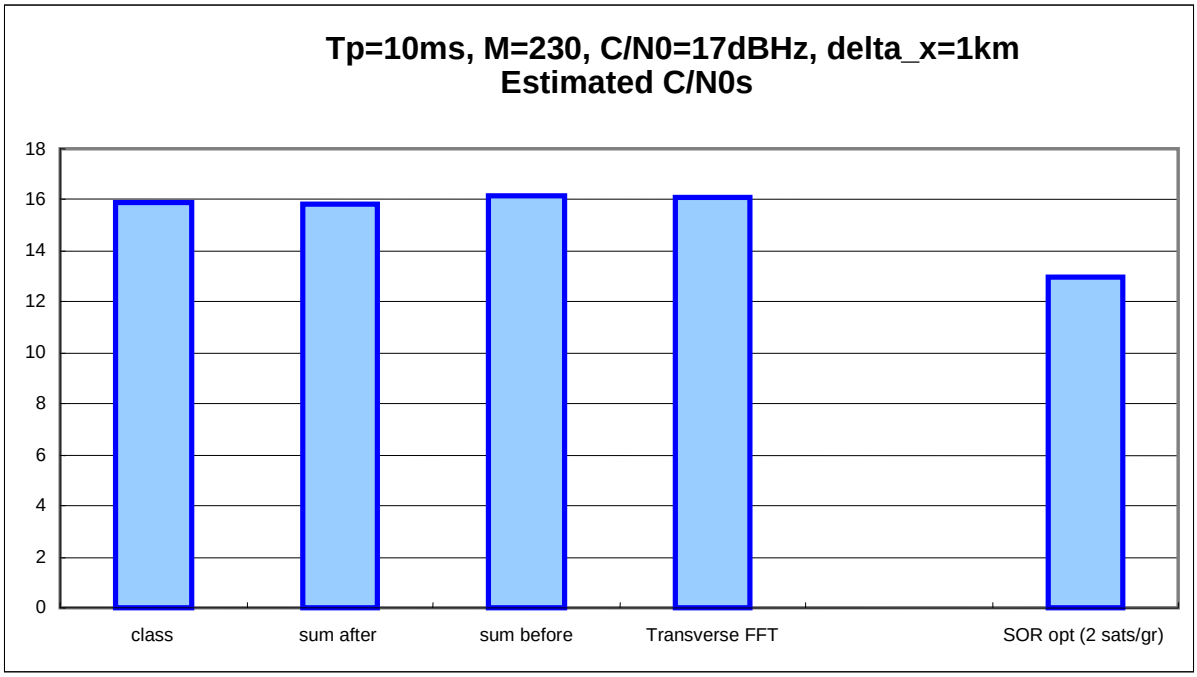

Fig VI-13: Estimated C/N_0 for a signal of $17 dBHz$, with fixed M and T_p

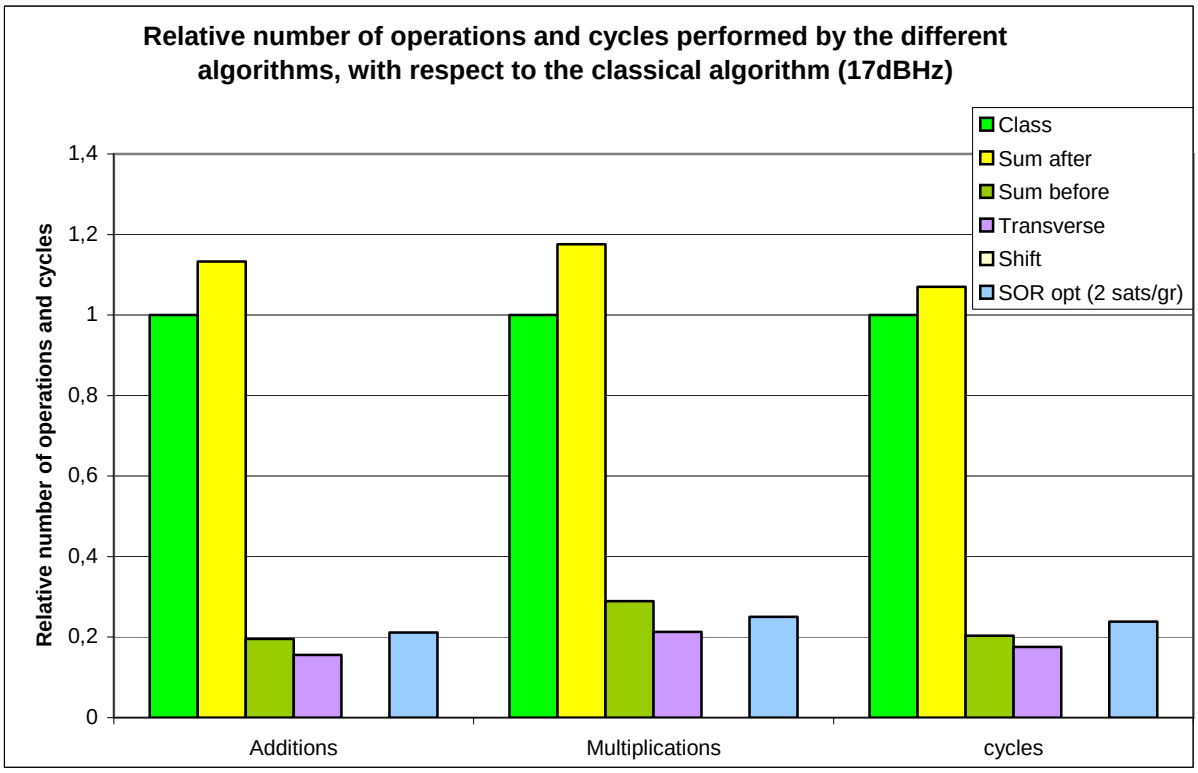

Fig VI-14 : Number of operations and cycles needed for $C/N_0 \cong 17\ dBHz$, $T_p = 10\ ms$, $M = 230$

In this case, the FFT Shift could not provide the right Doppler and code delay for signals at 17 *dBHz* , even for higher dwell times up to $3\ s$.

The sum before as predicted in Chapter V, did not induce any loss in C/N_0 in any of the tests. The same goes for the transverse FFT. Rather a small increase in the sensitivity is noticed for this algorithm and the other "mono- satellite" algorithms. This is explained by the use of 2ms of signal for 1ms of correlation.

Conclusions

- Gathered results of the complexity and the sensitivity tests show that in similar conditions, the "mono-satellite" algorithms have approximately the same sensitivity performance as the classical algorithm.
- An exception is made for the Shift algorithm which introduced an approximate loss of 1 *dB*, and could not deliver the right correlation peak for weak signals (17 *dBHz*).
- As for the optimised SOR algorithm, significant losses in sensitivity were observed.
- The optimised SOR complexity results (refer to figure VI-3) showed little difference for different number of satellites per group (or in other words different number of groups processed), whereas the loss greatly increases with the number of satellites per group. Consequently, in this case, groups of 2 satellites must rather be considered in order to limit the loss in C/N_0 ratio.

One way to compensate for these losses is to process longer blocks of signal. But this may increase the acquisition time needed. This is why further tests were conducted in order to compare the minimum time needed for each of these algorithms to successfully acquire a signal with a given C/N_0 . These tests are described next with the results obtained.

VI.3 Sensitivity limit performance evaluation

This test considers the same signals with the three characteristic C/N_0 ratios. The focus is put on the minimum time needed for each algorithm to successfully acquire a signal with a given C/N_0. The coherent integration duration is the same for all of the algorithms, in order to insure that the number of frequency bins tested is the same, for the sake of fair comparison between the algorithms. It is mainly the number of non-coherent integration M which is optimised. The minimum required M is searched for each satellite for each of the algorithms. The final value held for M is the one that insures a successful acquisition for a predefined number of satellites. It represents the mean value over ten tests (we could not conduct more tests due to lack of time). The uncertainty on the user position is again chosen according to the considered C/N_0. The parameters used for this test are illustrated in table VI-4.

C/N_0 $(dBHz)$	42	27	17
T_p (ms)	1	4	10
M	Variable	Variable	Variable
Δx (km)	30	10	1
Number of satellites successfully acquired	9/9	7/9	4/9

Tab VI-4: parameters used for sensitivity limit test

The choice of the number of satellites successfully acquired for each C/N_0 value was based on results obtained in chapter IV.

VI.3.1 Rural environments

The parameters used in this case are: $C/N_0 \cong 42\ dBHz$, $T_p = 1\,ms$, $\Delta x = 30\,km$

In this experiment, the minimum value of *M* needed to successfully acquire 9 satellites out of 9 visible satellites is first evaluated and the resulting algorithm complexity in terms of arithmetic operations is reported here. Since *M* will be different from one algorithm to another, the observation time of the signal used for acquisition will also be different; hence, the signal observation time is further considered when computing the final acquisition time. Only the acquisition complexity is computed here in terms of number of arithmetic operations and processor cycles, reconsidering the TM320 C64x processor. The results are depicted in figures VI-15 and VI-16.

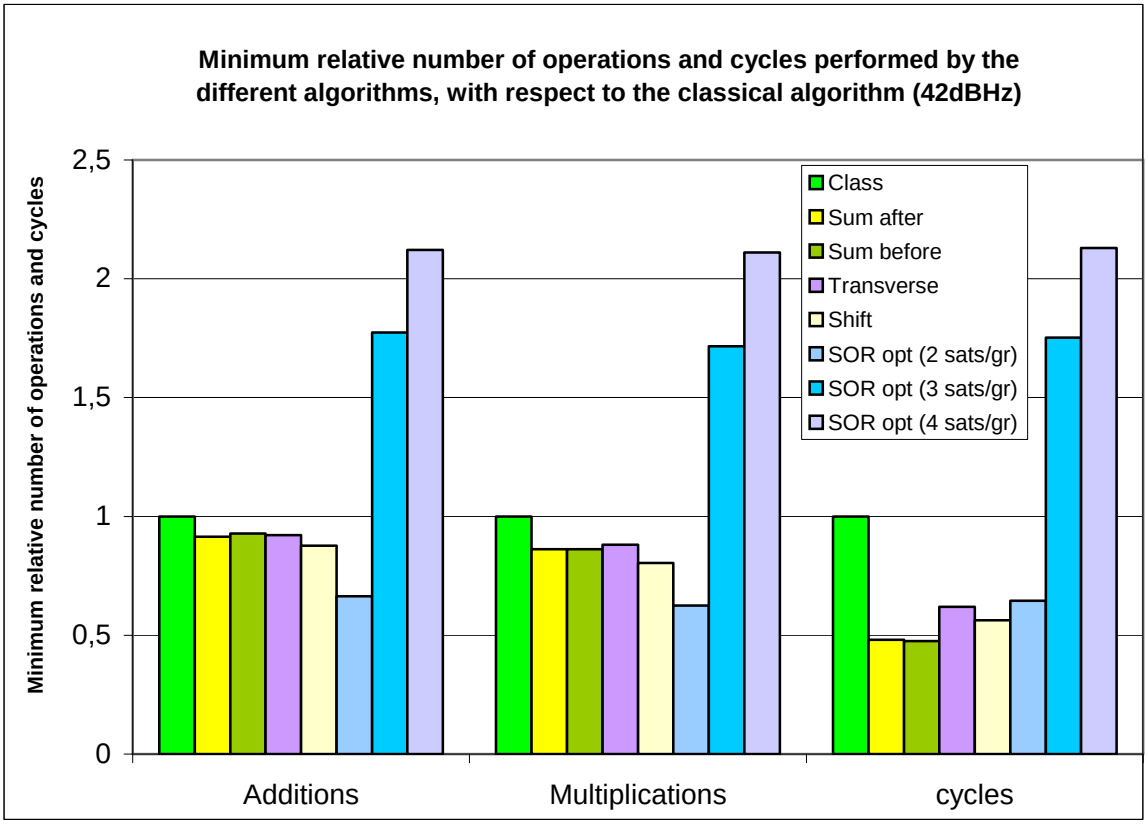

Fig VI-15: Minimum number of additions and multiplications needed by each algorithm to acquire a 9 satellites signal at $42 dBHz$

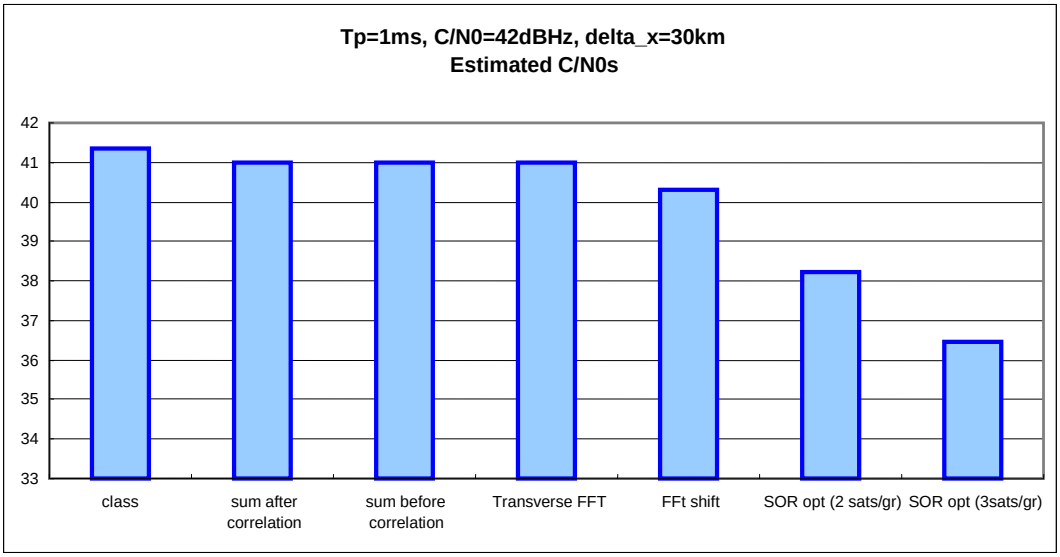

Fig VI-16: Estimated C / N_0 **for a signal of** $42\ dBHz$ **, with fixed** T_p

The "mono-satellite" algorithms are still much more comparable to the classical one in terms of sensitivity, which is compatible with results obtained before.

In terms of acquisition time also, they all have better performances than the Classical algorithm. This is because this test was conducted using a $1\,ms$ coherent integration as explained before. Note however, that at $T_p = 1\,ms$, and for equal values of *M*, the Classical

and the Sum after algorithms had performances better than the others in terms of complexity. This is not echoed in the result of figure VI-15. Indeed, the Classical algorithm needed longer non-coherent accumulations to provide a successful acquisition. This result highlights the need for linear correlation to enhance the algorithms sensitivity.

The SOR algorithm does not appear to be interesting at all in this case since it worsens the sensitivity by introducing losses and needs more time to acquire at once. In fact, the loss in the C/N_0 could not be compensated by longer integrations without increasing the overall time needed.

VI.3.2 Urban environments

The parameters used are: $C/N_0 \cong 27\ dBHz$, $T_p = 4\ ms$, $\Delta x = 10\ km$

This test has been conducted with the assumption that only 7 satellites out of 10 are needed to be successfully acquired in this case (based on results presented in Chapter IV). Thus, the minimum value of *M* retained is that corresponding to a successful acquisition of the first 7 satellites tested. Recall that these satellites are chosen out of all the visible satellites such that they have the highest elevation angles. The results are illustrated in figures VI-17 and VI-18.

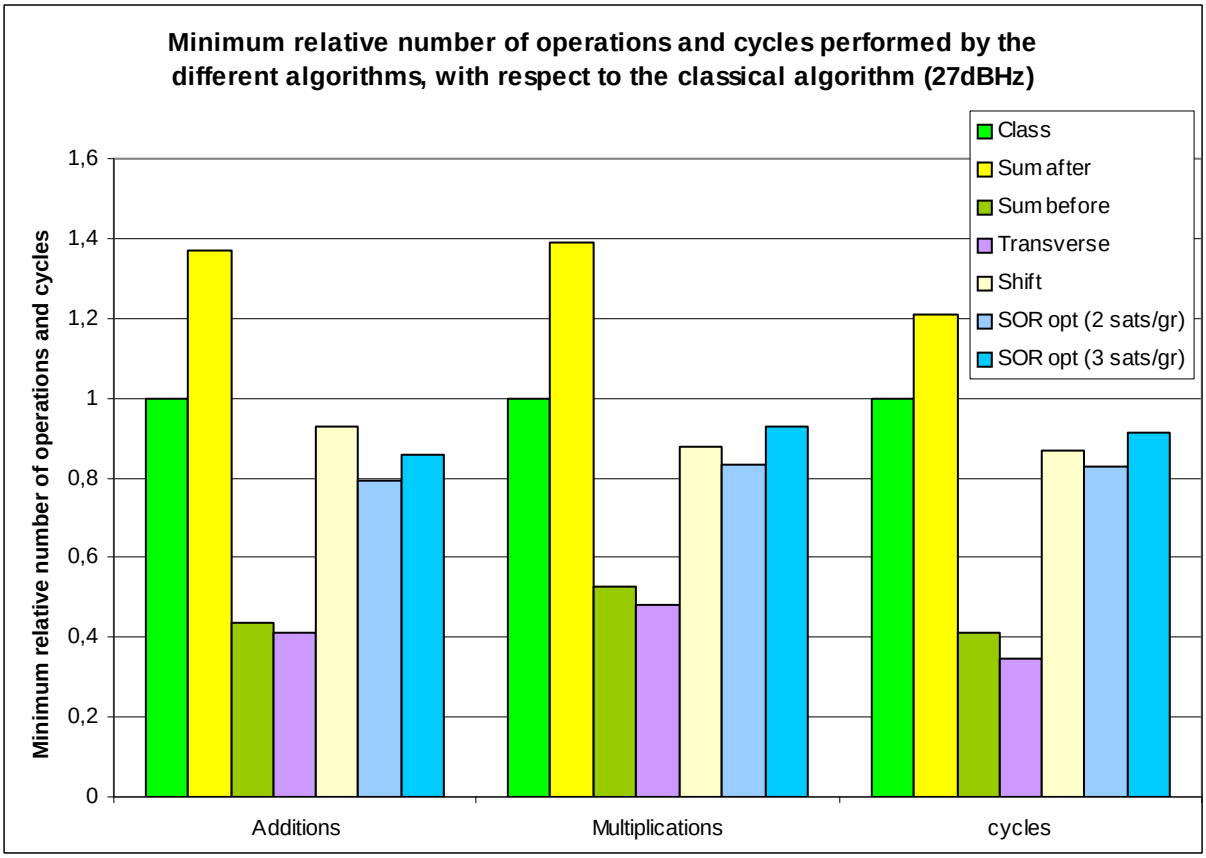

Fig VI-17: Minimum number of additions and multiplications needed by each algorithm to acquire a 10 satellites signal at $27dBHz$

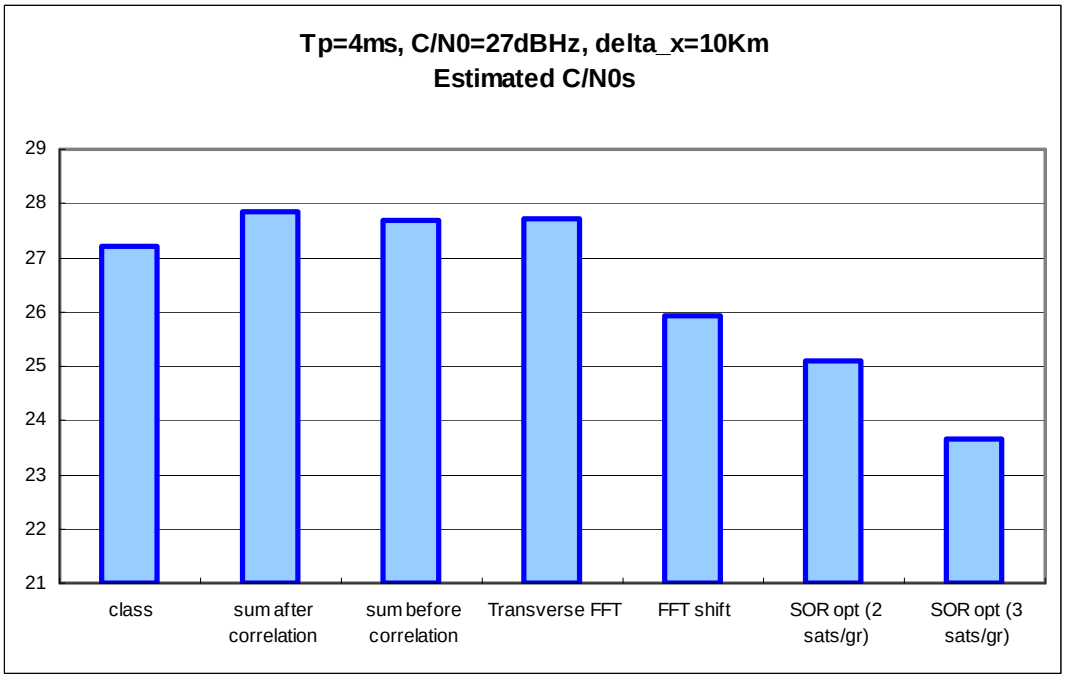

Fig VI-18: Estimated C/N_0 for a signal of $27\ dBHz$, with fixed T_p

In this experience the "mono-satellite" algorithms are faster than the Classical one, except for the Sum after correlation. The transverse FFT is the most interesting in this case. The Sum before is the closest in terms of speed to the transverse FFT, and they both do not present any C/N_0 losses. The optimised SOR needs more time but is more interesting than in the previous case. It is still however less interesting than the Sum before and the transverse FFT algorithms.

VI.3.3 Indoor environments

The parameters used here are: $C/N_0 \cong 17\ dBHz$, $T_p = 10\ ms$, $\Delta x = 1\,km$.

The number of satellites to be successfully acquired is set to 4 in this experiment, which corresponds to the minimum number of satellites needed to compute a position, since the availability in weak signal environments is always very low. The results are presented next.

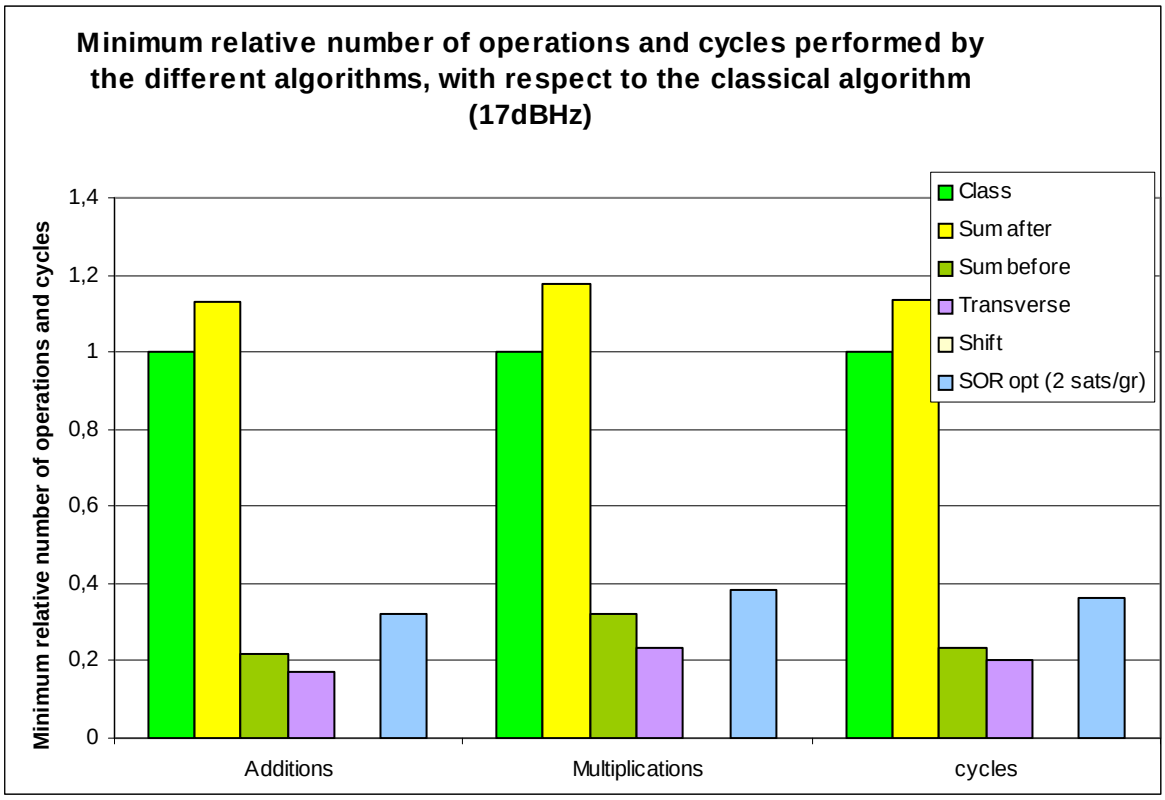

Fig VI-19: Minimum number of additions and multiplications needed by each algorithm to acquire a 10 satellites signal at $17\,dBHz$

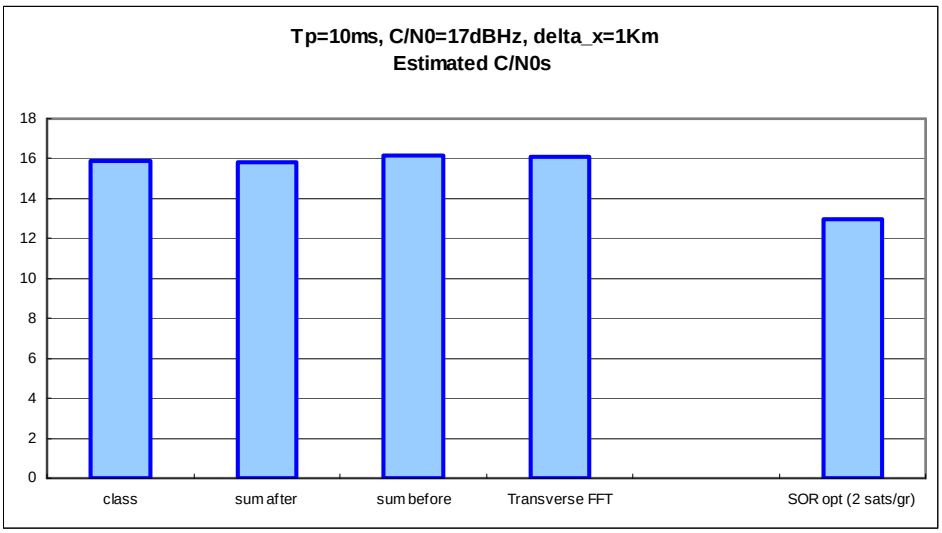

Fig VI-20: Estimated C / N_0 **for a signal of** $17\,dBHz$ **, with fixed** T_p

Here, the FFT Shift algorithm did not yield accurate results. And the best solution appears to be the Transverse FFT algorithm followed by the Sum before algorithm.

Conclusions

- In terms of sensitivity, the "mono-satellite" algorithms are much more comparable to the classical one, which is compatible with results obtained in the previous tests.

- In terms of acquisition time, they all have better performances than the Classical algorithm and the Sum after FFT-IFFT algorithm.
- The need for linear correlation to enhance the algorithms sensitivity was highlighted, since in rural environments, the Classical algorithm needed longer non-coherent accumulations to provide a successful acquisition.
- The SOR algorithm was not very interesting in this test since it worsens the sensitivity by introducing losses and needs more time to acquire at once.
- In indoors, the best solution appeared to be the Transverse FFT algorithm followed by the Sum before algorithm

VI.4 Memory requirements for each algorithm

A quick overview of the memory requirements for each algorithm shows that the transverse FFT and the SOR algorithms (since it is based on the transverse FFT algorithm) have the most stringent requirements, since T_p blocks of $2\,ms$ must be kept in memory in order to realize finer frequency search, even if a correlation is calculated each $2\,ms$ (refer to figure V-13). It is closely followed by the Classical and the Shift algorithms. The other algorithms only process $2\,ms$ blocks of signal at once. The Sum after and the Sum before algorithms have the lowest memory availability requirements. Indeed in these algorithms, at each iteration the current $2\,ms$ block is added to the previous one which can be deleted afterwards.

VI.5 Conclusion

In this chapter the performances of the advanced algorithms presented in chapter V were evaluated using three types of tests:

- the first test focuses on the algorithms complexity in terms of number of additions, multiplications and processor cycles to perform acquisition,
- the second test focuses on the sensitivity issues, by comparing the loss in the estimated C/N_0 induced by each algorithm,
- the third test compares the minimum time, evaluated in terms of number of arithmetic operations and number of processor cycles needed by the algorithms to acquire a signal at a given C/N_0 .

In the first two tests, the assumed T_p, M and C/N_0 values were the same for each algorithm; it was not the case for the third test where only the C/N_0 value was assumed to be the same. For all of the tests, signals generated by a Spirent STR4500 were used. Three characteristic C/N_0 ratios where chosen for these signals: 42 *dBHz* typical of rural environments, 27 *dBHz* typical of urban environments, and 17 *dBHz* typical of indoor environments.

The results show that the algorithms performance classification mainly depends on the number of coherent integrations, ie. T_p. This means that the algorithms performance classification does not depend on *M* (non-coherent accumulation). Indeed, the algorithms complexity is generally linear with *M* but non linear with T_p. An increased T_p induces a

larger number of data blocks to be processed for coherent integration, and in parallel more frequency bins to be explored thus implying a further increased complexity. But, an increased *M* only induces more data blocks to be processed.

For $T_p \geq 7\ ms$ - needed in constrained environments, the results highlighted a clear advantage of the Transverse FFT algorithm over the others, since it has the lowest complexity, and in the same time do not induce any sensitivity loss. It is followed by the Sum before. For $T_p \leq 7\ ms$, the Sum before is the most efficient, followed by the Transverse FFT. And for $T_p = 1\ ms$ the FFT Shift is the most efficient. It is followed by the Sum before, and the Transverse FFT is only the 5^{th} in this case. The Sum after algorithm had performances comparable to the Classical algorithm and even slightly worse in some cases.

Concerning the SOR algorithm introduced in this work, it may be relatively more interesting when *M* and T_p are preselected independently of the expected C/N_0 value, that is they are not optimised for the considered environment.

Yet, in terms of memory requirements, the Sum after and the Sum before algorithms have the lowest memory needs, whereas the Transverse FFT is the most constraining. Note that the optimised SOR algorithm is based on the Transverse FFT for the acquisition of the first satellite, and the Sum after for the acquisition of the all next satellites. This makes this algorithm as constraining as the Transverse FFT.

Résumé du chapitre 7 (Conclusion)

Les solutions de navigation de GNSS font de plus en plus partie de notre vie quotidienne, comme c'était le cas pour les téléphones cellulaires. Mais ces solutions GNSS et plus spécialement les solutions GPS, sont soumises à beaucoup de problèmes, surtout dans les environnements indoors, comme la puissance du signal reçu qui est très faible, les multitrajets, les interférences, etc.

L'objectif principal de cette thèse était de caractériser le canal GPS d'abord et de trouver par la suite des solutions en soft qui permettent d'améliorer le processus d'acquisition dans les environnements fortement contraints.

Ainsi, dans la première partie, l'impact de multitrajets et de intercorrélations sur le processus d'acquisition de signaux GPS a été étudié pour les environnements indoors et urbains. Pour les environnements indoors, un modèle du canal variant avec le temps a été développé basé sur une analyse statistique effectuée par l'ESA ; alors que pour les environnements urbains, le canal a été caractérisé en utilisant le modèle LMMCM du DLR.

Dans la deuxième partie, les différentes des techniques avancées d'acquisition GPS qui ont été considérées, ont surtout visé la réduction du temps de calcul (donc indirectement le TTFF), sans affecter la sensibilité de récepteur. Les performances de ces algorithmes ont été comparées.

Conclusions

Pour les cas indoors, les résultats sur la caractérisation du canal montrent que les répliques de multitrajets ne perturbent pas les performances de l'acquisition, que ce soit en présence ou en absence du LOS, car leurs Dopplers et leurs délais sont dans les limites d'erreurs tolérées en acquisition pour ces deux paramètres. Par conséquent, ils ne sont pas ou très difficilement détectés pendant l'acquisition. Cependant, il faut toujours garder en tête que poursuivre un mulitrajet n'est pas désiré dans un récepteur GPS. Par ailleurs, les simulations mettent en évidence des atténuations relatives de multitrajets comparés au LOS compris entre 14 et 17 *dB*. Finalement, nous avons remarqué que dans certains cas les multitrajets impliquent une petite augmentation du niveau du bruit : 1 *dB* au maximum. D'autre part, il a été souligné que les intercorrélations sont particulièrement inquiétantes car elles induisent des erreurs de l'ordre du *Km*.

Dans les milieux urbains et les environnements du type canyon, les multitrajets ne perturbent pas non plus l'acquisition, puisque les délais maximaux trouvés étaient dans ce cas-là généralement inférieur à la durée d'1/2 chip du code C/A. Les résultats ont en outre mis en évidence une corrélation assez claire entre les délais maximaux et l'angle d'élévation des satellites : Ceux-ci diminuent avec l'augmentation des angles d'élévation satellites (des délais de l'ordre de $50\,\eta s$ ont été trouvés à un angle d'élévation de 90 °). Dans ces environnements, nous avons relevé une atténuation relative des multitrajets par rapport au LOS qui varie entre –5 *dB* et –18 *dB*. Comparé aux atténuations des multitrajets en indoors (14 à 17 *dB*), ils sont

généralement moins atténués. Les pics d'intercorrélation se sont ont générés de très grandes erreurs dans ce cas-là aussi. En effet, les pics correspondants peuvent se produire à des délais aléatoires, à l'intérieur d'une période donnée du code, alors que ceux relatifs aux multitrajets dépendent du retard du LOS (ils ont des retards généralement proches) et ils sont progressivement atténués quand les délais augmentent. Dans tous les cas, le LOS a pu atteindre le récepteur la plupart du temps. Mais, dans les cas où il n'était pas disponible, un écho a plutôt été acquis et des problèmes d'intercorrélation sont apparus. Il est à noter cependant que selon l'application visée, il serait préférable de fournir aux boucles de poursuite des valeurs d'initialisation, qui peuvent être une bonne première approximation, voire de fournir une position avec un signal reflété plutôt que de ne pas être capable de déterminer une position du tout.

Toutes ces observations ont ouvert la voie à étudier l'HSGPS et l'AGPS d'une part, et à considérer des algorithmes de traitement de signaux GPS plus performants dans une deuxième partie de cette thèse.

Ainsi, dans cette deuxième partie, plusieurs tests ont été d'abord réalisés pour illustrer les performances de l'HSGPS et de l'AGPS. Le BT338 a été utilisé comme récepteur HSGPS, alors qu'une solution de Thalès Alenia Space a été utilisée pour tester le mode AGPS. Comparé à un récepteur classique, les récepteurs HSGPS bénéficient d'une plus grande disponibilité dans les environnements contraints : la position a pu être obtenue avec le récepteur HS dans les canyons urbains, pendant qu'un récepteur conventionnel ne pouvait pas produire une position dans de tels environnements. Les résultats obtenus dans les environnements urbains ont été répercutés par ceux des environnements indoors. En effet, dans des environnements indoors semblables, les récepteurs conventionnels ne pouvaient pas opérer, pendant que l'unité HS pouvait toujours fournir des positions. Ce résultat est confirmé par Karunanayake, parmi d'autres, qui a constaté que le seuil de poursuite des récepteurs Haute Sensibilité est environ à 18 *dBHz*, c'est à dire environ 14 *dB* en dessous de la limite de poursuite du récepteur GPS conventionnel évalué au cours de cette thèse et trouvée à 32 *dBHz*. Le BT338 utilisé dans les tests réalisés au cours de cette thèse a fourni un seuil de poursuite de 10 *dBHz*! Karunanayake a aussi constaté que le seuil d'acquisition est à 32 *dBHz* environ, montrant ainsi que le HSGPS n'est pas très robuste pour être utilisé tout seul dans les environnements dégradés. Mais, généralement, un niveau dégradé de performance de positionnement, notamment la précision, est observé quand la comparaison est possible entre le récepteur HS et les récepteurs conventionnels, comme montré dans plusieurs références. En bref, les applications qui utiliseront des récepteurs HSGPS doivent trouver un équilibre entre la disponibilité de solution et la précision de la position à moins que la détection et la réjection d'erreurs ne soient intégrés pour garantir une navigation fiable. L'AGPS améliore essentiellement la sensibilité du récepteur pendant l'acquisition, permettant ainsi de fournir une position GPS dans des conditions difficiles. Il bénéficie en outre d'une bonne précision comparé à la technique HSGPS. De plus, il diminue radicalement le TTFF qui est très important pour les applications commerciale temps réel. Pour l'AGPS le seuil de la poursuite a été trouvé à environ 19 *dBHz*. En raison du manque de temps, le TTFF obtenu avec l'AGPS n'a pas été étudié. Cependant Karunanayake a constaté que le TTFF est considérablement plus réduit en cas d'AGPS grâce aux données d'assistance. Il peut être conclu que l'assistance fournie une aide "grossière" qui n'est pas utile dans l'amélioration de la performance de la poursuite (le même seuil de poursuite que le récepteur HSGPS). En effet, quand le récepteur est dans le mode poursuite, il possède une information de temps et de position beaucoup plus précise. L'AGPS utilise le réseau sans fil pour fournir des données d'assistance au GPS mobile et est ainsi une solution inhérente pour les techniques hybrides. En plus, l'AGPS peut

facilement intégrer les techniques de Hautes Sensibilité. En effet, les développements récents de la technique d'AGPS ont permis de réaliser de longues intégrations cohérentes en fournissant le message de navigation, une information de temps, l'almanach et une position approchée via des canaux de communications différents. Cette assistance permet des intégrations plus longues que $20\,ms$ et peut améliorer le timing du récepteur pour diminuer les restrictions causées par une mauvaise compensation du Doppler. En résumé, l'AGPS fournit une meilleure sensibilité en acquisition et des performances de poursuite semblables aux récepteurs HSGPS. Comme cette thèse se focalise surtout sur les méthodes d'amélioration de l'acquisition, c'est l'AGPS qui a été choisi dans ce contexte. Il est important de rappeler cependant que l'utilisation de l'AGPS n'interdit l'utilisation de l'HSGPS pour le compléter.

L'utilisation d'AGPS doit être en plus couplée avec les algorithmes avancés d'acquisition. L'amélioration vise essentiellement du TTFF, en essayant de ne pas affecter la sensibilité de récepteur de façon significative. Chaque algorithme a été théoriquement décrit et analysé en présentant ses avantages et inconvénients.

Ces algorithmes peuvent être divisés en deux catégories :

- Les algorithmes "mono-satellites" qui acquièrent les satellites un par un et améliorent l'acquisition de chaque satellite. Les algorithmes considérés sont dans ce cas-là: FFT classique, la corrélation moyennée, l'intégration cohérente en sommant après FFT-IFFT, l'intégration cohérente en sommant avant FFT-IFFT, la FFT transverse, et la FFT shift.
- L'algorithme "multi-satellite" qui acquière plus d'un satellite en parallèle, permettant ainsi de réduction la complexité, le SOR. Un algorithme combiné a été aussi considéré (SOR optimisé), où le SOR a été couplé avec la FFT transverse pour acquérir le premier satellite.

Une optimisation commune a été aussi considérée pour les algorithmes "mono-satellites", qui est un résultat de la propriété de la FT : la réplique de code est générée une fois pour toutes au début du processus d'acquisition, au lieu de la générer à chaque itération, pour chaque case fréquence et pour chaque accumulation non-cohérente.

Après avoir décrit ces algorithmes, un ensemble d'expériences a été réalisé pour les comparer l'un avec l'autre en mettant en relief leurs avantages et inconvénients respectifs. Dans tous les tests, des signaux générés par un Spirent STR4500 ont été utilisés. Trois rapports C/N_0 différents ont été considérés : 42 *dBHz* typique d'environnements ruraux, 27 *dBHz* typique d'environnements urbains et 17 *dBHz* typique d'environnements indoors. La performance des algorithmes du point de vue de la complexité et de la sensibilité a été évaluée en utilisant trois types de tests :

- Le premier s'est concentré sur la complexité des algorithmes (le nombre d'additions, multiplications et cycles de processeur pour exécuter l'acquisition) pour des paramètres semblables. Les résultats ont montré que la performance des algorithmes dépend surtout du nombre d'intégrations cohérentes ; en d'autres termes, la classification des algorithmes est la même quelle que soit la valeur de *M*, mais ce n'est pas le cas pour toutes les valeurs de T_p.

- Le deuxième test s'est plutôt focalisé sur la sensibilité, en comparant la perte dans l'estimation du rapport C/N_0 induite par chaque algorithme, encore une fois pour des paramètres égaux.
- Finalement, le troisième a comparé le temps minimal, évalué du point de vue du nombre d'opérations arithmétiques et du nombre de cycles processeur nécessaires pour chaque algorithme pour acquérir un signal à un C/N_0 donné.

Les résultats montrent que la classification de performance d'algorithmes dépend surtout du nombre d'intégrations cohérentes et ne dépend pas de *M*, car la complexité n'augmente pas linéairement avec la durée d'intégration cohérente.

Pour un $T_p \geq 7\ ms$ - nécessaire pour des environnements sévères, les résultats ont montré un avantage net de la FFT transverse sur les autres algorithmes, car elle présente une complexité minimale, et en même temps ne conduit pas à des pertes en sensibilité.
L'algorithme de la FFT transverse est suivi par l'algorithme de la sommation avant corrélation.
Pour un $T_p \leq 7\ ms$, l'algorithme de la sommation avant corrélation est le plus performant, suivi par la FFT transverse.
Pour un $T_p = 1\ ms$, l'algorithme de la FFT shift est le plus efficace. Il est suivi de l'algorithme de la sommation avant corrélation. La FFT transverse n'est plus que le 5^{eme} algorithme en termes de performances en acquisition. L'algorithme de la sommation après corrélation a des performances comparables à l'algorithme de la FFT classique, voire même pires dans certains cas.
En ce qui concerne l'algorithme SOR introduit dans ce manuscrit, il peut être relativement plus intéressant quand M et T_p sont présélectionnés indépendamment de la valeur du rapport C/N_0, donc en d'autres termes si ces deux paramètres sont légèrement surestimés.

Finalement, en termes d'occupation mémoire, les algorithmes de la sommation après et avant corrélation ont des besoins en mémoires assez faibles, alors que l'algorithme de la FFT transverse est plus contraignant en termes de mémoire. Il est à noter que l'algorithme SOR est basé sur la FFT transverse pour l'acquisition du premier satellite, et l'algorithme de la sommation après corrélation pour l'acquisition des autres satellites. Ceci rend cet algorithme aussi contraignant qu'en mémoire que la FFT transverse.

Recommandations pour des travaux futurs

Les résultats présentés dans cette thèse montrent que pour les applications urbaines et indoors un récepteur GPS classique n'est pas suffisant. Et même l'AGPS n'est pas très efficace dans de tels environnements. En effet, des problèmes de précision et de disponibilité étaient mis en évidence dans ce type d'environnements, surtout en étage d'acquisition du signal : la disponibilité était d'environ 85 % et l'erreur 3D a atteint 104 *m*! Dans des environnements indoors très sévères, le récepteur AGPS ne pouvait pas fournir une solution du tout.

Ce résultat suscite le besoin d'explorer principalement deux axes de recherches :
- L'hybridation avec d'autres systèmes dans des environnements très sévères
- Le traitement des futurs signaux GNSS

En ce qui concerne l'hybridation, une des augmentations les plus importantes actuellement considérées avec le GPS est l'hybridation GPS/INS (le Système de Navigation Inertielle). Les résultats de ce type de couplage montrent une meilleure performance en navigation [*Kubrak et al.*, 2005], [*Singh*, 2006] et [*Gao et al.*, 2006]. D'autres systèmes complémentaires peuvent aussi être utilisés surtout en indoors, comme les répéteurs GPS, les pseudolites, ou même le système WiFi pour combler l'absence du GPS.

En outre, de nouveaux signaux GNSS seront disponibles avec l'arrivée du GPS modernisé, de Galileo et du GPS III. On s'attend à ce que ces signaux offrent de meilleures performances de disponibilité et de précision : en effet, ils ont des niveaux de puissance plus élevés que les signaux GPS sur L_1 (environ 5 *dB*) et incorporent un canal dataless (sans bits de données) qui permet de plus longues intégrations cohérentes sans être limité par la durée d'un bit de données de 20 *ms*.
En outre, ils utilisent des codes PRN ayant des périodes beaucoup plus longues, résultant ainsi en une réduction des problèmes d'intercorrélation via un meilleur isolement entre les pics d'autocorrélation secondaires et les pics d'intercorrélation. Cela implique cependant un temps d'intégration plus long, et plus de cases Doppler à explorer, augmentant ainsi la complexité. Finalement, la disponibilité est évidemment améliorée avec la présence de satellites des deux systèmes Galileo et GPS. Dans ce cas-là, les satellites présentent des géométries bien meilleures ce qui a pour effet d'améliorer la précision de la solution de positionnement.
Un des inconvénients de tels signaux est que leur fonction de corrélation a un lobe principal plus étroit, avec deux lobes secondaires sur chaque côté, qui sont beaucoup plus importants que ceux de la fonction d'autocorrélation du GPS. Un lobe principal plus étroit exige une résolution temporelle plus petite. Ceci entraîne une augmentation du temps nécessaire pour acquérir et poursuivre le signal. Plusieurs solutions sont disponibles pour résoudre un tel problème. Classiquement on pourrait réaliser plus de tests pendant l'acquisition sur les lobes précédents et lobes suivants afin de détecter une éventuelle erreur de détection. Une autre solution serait de poursuivre l'acquisition et de vérifier la fiabilité de la solution pendant la phase de poursuite en utilisant la méthode du BUMP and JUMP par exemple [*Fine et al.*, 1999], ou aussi l'algorithme ASPeCT [*Julien, 2005*].
Une autre solution consisterait aussi d'utiliser un récepteur bi-fréquence. En effet, les récepteurs bi fréquence peuvent réaliser des mesures différentielles parce qu'ils peuvent traiter deux signaux en parallèle, comme les signaux GPS L_1 et L_{2C}, ou d'autres signaux ayant des fréquences porteuses différentes par exemple. Ils s'avèrent aussi très intéressants pour traiter les signaux BOC de Galileo : ils permettent de filtrer chacun des lobes du signal, puis de les translater en fréquence de sorte à n'en former qu'un seul lobe, ramener ainsi la modulation QPSK utilisée en une modulation BPSK, qui est plus facilement traitée par le récepteur [*Heiries et al.*, 2004].

Chapter 7

Conclusions and recommendations for future work

Contents

GNSS navigation solutions are slowly becoming part of our daily life, as was the case for cellular phones. But these GNSS solutions, and more specifically GPS L_1 solutions, are subject to many problems, especially in indoor environments, such as received signal weakness, multipaths, interferences, etc.

The main objective of this thesis was to characterize the GPS channel first, and then to find optimal software solutions to improve the acquisition process in constrained environments.

Thus, in the first part, the impact of multipaths and cross-correlations on the GPS signals acquisition scheme was derived for indoor and urban environments. For the indoor environments, a time varying model of the channel was developed based on a statistical analysis performed by the ESA [*Pérez-Fontán et al., 2004*], while for the urban environments the channel was characterized using the DLR LMMCM model developed by Steingass et al. [*2005*].

In the second part, the different optimised GPS acquisition techniques that were considered, mainly aimed at reducing the TTFF without affecting the receiver sensitivity, as it was shown that these two requirements have conflicting goals. These algorithms performances were compared with each other.

The conclusions derived from the results presented through out this thesis and recommendations for future work are respectively addressed in sections VII.1 and VII.2 below.

VII.1 Conclusions

For indoor cases, results on channel characterization show that multipaths replicas do not disturb the acquisition performance either in the presence or in the absence of LOS since their Doppler and code delay are within the acquisition error limits for these two parameters. Consequently, they are not or hardly evidenced during acquisition, however one must keep in mind that locking on a mulitpath replica is not desired in a GPS receiver. Besides, simulations show relative attenuations of multipath replicas compared to the LOS between 14 and 17 *dB*. Last, we have observed that in some cases multipaths induces a small increase in the noise floor: 1 *dB* as a maximum. On the other hand, it was highlighted that cross-correlation are particularly disturbing since they induce very high range errors (in the *Km* level).

For urban downtown and canyon environments, the multipaths replicas also do not disturb acquisition, since the maximum excess delays found in this case were generally lower than the C/A code half chip duration of $0.5\,\mu s$. Results also evidenced a clear correlation between the maximum excess delays and the satellite elevation angle: the delays decrease with increasing satellite elevation angles (delays of the order of $50\,\eta s$ were found at an elevation angle of 90°). In these environments, we observed that the multipaths relative attenuation with respect to the LOS vary between $-5\,dB$ and $-18\,dB$. Compared to indoor multipaths replicas attenuations (14 to 17 *dB*), they are generally less attenuated. Cross-correlation peaks resulted in very large error also in this case. Indeed, the corresponding peaks may occur at random code delays, whereas the multipaths delays depend on the LOS delay (they have generally close delays), and they are progressively attenuated with increasing delays. In all cases the LOS could reach the receiver most of the time. But could be non available in some cases inducing the acquisition of echo only signals and to cross-correlation problems as well. Yet when the conditions are bad, depending on the application, it may be better to provide the tracking loops with these initialisation values, which may be a good first approximation, and even to do the position determination with a reflected signal than not being able to determine a position at all.

All of these observations paved the way for studying the HSGPS and AGPS systems, and for considering more performant signal processing algorithms in a second part of this thesis.

In the second part of this thesis, many tests were first conducted in order to illustrate the HSGPS and AGPS performances. The BT338 was used as an HSGPS receiver, while a Thalès Alenia Space solution was used in AGPS mode. Compared to a classical receiver, the HSGPS receivers result in higher availability of observations in constrained environments: position fixes could be obtained with the HS receivers in urban canyons, while a conventional receiver could not yield a position in similar environments. The results in urban environments were echoed by those in indoor environments, where in similar indoor areas, the conventional receivers could not operate while the HS unit could still provide positions. This result is confirmed amongst others by Karunanayake who found that the tracking threshold of the High Sensitivity receivers is approximately at 18 *dBHz*, this is about 14 *dB* lower than the tracking limit of the standard mode GPS receiver tested in the course of this thesis, and found at about 32 *dBHz*. The BT338 used in the tests conducted in the course of this thesis yielded a tracking threshold of 10 *dBHz*! Karunanayake also found that the acquisition threshold is at 32 *dBHz* approximately, rendering that the HSGPS by itself is not robust enough to be used in degraded signal environments. But, generally, a degraded level of positioning accuracy

performance is observed when comparison is possible between the HS receiver and conventional receivers, as shown in many references. In short, applications that will use HSGPS must balance solution availability with positioning accuracy unless fault detection and exclusion is integrated to ensure reliable navigation. The AGPS essentially enhances the acquisition sensitivity of the receiver, thus enabling GPS positioning in difficult conditions. It also has good accuracy performance compared to the HSGPS technique. Moreover, it dramatically decreases the TTFF which is very important for beneficial real time commercial applications. The AGPS tracking threshold was found at approximately 19 *dBHz*. Due to lack of time, the AGPS TTFF was not studied. However this was done by Karunanayake et al. [*2004*] who found that the TTFF is considerably lower in the case of AGPS thanks to the AD. It can be concluded that aiding provides "coarse" assistance which is not useful in improving tracking performance (the same tracking threshold as the HSGPS receiver) because when the receiver is in tracking mode, it has a much more precise GPS time and location. The AGPS uses the wireless network to supply assistance data to handset GPS receivers, and thus is an inherent solution for hybrid techniques. For example, it is easy to augment the assistance data message with the handset to BTSs distances measured by the network equipment. In addition, AGPS can easily integrate High Sensitivity issues. Indeed, recent developments of AGPS have enabled the use of long coherent integrations by providing the navigation message, timing information, almanac, and approximate position through alternate communications channels. This assistance allows integrations longer than 20 *ms*, and may improve receiver timing to lessen the limitations caused by Doppler mismatch. In short, AGPS provides greater acquisition sensitivity and similar tracking performance as HSGPS receivers. Finally, since this thesis mainly focuses on methods to enhance the acquisition scheme, it is the AGPS that was chosen in this context. Recall however that using AGPS does not prevent the use of HSGPS to complement it.

The use of AGPS must be further coupled with improved acquisition algorithms for better performance. The improvement essentially deals with the TTFF, while trying not to dramatically affect the receiver sensitivity. Each enhancement was theoretically described, and analysed through the presentation of its advantages and drawbacks.

The considered algorithms may be divided into two categories:

- "mono-satellite" algorithms which acquire the satellites one by one and enhance the acquisition of each satellite. The algorithms considered in this case are: the classical FFT based algorithm, the average correlation, the coherent integration by summing after FFT-IFFT, the coherent integration by summing before FFT-IFFT, the transverse FFT, the FFT shift algorithm.

- "multi-satellite" algorithm which acquires more than one satellite at once thus allowing for reduction of complexity by eliminating redundancy between the iterations needed to acquire different satellites, the SOR. A combined algorithm was also considered (the optimised SOR), where the SOR was coupled with the transverse FFT to acquire the first satellite. It was referred to as optimised SOR.

A common optimisation was also considered for the "mono-satellite" algorithms, which is a result of the time shift property of the FT. It consists in generating the code replica once and for all at the beginning of the acquisition process, instead of generating it at each iteration, i.e. for each frequency bin and each non-coherent accumulation. Classically this is

done in order to compensate for the code Doppler. But this may rather be performed in the frequency domain in the advanced algorithm. Thus the code is generated and translated to the frequency domain at the beginning, and only a multiplication by a complex exponential is performed within the loops to compensate for the code Doppler.

After having described these algorithms, a specific set of experiments were conducted to compare them with each other while highlighting their respective advantages and drawbacks. For all of the experiments, signals generated by a Spirent STR4500 were used. Three C/N_0 ratios where chosen for these signals: 42 *dBHz* typical of rural environments, 27 *dBHz* typical of urban environments, and 17 *dBHz* typical of indoor environments. The algorithms performance in terms of complexity (which directly translates in TTFF) and sensitivity were evaluated using three types of tests:

- The first one focused on the algorithms complexity (number of additions, multiplications and processor cycles to perform acquisition) for similar parameters. The results showed that the algorithms performance mainly depends on the number of coherent integrations, meaning that the algorithms classification is the same whatever the value of *M*, but this is not the case for all values of T_p.

- The second test rather focused on sensitivity issues, by comparing the loss in the estimated C/N_0 induced by each algorithm, again for equal parameters.

- Finally, the third one compared the minimum time, evaluated in terms of number of arithmetic operations and number of processor cycles needed by the algorithms to acquire a signal at a given C/N_0.

The results show that the algorithms performance classification mainly depends on the number of coherent integrations, ie. T_p, and does not depend on *M*, since the complexity does not linearly increases with the number of coherent integration.

For $T_p \geq 7\ ms$, the results highlighted a clear advantage of the Transverse FFT algorithm over the others: it has the lowest complexity, and in the same time do not induce any sensitivity loss. It is followed by the Sum before. Such coherent durations are generally needed for indoor and urban canyons environments. For $T_p \leq 7\ ms$, the Sum before is the most efficient, followed by the Transverse FFT. And for $T_p = 1\ ms$ the FFT Shift is the most efficient. It is followed by the Sum before, and the Transverse FFT is only the 5^{th} in this case. The Sum after algorithm had performances comparable to the Classical algorithm

The optimised SOR algorithm is interesting when the algorithms are compared for similar parameters, rather than in the case of the sensitivity limit test, that is when *M* and T_p are preselected, based on assumptions on the C/N_0, with a margin leading to over estimation of these parameters.

In terms of memory requirements, the Sum after and the Sum before algorithms have the lowest memory needs, whereas the Transverse FFT is the most constraining. The optimised SOR algorithm being based on the Transverse FFT for the acquisition of the first

satellite, and the Sum after for the acquisition of the all next satellites is as constraining as the Transverse FFT.

VII.2 Recommendations for future work

The results presented in this thesis show that for urban and indoor applications the GPS alone is not sufficient at all. And even AGPS is not very efficient in such harsh environments. Indeed some availability and accuracy problems were evidenced in light indoors and urban environments, especially in the case of signal acquisition: the availability was about 85% and the 3D error standard deviation reached 104 *m*! In deep indoors the AGPS receiver could not deliver a solution at all.

This result raises the need for two major axes of research:
- Hybridisation with other systems in very harsh environments
- Future GNSS signal processing

In the case of hybridisation, one of the most important augmentations currently considered with the GPS is the GPS/INS (*Inertial Navigation System*) hybridisation. Results on this kind of system coupling exhibit better navigation performance [*Kubrak et al., 2005*], [*Singh, 2006*] and [*Gao et al., 2006*]. Other complementary systems may also be used especially indoors, like GPS repeaters, pseudolites, or even WiFi system to fill the lack of GPS for indoor or harsh positioning.

Besides, new GNSS (*Global Navigation Satellites Systems*) signals will be available with the arrival of modernized GPS, Galileo and GPS III (more particularly BOC(1,1) signals). These signals are expected to offer better accuracy and availability performance: indeed, they have power levels higher than the L_1 GPS signals (about 5 *dB*) and incorporate a dataless channel which allows for longer coherent integrations without being limited by the 20 *ms* duration of a data bit.
Furthermore, they use PRN codes with much longer periods, thus allowing for reducing the cross-correlation problems through an improved isolation of auto-correlation secondary peaks and cross-correlation peaks. This however induces longer integration time, thus implying more Doppler bins to be explored, hence increasing complexity.
On the other hand, the availability is obviously increased with the presence of satellites from both GPS and Galileo systems. In this case better satellites geometries are available for the receivers.
A disadvantage of such signals is that their correlation function has a narrower main lobe, with two secondary lobes on each side, that are much more important than the GPS L_1 signal secondary lobes. A narrower main lobe requires a lower time resolution. This results in a higher time consumption to acquire and track signal. Many solutions are available to resolve such problem. A basic one would be to carry out further tests during acquisition on the preceding and succeeding lobes. Another solution would be to proceed with the acquisition and to compensate for this problem during the tracking phase using the BUMP and JUMP method for example [*Fine et al., 1999*], or ASPeCT [*Julien, 2005*].
Yet another solution also is to use a dual band receiver. Indeed, dual band receivers allow for differential measures because they can process two signals at once, like the GPS L_1 and L_{2C} signals, or other signals with different carrier frequencies for example. They are also very interesting in the frame of the BOC Galileo signal: by allowing for filtering each of the signal

lobes the latters can be translated to the same central frequency, and the QPSK scheme used for this modulation is converted to BPSK scheme, which is more easily processed by the receiver [*Heiries et al., 2004*].

Bibliography

[*3GPP, 2006*] - http://www.3gpp.org/ftp/Specs/html-info/44031.htm

[*Akopian et al., 2005a*] - Akopian David, Sagiraju Phani K., Agaian Sos, Raju G. V. S, Sudharsanan Subramania, Bove V. Michael, Panchanathan Sethuraman, *"A reduced complexity frequency domain acquisition of DS-SS signals for embedded applications"*, in proceedings of IS&T/SPIE's Symposium on Electronic Imaging: Science & Technology, Jan. 2005, San Jose, California, USA.

[*Akopian et al., 2005b*] - Akopian D., Turunen S., *"System for method for fine acquisition of a spread spectrum signal"*, US patent, 6909736, 2005

[*Akopian, 2001*] - D. Akopian, *"A fast satellite acquisition method"*, in proceedings of ION GPS, September 2001, Salt Lake City, Utah, USA

[*Akos, 1997*] - Akos, D., *"A Software Approach to Global Navigation Satellite System Receiver Design"*, Ph. D. Dissertation, August 1997, available at:

[*Akos et al., 2000*] - Denis M. Akos, Per-Ludvig Normark, Jeong-Taek Lee, Konstantin G. Gromov, James B. Y. Tsui, John Schamus, "*Low Power Global Navigation Satellite System (GNSS) Signal Detection and Processing*", in proceedings of ION GPS, September 2000, Salt Lake City, Utah, USA

[*Agarwal et al., 2002*] - N. Agarwal , J. Basch, P. Beckmann, P. Bharti S. Bloebaum, S. Casadei, A. Chou, P. Enge, W. Fong N. Hathi, W. Mann, J. Stone, J. Tsitsiklis, B. Van Roy, P. Enge, B. Van Roy, A. Sahai, J. Tsitsiklis, "*Algorithms for GPS operation indoors and downtown*", GPS Solutions (2002) 6:149–160, 13 November 2002, Springer-Verlag

[*Assistant Secretary of Defense, 2001*] - Assistant Secretary of Defense, Defense Pentagon, "*Global Positioning System Standard Positioning Service Performance Standard*", October 4, 2001, Washington DC

[*Bastide et al., 2002*] - Frédéric Bastide, Olivier Julien, Christophe Macabiau, Benoît Roturier, "*Analysis of L5/E5 Acquisition, Tracking and Data Demodulation*", in proceedings of ION GPS, September 2002, Portland, OR

[*Biacs et al., 2002*] - Z. Biacs, G. Marshall, M. Moeglein, W. Riley, "*The Qualcomm/SnapTrack Wireless-Assisted GPS Hybrid Positioning System and Results from Initial Commercial Deployments*", in proceedings of ION GPS, September 2002, Portland, Oregon

[*Camp et al., 1998*] - Camp Jr, Thomas O., Makovicka Thomas J., *"Stand alone positioning system (GPS) and method with high sensitivity"*, US Patent, 6075987, 1998

[*Chandra, 2002*] - Ashok Chandra, *"Indoor Radio Mobile Communication"*, in proceedings of the ION GPS, September 2002, Oregon, Portland

[*Changlin, 2003*] - Changlin Ma, *"Techniques to Improve Ground-Based Wireless Location, Performance Using a Cellular Telephone Network"*, PhD thesis, June 2003

[*Clinton, 2000*] - W. Clinton, *"Improving the Civilian Global Positioning System (GPS)"*, White House Fact Sheet, May 1, 2000

[*Coenen et al., 1992*] – A.J.R.M. Coenen, D.j.R. van Nee, *"Novel fast GPS/Glonass code acquisition technique using low update rate FFT"*, in proceedings of IEEE Electronic Letters, vol. 28, no. 9, 1992

[*Collin et al., 2003*] - J. Collins, H. Kuusniemi, O. Mezentsev, G. MacGougan, G. Lachapelle, "*HSGPS under heavy Signal Masking – Accuracy and Availability Analysis"*, in proceedings of the 6th Nordic Radio Navigation Conference and Exhibition, NORNA 2003, Stockholm-Helsinki

[*Correia, 2000*] - Paul Correia, *"Guide pratique du GPS"*, Eyrolles, 2000

[*Deshpande, 2004a*] - S. Deshpande, M.E. Cannon, *"Analysis of the Effect of GPS Receiver Acquisition Parameters"*, in proceedings of ION GNSS 2004, September 2004, Long Beach, California

[*Deshpande, 2004b*] - S. Deshpande, M.E. Cannon, *"Interference Effects on the GPS Signal Acquisition"*, in proceedings of ION NTM 2004, January 2004, San Diego, California

[*Djebbouri et al., 2003*] - Mohamed Djebbouri, Djamel Djebouri, *"Fast GPS Satellite Signal Acquisition"*, in proceedings of ElectronicsLetters.com, First of October 2003

[*Djuknic, 2001*] - Goran M. Djuknic, Robert E. Richton, *"Geolocation and Assisted GPS"*, February 2001

[*DoD, 1995*] - Department of Defense/Department of transportation, "*1994 Federal Radionavigation Plan"*, National Technical Information Service, May 1995, Spring-field, VA

[*El Natour et al., 2005*] - Hanaa El Natour, Anne-Christine Escher, Christophe Macabiau, Marie-Laure Boucheret, *"Impact of multipath and cross-correlation on GPS acquisition in indoor environment"*, in proceedings of the ION NTM 2005, San Diego, California

[*El Natour et al., 2006a*] - Hanaa El Natour, Anne-Christine Escher, Christophe Macabiau, Michel Monnerat, Marie-Laure Boucheret, *"A new algorithm to reduce AGPS acquisition TTFF"*, in proceedings of the ION NTM 2006, Monterey, California

[*El Natour et al., 2006b*] - Hanaa El Natour, Anne-Christine Escher, Christophe Macabiau, "Analysis of the GPS acquisition environment: Indoors and outdoors", in proceedings of the ICTTA 2006 conference, Damascus, Syria

[*El Natour et al., 2006c*] - Hanaa El Natour, Anne-Christine Escher, Christophe Macabiau, Olivier Julien, "*Enhanced Global Solution for GPS Acquisition in all Types of Environments*", in proceedings of the ION GNSS September 2006, Fort Worth, Texas

[*Escher, 2003*] – Anne-Christine Escher, *""*, PHD thesis, available at

[*FCC, 2000*] - Federal Communications Commision, USA, OET BULLETIN No. 71, Guidelines for Testing and Verifying the Accuracy of Wireless E911 Location systems, www.fcc.gov/Bureaus/Engineering Technology/Documents/bulletins/oet71/oet71.pdf. http://www.fcc.gov/oet/info/documents/bulletins/

[*Fine et al., 1999*] - Fine, P., Wilson, W., *"Tracking Algorithm for GPS Offset Carrier Signals"*, in proceedings of the ION National Technical Meeting, 1999, January 25-27, San Diego, California, USA

[*Gao et al., 2006*] - Guojiang Gao, Gérard Lachapelle, *"INS-Assisted High Sensitivity GPS Receivers for Degraded Signal Navigation"*, in proceedings of the ION GNSS, September 2006, Fort Worth TX

[*Garin et al., 1999*] - Garin, L. J., M. Chansarkar, S. Miocinovic, C. Norman and Hilgenberg, *"Wireless Assisted GPS-SiRF Architecture and Field Test Results"*, in proceedings of ION GPS 1999, September 14-17, Nashville

[*Germroth et al., 2005*] - Matthew Germroth, Laurence Carstensen, *"GIS and Satellite Visibility: Viewsheds from Space"*, in proceedings of ESRI International Conference, 2005, Virginia Tech, Blacksburg

[*Gligorevic, 2002*] - Snjezana Gligorevic, *"Joint Channel Estimation And Equalization For Fast Time-Variant Multipath Channels"*, in proceedings of the IEEE PIMRC 2002

[*Goran et al., 2001*] - Goran M. Djuknic, Robert E. Richton, *"Geolocation and Assisted GPS"*, February 2001, Bell Laboratories, Lucent Technologies

[*Hashemi, 1993*] - Homayoun Hashemi, *"The Indoor Radio Propagation Channel"*, in proceedings of the IEEE, vol. 81, July 1993

[*Heiries et al., 2004*] – Vincent Heiries, Daniel Roviras, Lionel Ries, Vincent Calmettes, *"Analysis of Non Ambiguous BOC Signal Acquisition Performance"*, in proceedings of International Technical Meeting of the Satellite division, 2004, September 21-24, Long Beach, California, USA

[*Holmes, 1990*] - Jack J. Holmes, *"Coherent Spread Spectrum Systems"*, Robert E. Krieger Publishing Company, 1990

[*Holmes, 2000*] - Jack J. Holmes, *"Code Tracking Loop Performance Including the Effect of Channel Filtering and Gaussian Interference"*, in proceedings of the ION Annual Meeting, 2000, June 26-28, San Diego, California, USA

[*ICD200C, 2000*] – GPS Interface Control Document, NAVSTAR GPS Space Segment / Navigation User Interfaces, IRN-200C-004

[*J. Miller, 1995*] - Michael J. Miller, Branka Vucetic, Les Berry, *"Satellite communications: Mobile and Fixed Services"*, Kluwer Academic Publishers, Norwell, 1995, Massachusettes, USA

[*Julien, 2005*] – Olivier Julien, *"Design of Galileo LF1 Receiver Tracking Loops"*, PhD Thesis, available at: http://www.geomatics.ucalfauy.ca/links/GradThesis.html

[*Kaplan, 1996*] - Eliott. D Kaplan, *"Understanding GPS: Principles and Applications"*, March 1996, Artech House, Norwood, MA, 1996

[*Karunanayake et al., 2004*] - Karunanayake, M. D., M. E. Cannon, G. Lachapelle, & G. Cox, *"Evaluation of Assisted GPS (AGPS) in Weak Signal Environments Using a Hardware Simulator"*, in proceedings of ION GNSS, September 2004, Long Beach, California

[*Kavak et al., 1999*] – Adnan Kavak, Weidong Yang, Sang-Youb Kim, Kapil R. Dandekar, Guanghan Xu, *"Experimental Studies of Indoor Propagation Characteristics of a Smart Antenna System at 1.8 GHz"*, in proceedings of SPIE Vol. 3708, p. 98-107, Digital Wireless Communication, 1999

[*Kennedy, 2002*] - Michael Kennedy, *"The Global Positioning System and GIS : An Introduction"*, Second Edition, London and New York, Taylor & Francis, 2002

[*Klukas, 1997*] – R. W. Klukas, *"A Superresolution Based Cellular Positioning System Using GPS Time Synchronisation"*, Ph.D. thesis, available at: http://plan.geomatics.ucalgary.ca/publications.php

[*Klukas et al, 1998*] – R. W. Klukas, G. Lachapelle, M. Fattouche, *"Cellular telephone positioning using GPS time synchronisation"*, GPS World, Vol. 9, No. 4, April 1998, pp. 49-54

[*Kowoma, 2005*] - www.kowoma.de/en/gps/history.htm

[*Krasner, 1998*] - Norman F. Krasner, *"GPS receiver and method for processing GPS signals"*, US Patent, 5781156, 1998

[*Krasner, 2001*] - Norman F. Krasner, *"Reducing satellite signal interference in a global positioning system"*, US Patent, 6236354, 2001

[*Kubrak et al., 2005*] – Damien Kubrak, Christophe Macabiau, Michel Monnerat, *"Performance Analysis of MEMS based Pedestrian Navigation Systems*", in proceedings of ION GPS/GNSS, September 2005, Long Beach, California

[*Lachapelle et al., 2004*]- Gérard Lachapelle, H. Kuusniemi, Diep T.H. Dao, G. MacGougan, M.E. Cannon, *"HSGPS Signal Analysis and Performance under various Indoor Conditions"*, in proceedings of the journal of the Institute Of Navigation, Vol. 51, No 1, spring 2004, USA

[*Lachapelle et al., 2003*]- Gérard Lachapelle, H. Kuusniemi, Diep T.H. Dao, G. MacGougan, M.E. Cannon, *"HSGPS Signal Analysis and Performance under various Indoor Conditions"*, in proceedings of the ION GPS/GNSS conference, September 2003, Portland, Oregon

[*LaMance et al., 2002*] - John J. LaMance, J. DeSalas, J. Jarvinen, *"Assisted GPS : A Low-Infrastructure Approach "*, GPS World, Vol. 13, No. 3, March 2002, pp. 46-51

[*Lin et al., 2002*] – Lin D. M., J. B.Y. Tsui, L. Lee, Y. T. Liou, J. Morton, *"Sensitivity Limit of A Stand-Alone GPS Receiver and An Acquisition Method*", in proceedings of ION GPS, September 2002, Portland, Oregon

[*Macabiau, 2001*] – Christophe Macabiau, *"Communications par Spectre Etalé"*, Lecture Notes.

[*MacGougan, 2003*] – Glenn D. MacGougan, *"High Sensitivity GPS performance Analysis in Degraded Signal Environments"*, PhD thesis, available at www.geomatics.ucalgary.ca/links/GradTheses.html

[*Mangold et al., 1998a*] – Stefan Mangold, Matthias Lott, Communication Networks, Aachen Dave Evans, Rob Fifield, *"Indoor Radio Channel Modelling – Bridging form Propagation Details to Simulation"*, in proceedings of IEEE international conference on Personal, Indoor and Mobile Communications, Vol. 2, pp. 625-629, 1998

[*Mangold et al., 1998b*] – Stefan Mangold, Matthias Lott., *"Indoor Radio Channel Models based on Measurements and Ray-Tracing at 5.2 GHz"*, in proceedings of ITG-Workshop Wellenausbreitung bei Funksystemen und Mikrowellensystemen, pp. 29-52, May 1998, Oberpfaffenhofen, Germany

[*Mathieu, 2006*] - Bernard Mathieu, CNES, "*Point de situation des programmes EGNOS et Galileo*", Power Point Presentation, Localisation – Navigation Journey, December 7, 2006, Cité de l'Espace, Toulouse, France

[*Mattos, 2003*] – Philip G. Mattos, "*Solution of the Cross-Correlation and the Oscillator Stability Problems for Indoor C/A Code*", in proceedings of the ION GPS/GNSS 2003, September 2003, Portland, Oregon

[*Mitra et al., 1993*] – Sajit K. Mitra, James F. Kaiser, *"Handbook of Digital Signal Processing "*, John-Wiley & sons, 1993

[*Mudhafar, 2002*] - Hassan-Ali Mudhafar, Kaveh Pahlavan, *"A New Statistical Model for Site-Specific Indoor Radio Propagation Prediction Based on Geometric Optics and Geometric Probability"*, in proceedings of IEEE Transactions On Wireless Communications, Vol. 1, No. 1, January 2002

[*Norman, 2001*] - Charles R. Cahn, Charles P. Norman, *"Strong signal cancellation to enhance processing of weak spread spectrum signal"*, US patent, 6282231, 2001

[*O'Driscoll, 2006*] – Cillian O'Driscoll, *"Performance Analysis of the Parallel Acquisition of Weak GPS Signals"*, PhD thesis, 2006, University College Cork, Cork, Ireland

[*Parkinson, B.W. 1996*] – B.W. Parkinson, *"Introduction and Heritage of NAVSTAR, the Global Positioning System"*, in "Global Positioning System: Theory and Applications, Vol. I", Progress in Astronautics and Aeronautics Volume 164, AIAA, pp. 3-28.

[*Parsons, 1992*] – David Parsons, *"The Mobile Radio Propagation Channel"*, BPCC Wheatons Ltd, GB

[*Pérez-Fontán et al., 2004*] – F. Pérez-Fontán, B. Sanmartín, A. Steingass, A. Lehner, J. Selva, E. Kubista, Joanneum Research. Graz. Austria, B. Arbesser-Rastburg, *"Measurements and Modeling of the Satellite-to-Indoor Channel for Galileo"*, in proceedings of ENC-GNSS, 8th European Navigation Conference GNSS, May 2004, Rotterdam, The Netherlands

[*Peterson et al., 1995*] – R.L. Peterson, R.E. Ziemer, D. E. Borth, *"Introduction to Spread Spectrum Communications"*, Prentice Hall.

[*PriceWaterHouseCoopers, 2001*] – PriceWaterHouseCoopers, *"Inception Study to Support the Development of a Business Plan for the GALILEO Program"*, Report TREN/B5/23-2001, Prepared for the European Community under contract ETU-B6613-E4-PWC-2001-S12.321824.

[*Proakis, 1995*] - J. G. Proakis, "Digital Communications", Third Edition, McGraw-Hill, 1995

[*Psiaki et al., 2001*] - Mark L. Psiaki, Cornell University, *"Block Acquisition of Weak GPS Signals in a Software Receiver"*, ION GPS 2001, September 2001, Salt Lake City, Utah

[*Ray, 2002*] - Ray, J., *"Mitigation of GPS Code and Carrier Phase Multipath Effects Using a Multi-antenna System"*, PhD thesis, available at: www.geomatics.ucalgary.ca/links/GradTheses.html.

[*Rossatti, 2001*] - Claudio Rossatti, *"Evaluation de la gestion de la position pour les systèmes mobiles"*, final report, December 2001

[*Saleh et al., 1987*] – Adel A.M. Saleh, Reinaldo A. Valenzuela, *"A statistical model for indoor multipath propagation"*, in proceedings of the IEEE journal on selected areas in communications, Vol. SAC-5, No. 2, February 1987

[*Shewfelt et al., 2001*] - John L. Shewfelt, Robert Nishikawa, Chusk Norman, Geoffrey F. Cox, *"Enhanced Sensitivity For Acquisition in Weak Signal Environments Through the Use of Extended Dwell Times"*, in proceedings of ION GPS, September 2001, Salt Lake City, Utah

[*Singh, 2006*] – Sanjeet Singh, *"Comparison of Assisted GPS and High Sensitivity GPS in Weak Signal Conditions"*, Master Of Science thesis, available at www.geomatics.ucalgary.ca/research/publications/GradTheses.html

[*Spilker, 1997*] - J.J. Spilker, *"Fundamentals of Signal Tracking Theory"*, in "Global Positioning System: Theory and Applications", Vol. I, Progress in Astronautics and Aeronautics Volume 164, 1997, pp. 245-328

[*Spilker, 1996*] - J. J. Spilker, *"Signal Structure and Theoretical Performance"*, in "Global Positioning System: Theory and Applications", Vol. I, Progress in American Institute of Aeronautics and Astronautics, 1996, pp. 89–21

[*Sorrells et al., 2000*] – Sorrells David F., Bultman Michael J., Cook Robert W., Looke Richard C., Moses Jr., Charley D., Rawlins Gregory S., Rawlins Michael W., Smith Francis J., *"Frequency synthesizer using universal frequency translation technology"*, US Patent, 6694128, 2000

[*Sorrells et al., 2002*] – Sorrells David F., Bultman Michael J., Cook Robert W., Looke Richard C., Moses Jr., Charley D., *"Applications of universal frequency translation"*, US Patent, 7016663, 2002

[*S. Rappaport, 1996*] - Rappaport, Theodore S., *"Wireless Communications – Principles & Practice"*, IEEE Press, 1996, pp 130.

[*Starzyk et al., 2001*] - J. A. Starzyk, Z. Zhu, *"Averaging Correlation for C/A Code Acquisition and Tracking in Frequency Domain"*, in Circuits and Systems, MWSCAS 2001, proceedings of the 44th IEEE 2001 Midwest Symposium, Dayton, Ohio

[*Steingass et al., 2005*] - Alexander Steingass, Andreas Lehner, *"A Channel Model for Land Mobile Satellite Naviagtion"*, GNSS 2005 Conference, July 19-22, 2005, Munich, Germany

[*Steingass et al., 2004*] - Alexander Steingass, Andreas Lehner, "*Measuring the Navigation Multipath Channel – A Statistical Analysis"*, in proceedings of the ION GNSS 17th International Technical Meeting of the Satellite Division, 21-24 September 2004, Long Beach, California

[*Titus Lo et al., 1994*] - Titus Lo, John Litva, Henry Leung, *"A New Approach for Estimating Indoor Radio Propagation Characteristics"*, IEEE Transactions on Antennas and Propagation, Vol. 42, No 10, October 1994

[*Tsui et al., 2000*] - Y. Tsui, J. Bao, *"Fundamentals of Global Positioning System Receivers: A Software Approach"*, John Wiley & Sons Inc., New York, NY, 2000.

[*Turetzky et al., 2004a*] – Gregory Bret Turetzky, Charles P. Norman, Henry D. Falk, *"Location services system that reduces auto-correlation or cross-correlation in weak signals"*, U.S. patent, 6707423, 2004.

[*Turetzky et al., 2004b*] – Gregory Bret Turetzky, Charles P. Norman, Henry D. Falk, *"Communications system that reduces auto-correlation or cross-correlation in weak signals"*, U.S. patent, 6680695, 2004.

[*Van Dierendonck, 1996*] - A. J. Van Dierendonck , *"GPS Receivers"*, *in "Overview of GPS Operation and Design, Global Positioning System: Theory and Applications"*, Vol. I, American Institute of Aeronautics and Astronautics Inc., Washington, DC

[*Van Diggelen, 2001a*] - F. van Diggelen, C. Abraham, *"Indoor GPS Technology"*, in proceedings of CTIA Wireless-Agenda, May 2001, Dallas

[*Van Diggelen, 2001b*] - F. Van Diggelen, C. Abraham, *"Indoor GPS, The No-Chip Challenge"*, GPS World, 12(9), pages 50–58

[*Van Nee et al., 1991*] - D.J.R. Van Nee, A.J.R.M. Conen, "*New Fast GPS code acquisition technique using FFT"*, in proceedings of IEEE Electronic letters, Vol. 27, No, 2, pp. 158-160**.**

[*Ward, 1996*] - P. Ward, *"GPS Satellite Signal Characteristics, Understanding GPS Signal Characteristics"*, chapter 4, pages 83–116, Artech House, Inc., 685 Canton Street, Norwood, MA 02062.

[*Watson, 2005*] – John Robert A. Watson, *"High-Sensitivity GPS L1 Signal Analysis for Indoor Channel Modelling"*, PhD thesis, available at:
http://www.geomatics.ucalgary.ca/links/GradTheses.html

[*Wells, 1987*] - David Wells & al., *"Guide To GPS Positioning"*, Canadian GPS Associates, May 1987

Appendix A

GPS Navigation Message structure

This appendix briefly details the structure of the GPS navigation message.

The navigation message broadcasted by the GPS satellite contains information about the message transmission time, the position and the operating conditions of the satellites, the signal propagation delay, the correction to be made in order to correct the UTC (*Universal Time Clock*) clock, and the constellation conditions. This message is composed of the binary data, which is transmitted over the L_1 and L_2 carriers at 50 bits/*s*. It is divided into frames of 1500 bits. Each of these frames is comprised of 5 sub-frames of 300 bits each, and having a duration of 6 *s*. Each subframe is composed of 10 words of 30 bits each. This data signal has a period of 25 frames, in other words it repeats every 37500 bits, or 12.5 min.

Figure A-1 below illustrates the structure of these frames:

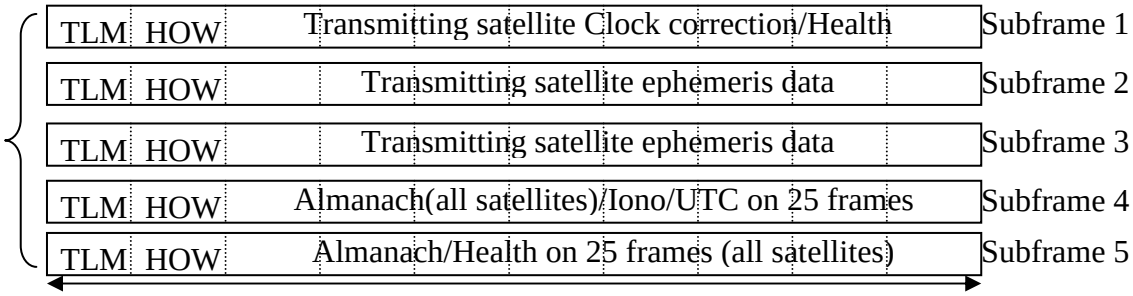

Total duration of one sub-frame: 300/50=6 seconds

Fig. A-1 : GPS Navigation Message structure (one frame)

where **TLM** stands for TeLeMetry. All the sub-frames begin with a telemetry word destined to measure the satellite distance precisely. It has a preamble of 8 bits which is always the same (10001011) and known by all the receivers so that they can identify the beginning of a frame. This allows the receiver to measure the moment when the message arrived more precisely. Moreover, it has 16 data bits, and six parity bits.

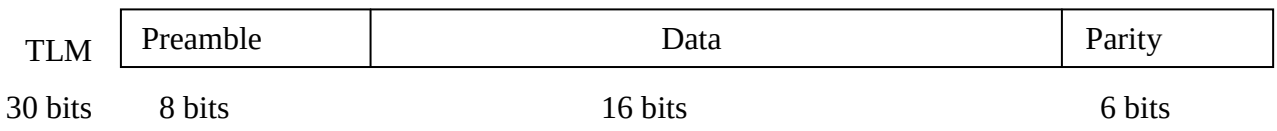

HOW stands for Hand Over Word, it allows to identify the time at which the last bit of the subframe was emitted.

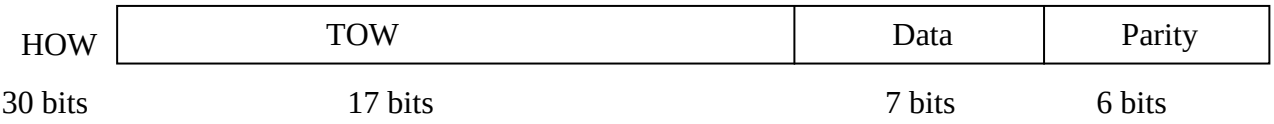

The first 17 bits are called Time Of Week; they provide the number of transmitted subframes since the beginning of the week (Sunday midnight). And knowing that each subframe has a duration of six seconds, the receiver can calculate the exact time. This is a mean of updating the GPS receiver clock every 6 seconds. The 7 data bits enable the receiver to identify the number of the emitted subframe and also informs about the validity of the received message.

The satellite conditions and clock corrections part of the first subframe is composed of the remaining 240 bits. The first ten bits of word three define the number of weeks passed since the 6th of January 1980, such that this number is reinitialized every 1024 weeks that is a little less than 20 years. The GPS receiver must keep the date when this happens so that it remains updated. The four bits that follow define the URA (*User Range Accuracy*). The URA gives the worst predicted precision for the 30 seconds to come, and is rated from 0 for the best precision and 15 for the worst. But this value for the accuracy does not take into account the delays introduced by the ionosphere layers. Six other bits give information about the satellite operation, and indicate if the satellite can be used or not. When the satellite operation mode is normal, this field is set to zero. A field called the IODC (*Issue Of Data Clock*), composed of ten bits, allows the receiver to know if one or more correction parameters were modified. The receiver can then be updated. Another field called t_{GD} is composed of 8 bits, and gives an estimate of the corrections to be made to the satellite differential group delay. This sub-frame contains in summary all the corrections concerning the calculation of the clock and the position of the satellite.

The second and the third subframes give the satellite ephemeris. They define the actual orbital of the satellite with respect to the GPS clock. This information remains valid and can be used by the receiver for two to four hours without a significant error. An 8 bits field, the IODE (*Issue Of Data Ephemeris*), has the same functionality as the IODC, but it concerns the satellite ephemeris parameters. It must also be equal to the first 8 bits of the IODC field.

The fourth subframe contains general information concerning the clock drift between the GPS and the UTC clock. It gives the configuration of the 32 satellites, and the signals propagation delay model through the ionosphere layers. It also gives with the fifth sub-frame the satellites almanac[1] and their operation conditions. A 22 characters message can also be sent in the fifth subframe.

[1] Subframe 4 gives almanac data for satellites 25-32, and subframe 5 gives almanac data for satellites 1-24.

Appendix B

GPS link budget

This appendix provides the material to derive the GPS signal transmission link budget.

The satellite downlink losses may be modelled as in figure B-1:

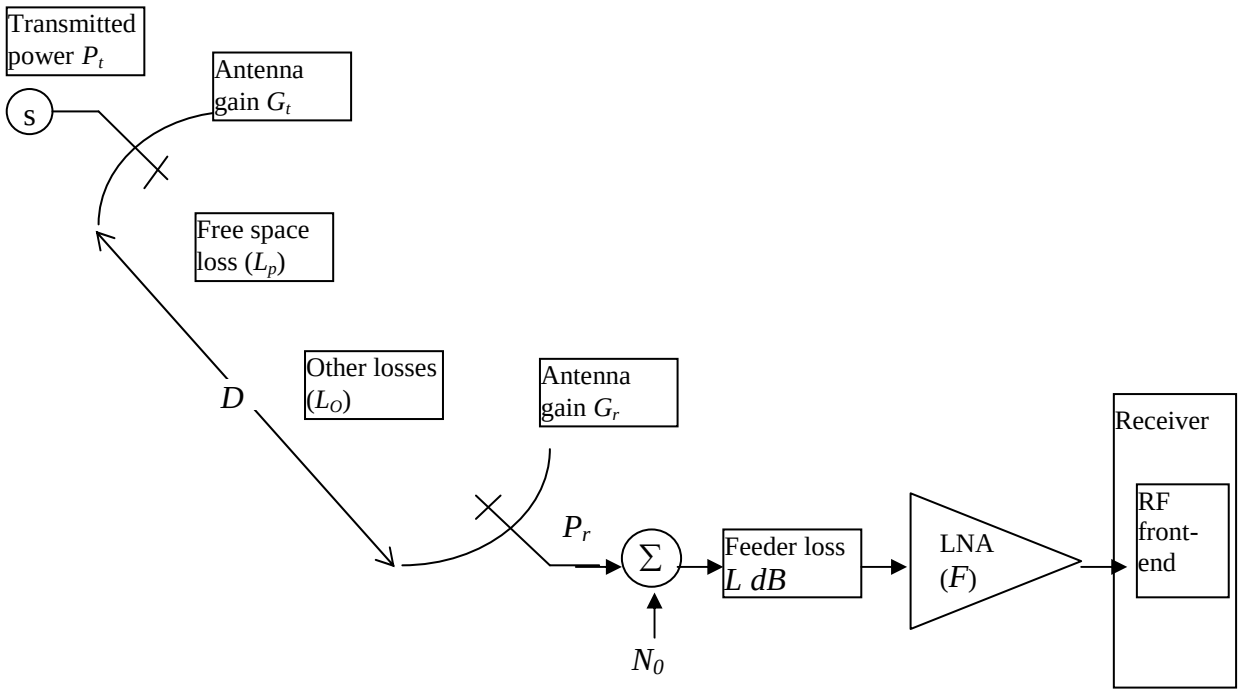

Fig. B-1 Different GPS signal loss sources

Where F is the noise factor.

G_t is the maximal transmitting antenna gain (assumed to be a directional antenna).

G_r is the maximal receiving antenna gain (assumed to be a directional antenna).

N_0 is the equivalent noise generated by all noise sources, placed at the input of the receiver

B.1 The power of the Radio Frequency signal

First, the L_1 carrier power $P_{c/A}$ is calculated at the output of the receiving antenna, as a function of the received power P_r [*Akos, 1997*], [*Spilker, 1996*].

The received flux density at any distance R on the bore sight of the transmit antenna is given by: $W_d = \frac{P_t G_t}{4\pi R^2}$ (W/m^2), where the numerator represents the EIRP (*Effective Isotropic Radiated Power*), $EIRP = P_t G_t$ (W).

If the receiving antenna was ideal, then the received power would be expressed as: $P_r = W_d A_r$, where A_r is the aperture area. But in practice, the effective aperture area is given by: $A_e = \eta_e A_r$, where η_e is the aperture efficiency of antenna. In this case, the power received by the antenna becomes:

$$P_r = \frac{P_t G_t A_e}{4\pi R^2} \qquad \textbf{(B-1)}$$

The maximum gain of the receiving antenna is related to its effective area by a fundamental relationship in antenna theory: $G_r = \frac{4\pi A_e}{\lambda^2}$

where λ is the signal carrier wavelength ($\cong 19\,cm$ for the L_1 carrier).
Hence, by substituting A_e by its value in the expression of the received power equation B-1, P_r becomes:

$$P_r = P_t G_t G_r \left[\frac{\lambda}{4\pi R}\right]^2 \qquad \textbf{(B-2)}$$

This is called the Friis transmission equation. This equation can be otherwise written as: $P_r = EIRP + 10\log G_r - L_p$. According to the definitions given previously, P_r corresponds to the received carrier power C.

The total transmitted power P_t is calculated by recalling that an L_1 carrier transmitted signal in a GPS system has an initial power of 50 W for both the C/A and P codes, and that the power consumed by the C/A code is half that consumed by the P code. In this case, we have: $P_{L_1} = 50W = P_{c/A} + P_P$ with $P_P = \frac{1}{2} P_{c/A}$. This gives: $P_{c/A} = P_t = \frac{2}{3} 50\ W = 33\ W$ or $P_t = 10\log 33 = 15.2\ \ dBW$.

Furthermore, we set $G_t = G_{t\max} = 13.2\,dB$, which is the maximum GPS transmitting antenna gain at its edges; we assume the antenna loss pointing is compensated by the pattern. This gives $EIRP = 15.2 + 13.2 = 28.4\ \ dBW$.

The last term of equation B-2 is the inverse of the free space loss expressed as: $L_p = \left[\frac{4\pi R}{\lambda}\right]^2$

with $\lambda = \frac{c}{f} = \frac{3 \cdot 10^8}{1575.42 \cdot 10^6} m$, where c is the velocity of light, and f is the carrier frequency.

$R \cong 20200000\ m$ at the zenith point, and $\cong 26000000\ m$ in the azimuth direction.

The inverse of the free space loss is then calculated as follows

- for $R \cong 20200000\ m$:

$$20\log\lambda - 20\log 4 - 20\log\pi - 20\log R$$

$$= 20\log\frac{3 \cdot 10^8}{1575.42 \cdot 10^6} - 12 - 20\log\pi - 20\log 20200000 = -182.5\ dB$$

- For $R \cong 26000000\ m$:

$$20\log\lambda - 20\log 4 - 20\log\pi - 20\log R$$

$$= 20\log\frac{3 \cdot 10^8}{1575.42 \cdot 10^6} - 12 - 20\log\pi - 20\log 26000000 = -184.7\ dB$$

In what follows, the calculations will only be performed assuming that $R \cong 26000000\ m$, that is considering the worst case.

Last, it is assumed that $G_r = 0\ dB$, hence we get $C = P_r = 28.4 - 184.70 = -156.3\ dB$

In practice, other losses must be considered such as rain or dust attenuation, losses due to ionospheric and tropospheric attenuation (which are very negligible for the *L* band), losses associated with the transmitting antenna like the feeder losses and loss of gain due to pointing error, and losses associated with the receiving antenna. But for the sake of simplicity, these losses will not be considered here. Note that the tropospheric delay can be modelled and the ionospheric errors can be corrected in a two-frequency receiver [*Wells, 1987*].

B.2 The noise power spectral density N_0

It is defined as:

$N_0 = k \cdot T$,

where *k* is the Boltzmann constant, $k = 1.3806503 \times 10^{-23}\ \mathrm{m^2 kg\, s^{-2}\, K^{-1}}$, and *T* is the system typical temperature, $T = \underbrace{T_A}_{antenna} + (L-1) \cdot \underbrace{T_c}_{feeder} + L \cdot \underbrace{T_R}_{LNA+receiver}$.

The expression of *T* assumes that the result takes into account all of the noise sources in the receiver:

- L is the feeder loss, it is equal to $0.4\ dB$
- $T_c = T_0 = 290°K$, this is the ambient temperature
- $T_R = (F-1) \cdot T_0$ (where F is the receiver noise factor, it ranges from 1 *dB* to 4 *dB*)
- $T_A = 130°K$

This yields: $T = T_A + (LF - 1) \cdot T_0$. Thus the system temperature is given as

$$\begin{cases} T = 130 + \left(10^{0.04} \cdot 10^{0.1} - 1\right) \times 290 \cong 240°K = 23.8\ dBK \\ T = 130 + \left(10^{0.04} \cdot 10^{0.4} - 1\right) \times 290 \cong 639°K = 28.0\ dBK \end{cases}$$

And the noise power spectral density is,

$$\begin{cases} N_0 = \overbrace{-228.6}^{10\log k} + 23.8 = -204.8\ dBW/Hz \\ N_0 = -228.6 + 28.0 = -200.6\ dBW/Hz \end{cases}$$

Finally, the carrier to noise density ratio at the output of the receiving antenna is:

$$\begin{cases} \frac{C}{N_0} = -156.3 + 204.8 = 48.5\ dBHz \\ \frac{C}{N_0} = -156.3 + 200.6 = 44.3\ dBHz \end{cases}$$

The carrier to noise ratio *C*/*N* at the output of the selective filter is given by: $\frac{C}{N_0 B}$

where the carrier power *C* is –156.3 *dBW*,
and the noise power is $\sigma_b^2 \approx N_0 B$, where *B* is the front end filter double sided bandwidth.

The bulk of the GPS signal power, about 90%, is contained within the null-to-null bandwidth of the broadcast signal. The carrier to noise ratio is thus equal to:

$$\begin{cases} for\ B_{RF} = 2\,MHz, \frac{C}{N_0 B} = 48.5 - 63 = -14.5\ dB \\ for\ B_{RF} = 20\,MHz, \frac{C}{N_0 B} = 44.3 - 73 = -28.7\ dB \end{cases}$$

, with $F = 1\,dB$, that is the best case.

Hence, the GPS signal is well below the noise floor and is not visible with a spectrum analyzer even at its spectral peak.

The signal to noise ratio being negative, the signal fed to the ADC at the RF front-end is totally buried in the noise. It can be seen from the last equation that the low signal to noise ratio value is essentially due to the large signal bandwidth. Thus, extracting the useful information from such a received signal is very difficult: one cannot even know whether there is a signal or not.

Appendix C

Doppler shift due to satellite or user motion, time and position uncertainty

In this appendix, the Doppler shift is computed depending on different parameters, namely, the relative satellite-user motion, the time uncertainty and the position uncertainty.

C.1 Uncertainty on the Doppler shift due to a user's position uncertainty

T

he angular velocity of the satellite in its orbit is given as [*Kaplan, 1996*]:

$$\frac{d\theta}{dt} = \frac{2\pi}{11\times 3600 + 58\times 60 + 2.05} = 1.458\times 10^{-4}\, rad/s,$$

where *dt* corresponds to half a sidereal[2] day (11 hrs, 58 min, 2.05 *s*) in seconds. This is the time taken by the GPS satellites to rotate once around the earth.

The speed of the satellite is:

$v_s = \frac{r_s d\theta}{dt} \cong 26560\times 1.458\times 10^{-4} \cong 3874\ m/s$, r_s is the average radius of the satellite orbit.

The Doppler shift is caused by the v_d component of the satellite velocity, represented in figure C-1 below.

[2] The sidereal day is slightly different from an apparent solar day. The apparent solar day is the time between two successive transits of the sun across the local meridian and has 24 hours. It is the time used daily. The sidereal day is the time for the earth to turn one revolution. The mean sidereal day is 23h 56min 4.09s. Half a sidereal day is 11h 58min 2.05s. This is the time for the satellite to rotate once around the earth.

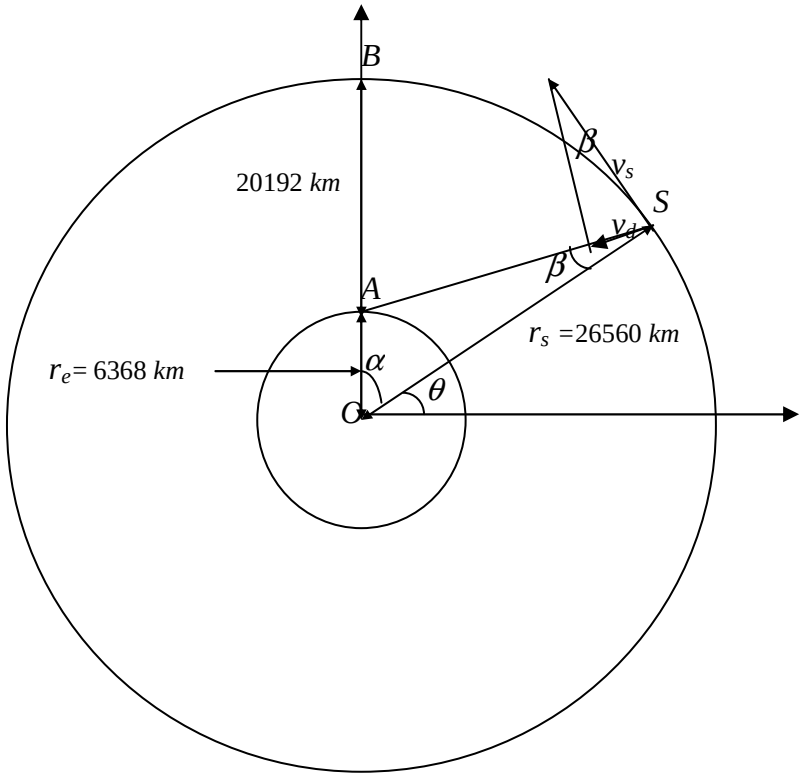

Fig. C-1: Doppler Shift due to satellite motion

The Doppler frequency caused by v_d toward the user is:

$v_d = v_s \cdot \sin\beta$.

Applying the cosine law in the OAS triangle gives:

$AS^2 = r_e^2 + r_s^2 - 2r_e r_s \cos\alpha = r_e^2 + r_s^2 - 2r_e r_s \sin\theta$.

And the sine law leads to:

$$\frac{\sin\beta}{\sin\alpha} = \frac{\sin\beta}{\cos\theta} = \frac{r_e}{AS}.$$

Hence v_d can be computed as:

$$v_d = \frac{v_s r_e \cos\theta}{AS} = \frac{v_s r_e \cos\theta}{\sqrt{r_e^2 + r_s^2 - 2r_e r_s \sin\theta}}.$$

As it can be expected, for $\theta = \pi/2$, $v_d = 0$ and it is intuitively maximal when the satellite is at a horizontal position with respect to the user. This may be easily verified by the calculation of the maximum value of v_d which is the one that cancels its time derivative with respect to θ given as:

$$\frac{dv_d}{d\theta} = \frac{v_s r_e \left[r_e r_s \sin^2\theta - (r_e^2 + r_s^2)\sin\theta + r_e r_s \right]}{\left(r_e^2 + r_s^2 - 2r_e r_s \sin\theta \right)^{3/2}}.$$

Setting $\frac{dv_d}{d\theta} = 0$ gives $\sin\theta = \frac{r_e}{r_s} \Rightarrow \theta \cong 0.242\ rad$. At this angle the satellite is at the horizontal position referenced to the user as expected; and the maximum value of v_d is then:

$$v_{d\max} = \frac{v_s r_e \sqrt{1 - r_e^2 / r_s^2}}{\sqrt{r_e^2 + r_s^2 - 2 r_e r_s \, r_e / r_s}} = \frac{v_s r_e}{r_s} = \frac{3874 \times 6368}{26560} \cong 929 \; m/s \, .$$

For the L_1 frequency, the maximum Doppler frequency shift is:

$$f_d = \frac{L_1 v_{d\max}}{c} = \frac{1575.42 \times 929}{3 \times 10^8} \cong 4.9 \; kHz \, .$$

This is the Doppler shift caused by the satellite motion. The user motion also affects the Doppler shift. If the user is moving towards the satellite, the overall Doppler shift is increased. Otherwise, it is reduced. However, a walking user does not usually move at a high speed, thus the resulting Doppler shift is very small:

$f_d \cong 3 \; Hz$ for a user walking at 2 *m*/*s*.

However, the Doppler shift resulting from a land vehicle must be considered if the Doppler bins used for acquisition are small. For a car moving at 50 *km*/*h* for example, the resulting Doppler frequency is of:

$$f_d = \frac{L_1 v_d}{c} = \frac{1575.42 \times 13.9}{3 \times 10^8} \cong 73 \; Hz$$

Concerning the Doppler frequency shift on the C/A code, it is quite small because of the low frequency of the C/A code:

$$f_{dc} = \frac{f_c v_{d\max}}{c} = \frac{1.023 \times 10^6 \times 929}{3 \times 10^8} \cong 3.2 \; Hz \qquad \textbf{(C-1)}$$

C.2 Uncertainty on the Doppler shift due to a user's position uncertainty

In the previous section we proved that: $v_d = v_s \cdot \sin\beta$. In the case of an uncertainty on the user position, figure C-2 becomes:

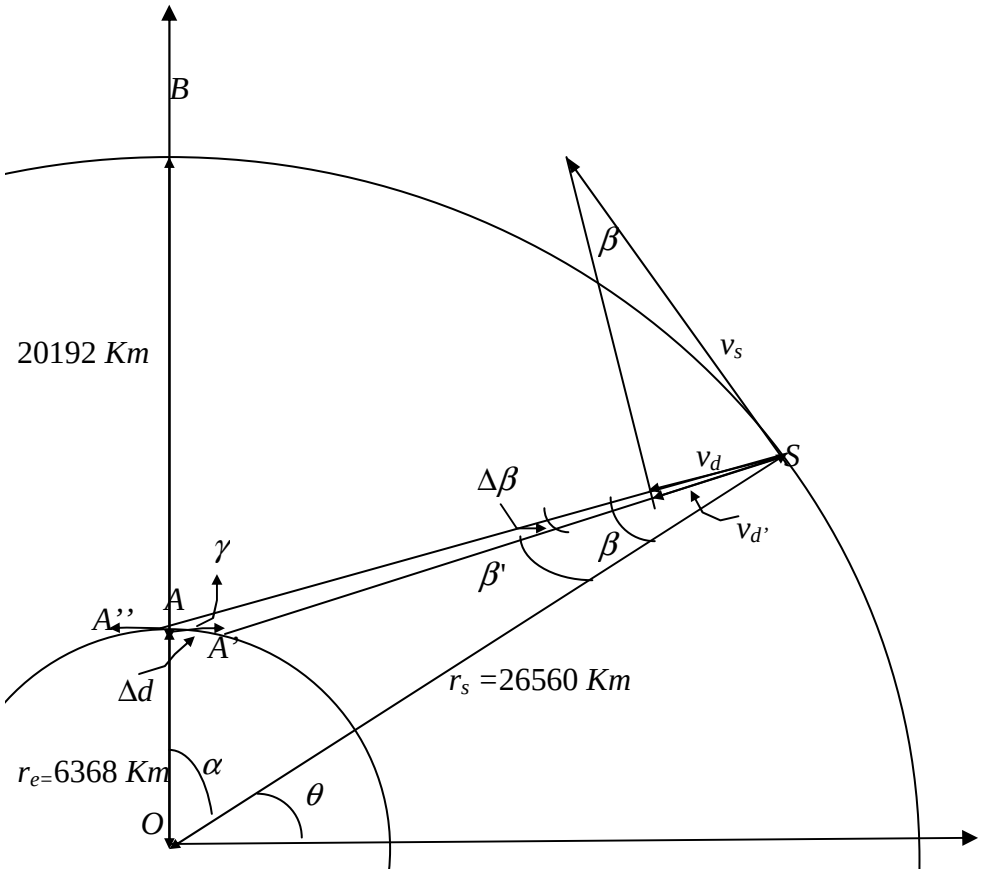

Fig. C-2: Doppler Shift due to user position uncertainty

In the case of AGPS, the ephemeris data is transported over the GSM radio interface and the user's position is known to be in the serving cell. Thus the maximum uncertainty on the user's position is $\Delta d_{\max} = 15\,km$, which corresponds to the maximum cell radius in a GSM network. This distance has a circular shape, but compared to the perimeter of the earth it is reasonable to consider it as a segment[3].

Figure C-2 shows that $v_d' = v_s \cdot \sin\beta'$, with $\beta = \beta' + \Delta\beta$. Thus by replacing β in the expression of v_d' we have:

$$v_d' = v_s \sin(\beta - \Delta\beta) = v_s \sin\beta\cos\Delta\beta - v_s \cos\beta\sin\Delta\beta \qquad \textbf{(C-2)}$$

The sine rule applied to the triangle AA'S gives:

$\sin\Delta\beta \cdot A'S = \sin\gamma \cdot \Delta d$ that is $\sin\Delta\beta = \dfrac{\sin\gamma \cdot \Delta d}{A'S}$,

with $A'S = \sqrt{AS^2 + AA'^2 - 2AS \cdot AA' \cdot \cos\gamma}$, and $AS = \sqrt{r_e^2 + r_s^2 - 2r_e \cdot r_s \cdot \sin\theta}$.

The maximum value of $\sin\Delta\beta$ is obtained by a Matlab algorithm which plots $\sin\Delta\beta$ as a function of γ and θ, and gives the maximum result and the corresponding teta and gamma. Figure C-3 shows the obtained graph.

[3] The earth's perimeter is $P_E = 2\pi r_e = 40011.324\,km$, and $\Delta d / P_E \cong 0.000375 <<< 1$

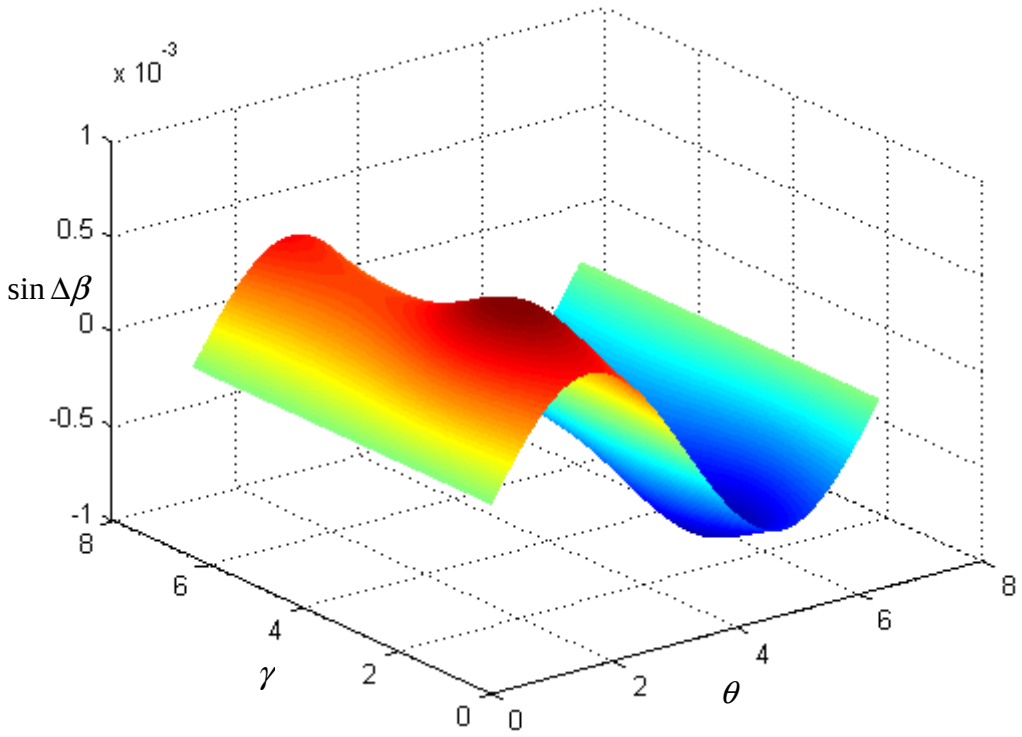

Fig. C-3: $\sin\Delta\beta$ **as a function of** γ **and** θ

The maximum value of $\sin\Delta\beta$ over the range $[0;2\pi]$ for both γ and θ is 7.4287e-004. It is reached for $\gamma=\theta=1.57\,rad$. This maximum value of $\sin\Delta\beta$ allows us to consider it as small and to make the following approximations:
$\cos\Delta\beta\cong 1$ and $\sin\Delta\beta=\Delta\beta$.
Reporting these approximations in equation C-1 yields:
$v_d'=v_s\cdot\sin\beta-v_s\cdot\Delta\beta\cdot\cos\beta=v_d-\Delta v_d$, with $\Delta v_d=v_s\cdot\cos\beta\cdot\Delta\beta$.

The same can be applied for A'' (triangle AA''S), and we get as a result:
$\Delta v_d=-v_s\cdot\cos\beta\cdot\Delta\beta$.
Δv_d is maximum when $\cos\beta$ and $\Delta\beta$ are maximum. This is the case for $\beta=0°$, and for $\Delta\beta=7.4287\text{e-}004\,rad$, that is when the SV is just at the vertical of the user, which gives:
$\Delta v_{d\max}=2.8779\,m/s$

Therefore, $\Delta f_{d\max}=\dfrac{L_1\cdot\Delta v_{d\max}}{c}=15.2\ Hz$, and the Doppler shift uncertainty resulting from a user position uncertainty is reduced to the range $[-15.2\ Hz;+15.2\ Hz]$.

C.3 Impact of time uncertainty on the Doppler shift

A time uncertainty engenders a satellite position uncertainty. This implies an uncertainty on the angle θ. Figure C-4 below, illustrates the impact of time uncertainty on the satellite estimated position, and thus on the estimated Doppler shift.

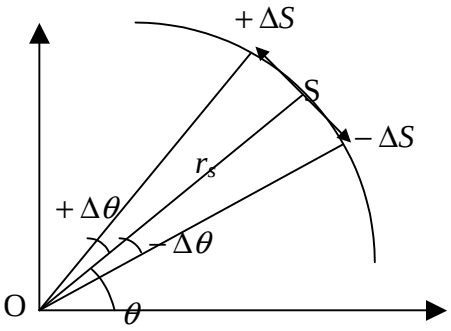

S is the actual satellite position

O is the center of the Earth

r_s is the satellite orbital radius of approximately 26560 *km*

Fig. C-4 : Impact of time uncertainty

As already mentioned, the time uncertainty in a GSM network is in general of 2 *sec*. If the satellite is supposed to have a linear velocity of $v_s = 3874\ m/s$, a 2 *sec* uncertainty yields a 7748 *m* error on the satellite position. For an approximately circular satellite orbital, this results in an error $\Delta\theta$ such that:

$$\Delta\theta = \frac{7748}{r_s} = 3\times10^{-4} = 0.0003\,rad$$

This result allows us to make the following approximations:

$$\cos\Delta\theta \cong 1,\ \sin\Delta\theta \cong \Delta\theta \qquad \textbf{(C-3)}$$

Now if we reconsider the expression of v_d obtained in the previous section: $v_d = \frac{v_s r_e \cos\theta}{\sqrt{r_e^2 + r_s^2 - 2r_e r_s \sin\theta}}$. With an uncertainty of $\Delta\theta$, the new expression of v_d becomes:

$$v_d' = \frac{v_s r_e \cos(\theta+\Delta\theta)}{\sqrt{r_e^2 + r_s^2 - 2r_e r_s \sin(\theta+\Delta\theta)}} = \frac{v_s r_e\left(\cos\theta\cos\Delta\theta - \sin\theta\sin\Delta\theta\right)}{\sqrt{r_e^2 + r_s^2 - 2r_e r_s(\sin\theta\cos\Delta\theta + \cos\theta\sin\Delta\theta)}}.$$

By taking into account the approximations considered above, the expression of v_d' becomes:

$$v_d' = \frac{v_s r_e\left(\cos\theta - \Delta\theta\cdot\sin\theta\right)}{\sqrt{r_e^2 + r_s^2 - 2r_e r_s(\sin\theta + \Delta\theta\cdot\cos\theta)}} = \frac{v_s r_e\cos\theta - v_s r_e\Delta\theta\cdot\sin\theta}{\sqrt{r_e^2 + r_s^2 - 2r_e r_s\sin\theta - 2r_e r_s\Delta\theta\cdot\cos\theta}}$$

$$v_d' = \frac{v_s r_e\cos\theta - v_s r_e\Delta\theta\cdot\sin\theta}{\sqrt{r_e^2 + r_s^2 - 2r_e r_s\sin\theta}\sqrt{1 - \frac{2r_e r_s\Delta\theta\cdot\cos\theta}{r_e^2 + r_s^2 - 2r_e r_s\sin\theta}}}$$

Let us set $Q = \frac{2r_e r_s\Delta\theta\cdot\cos\theta}{r_e^2 + r_s^2 - 2r_e r_s\sin\theta}$. A Matlab algorithm is used to find the maximum value of this ratio, as a function of θ. The resulting graph is shown in figure C-5, below.

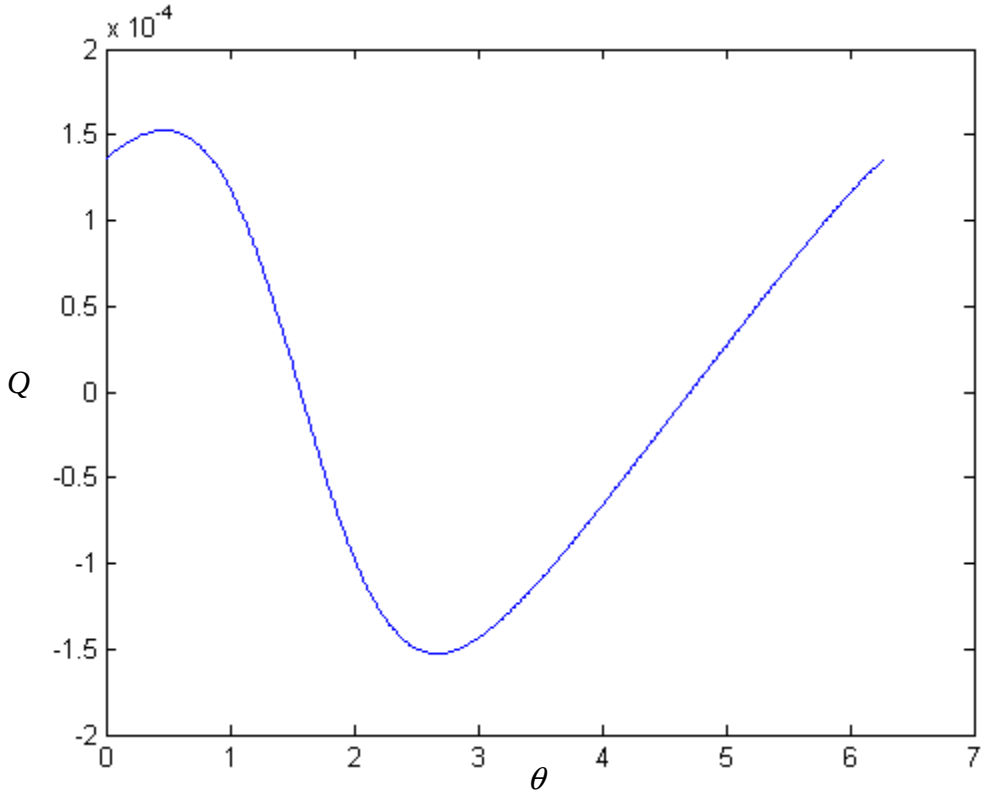

Fig. C-5 : Q as a function of θ

Figure C-5 shows that the maximum of *Q*, that is equal to 1.5263e-004, is reached for $\theta = 0.47\ rad$. Thus it is possible to make the approximation that $\sqrt{1-\frac{2r_e r_s \Delta\theta \cdot \cos\theta}{r_e^2 + r_s^2 - 2r_e r_s \sin\theta}} \cong 1 + \frac{r_e r_s \Delta\theta \cdot \cos\theta}{r_e^2 + r_s^2 - 2r_e r_s \sin\theta}$. In this case, the maximum value for the ratio $\frac{r_e r_s \Delta\theta \cdot \cos\theta}{r_e^2 + r_s^2 - 2r_e r_s \sin\theta}$ is 7.6315x10^{-5}, and it can be neglected with respect to 1.

The final expression of v_d' becomes:

$v_d' = \frac{v_s r_e \cos\theta - v_s r_e \Delta\theta \cdot \sin\theta}{\sqrt{r_e^2 + r_s^2 - 2r_e r_s \sin\theta}} = v_d - \Delta v_d$, with $\Delta v_d = \frac{v_s r_e \Delta\theta \cdot \sin\theta}{\sqrt{r_e^2 + r_s^2 - 2r_e r_s \sin\theta}}$.

In the case of a negative $\Delta\theta$, the same can be applied and we obtain a positive Δv_d. Now, the maximum value of Δv_d is obtained when $\sin\theta$ and $\Delta\theta$ are maximum, i.e., for $\sin\theta = 1$ and $\Delta\theta = 0.0003$. Thus, $\Delta v_{d\max} = 2.5129\ m/s$.

The corresponding Doppler uncertainty is: $\Delta f_{d\max} = \frac{L_1 \cdot \Delta v_{d\max}}{c} = 13.2\ Hz$. Thus the Doppler shift resulting from a propagation time uncertainty lies in the range $[-13.2\ Hz; +13.2\ Hz]$.

C.4 Impact of a user position uncertainty on the determination of the code delay

The pseudo range equation is as follows:

$$\hat{\rho} = \|r_s - r_u\| + c \cdot \left(d\hat{t} - d\hat{T}\right) + d\rho = \hat{\tau} \times c$$

where $\hat{\rho}$ is the predicted pseudo range,

r_s is the satellite position,

r_u is the receiver position,

$d\hat{t}$ is the estimated satellite clock drift with respect to GPS time,

$d\hat{T}$ is the estimated receiver clock drift with respect to GPS time,

$d\rho$ stands for different errors affecting the GPS signal (errors due to the troposphere, the ionosphere, ….),

$\hat{\tau}$ is the predicted propagation delay,

c is the light velocity

Figure C-6 below, shows the case where the uncertainty on the user position is maximal, 15 *km*, which corresponds to the maximal allowed radius for a GSM cell.

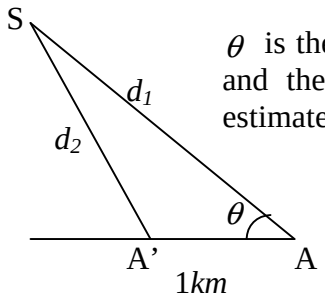

θ is the elevation angle, i.e., the angle between the user-to-satellite LOS and the horizontal plane, A is the real user position, and A' is the estimated user position

Fig. C-6 : Impact of a user position uncertainty

The cosine rule applied to the AA'S triangle gives:

$d_2 = \sqrt{AA'^2 + d_1^2 - 2AA' \cdot d_1 \cos\theta}$ and $d_2 - d_1 = \sqrt{AA'^2 + d_1^2 - 2AA' \cdot d_1 \cos\theta} - d_1 = \Delta d$,

where Δd is the error on the user to satellite predicted geometrical distance. This error is maximal for $\theta = 0°$, which corresponds to:

$$\Delta d_{\max} = \sqrt{(AA'^2 + d_1)^2} - d_1 = AA' = 15\ km$$

This yields an error of $\frac{15000}{3 \cdot 10^8} \cdot f_c = 51.15\ chips$ on the code delay.

On the other hand, the uncertainty on the user clock generates generally an error of $\pm 1kHz$ on the Doppler frequency, and 10 *cm* on the user position. But this error can be neglected with respect to the code delay.

Appendix D

GSM positioning techniques

Cellular network based localization techniques are either hold out by the network, "network centric" techniques, by the MS (*Mobile Station*), "handset centric" techniques, or by the two of them, "hybrid" techniques [*Rossatti, 2001*], [*Changlin, 2003*]. Most of this appendix relies on [*Rossatti, 2001*].

In network based techniques, the MS itself is totally passive. The network makes all the needed location measurements and calculates the MS position. These are done by means of the BSC (*Base Station Controller*), the MSC (*Mobile Switching Center*) or an equipment such as a LMU (*Location Measurement Unit*), a MLC (*Mobile Location Center*) or a SMLC (*Serving Mobile Location Center*)[4]. The last three equipments are to be added to the network for location purposes. Such a technique eventually requires costly modifications to be done by the operator to accommodate a wide range of hardware products. More specifically, these modifications involve changes or updates of the BTS (*Base Transceiver Station*), the Base Station Controllers and/or the MSC.

In the second technique, the localization procedure is implemented in the mobile phone: It makes location measurements and calculates its own position. The calculation of the user position in this case can be assisted by the network. Thus, it may assist the MS in location estimation. This method doesn't require changes to be made in the mobile network, but simply updating or eventually changing the MS.

The hybrid localization technique is in reality still mainly based on the network which makes most of the positioning functionalities. The MS can make some location measurements or other similar tasks to assist the network. This method still has a great disadvantage because it requires changes to be made to the network or to the MS.

[4] The LMU measures the physical signals, and can be integrated in the BTS, related to the Base Station Controller BSC or through a radio interface to the BTS.
The SMLC demands an MS localization, and in certain cases contains some network info (topology,.....)

There is another type of cellular network based techniques. It consists in a micro-localization by means of an IR (*Infra-Red*) or a Bluetooth interface for example. But obviously this solution is limited by the distance between the receiver and the transmitter. Moreover, it is not secure, because personal information will transit in a network other than the cellular network and the server permanently knows the user position.

In what follows, several cellular network wireless location techniques are overviewed.

D.1 Network centric techniques

D.1.1 The Cell-ID or COO (*Cell Of Origin*)

An inherent feature of all cellular systems is the ability to identify a cell by identifying the corresponding BTS. In fact, each BTS has a code that identifies it uniquely and internationally: the CGI (*Cell Global Identifier*). Thus, the extra work to be done in this method, is just to associate this Cell-ID with a location information of the BTS, such as its (X,Y) coordinates. No additional calculations are needed. The computation time is only that of the research in a pre-prepared data base. Thus, this method is fast and interesting for applications requiring high capacity but low precision. In fact, the accuracy of the Cell-ID technique is of the order of the cell size, which is about a few hundred meters in GSM networks, in urban areas, but reaches 35 *km* in rural areas. If in addition, the cells are sectorised, the precision is improved, and becomes of the order of a sector. But, in practice, the real covered zone may differ from the predicted one. This increases the lack of precision of this technique. This method can be enhanced by considering the signals received by the mobile from neighbouring cells. In this case, the position is determined as the intersection of different areas. But the precision is just a little bit enhanced; it still depends on the cell size, and requires a longer computation time. The figure below illustrates the principle of the Cell ID wireless location technique.

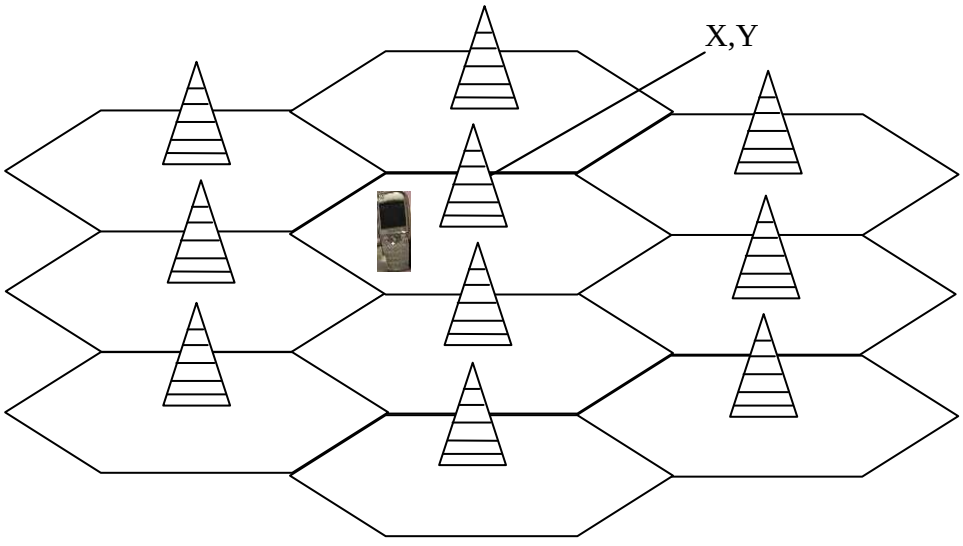

Fig. D-1 : Cell ID wireless location technique

D.1.2 The AOA (*Angle Of Arrival*) method

This method was first used during the development of radar, sonar and antenna array[5] techniques. It is based on array signal processing techniques. Each BTS is equipped with special antenna arrays and location receivers enabling it to determine the AOA of the MS signal. And the final location of the mobile is the intersection of different apparent arrival directions calculated by different BTSs. Thus at least two BTSs are needed, but three or more are often used to increase accuracy and reduce uncertainty due to multipath. No modifications are needed to be done to the MS.

The accuracy of this method depends on the distance between the MS to be located and the BTS. The further is the MS from the BTS, the larger is the localization uncertainty. Obviously, this type of measurement is greatly distorted when no LOS (*Line Of Sight*) exists between the MS and the antenna arrays, and the localization accuracy is thus degraded. Figure D-2 below illustrates the principle of the AOA location technique.

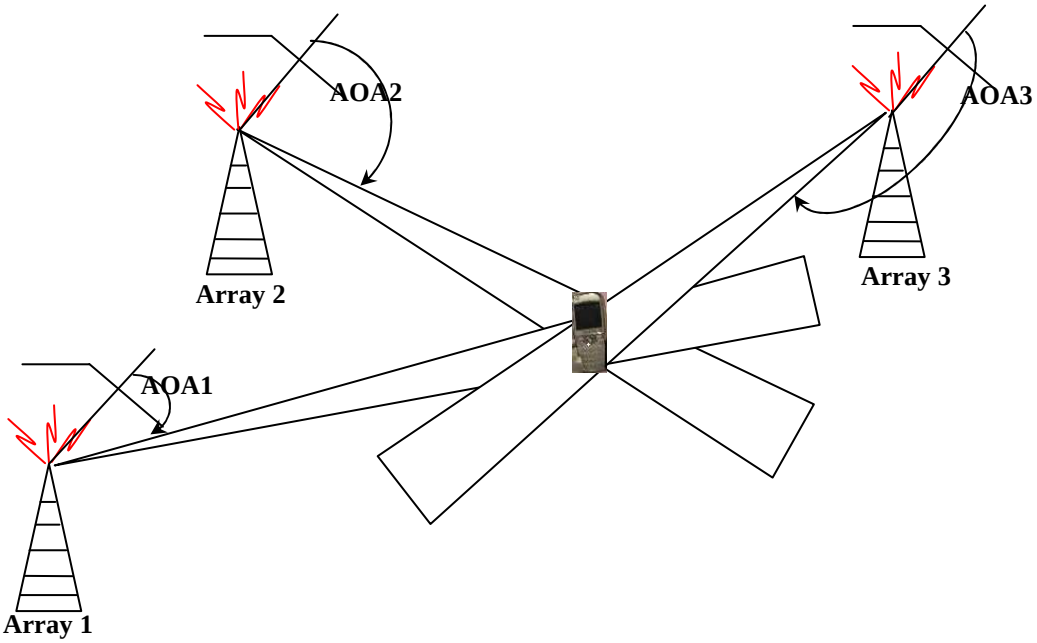

Fig. D-2: AOA wireless location technique

D.1.3 The TOA (*Time Of Arrival*) method

The principle here is to measure the absolute signal transmission time between the MS and the BTS. The MS signal must be received by at least three BTSs which measure the TOA independently. The data is sent to a PDE (*Position Determination Equipment*) that must be added to the network. The PDE multiplies the different received TOAs by the signal propagation velocity, which is equal to the velocity of light, and can compute the distance

[5] Antenna array: An assembly of antenna elements with dimensions, spacing and illumination sequence such that the fields for the individual elements combine to produce a maximal intensity in a particular direction, and minimum field intensities in other directions.

separating each BTS from the MS to be located. The MS is therefore located on a circle centred on the BTS, and having as radius the calculated MS-BS distance.

The intersection of three such circles determines the MS location. As a consequence of this dialogue between BTSs and the PDE, signalling is increased.

Furthermore, this method requires that all the BTSs be precisely synchronized to each other, and that the MS also be synchronized to the network. This makes it possible to be implemented only in fully synchronized networks, as for example in the IS-95 CDMA systems. Moreover it involves mathematic calculations. The principle of the TOA wireless location technique is illustrated in figure D-3 below.

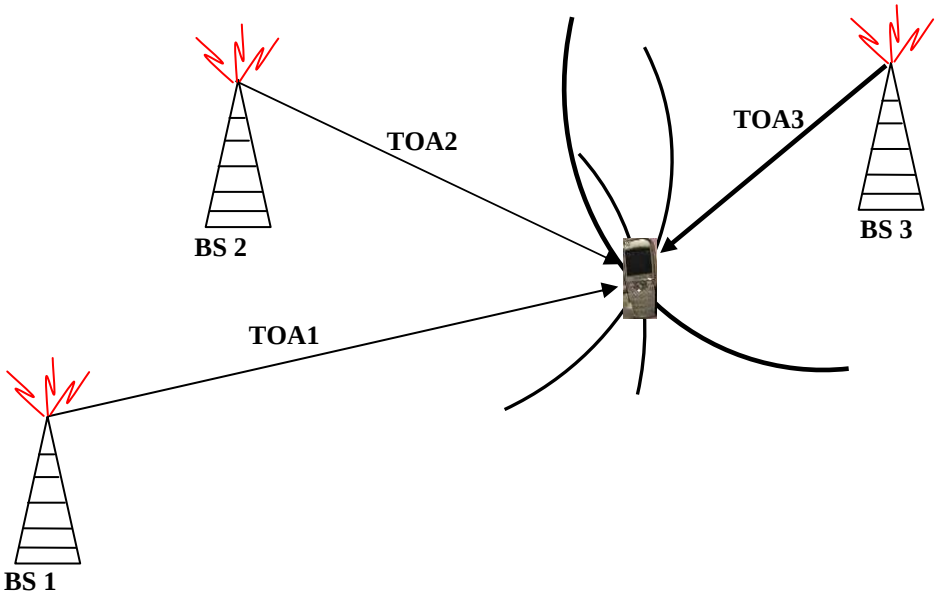

Fig. D-3: TOA wireless location technique

D.1.4 The TDOA (*Time Difference Of Arrival*)

The measurement made in this method is the relative signal transmission times which are equivalent to distance differences. The MS signal is monitored by at least three BTSs using dedicated location receivers. Each TDOA measurement defines a hyperbola. The location is determined as the intersection of three hyperbolic surfaces corresponding to three different BTSs. In fact, each two of these BTSs allow determining a hyperbola with the two BTSs as the foci. The TDOA method is illustrated in figure D-4 below.

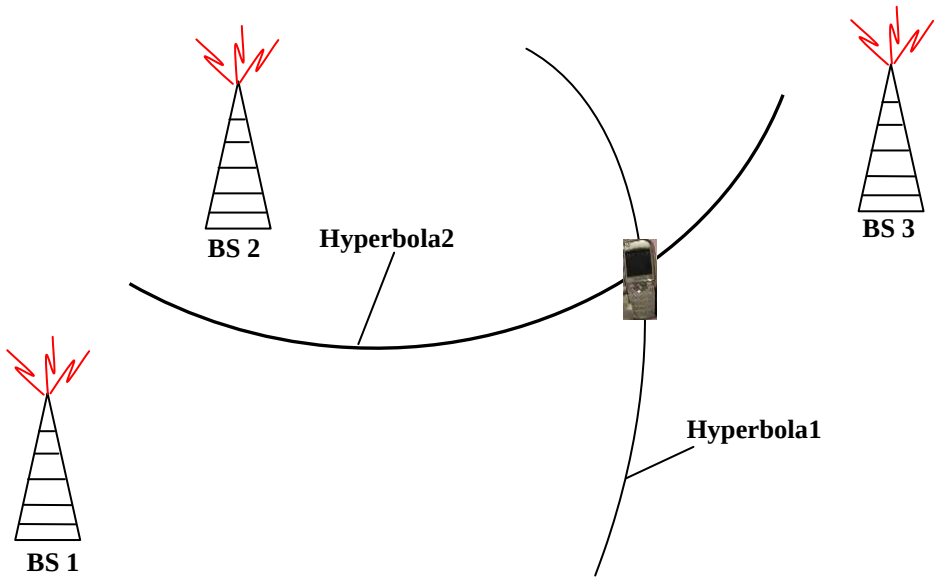

Fig. D-4: TDOA wireless location technique

All over the hyperbola, the two signals have the same phase shift between each other. This method requires a strict time synchronism among all of the BTSs, however the MS doesn't need to be synchronized since its clock bias is the same with respect to all the BTSs and will be cancelled out by differencing any two TOA measurements. Synchronizing the BTSs can be done by either synchronizing all the BTSs physically or by bringing them to a common reference time by measuring time differences between the BTSs. If this is done, the accuracy of this method can be of the order of a few tens of meters [*Rossatti, 2001*].

In the case where the MS is covered by just one cell, this method becomes inefficient. Unfortunately, this is generally the case in rural areas. Furthermore, the computation time is greater than in the precedent techniques, because complex mathematics calculations are needed.

On the other hand, the implementation of this method may be costly because the operator must update all the BTSs software and eventually add some equipment, like the PDE.

D.1.5 The TA (Timing Advance)

The use of the TDMA technique in GSM networks creates a problem of a general non synchronism between the MSs and the BTSs. Moreover, when the signal travels from the BTSs to the MS and vice-versa, it is delayed by a fraction of time. This delay is essentially a function of the signal propagation time, and is not always the same due to the mobility of the MS. Thus, it is possible that a signal occupies part of another TDMA slot, which is normally reserved to another user. In order to solve this problem, the GSM protocol defines a TA (*Timing Advance*) field calculated by the BTS and sent back to the MS to correct the signals emission time. In UMTS networks, the TA will be much more precise then in the GSM networks, because it will be based on a CDMA technology. This technique is illustrated in figure D-5.

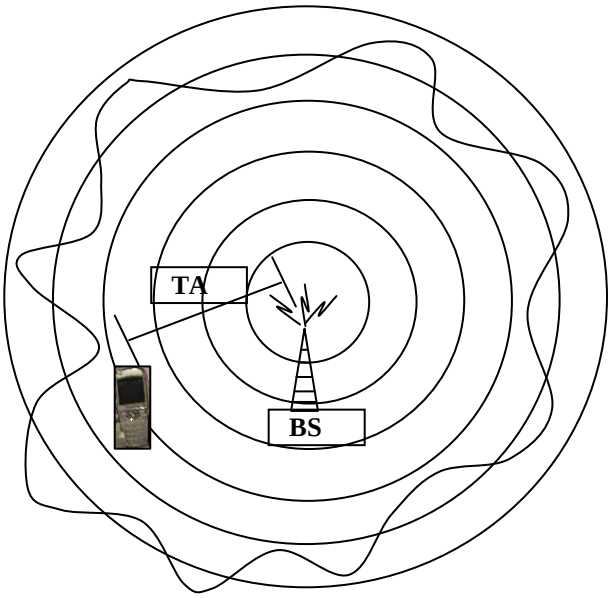

Fig. D-5: TA wireless location technique

The value of the TA being directly proportional to the distance between the MS and the BTS, it can be used to locate the MS. It is comprised between 0 and 63 (it is a 6 bits field, where one bit corresponds to a delay of 3.7 μs). Hence, it identifies rings of 550 meters large, centered on the BTS. The precision is directly related to the distance between the MS and the BTS, because the more the radius is large the more the surface of one ring is large also. This method involves at least three BTSs, and the accuracy is thus enhanced.

No modifications to handsets are needed, but the minors changes must be made to the BTSs software.

D.1.6 Multipath fingerprint

In this technique, the MS location is found by matching the multipath-produced "fingerprint" of the signal received by one or more BTSs with predetermined location/fingerprint database. This requires a continuous database management and updating.

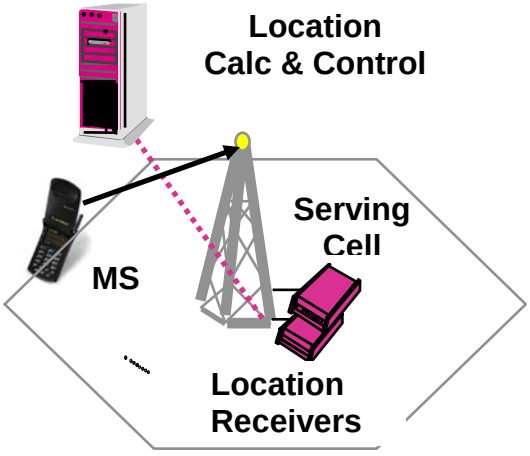

Fig. D-6: Multipath fingerprint wireless location technique [*Rossati, 2001*]

Implementing this method involves network based location calculation and control. It also needs location receivers to be added. No changes have to be made to the handset.

D.2 Handset centric techniques

Only one wireless location technique is completely based on the MS: the OTD method described next.

D.2.1 OTD (Observed Time Difference)

(Also called E-OTD (*Enhanced-OTD*) in GSM networks).

This technique is similar to the TDOA method except in the fact that the measurements are rather made by the MS, which monitors signals from at least three BTSs and observes the time differences of arrivals. The BTSs locations are known and fixed, and the position can be calculated by triangulation after subtracting the OTD from the RTD (*Real Time Difference*).

In this case also, the BTSs must be synchronized to a common reference time, and in addition the MS must also be synchronized with the BTSs. Figure D-7 below illustrates the OTD technique.

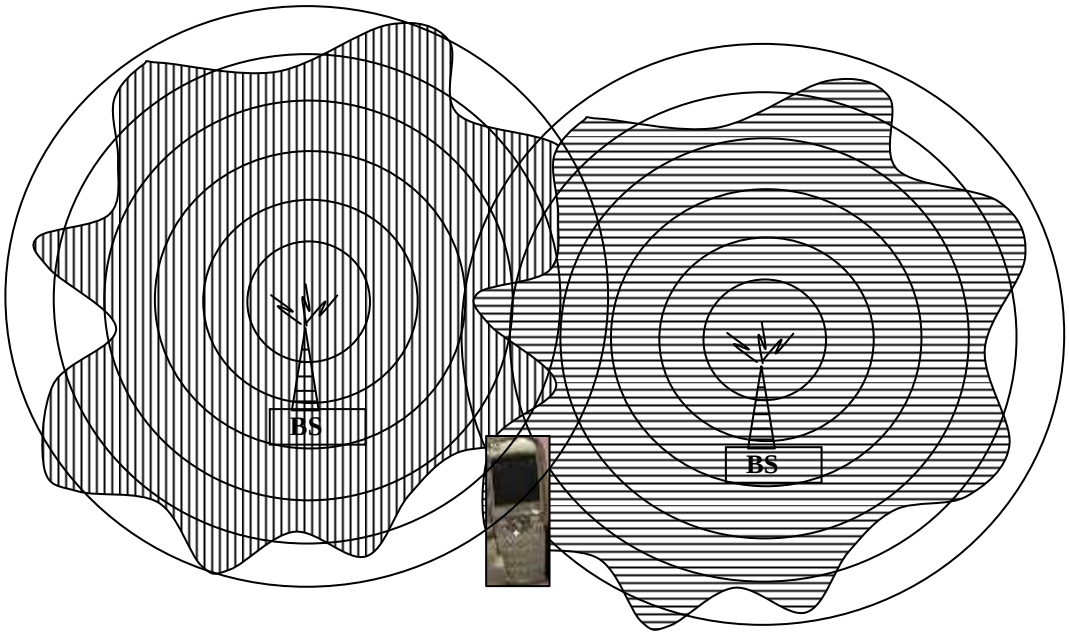

Fig. D-7 : OTD wireless location technique

The precision of this method is limited by the time measurement done by the MS clock. The accuracy of the measurements is between 100 and 500 m [*Rossatti, 2001*]. But this is subject to the synchronization between the BTSs. Actually, in the GSM network for example, the BTSs are not synchronized, however it will probably be the case for the GPRS and the future cellular networks. Thus applying this method in present is costly. Furthermore, in rural areas where the MS cannot receive signals from three BTS at a time, the accuracy of this technique is greatly degraded.

On the other hand, the MS needs an additional hardware component to enable it to measure the OTD of the two incoming signals with two different carrier frequencies, the most precisely possible. In parallel, changes must be made to the phone software in order to treat this information.

D.3 Hybrid network based techniques

D.3.1 The E-FLT (Enhanced Forward Link Triangulation)

This solution is exclusively implemented in CDMA environments. It is primarily based on TDOA using forward-link signals received by MS. The performance can be enhanced by complementary methods, including pattern matching of RF characteristics, statistical modeling, round trip delay measurements, and AOA. The E-FLT location method is illustrated in figure D-8 below

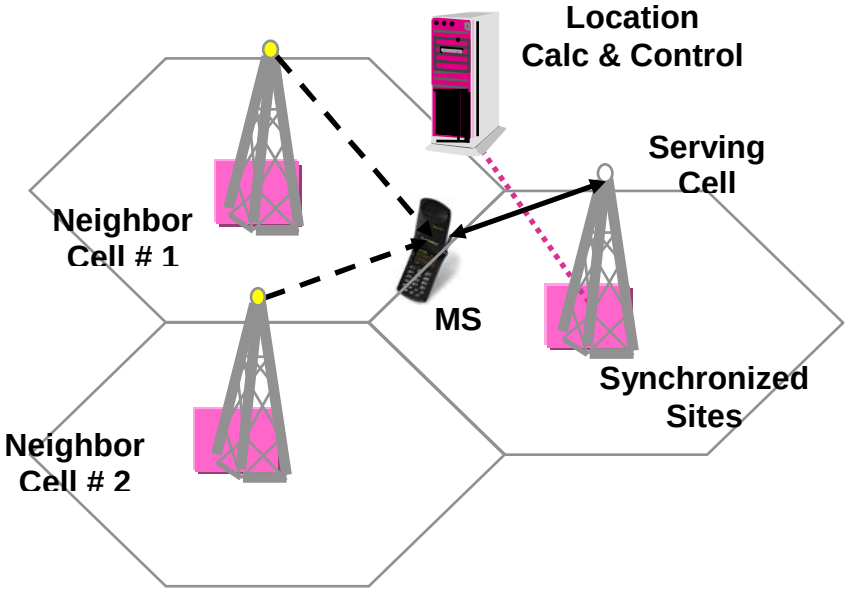

Fig. D-8: E-FLT wireless location technique [*Rossatti, 2001*]

The E-FLT method needs location calculation and control to be made by the network. It also claims synchronization between the BTSs and the MSs.